STUDY OF SURFACE PROPERTIES AND RESIDUAL STRESSES OF ALUMINIUM MATRIX COMPOSITES AFTER ELECTRIC DISCHARGE MACHINING

A THESIS

Submitted in fulfillment of the requirements

for the award of the degree

of

DOCTOR OF PHILOSOPHY

in

MECHANICAL ENGINEERING

By

SARABJEET SINGH SIDHU

(Reg. No. 950808009)

DEPARTMENT OF MECHANICAL ENGINEERING

THAPAR UNIVERSITY

PATIALA–147 004(INDIA)

2014

PREFACE

This research work was carried out by the author under the guidance of Dr. Ajay Batish, Professor & Head, Department of Mechanical Engineering at Thapar University, Patiala and Dr. Sanjeev Kumar, Associate Professor, Department of Mechanical Engineering, PEC University of Technology, Chandigarh.

The Electric discharge machine, weighing machine, micro-hardness measuring apparatus and other facilities are available at Central Institute of Hand Tools, Jalandhar. Some instrument like Surface roughness and optical Image analyzer available in metallurgical lab at IMTT, Batala.

For analyzing residual stress and microstructure of machined samples, X-ray diffraction and scanning electron microscope apparatus available at IIT, Ropar (Punjab) was used.

Several research papers were published out of this research work.

The list of Journals/ Conference in which the papers finds places is given below:

Journals:

1. Sarabjeet Singh Sidhu, Ajay Batish and Sanjeev Kumar, EDM of metal matrix composite for parameter design using lexicographic goal programming, Materials and Manufacturing Processes (***Taylor and Francis***), 28 (2013) 495-500.

2. Sarabjeet Singh Sidhu, Ajay Batish and Sanjeev Kumar, Neural-Network–Based modeling to predict residual stresses during electric discharge machining of Al/SiC-MMCs, Proceedings of The Institution of Mechanical Engineers Part: B 2013 (***SAGE Publications***), 227 (2013)1679-1692.

3. Sarabjeet Singh Sidhu , Ajay Batish and Sanjeev Kumar, Fabrication and electrical discharge machining of metal-matrix composites: A review, Journal of Reinforced Plastics and Composites (***SAGE Publications***),32 (2013) 1308-1318.

4. Sarabjeet Singh Sidhu, Sanjeev Kumar and Ajay Batish, Electric discharge machining of 10vol% Al_2O_3/Al metal matrix composite-An experimental study, Materials Science Forum, 751 (2013) 9-19.

5. Sarabjeet Singh Sidhu, Ajay Batish and Sanjeev Kumar, Study of surface properties in particulate reinforced MMC using powder-mixed EDM, Materials and Manufacturing Processes ***(Taylor and Francis***), 29 (2014) 46-52.

Conference:

1. Sarabjeet Singh Sidhu, Ajay Batish and Sanjeev Kumar, Electric discharge machining of Al-10% Al_2O_3 metal matrix composite, Proceeding of the third and twenty fourth All India Manufacturing Technology, Design and Research Conference (**AIMTDR-2010**), Visakhapatnam, Dec 13-15,2010,pp. 1211-1216.
2. Sarabjeet Singh Sidhu, Ajay Batish and Sanjeev Kumar, ED Machining of particulate reinforced MMCs, International Conference on Emerging Trends in Engineering and Technology, Miami 10-11 March, **2014**. Paper Published in "International Journal of Mechanical Industrial Science and Engineering, 8 (2014)7-13.

Sarabjeet Singh Sidhu

ACKNOWLEDGEMENT

The author wishes to express his deep sense of gratitude to Dr. Ajay Batish, Professor and Head, Department of Mechanical Engineering, Thapar University Patiala and Dr. Sanjeev Kumar, Associate professor, Department of Mechanical Engineering, PEC University of Technology, Chandigarh, for having given me an opportunity to do research in the area of Electric discharge machining and for inspiring guidance given throughout this research work.

Heartfelt thanks are due to Dr. K.K. Raina (Director, Thapar University, Patiala) and Dr. P.K. Bajpai (Dean, Research and Sponsored Projects, T.U. Patiala) and Dr. Tarun Nanda (Ph.D. Coordinator MED) for their encouragement and support during this research work.

The author wishes to place his profound gratitude to Dr. O.P. Pandey, Senior Professor (School of Physics & Materials Science, Thapar University) and Dr. Vinod Kumar Associate Professor (Department of Mechanical Engineering, Thapar University).

The author is grateful to Dr. Mark A. Occhionero (Senior Research Scientist, Ceramic Process System (CPS), 111 South Worcester Street, Norton, MA, USA) and Mr. Allen Drake (Director, Sales & Marketing, Metallic Composites for 21st Century) MC-21, Inc. 5100, Convair Dr. Carson City, NV 89706) for providing particle reinforced metal matrix composite for my research work. The author wishes to place on record his profound gratitude to Dr. Thomos L. Satty, Professor (founder of AHP technique).

I am thankful to Dr. Harpreet Singh, Associate Professor, School of Mechanical, Materials & Energy Engineering, IIT Ropar for providing me facilities in carrying out the X-Ray diffraction and SEM for analyzing the machined sample.

My firm faith in the Almighty God has led me to face all the problems with smile and helped me to cross all the bridges which came my way during this journey of success.

Last, but not the least, my family deserves special mention for the love, affection and blessing showered on me to undertake and successfully complete this research work leading to Ph.D. degree. Special one deserves special acknowledgement.

Sarabjeet Singh Sidhu

CERTIFICATE

Certified that the work which is being presented in this thesis entitled **"Study of surface properties and residual stresses of aluminium matrix composites after electric discharge machining"** by Mr. Sarabjeet Singh Sidhu in fulfillment of the requirements for the award of degree of **Doctor of Philosophy** and submitted to the **Department of Mechanical Engineering, Thapar University, Patiala**, is an authentic record of research work carried out by him under our guidance. The matter contained in this thesis work has not been submitted for the award of any other degree.

23/5/14

(Dr. Ajay Batish)
Professor & Head
Department of Mechanical Engineering,
Thapar University,
Patiala.

(Dr. Sanjeev Kumar)
Associate Professor
Department of Mechanical Engineering,
PEC University of Technology,
Chandigarh.

ABSTRACT

With the emergence of newer technologies, many advanced engineering applications require materials with enhanced properties and controlled coefficient of thermal expansion. One such class of materials are metal matrix composites (MMCs) that have reinforcements (such as fibers or particles) supported by binder (matrix) material. Particulate reinforced MMCs combine a conductive matrix which has been embedded with hard ceramic particles with an average size scale ranging from the molecular level to few microns. Such materials have vastly improved properties and are particularly difficult to machine with conventional machining methods. The use of traditional machinery to machine MMCs results in large tool wear due to the presence of abrasive nature of reinforcement. Electric Discharge Machining (EDM) provides an effective alternative to machine such materials especially when complex geometries are required.

This research work has been conducted in three stages of experimentation. In Stage I, the experimental study was undertaken to identify the significant factors that affect the output responses while machining of 10vol%Al_2O_3/Al composite material. The material removal rate (MRR) and tool wear rate (TWR) have a direct relationship with current and an inverse relationship with pulse-on time. The results were optimized using Lexicographic Goal Programming (LGP) to predict the ideal parametric combinations for machining of MMCs. Optimal conditions for the significant parameters were listed depending upon the requirements of the machining process which may vary for rough machining (higher material removal rate) and finish machining (lower surface roughness). The mean thickness of the recast layer formed after machining was also studied.

The results at this stage of experimentation show that all the responses (MRR, TWR, and SR) have a direct relationship with current but an inverse relationship with pulse-on time. This is because the increased pulse-on time decreases the frequency of spark occurrence. A non-linear mathematical model was developed to predict the optimum machining response parameters. The LGP proved to be a powerful tool in determining the setting of response parameters under given constraints. The recast layer thickness is significantly affected by current and pulse-on time. Also, the pulse-on time is highly significant in determining the thickness of recast layer. The formation of clusters or uneven distribution of reinforced particles deteriorates the properties of the machined surface; hence due to least presence of reinforced particles in recast layer, it is desirable to remove it.

For the next stages of study, the kerosene dielectric medium was replaced with EDM oil for enhanced transfer of spark energy and least deposition of carbon particles on both the electrodes. The diameter of the selected tool electrode was also increased for a detailed study of responses.

During Stage II, two variants of MMCs (65vol%SiC/A356.2; 10vol% SiC-5vol% quartz/Al) were machined and the material removal rate (MRR), surface roughness (SR) and residual stresses were measured. A method to obtain more reliable global weights of three different responses has been described for electric discharge machining (EDM) of different types of particulate reinforced metal matrix composites using the Analytic Hierarchy Process (AHP). Five different process parameters were varied to evaluate their effects on MRR, SR and residual stresses using a standard Taguchi's orthogonal array L_{18}. The machining process parameters such as electrode material (Copper, Graphite and Copper-Graphite composite), peak current, pulse-on/off time and dielectric medium were varied during the study. The residual stresses induced due to subsequent heating, and cooling shocks during the electric discharge process are of primary concern during machining. Artificial Neural Network (ANN) modeling technique was implemented to predict the residual stresses. The capability of ANN to predict residual stresses during EDM has been achieved with feed forward back propagation neural architecture with two hidden layers. The model accurately predicts the residual stresses and can be used as a reliable tool for study of residual stresses in case of complex problems that involve qualitative and quantitative factors.

MMCs with low coefficient of thermal expansion and high reinforced particles exhibit lower residual stresses. Also, better conductive electrode materials used during machining cause lower residual stresses. Pulse-off time was identified as the most significant factor resulting in residual stresses in both the MMCs. The increase in pulse-off time causes a steep rise in residual stresses due to extended solidification period while pulse-on time has no effect. The addition of powder in the dielectric lowers the residual stresses. However, the conductivity of powder particles has no effect on residual stresses. The pulse-off time which had no significant effect on MRR or SR, had the largest effect on residual stresses followed by powder mixed dielectric, current and the type of electrode used. The XRD patterns clearly indicate the formation of new phases on the machined surface. The peak intensity after machining is reduced due to dislocation of atomic layer resulting in residual strains.

The process conditions that affected the three responses were identified and optimized together using AHP and the most suitable process parameter settings for machining of MMCs. It reveals that machining of work piece with graphite electrode and higher setting of pulse-on time with lowest pulse-off time in the presence of suspended particles in the dielectric gives minimum residual stresses with desired MRR. Due to the presence of dense ceramic reinforced particles in Sample I as compared to Sample II, the desired results were obtained at intermediate level of current and choice of higher conductive powders in a dielectric medium. Also, copper powder in the dielectric medium resulted in an optimal solution for 10vol%SiC-5vol% quartz/Al MMC and graphite powder gave better results for 65vol%SiC/A356.2 metal matrix composite.

Higher density of reinforced particles in the matrix results in lesser MRR, SR and residual stress as ceramic particle act as a shield of matrix material against sparks energy. MRR was observed to decrease when the pulse-on time was stepped up from 10 to 30 µs, further it increases drastically as prolonged pulse-on time causes intense melting and evaporation of matrix material and easy removal of reinforced particles by spalling mechanism.

Stage III reports the optimal process conditions for machining of three different types of MMCs; namely 65vol%SiC/A356.2, 10vol% SiC-5vol% quartz/Al and 30vol%SiC/A359 using EDM process. MRR, TWR, SR, residual stresses, micro-hardness and recast layer were evaluated after each trial and contributing process parameters were identified using Taguchi L_{27} orthogonal array. Each work piece was examined by X-ray diffraction (XRD) followed by Scanning Electron Microscope (SEM) for surface integrity and material deposition.

In this stage of study, the effect of material properties and machining parameters on the residual stresses of a machined surface during EDM was investigated by measuring the shift in selected peak at highest angle by Diffractometer method. It was observed that the residual stresses are tensile as well as compressive in nature due to conflicts in thermal properties of matrix and reinforced particles. The surface residual stresses were observed to be mainly dependent upon concentration/ particle size and the conductivity of the work piece. The residual stresses increased with an increase in pulse-off time due to higher re-solidification time of the recast layer (as observed in Stage II experimental plan). The depositions on the work piece due to the presence of copper powder in dielectric resulted in higher residual stresses as compared to conditions where graphite powder is mixed.

Due to weak bonding in composite electrode (Cu-Gr composite), significant quantities of disintegrated particles were deposited to form thick recast layer on the work piece.

The study also reports the phenomenon of surface modification while machining with EDM process. The density of reinforced ceramic forming oxides at elevated temperature (above 1700^0C) was the most significant factor affecting micro-hardness on the machined surface. The XRD spectra revealed formation of copper oxide as the major transferred element from electrode/ dielectric medium. The deposition of carbon was observed when the machining parameters setting were at the highest level. Finally, the cross-sectional view of recast layer analysis reflected the profile of sparks generated during EDM.

The SEM analysis revealed that the thickness of recast layer was maximum for dense reinforced particles MMCs due to the higher heat absorption tendency of doped particles. Hence, high density reinforcement also showed high extent cross-sectional residual stress distribution. It also depended upon the size of reinforced particles. The powder mixed EDM with copper as an additive showed the least recast layer thickness due to improved electric conductivity and consistent discharges.

LIST OF TABLES

LIST OF FIGURES

ABBREVIATIONS

Symbol	Definition
EDM	Electric discharge machining
MMC	Metal matrix composite
ANN	Artificial neural network
AHP	Analytical hierarchy process
ANOVA	Analysis of variance
CR	Consistency ratio
CI	Consistency index
RI	Random index
λ_{max}	Maximum Eigen value
Phi(φ)	Angle of rotation in the plane of the sample, [^{0}]
Psi(ψ)	Angle between the normal of the sample and the normal of the diffraction plane, [^{0}]
θ	Angular position of the diffraction line according to Bragg's Law, [^{0}]
d_0	Strain free inter-planar spacing, [A^0]
$d_{\varphi\psi}$	Inter-planar spacing of the plane measured in the direction defined by phi(φ), psi(ψ), [A^0]
$\epsilon_{\varphi\psi}$	Lattice strain measured in the defined direction
a+	Average of lattice strain for positive and negative(ψ) tilt
σ_{φ}, τ_{φ}	Normal stress and shear stress in the chosen direction, [MPa]
σ_{11}, σ_{22}, σ_{33}	Principal stresses in the principal directions, [MPa]
S_1,1/2S_2	X-ray elastic constants, [MPa^{-1}]
E	Elastic modulus, [GPa]
ν	Poisson's ratio
λ	X-ray wavelength, [A^0]
{hkl}	Miller indices of the crystalline plane
n1,n2	1st and 2nd hidden layer of ANN
E_r	Error signal in the rth neuron for the network
T_{or}	Desired value for the rth output neuron
O_{or}	Network value for the rth output neuron

CONTENTS

CHAPTER – 1
INTRODUCTION

The desire for higher efficiency in modern technology drives the human ability toward the direction of evolution of materials having higher specific properties. One such candidate that satisfies the need of technologies related to aerospace, automobiles, electronic, military equipment, and other industries is designated as composite materials. The ability of "combined action" of composite material was first utilized back in 17^{th} century in the era of Mongolian's to develop a higher strength to weight ratio for archery bow weapons [1]. From 1940's a revolution of composite material started and attracted various researchers and industrialists [2]. The composite materials are classified on the basis of the matrix material and the kind of filler or reinforced material used.

Metal matrix composites (MMCs) are the judicious combinations of two or more materials (one of which is metal) in which the tailored properties are achieved by systematic combination of different constituents. Conventional materials have limitations in terms of properties of strength, stiffness, coefficient of expansion and density. Composite materials can be tailored for desired properties by appropriately choosing their constituents, their distributions, their proportions, their morphologies, degree of crystallinity, crystallographic textures, as well as the structure and composition of the interface between the components. Due to these properties of tailorabilty composite materials can be designed to satisfy the needs of technologies relating to the aerospace, automobile, electronics, construction, energy, biomedical industries. They are also used in various applications such as electronic packaging and thermal management solutions such as microprocessor lids, flip chip lids, microwave housing, optoelectronic housing, armors etc. with the potential to replace existing high cost alloy materials such as titanium-based alloy etc.

The metal matrix composites are also known as cermets (Meaning ceramic-metal combinations) that contain a fraction of ceramic (e.g. Silicon carbide, tungsten carbide etc.). The volume fraction of ceramic and its type determine their application, for example the low volume fraction (15%) tungsten carbide particles ceramic are used in cutting tools such as drills. These are also used in resistors and other electronic components that need to withstand high temperatures. Metal matrix composites containing SiC ceramic at high volume fraction (up-to 65%) are used as heat sinks and housing of microelectronics due to its low coefficient of thermal expansion. The MMCs contain graphite flakes as a

reinforced or fillers and are used as self lubricating piston cylinders for automobile engines.

The particles reinforced MMCs produced by foundry technique find a wide variety of application as shown in Table 1.1.

Table 1.1 Selected MMCs and their potential application [3, 13]

Composites	Application	Features
Aluminum/graphite	Bearings	Cheaper, lighter, self lubricating, conserve Cu, Pb, Sn, Zn etc.
Aluminum/ Al_2O_3, Aluminum/ SiC	Automobile pistons, cylinder liners, piston rings, connecting rods	Reduced wear, anti-seizing, lighter, conserve fuel
Aluminum/SiC , Aluminum/glass or carbon micro-balloons	Turbo-charge impellers	High temperature use, ultra light material
Copper/graphite	Sliding electrical contacts	Excellent conductivity and anti-seizing properties.
Aluminum/zircon, Aluminum/silica	Cutting tools, machine shrouds, impellers	Hard, abrasion resistant materials
Aluminum/ char, Aluminum/clay	Low-cost low-energy material	----
Aluminum/ boron carbide	Drive shaft	High energy transfer
Monofilament silicon carbide fibers in titanium matrix	F-16 fighting falcon	Excellent wear resistant use as jets landing gear

A variety of methods for producing MMCs including foundry technique, have recently become developed. The advantages of preparing MMCs by these techniques are its cost effectiveness, and simple fabrication method. In manufacturing, foundry process is used produce a large volume of complex shaped components at high production rates, required by automobile and other consumer-oriented industries.

The cast MMCs are made by introducing ceramic particulates into molten or partially solidified metal, followed by casting these slurries in the molds. The fabrication of MMCs often involves the use of an intermediate called preform, in the form of sheets,

cylinders or near-net shape. The preform contains the reinforcements, which are held together by a binder that can be polymers (e.g. acrylic, styrene), a ceramic (e.g. silica, aluminum meta-phosphate) or a matrix material itself. The basic requirements of casting of MMCs are the proper wettability of ceramic phase and the molten metal alloy and these can be achieved by uniform dispersions into the molten metal or by pressure infiltration of molten metal into the perform of ceramic phase.

Various methods of uniform distribution of ceramic particulates into molten melts are:

- Addition of particles to a vigorously agitated fully or partially molten alloy [5-7].
- Injection of discontinuous phase into the melt with injection gun [8].
- Dispersion of pellets or briquettes, formed by compressing powders of base alloys and ceramic phase, into a mildly agitated melt [9].
- Addition of powder to an ultrasonically irradiated melt. The pressure gradients caused by cavitations phenomena promotes homogenous mixing of ceramic in the metallic melts.
- Addition of power to an electromagnetically stirred melts. The turbulent flow caused by the electromagnetic stirring is used to obtain a uniform suspension.

The distribution of ceramic/filler phase in the cast structure principally determines its properties. The various factors on which the distribution depends are rate of cooling, viscosity of solidifying melts, shape, size and volume fraction of ceramic particles, thermal properties of ceramic matrix phase, morphology of crystallization phase and their interaction with particles, entrapment and pushing of particles during solidification process and clustering of particles.

The most popular method of fabricating metal-matrix composites is the infiltration of a preform by liquid metal, typically under pressure as shown in Figure 1.1.

This process overcomes disadvantages of suspended particles to experience buoyancy-driven movement (such as graphite, mica, talc, porous alumina) or setting and segregate down (such as SiC, SiO_2, TiO_2, ZiO_2) near the bottom of the melts. In this process, the temperature of liquid melts need to be above the solidus temperature i.e., the temperature above which liquid exists, such that the liquid metal coexist with the solid metal unless the temperature is above the liquidus region.

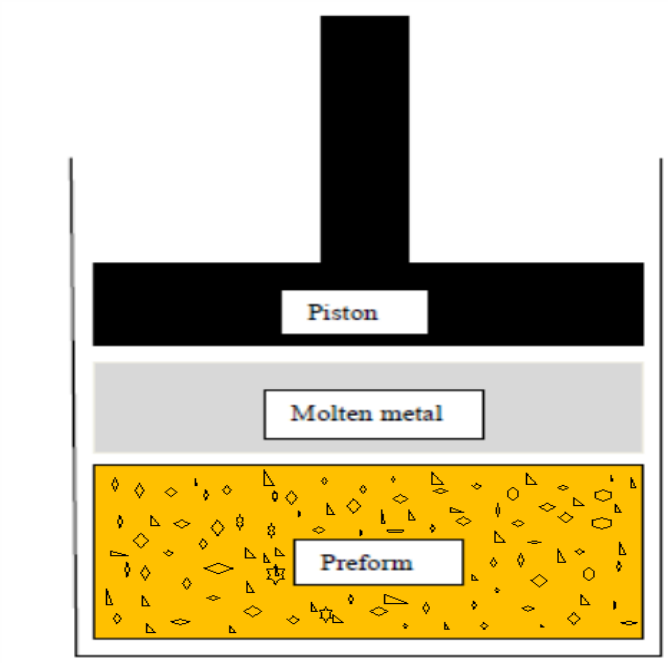

Figure 1.1 Schematic diagram showing fabrication of MMC by infiltration process

The development of conventional machine tools such as lathe, shaper and milling where high speed steel or tungsten carbide are used as tool to improve the material removal rate (MRR) by many folds and reduce the machining time. These tool materials perform well as alloy or hard material where the material properties are almost uniform, but in case of MMCs the presence of ceramics limits the application of these tools.

These limitations were overcome with the advent of nonconventional machining processes where machining was done with the help of electric sparks, high velocity materials jets, pulse magnetic fields, light beams and chemical reactions. These processes are also known as modern machining processes or advanced machining processes or newer machining process and are characterized by the absence of plastic deformation and chip formation. The various modern machining processes and their mechanism of stock removal are listed in Table 1.2.

Among various advanced machining processes EDM has been increasingly used in the industry, due to its ability to machine parts independent of workpiece properties as well as its capability to machine complex shapes. Since EDM is already being used for the manufacture of press tools, dies and punches where a hard and abrasion-resistant machined surface is a major requirement, researchers have explored ways to adapt this technique for optimizing the machining time with minimum surface distortion. Efforts are being made to machine components with an aim to increase their working life and wear resistance.

Table 1.2 Classification of non-conventional manufacturing processes [4]

Energy type	Basic mechanism	Transfer media	Energy medium source	Processes
Mechanical	Erosion	High velocity particles	Pneumatic/ Hydraulic pressure	Abrasive jet machining, ultrasonic machining, Whirling jet machining.
	Shear	Physical contact	Cutting tool	Conventional machining
Electrochemical	Ion displacement	Electrolyte	High current	Electrochemical machining
Chemical	Chemically reactive agent	Reactive environment	Corrosive agent	Chemical etching/machining
Thermoelectric	Fusion	Hot gases electrons	Ionized material high voltage	Ion beam machining, Electric discharge machining
	Vaporization	Radiation	Amplified light	Laser beam machining
		Ions stream	Ionized material	Plasma arc machining

1.1 WORKING PRINCIPLE OF EDM

The EDM process works on the principle of thermal energy generated due to the excitation of progressive rectangular electric pulses which results in formation of plasma channel. The thermoelectric energy (spark) is generated between the work piece and tool electrode in the presence of dielectric medium (Figure 1.2). The spark gap (distance between work piece and tool electrode) separated by insulating dielectric which helps to control the vigorous nature of spark and also restrict the electrolysis effects on the electrodes. The workpiece is mounted on the table of the machine and tool (electrode) is attached to the ram of machine. The advancing of tool electrode into the work piece is controlled automatically by a servo- control system. During EDM process, pulsed DC of 80-100V and approximately 5Hz -5kHz frequency is passed through the electrodes, which

is separated by a small gap (10-100μm) for precise machining. A small gap is maintained between two electrodes for spark to occur. For this purpose, a tool driven by the servo-system is continuously moved towards the work piece. Localized electrical breakdown of the dielectric occurs and sparks are generated at the closest locations (smallest gap) between the two electrode surfaces where local electric field is highest. The high electric field loses the negatively charged particles (electrons) from the cathode surface and moves towards the anode surface under the influence of the electric field forces. During this movement, the electrons strike with neutral molecules of the dielectric; thus an ionization channel is formed establishing conductivity. In this channel, there is a continuous flow of a considerable amount of electrons towards the anode and that of ions towards the cathode. The kinetic energy is converted into heat energy, thus heating the anode as a result of bombardment of electrons and heating the cathode due the bombardment of ions. The thermal energy generates plasma between the electrodes with a temperature range of 8000^0C to 1200^0C [10] or as high as 20000^0C [11] thus, initializing the heating and melting (i.e. eroding) of a substantial amount of material from the surfaces of both the electrodes. When the pulsating current is turned off, the plasma channel breaks down causing sudden reduction of temperature thereby allowing the dielectric to circulate between the electrode gap and flushing the molten metal from the poles surface in the form of microscopic debris. Since there is no direct contact between the work piece and the tool electrode, this eliminates the problem of mechanical stress, chatter or vibration. The conductive material of any hardness can be machined with this process.

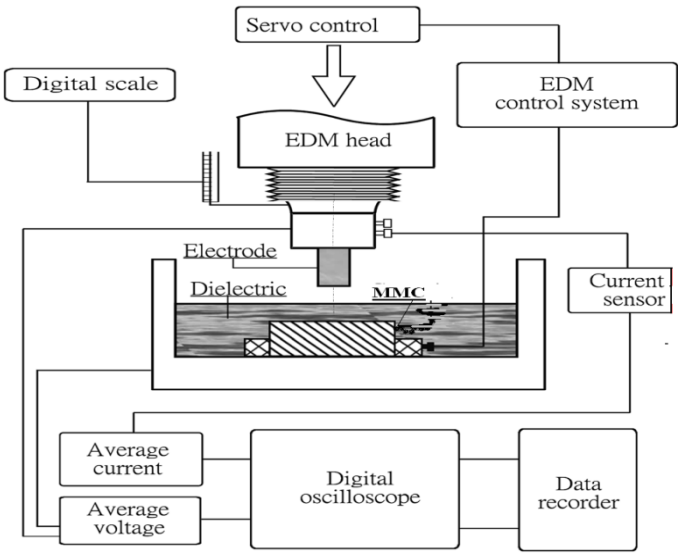

Figure 1.2 Schematic diagram of basic EDM system [35]

Usually, components made by EDM process are machined in two stages viz.

- *Rough machining* at high MRR which may have poorer surface finish.
- *Finish machining* at low MRR with high surface finish.

As the spark duration is only a few micro-seconds, this surface is immediately quenched by the flowing dielectric. Variation in process parameters such as pulse wave form, current intensity, flushing, type of dielectric and electrode material properties such as thermal conductivity, electrical resistivity and heat diffusivity have considerable impact on the surface finish, hardness and dimensional accuracy of the machined surface [12, 13].

Some powder additives suspended in the dielectric fluid also significantly affect the properties of the machined surface. These particles facilitate the ignition process by creating a higher discharge probability and lowering the breakdown strength of the insulating dielectric. This results in a strong corrosion resistant surface having high micro-hardness and less micro-cracks [14, 15].

To enhance the performance of EDM process, powder is mixed in the dielectric and the process is called powder/additives mixed electric discharge machining (PMEDM). The mixed additive reduces the insulating strength of dielectric fluid and increases the inter electrode gap from 25-50 to 50-150μm [16], resulting in an effective transfer of energy as the chain of powder particles helps in bridging the gap. The process becomes more stable thereby improving material removal rate, surface quality, and surface integrity of the machined surface. Jeswani [17] reported increase in MRR by 60% and tool wear by 15% when graphite powder (4g/l) is mixed in kerosene dielectric. Wong et al. [18] suggested the importance of the appropriate combination of powder and the work piece material for superior surface finish. They used graphite, silicon, aluminum crushed glass silicon carbide and molybdenum sulphide with different grain size for machining. Aluminum powder was reported to give mirror finish on SKH-51 work piece but not on SKH-54 work piece.

1.1.1 Phenomenon of material removal

While several theories of how EDM works have been advanced over the years, Patel et al. [19] investigated in the theoretical models of the EDM process and reported that spark is caused as a result of release of electrical energy, which produces thermal and mechanical energy. This result in heating of the work piece and the tool material to melting and

vaporizing temperature and the melts is thrown out in an explosive manner by the mechanical and electrical forces [20]. The process leaves tiny craters on the surface of both the electrodes (work piece and tool). If the spark energy is high, the craters will be relatively larger, producing a rough surface. This type of erosion is called “roughing”. The amount of material eroded from the work piece and the tool electrode depends upon the contributions (in the form of kinetic energy) of electrons and ions respectively. The particles removed are carried off from the gap by the dielectric with the aid of a pressure flushing arrangement. The rate of stock removal is dependent on the polarity of the work piece and the tool electrode [21]. The polarity normally used is straight (normal polarity) in which tool is negative (-ve) and work piece is positive (+ve), while in reverse polarity, the tool is +ve and work piece is -ve The dielectric liquid has the function of reducing the cross-sectional area of the discharge channel to increase the energy density, thus concentrating the energy of spark on to a small area. Dielectric also acts as a shielding medium to prevent the oxidation of work piece during spark discharge.

The four illustrations given in Figure1.3 (a), (b), (c) and (d) show the steps during a single EDM cycle. In Figure 1.3 (a), voltage is increasing leading to creation of ionized channel between the electrodes, but current is still zero. As the voltage reaches its peak, insulating properties of the dielectric fluid begin to decrease along a narrow channel centered in the strongest part of the field.

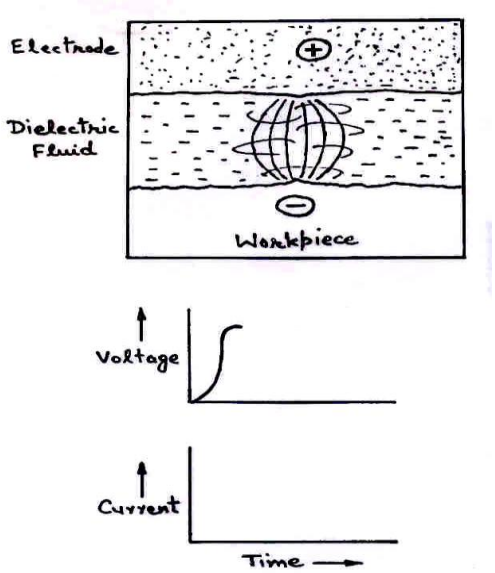

Figure 1.3 (a) First stage of a single EDM cycle [23]

A current is established as the number of ionic particles increases and the fluid becomes less of an insulator. This stage is depicted in Figure 1.3 (b).

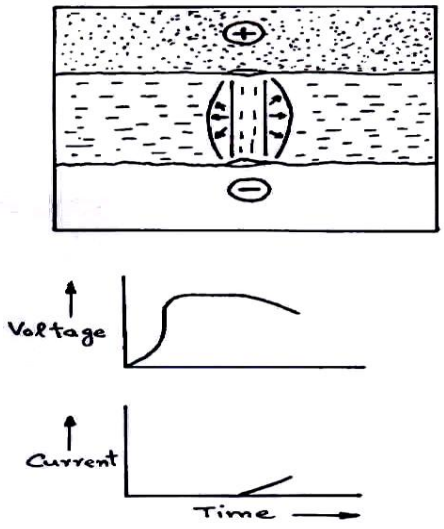

Figure 1.3 (b) Second stage of a single EDM cycle [23]

These ions are attracted by the extremely intense electromagnetic field that has built up. Voltage and current stabilizes towards the end of pulse-on time (Figure 1.3 (c)). Heat and pressure within the plasma channel reaches the maximum. The layer of material directly under the discharge column is in the molten state, but is held in place by the pressure of vapour bubble. More material is vaporized from the surfaces of work piece and tool electrode

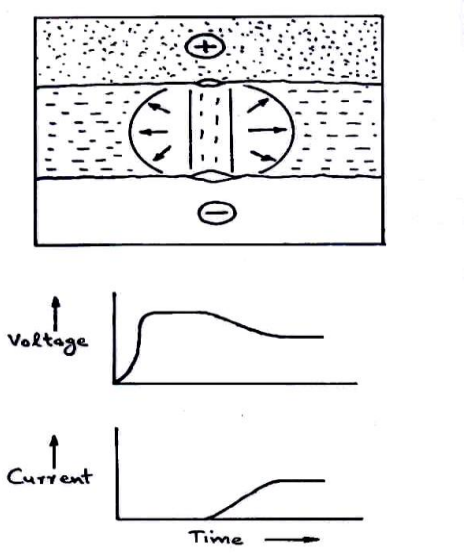

Figure 1.3 (c) Third stage of a single EDM cycle [23]

As the voltage and current drop to zero value, temperature decreases rapidly and then plasma channel collapses, causing the molten material to be flushed away by the flowing dielectric [Figure 1.3 (d)].

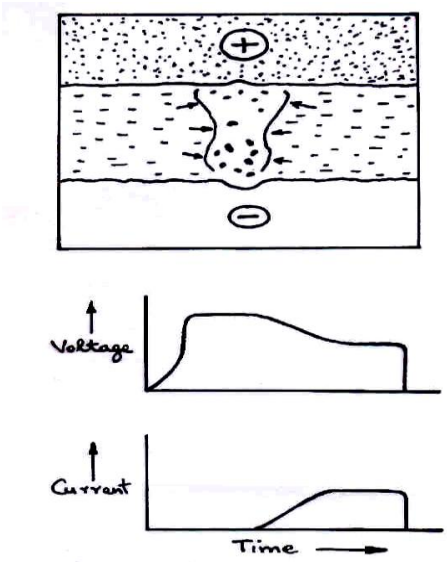

Figure 1.3 (d) Final stage of a single EDM cycle [23]

1.1.2 Surface characteristics of ED-Machined surface

EDM can be employed for electrically conductive material irrespective of its hardness and other mechanical and physical properties. The process can perform different kind of operations such as drilling, slotting etc. The resulting surface consists of a series of randomly distributed overlapping craters with the depth to diameter varying from 5 to 50μm. It gives a high degree of repeatability and high accuracy of the order of 0.025 mm to 0.127 mm. At lower spark energy, the surface finish is comparable to that in turning, planing or milling [22]. Microscopic examination of the machined surface reveals three kinds of layers, namely (i) Recast layer (ii) Heat affect zone and (iii) Converted layer.

The examination of a section of the surface layer produced by EDM (Figure 1.4) reveals that if the molten material from the work piece is not flushed out quickly, it will re-solidify and harden due to the cooling effect of the dielectric, and will get adhered to the machined surface. The depth of this top melted zone (about 2.5 to 50 μm) depends on the pulse energy and duration. This thin layer is known as recast layer. The surface is porous and may contain micro cracks. Below the top layer is a "heat affected zone (HAZ) in which chemically affected layer with changes in the average chemical composition and possible phase changes. Heating and cooling and diffused material are responsible for this zone. Thermal residual stresses, grain boundary weaknesses and grain boundary cracks are some of the characteristics of this zone. There is a plastically deformed zone with micro and macro strains characterized by the presence of twinning slip and phase changes.

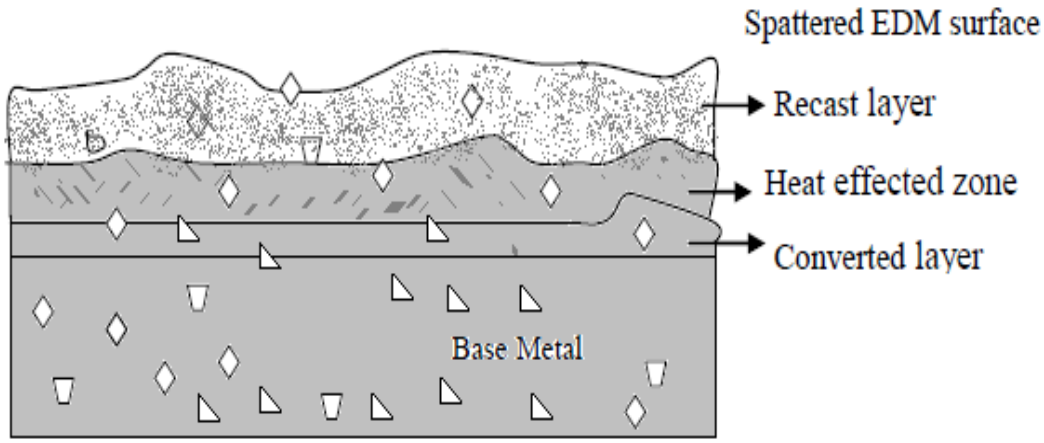

Figure 1.4 Surface layers after electrical discharge machining

Conversion zone is identified below the HAZ and is characterized by change in grain structure from the original structure. Excessive local thermal expansion and contraction rate causes severe slip twining and cleavage on or near the crater or the eroded layer which results in residual stress which is tensile in nature. These stresses are present in extremely narrow superficial zone and depends upon the magnitude of spark energy [87-89].

1.2 RESIDUAL STRESSES

The components during service are subjected to various types of stresses and there are modern techniques to measure them, but are not sufficient to predict the component's life. Residual stresses in a work piece are the function of its material processing and machining history. The residual stresses are system of stresses which can exist in a body/structure in the absence of loading of thermal gradients. These stresses may be due to manufacturing methods, surface treatments, coatings or phase transformations.

These stresses can enhance or impair the functional behavior of machined part. The ED-machined work piece has to be described precisely and this includes an important factor known as residual stress especially on the surface layer. The presence of residual stresses combined with external stresses cause unexpected failures. For many applications, the surface properties are the dominant factor for the functional behavior of the whole component. Figure 1.5 represents some of the effects of residual stress on the machined component. When the high frequency current is in off mode, the plasma breaks down causing sudden reduction of temperature. This results in imploring of the plasma channel by the circulating dielectric fluid and flushing of the molten material in the form of flares

[35]. Due to rapid high temperature melting and cooling process, subsurface defects such as cracks, spalling, porosity, residual stresses, metallurgical transformations are formed on the machined surface [2].

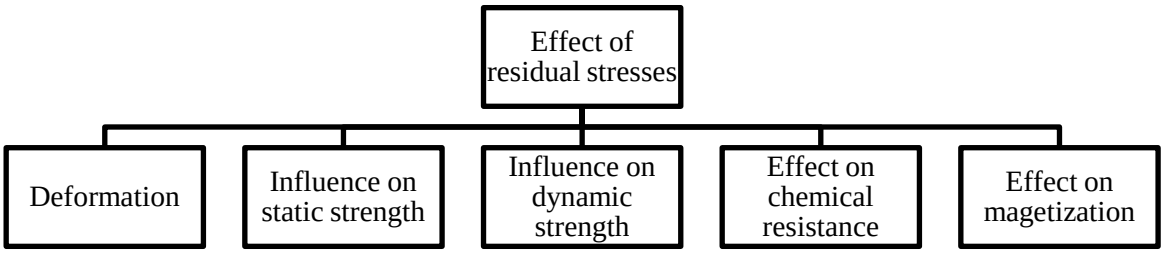

Figure 1.5 Effects of residual stresses

In addition to these, there are other effects such as optical, acoustical or thermal results of residual stresses.

- Deformation by residual stresses: Residual stress act in a body without external forces or moments. The machined work piece develops the internal forces due to plastic deformation or metallurgical transformations. These stresses have only limited depth of penetration, which caused disturbance of equilibrium state of the work piece causing deformation.
- Influence on static strength: The machined component may consist of plastically deformable material. The surface white layer which is brittle in nature, have residual stresses which may lead to cracks if the resulting stresses exceeds the strength of the material at any point.
- Influence on dynamic strength: The influence of residual stresses on fatigue strength results in fracture of the parts. Thus, not the average values of the applied stress but the local induced stresses (residual stresses) are more relevant in failure. This evaluation is necessary in those machining processes which generate scattering stress distributions such as grinding process etc.
- Effect on chemical resistance: If certain metals are subjected to stress and are exposed to the corrosive environment over a period of time, stress corrosion can

be observed. The conditions under, which this effect arises, are specific sensitivity of the material, the existence of residual stresses in the surface and presence of corrosive medium. The cracks may be generated on the surface of work piece due to stress corrosion. There are different theories about the dominant processes during stress corrosion. The electrochemical hypothesis assumes potential difference between the precipitations at the grain boundaries or in grains and the adjacent matrix so that the precipitates are dissolved anodically. These are the main causes of failure in chemical plants.

- Effect on magnetization: This effect is related to the ferromagnetic materials. The magnetic property of this material depends upon its physical state. Micro-cracks for instance act as a disturbance of the magnetic flux in a material.

1.2.1 Types of residual stress

Residual stresses in a work piece are not necessary to maintain equilibrium between the body and environment. They may be categorized by causes (e.g. thermal or elastic mismatch) and by the scale over which they self-equilibrate, or according to the method by which they are measured. In the present study, the residual stresses are originated due to the misfits between different regions.

Three different additive kinds of residual stress in a polycrystalline material are distinguishable. These are categories according to their corresponding length scales [24], and are classified as macro residual stresses and micro residual stress.

- *Macro residual stresses*: As regards structural integrity considerations, continuum long range stresses, much larger than grain size, are generally of most concern and it are often termed as Type I. These stresses are generally of paramount concern.
- *Micro residual stresses (Two Types)*: These stresses results from the difference within the microstructure of the materials and its magnitude and nature changes over distances comparable to grain size of the material under analysis. These are further classified into two types:
    - *Grain- scale stresses* (Type II): These stresses may arise from grain to grain anisotropy. It varies on the scale on an individual grain. It may develop in multiphase materials as a result of the different properties of the phases.

- *Sub-grain-scale stresses* (Type III): These stresses exist within a grain, essentially as a result of defect, dislocations and precipitations or any other crystalline defects.

There are numerous methods for measuring residual stresses, out of these the commonly used methods of residual stresses determination are shown in Figure 1.6. The methods classified under mechanical stress measurement methods rely on the monitoring of changes in component distortion, either during the generation of the residual stresses or afterwards, by deliberately removing the material to allow the stresses to relax. However, most of these techniques make no differentiation between the measurement which include elastic changes and plastic deformations.

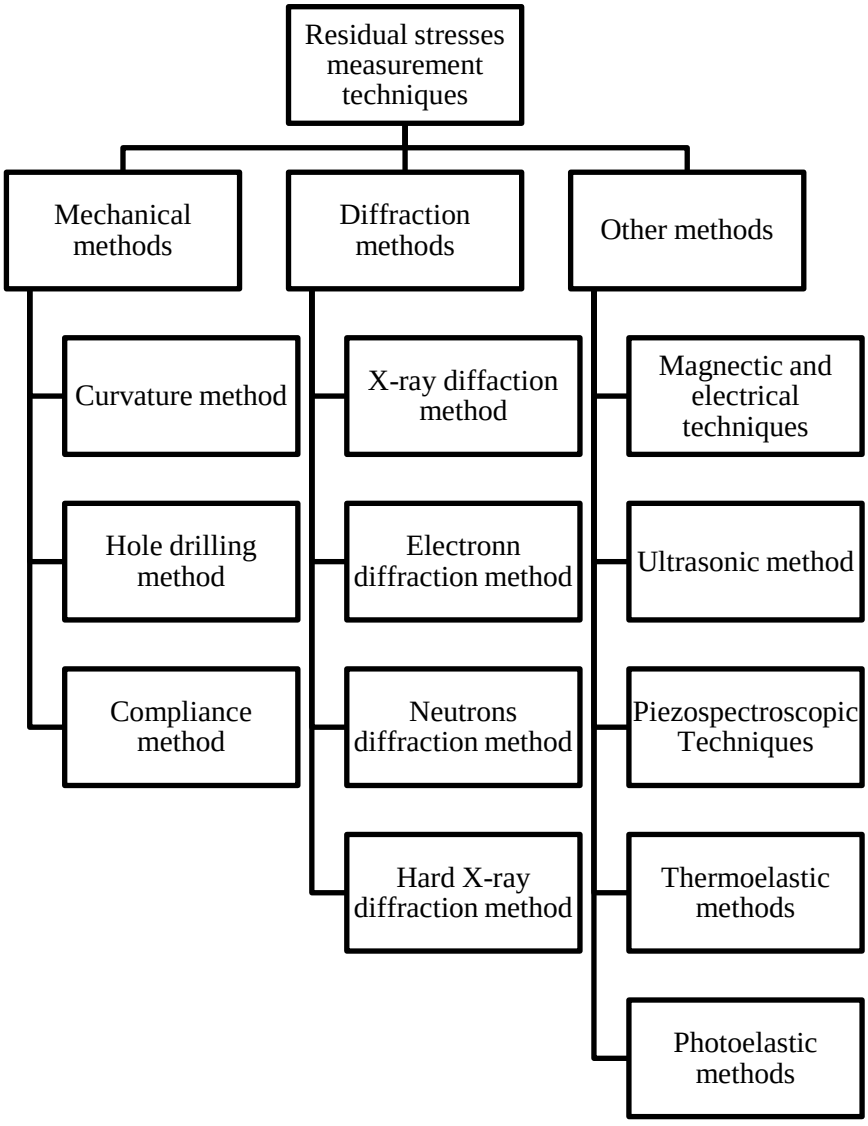

Figure 1.6 Classification of methods of residual stresses measurement techniques

One of the popular methods employed by the researchers is a Hole drill method. It is a destructive method, in which the depth of measurement is approximately 1.2 times the

diameter of the hole and its accuracy is limited to ± 50 MPa. Amongst the non-destructive techniques X-ray and Neutron method have the enormous advantage that repeated measurements are possible on the specimen. For example, one may measure stress before and after some treatment designed to produce or modify residual stress. One may measure residual stress on the machined component at various stages in its service life. In this technique, the measuring depth is ≤ 50μm for aluminum alloys with accuracy of ±20MPa, but this depth of measurement can be increased up to 200 mm by using neurons diffraction method. Ultrasonic method, magnetic methods, Raman method are some of the other non-destructive techniques used to measure residual stresses. The summary of commonly used techniques and their attributes such as resolution and penetration etc. are presented in Table 1.3.

Table 1.3 Summary of various stress measurement techniques [85]

Methods	Penetration	Spatial resolution	Accuracy	Comments
Hole drilling (Distortion caused by stress relaxation)	~1.2 x hole diameter	50 μm depth	± 50 MPa, limited by reduced sensitivity with increasing depth	Measures in-plane type I stress; Semi-destructive
Curvature (Distortion as stress arise or relax)	0.1-0.5 of thickness	0.05 of thickness; no lateral resolution	Limited by minimum measurable	Unless used incrementally, stress field not uniquely determined; Measures in-plane type I stress
X-ray diffraction (Atomic strain gauge)	≤ 50μm(Al); ≤ 5μm(Ti); ≤ 1mm (With layer removal)	1 mm laterally; 20 μm depth	± 20 MPa, limited by non-linearity's in $\sin^2\psi$ or surface condition	Non-destructive only as a surface technique: Sensitive to surface preparation ; Peak shift : Type I, II; Peak widths: Type II, III
Hard X-ray (Atomic strain gauge)	150-50 mm (Al)	20 μm lateral to incident beam; 1 mm parallel to beam.	± 10 x 10^{-6} strain, limited by grain sampling statistics	Small gauge volume leads to spotty powder patterns; Peak shift

Neutron (Atomic strain gauge)	200 mm (Al); 25 mm (Fe); 4 mm (Ti)	500 µm	± 50 x 10^{-6} strain, limited by counting statistics and reliability of stress free references	Access difficulties: low data acquisition rate : costly; Peak shift: Type I, II
Ultrasonic (Stress related changes in elastic wave velocity)	≥ 10 cm	5 mm	10%	Microstructure sensitive; Type I, II, III
Magnetic (Variations in magnetic domains with stress)	10mm	1 mm	10%	Microstructure sensitive; For magnetic material only; Type I, II, III
Raman	≤ 1 µm	≤ 1 µm approx.	Δλ~0.1 cm^{-1} = 50 MPa	Type : I, II

X-ray diffraction method is used for measurement near-surface stress. If the stress is to be measured at some point below the surface, material must be removed down to that point to expose a new surface for X-ray examination; and becomes a destructive method. However, in EDM process, the residual stresses present on the work piece ordinarily near-surface volume where the magnitude of stress is usually high and where failure usually originates.

1.3 CONCEPT OF DIFFRACTION STRESS ANALYSIS

A basic idea of diffraction stress analysis is explained in Figure 1.7 where the polycrystalline specimen is subjected to a tensile stress parallel to the surface.

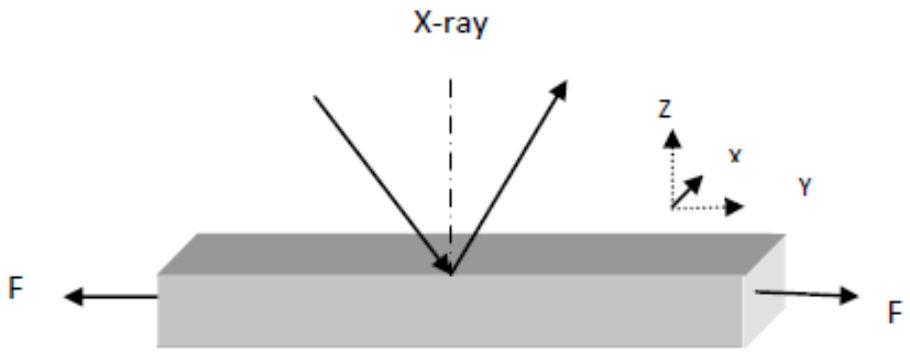

Figure 1.7 Specimen under pure tension, with diffraction plane parallel to axis

Due to tensile stresses, the lattice spacing changes in the lattice plane (hkl). A particular set of grains contributes to a particular (hkl) reflection in the para-focusing geometry. The grains in (hkl) plane which are parallel to the specimen surface get altered due to the tensile or compressive stresses. Measurement of the strain (Єy) in y axis by X-ray requires diffraction from the plane perpendicular to the axis of the specimen. With X-ray diffraction analysis, direction-dependent measurement of lattice strain is possible. A back reflection technique is used to measure the lattice spacing. The Bragg's law $\lambda = 2d\sin\theta$ relates the lattice d-spacing, wavelength of incident X-ray λ, and the diffraction angle θ in the lattice planes. This provides the measurement of strain in z direction (Єz) or lattice spacing is measured in the direction of diffraction vector and is calculated as equation (1.1)

$$\varepsilon_z = \frac{d_n - d_o}{d_o} \tag{1.1}$$

Where d_n is the spacing of the plane parallel to the specimen under stress and d_o is the spacing of the same plane in the absence of stress. The strain in Єy is calculated as Єy =ν Єz where ν is Poisson's ratio for the material, and its value ranges from 0.25 to about 0.45 for most metals and composite materials. The strain is related to the uniaxial stress (σy) in the direction of tensile force by Modulus of elasticity (E) and is given by equation (1.2)

$$\sigma_y = E\varepsilon_y \tag{1.2}$$

The above equation, the grains whose (hkl) planes are parallel to the surface of the bar (Figure 1.8, $N_p \perp$ to the atomic plane) are compressed i.e. reduction in d-spacing by the tensile stress are contributing the for stress measurement.

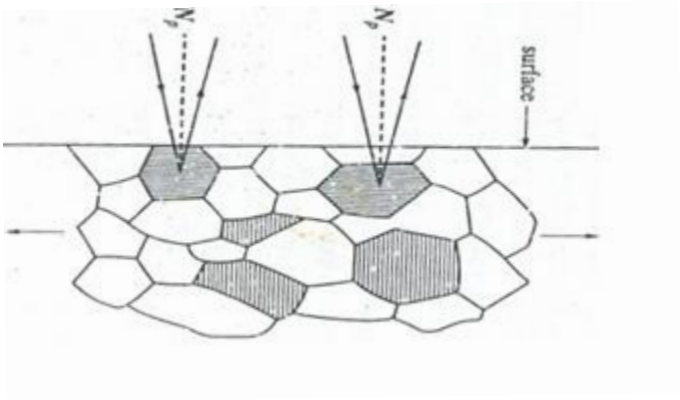

Figure 1.8 Diffraction from stained aggregate horizontal plane [109]

The variation of d-spacing with ψ-angle of the normal of (hkl) is shown in polar coordinate in Figure 1.9. The length and the direction of any vector in this diagram show the spacing and plane-normal direction, respectively, of any selected (hkl) set of plane. If the specimen were unstressed, the end of the d_0 vector would describe the dashed circle shown, because plane spacing is independent of plane orientation. This is not true if some stress is present; if the stress is tensile, d-spacing increase with ψ along the curve shown by the full line.

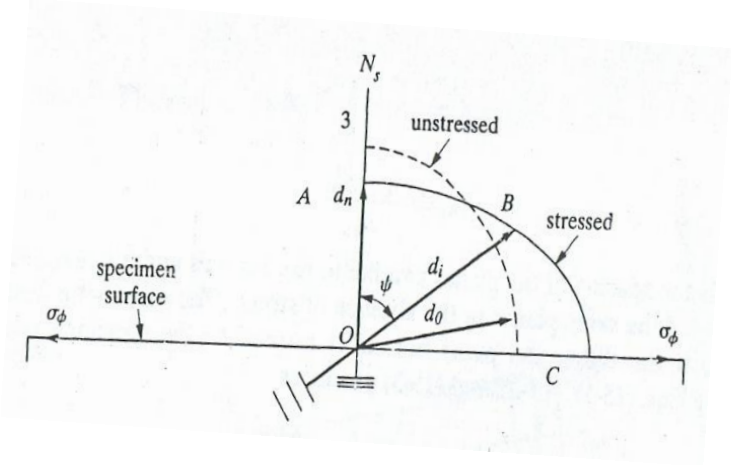

Figure 1.9 Vector diagram of plane d-spacing for stress [109]

In general, the residual stresses developed in the work piece are in two or more directions, thus forming a biaxial or tri-axial stress system. The direction of strain measurement is the direction vector and is identified by the angles ψ and φ, where ψ is the inclination angle of the specimen surface with respect to the diffraction vector and φ is the rotation of the specimen about the specimen surface normal as represented in (Figure 1.10).

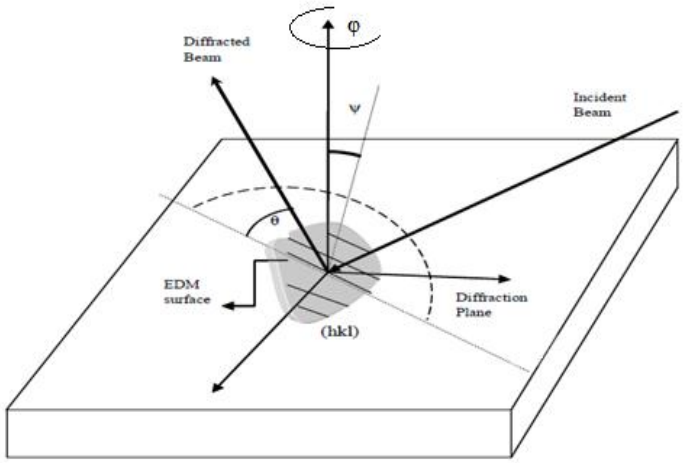

Figure 1.10 Schematic of concept of diffraction stress analysis

Based on the co-ordinate system, the relation between stress and strain full tensor is represented by equation 1.3

$$\epsilon_{\varphi\psi} = \frac{1}{2}S_2 \sin^2\psi(\sigma_\varphi - \sigma_{33}) + \frac{1}{2}S_2\,\tau_\varphi \sin(2\psi) + \epsilon_{\varphi 0^0} \quad (1.3)$$

Where

$$\epsilon\varphi\psi\ \ (lattice\ spacing\ in\ particular\ direction\ ) = \frac{d_{\varphi\psi} - d_0}{d_0}$$

$$\epsilon_{\varphi 0^0} = \frac{1}{2}S_2\,\sigma_{33} + S_1(\sigma_{11} + \sigma_{22} + \sigma_{33})$$

$$\sigma_\varphi(Measured\ normal\ stress\ Mpa) = \sigma_{11}\cos^2\varphi + \sigma_{12}\sin(2\varphi) + \sigma_{22}\sin^2\varphi$$

$$\tau_\varphi(Measured\ shear\ stress\ Mpa) = \sigma_{13}\cos\varphi + \sigma_{23}\sin\varphi$$

$$S_1 = -\frac{\nu}{E}$$

$$\frac{1}{2}S_2 = \frac{(1+\nu)}{E}$$

S_1 and $1/2S_2$ are the X-ray elastic constants (XEC's). The value of d_0 , E and ν are required for the above equation 1.3. Normally, d_0 is taken as experimentally measured d-spacing at ψ=0. This assumption is reasonable because elastic strains typically introduce a maximum of 0.1% difference between true d_0 and d measured at any ψ.

Further, d_0 is a multiplier to the slope of equation 1.3, and the net effect will therefore, be less than 0.1%, much less than that from other errors [109]. The value of X-ray elastic constant can be collected from the available literature.

The most common method used to determine the stress is $\sin^2\psi$ method and it was first introduced in 1961 [110]. A number of XRD measurements are made at different ψ tilts (Figure 1.10) and is used for stress determination because this allows the data to be fit with the least squares line, thereby increasing the robustness of the experimentation.

The inter-planner spacing, or 2θ peak position, is measured and plotted against $\sin^2\psi$. The sample calibration stresses is shown in Chapter 3. Figures 1.11 shows the three patterns of d vs. $\sin^2\psi$.

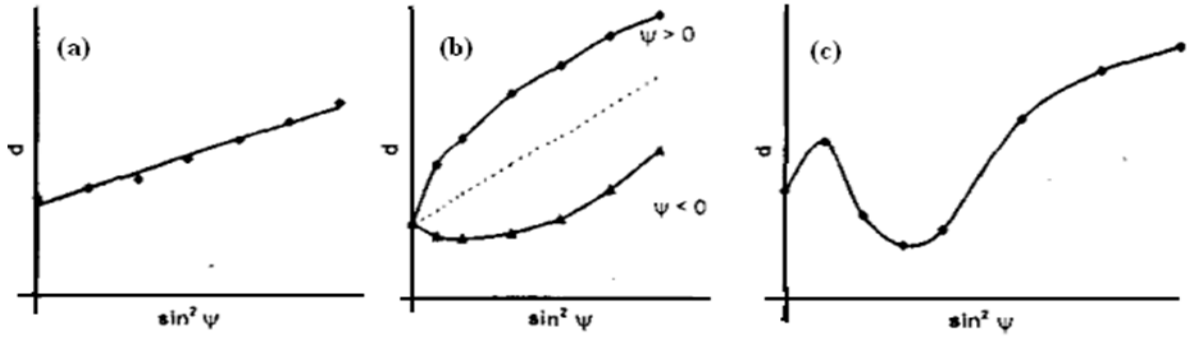

Figure 1.11 Different types of d-spacing vs. $\sin^2\psi$ plots

If shear stress components σ_{13} and σ_{23} are zero (τ_φ =0), the equation 1.3 shows the linear relationship between d and $\sin^2\psi$ as shown in Figure 1.11(a). The behavior in Figure 1.11(b) is termed as "psi-splitting", that is the d-spacing determined for positive and negative ψ. This splitting of the curve is due the presence of both shear components i.e. σ_{13} and σ_{23} (due to sin2ψ term). The full tensor equation 1.3 is derived on the assumption that the bulk material is elastically isotropic. This requires the random orientation of the crystallites. However, during metal processing a significant amount of texture or preferred orientation are present. In such cases the d vs. $\sin^2\psi$ plots shows an oscillatory behavior. In case of steep gradients the d vs. $\sin^2\psi$ plots are found to be slightly curved instead of a straight line. The strain $\epsilon_{\varphi\psi}$ depends upon the angles φ (phi) and ψ (psi). The alternatives measurement of stress is possible such as:

(1) The strains $\epsilon_{\varphi\psi}$ can be measured as a function of ψ for a fixed value of φ. This is the conventional ψ-differential method. Depending on how ψ is changed there are two techniques called the iso-inclination method and the side inclination method.

(2) The strain $\epsilon_{\varphi\psi}$ is measured as the function of φ for a fixed value of ψ. This is called the phi-integral method.

Any one of these techniques can be followed to determine strain and stress in the work piece. The diffractometer used for the measurement of residual stress are basically powder diffractometer, however, if required they can accommodate larger, heavier samples, although as it is usually desirable to use cut sections from large components. The maximum 2-theta accessible to the instrument is larger, typically 145^0-165^0 (2-theta) as the measurement can be made at high 2-theta values where the small changes in the d-spacing, due to strain, can be measured precisely. Residual stress diffractometers are classified as two types:

- Fixed, laboratory based system: This type of diffractometer is used in the present study in which the sample is placed within radiations enclosure instrument. These instruments are usually capable of other forms of X-ray diffraction analysis, for example, phase identification.
- Portable systems: These systems are designed specifically for stress analyses and are much smaller for ease of handling. They can be taken to a large structure (for example, a bridge) and placed on the component of interest.

1.3.1 Radiation selection for residual stress analysis

The choice of X-ray tube anode and therefore the wavelength of the incident X-rays is critical for the measurement of residual stress. During selection, three important criteria must be considered. These are:

- Sample fluorescence
- Diffraction angle
- Choice of crystallographic plane

Sample fluorescence: If the K-α component of the incident beam causes the sample to emit its own fluorescent X-rays, then radiation used for examination is not suitable. Consider an example of examining iron sample with copper K- α radiation. The K-α radiation of copper has slightly higher energy than that of iron K-α absorption edge. The copper K-α radiation is exactly the same energy to be absorbed by the iron atoms which results in emitting iron K-α radiation, a fluorescent effect. This fluorescence produces very high background and consequently a poor peak-to-background ratio. This may be improved by using a secondary monochromator, which filters the fluorescent radiation before it enters the X-ray detector. Usually, a longer wavelength radiation is selected for examining the iron sample, as these radiations will not have sufficient energy to cause florescence. For iron samples a good choice would be chromium anode X-ray tube.

Diffraction angle (2-theta): The change in d-spacing due to the strain in the sample is very small, that is typically in the third decimal place. For analysis, the wavelength that will give a reflection from the sample at the highest possible 2-theta angle is selected. At high 2- theta angles small change in the d-spacing will give measurable changes in 2-theta, although the peak shift are still only a few increments of degree. At low 2- theta angles the difference will be too small to be measured with any degree of precision. Ideally, the radiation source should be selected to give a reflection at Bragg angle greater than 125^0 (2-theta).

Choice of crystallographic plane: Different crystallographic planes vary in their deformation mechanism and give different responses for both elastic (residual stress) and inelastic strain (line broadening). Measurements at different crystallographic planes are generally not comparable. Also, measurement made with different radiations may not be comparable due to difference in its penetration depth of X-ray beam in the sample. If it is suspected that the sample is textured, the reflection with highest multiplicity is selected, as it reduces the oscillation in d vs. $\sin^2\psi$ plot. If the sample has a larger grain size it may also help to select the reflection with the highest multiplicity. Table 1.4 shows the recommended X-ray tube and {hkl} plane combinations for the variety of samples

Table 1.4 X-ray tube and {hkl} plane for some materials [109]

Material	Lattice structure	X-ray Tube anode	K-β filter	Wavelength A^0 (K-α)	2-Theta angle (Approx.)	{hkl}	Multiplicity
Ferrite α-iron	BCC	Cr K- α	V	2.2897	156.1	211	24
Austenite γ-iron	FCC	Mn K- α	Cr	2.1031	152.3	311	24
		Cr K- α	V	2.2897	128.8	220	12
Aluminum	FCC	Cr K- α	V	2.2897	139.3	311	24
		Cr K- α	V	2.2897	156.7	222	8
		Cu K- α	Ni	1.5406	162.6	333/511	32
		Cu K- α	Ni	1.5406	137.5	422	24
		Fe K- α	Mn	1.9360	127-131	311	24
Titanium alloy	Hexagonal	Cu K- α	Ni	1.5406	139.4	213	24
Copper	FCC	Cu K- α	Ni	1.5406	144.8	420	24
Tungsten	BCC	Co K- α	Fe	1.7889	136.6	222	8

1.4 TAGUCHI'S APPROACH FOR ROBUST DESIGN

Since, 1980's engineers and scientists have become aware of the benefits of using designed experiments and their new application areas. The characteristics of robust design, focused on one or more of the following:

- Designing a product that is insensitive to environmental factors, affecting the product performance.
- Designing product so that they are insensitive to variability transmitted by the component of the system.
- Designing processes so that the manufactured product will be as close as possible to the desired target specifications even though some process variables or raw material characteristics are impossible to control precisely.
- Determining the operating conditions for a process so that critical product characteristics are as close as possible to the target value and the variability around the target is minimized.

A Japanese engineer, Dr. Genichi Taguchi, introduced the approach based on classifying the variables in a process as either control (or controllable) variables or noise (or uncontrollable) variables and then finding the settings for the controlled variables that minimized the variability transmitted to the response from the uncontrolled variables. Taguchi's approach provides a powerful and efficient method for designing products operate consistently and optimally over the variety of conditions [25]. Due to limitations in handling the experimental data, the traditional "one factor at a time" approach is changed to varying many factors at a time through statistical experimental design techniques. This is done in conjunction with a change of attitude for dealing with the uncontrollable factors, removing the effect and not the cause, by appropriately tuning the controllable factors.

The controlled factors which are set by the manufacturer and cannot be directly changed by the customers are of three different types as shown in Figure 1.12. The factors which effect the responses of the process are referred to as target control factors or signal factors. The factors that effect the variability in the response are variability control factors. The factors which effect neither the mean response nor the variability, and thus are adjusted to fit the economic requirement are called cost factors. Noise factors are those over which the manufacturer has no direct control but which vary with the customer's environment and usage. These are categorized as: Outer noise; Inner noise; Product noise. The outer noise are the environmental factor such as ambient temperature, humidity pressure etc. The inner noise is function and time related such as deterioration, wear etc. The product noise manifests itself in part-to-part variations. The product may have sensitivity to all three forms of noise [26, 108].

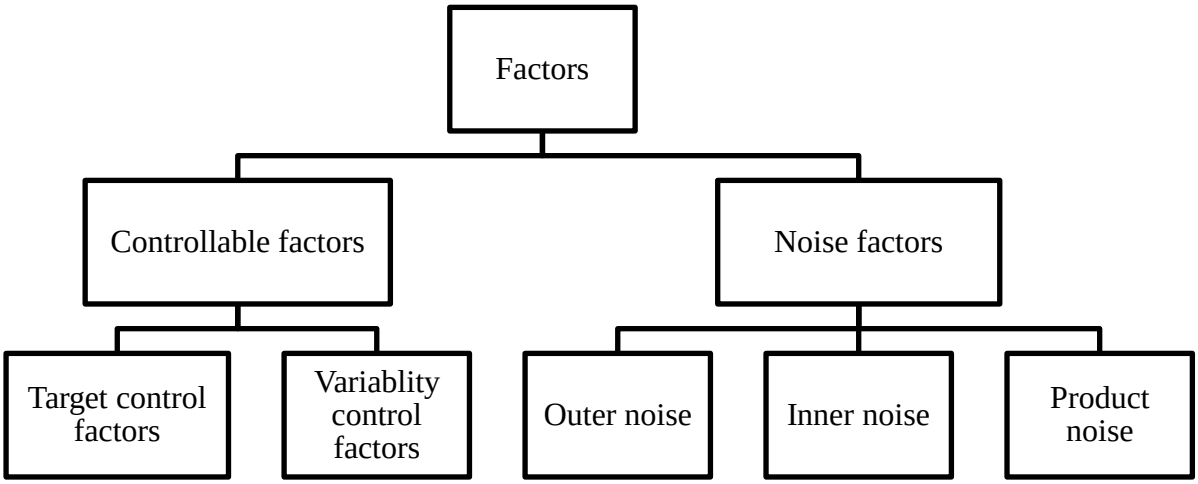

Figure 1.12 Controllable and noise factors

1.4.1 Steps in an experimental study

The essential steps suggested by Taguchi has suggested being taken in conducting the experimental study are discussed below [108].

1. Recognition of and statement of problem: This step concern with the clear understanding of the problem. The problem statement should be specific and if multiple responses are involved, that should be noted.
2. Determine the objective: This includes the identification of the performance characteristics and level of performance required when the experiment is completed.
3. Determine the measurement methods: In this step the performance characteristics are assessed after the experiment is completed.
4. Identification of factors: At this stage, the factors are identified that influence the performance characteristics. This involves a group of people who are associated with the product or process under investigation to collectively decide the controllable and uncontrollable factors, to define the experimental range and

appropriate factors levels. Brainstorming, flowcharts and fish bone charting is used to aid the creation of the factors to be investigated. A pilot experiment often aids the identification of factors.

5. Identification of interactions: The controlled factors that may interact are identified. These interactions use up some degree of freedom also and may dictate the size of the experimentation.
6. Linear graph analysis: The linear graph for the controlled factors and interaction are plotted. The desired factors and interaction may influence the selection of orthogonal array.
7. Selection of orthogonal array (OA): The orthogonal array, inner and outer, are the function of total degree of freedom required from the factors listed and the required linear graph.
8. Assignment of factors and interaction to column: The linear graph for an OA may have to be modified to fit the required form. The number of levels in a column may have to be modified at this time also.
9. Conduct the experimentation: The trial data sheets should be constructed to minimize the possibility of errors in setting the proper levels for the trials. Randomization strategies should be considered during the experimentation.
10. Analysis of data: The performance measures are evaluated for each trial of inner array and analysis is made using appropriate statistical techniques such as ranking method, ANOVA, S/N ANOVA, average graphs, interaction graphs etc.
11. Interpretation of results: The optimal levels of variability control factors and target control factors are identified from the information obtained after analysis phase. For variability control factors, the optimal levels are considered to be those which reduce the variations in responses of interest. For target control factors, the optimal levels are defined as those which bring the mean response nearest to the target value. The performance of product or process is then predicted at the optimal levels setting. Hence, at this stage the influential factors that effect the performance characteristics are identified.
12. Selection of optimum levels: The optimum levels of most influential control factors are selected for predicting the expected results. The influential factors are

the only one necessary to have the level set or controlled. The non influential factors should be set at level, where lowest cost is realized.

13. Confirmation experimentation: This stage demonstrates that the factors and levels chosen for the influential factors do provide the desired results. The non-influential factors should be set at their economical level during the confirmation test. If the results are not as expected then some important factors may have been left out during experimentation and more screening may need to be done and reiteration steps 4-13 may be necessary.

1.4.2 Selection of orthogonal array

The orthogonal array is special experimental design that requires comparatively small number of experimental trials to measure the effect of parameters included in the study. It is considered to be 'fractional factorial design' and composed of symmetrical subsets of all the combinations of the levels of input parameters corresponding to full factorial design [26]. The selection of factors and interactions is based on the previous experience of experimenter or literature review. Otherwise trial and error approach or pilot experimentation can be used to decide the severity of interaction between the factors. The levels of factors can also be decided by conducting a preliminary study.

The selection of orthogonal array depends on the following items:

- The number of factors and interactions of interest.
- The number of levels for the factors of interest.

The items are used to determine the total degree of freedom required for the experimentation. The total degree of freedom (f_a) for each factor is the number of levels (l_a) minus one i.e.

$$f_a = l_a - 1$$

The degree of freedom for interaction is the product of interacting factors degrees of freedom i.e.

$$f_{aXb} = (f_a)(f_b)$$

The minimum required degree of freedom in the experiment is the sum of the entire factors and the interactions degree of freedom.

The total degree of freedom available in the OA (f_{OA}) is equal to the number of trials minus one. The selection of particular OA for an experiment, the following inequality must be satisfied.

$$f_{OA} \geq (f_{axb} + f_a)$$

It may be possible that a number of alternate arrays qualify this condition. Then, the experimenter should try to find out which array could be more suitable from the point of view of the economy and the possible error in the results obtained through experimentation. Taguchi has provided two tools to aid in assignment of factors and interaction to OA. These are linear graphs and triangular tables.

1.5 MULTIPLE CRITERIA DECISION MAKING

The experimentation conducted using Taguchi's method successfully identifies the optimal process parameters for a single response characteristics. This single setting of process parameter may be optimal for one quality characteristic, but the same may yield sub-optimal results for the other quality characteristics. The suggested optimal setting has its own characteristic, application, advantages and limitations. Hence, it is necessary to go for global/ multiple optimizations of responses such that a single setting of parameters that are optimal for all the quality characteristics could be realized.

The decision for optimization often exhibits the presence of multiple, conflicting criteria for judging the alternatives. Thus, there is a need for making compromise or trade-offs regarding the outcomes of alternative courses of action. The methods used for making a decision in the presence of multiple, usually conflicting criteria is referred as Multiple Criteria Decision Making (MCDM).

MCDM problems can be broadly classified as "selection problem" or "mathematical programming problems". The focus of multiple selection problems is on selecting the best or preferred alternative(s) from the finite set of alternatives. The MCDM method that helps in identifying the "best" alternatives for such problems are referred to as the multiple criteria methods for finite alternatives. The focus of multiple criteria mathematical programming problems is to fashion or create an alternative when the possible number of alternative is high or infinite. These problems are usually modeled using explicit mathematical relationships, involving decision variables incorporated within constraints and objectives and it is represented as:

Objective function : $Max[f_1(x), f_2(x), f_3(x) \dots \dots . f_n(x)$

Subject to : $g_j(x) \geq 0, j = 1,2,3 \dots . . m.$

Some definitions:

The definition of critical terms used in MCDM problem and its solution methods are as follows:

- *Alternatives*: Alternatives are the possible courses of action or experimental trials in decision making problems.
- *Attributes*: These are the traits, characteristics, qualities or performance parameters of the alternatives. For example, if the decision situation is one of choosing the "best" EDM parameter setting, then the attributes could be MRR, tool wear rate (TWR), Residual stress etc. Attributes, from the decision making a point of view, are the description of the alternatives.
- *Objectives*: These are the direction of improvement or to do better as perceived by the decision makers. In an EDM process parameter setting, an objective may be to "maximize MRR" or "minimize TWR or residual stresses".
- *Goals*: These are specific (or desired) status of attributes or objectives. Goals are the targets or threshold of objective or attributes values that are expected to be attained as the best alternative.
- *Evaluation (Criteria)*: These are the rules of acceptability or standards of judgment for the alternatives. Therefore, criteria encompass attributes, goals and objectives.

A common problem in multiple criteria decision making (MCDM) with the use of differing units of evaluation measures is that relative rating of alternative may change merely because the units of measurement have changed. This problem can be solved by normalization. Normalization allows inter-criteria comparison.

In decision making, it is assumed that benefit criteria is one in which the decision maker prefers more of it (i.e. more is better) and a cost criteria is one in which the decision maker prefers less of it (i.e. less is better). In general, cost criteria can be transformed mathematically to equivalent benefit criteria by multiplying by -1 or taking the inverse of it.

The normalization of criteria can be achieved by linear normalization method, vector normalization, use of 10 raised to appropriate power or use of range equalization factors. Many MCDM methods require the use of relative importance weights of criteria. Many of these methods require ratio-scaled weights proportional to the relative value of unit changes in criteria value functions.

Of the many MCDM methods, few important methods that have higher potential to solve decision making problems in manufacturing environment. Figure 1.13 represented the classification of widely used MCDM method in the field of academic planning, accounting, environment, health planning, manpower planning, metal cutting, production planning and scheduling, waste disposal, supply chain management etc.

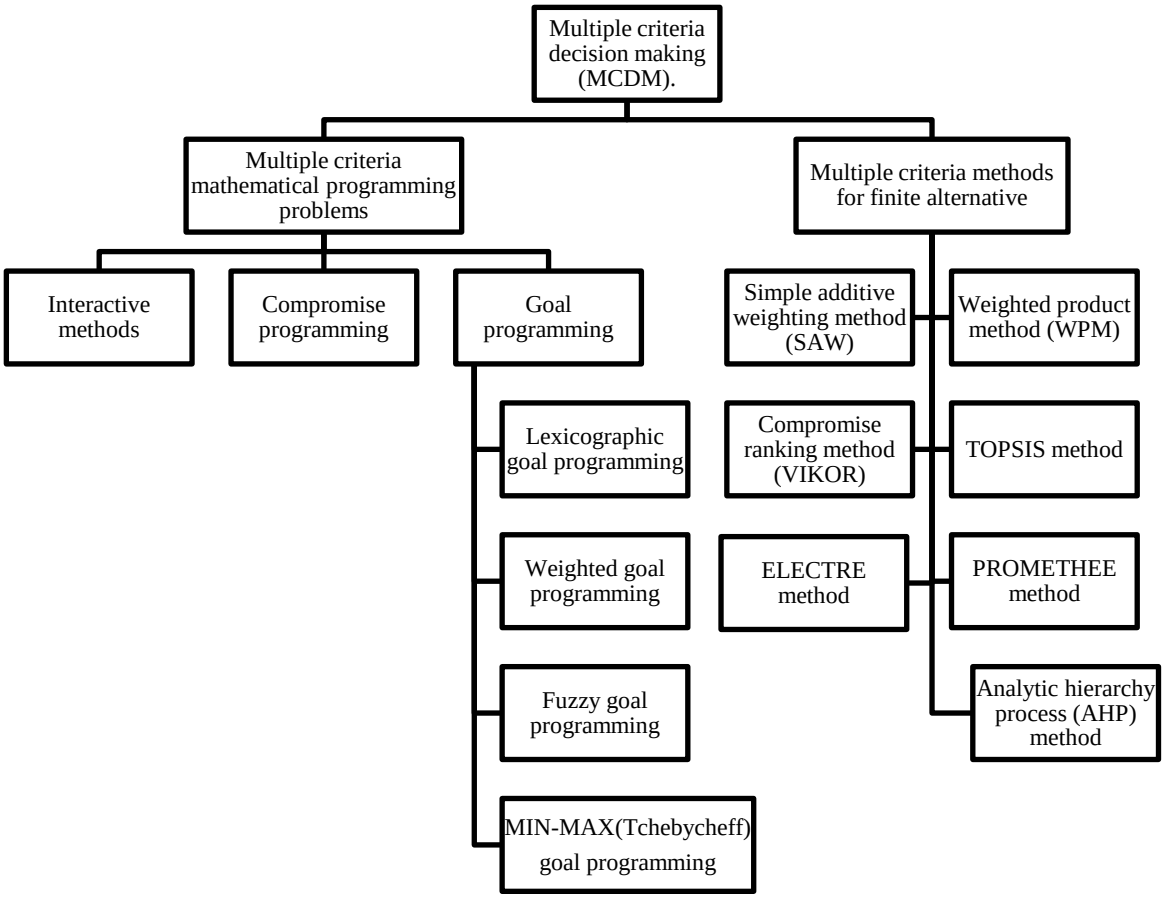

Figure 1.13 Classification of MCDM methods

1.6 OBJECTIVES & SCOPE OF THE WORK

The surface properties after EDM are affected by quenching, as the flowing dielectric causes thermal gradient and phase transformation which results in residual stresses. The chemical composition which, in EDM, may change under the influence of material transfer from the tool or dielectric media in which machining is taking place or both. Suitable operating parameters, electrode bodies or suspended powder in the dielectric fluid is important for carrying out desirable surface modifications on the machined surface.

This study is aimed at investigating the machining characteristic of MMCs using a different tool electrode in variant dielectric medium and to optimize these characteristics according to the desired objective. The most important characteristic, residual stress was modeled to predict the life of the machined component for industrial applications.

Following issues have been taken up during this research work.

1. The capability of electrical discharge machining to machine variant MMCs has been addressed.

2. Material removal rate (MRR), Tool wear rate (TWR), Surface roughness (SR) and surface integrity such as residual stress, induced micro-hardness, recast layer has been explored in EDM with different tool electrode and dielectric mediums.

3. The residual stress induced during EDM of MMCs has been modelled using Feed-Forward Backpropagation Neural Network technique.

4. Relation between different process parameters and response parameters has been established for collective optimization of machining parameters.

5. Material characteristic like microstructure, micro-hardness have been determined for the given work material.

6. The experimental results thus obtained have been globally optimized with suitable MCDM techniques, by which the service life of the machine component can be enhanced.

1.7 OVERALL METHODOLOGY OF THE STUDY

The overall methodology for the study has been divided into five phases:

- Detailed literature review
- Design of study
- Experimentation
- Analysis of the results
- Conclusions

Literature on EDM and its aspects has been reviewed to design a methodology for carrying out the analysis on machining of MMCs. A large number of the input process parameters can be varied in the EDM process, each having its own impact on output parameters such as material removal rate, tool wear rate, micro-hardness of the machined surface, surface finish and overall surface integrity. However, for the purpose of this experimentation, it was not necessary to vary all these parameters because the impact of some of them has already been well established by previous research work available in the literature. During the beginning of Design of Experment (D.O.E) phase, pilot experimentation was performed to establish the effective ranges of input parameters to study the capability of EDM to machine MMCs.

The study of process parameters in MMCs has been divided into three distinct stages:

Stage I: EDM of MMC with copper electrode.

Stage II: Powder mixed EDM of two different MMCs with copper, graphite and copper-

-graphite electrodes using L_{18} orthogonal array.

Stage III: Powder mixed EDM of three different MMCs with copper, graphite and

copper- graphite electrodes using L_{27} orthogonal array.

In Stage I , experimentation was done on Al-10%Al_2O_3 composite by selecting a full-factorial design to determine MRR, TWR, and SR with copper as a tool electrode. Commercial grade kerosene was used as the dielectric medium and the time for each cut was fixed at 20 minutes. In this stage, the most important factors such as current and pulse-on time and there levels were identified from the literature. The design was repeated for both the polarities (which can be positive or negative) to study the effect of polarity. The global performance of EDM process for best input parameters was

established by a multiple criteria decision making tool called Lexicographic Goal Programming.

Before starting Stage II, a literature review and pilot experimentation was carried out. For pilot experimentation Al-60%SiC MMC was selected to find out the most significant machining parameters and their levels that were conducive for favourable output response parameters.

The work piece selected for this experimental stage was Al-60%SiC composite and Al-10%SiC-5%quartz. Three variants of tool electrode were selected namely (i) copper, (ii) graphite, and (iii)copper-graphite composite. The dielectric mediums used were EDM oil and powder-mixed EDM oil. Based on the results, input machining parameters (workpiece, electrode, current, pulse-on/off time, dielectric medium) and their levels for actual experimentation on the work materials were finalized. Taguchi's method was used for the design of the study. The fractional factorial method developed by Taguchi is a technique that allows a process to yield most information using relatively few experiments when there are a large number of input variables.For this, Taguchi has defined a set of orthogonal arrays, each of which can be used in many experimental situations, and provides a standard method for analysis of the results. For this work, L_{18} orthogonal array was found to be most suitable. A specially designed tank was used for conducting experiments with powder mixed in the dielectric medium. This tank confined the additives to a very small region and isolated it from the main dielectric circulating and filtering system. A stirrer was used in this tank to maintain the circulation and consistency of the powder in the machining area. The results showed that the response parameters such as MRR, SR, residual stress were strongly influenced by control parameters (input parameters). The response variables (output parameters) were globally optimized by using multiple criteria method for finite alternative, known as Analytical Hierarchy Process. The results for most important response such as residual stress were modelled by using Artifical Neural Network technique.

In Stage III, the experimentation was conducted on three different types of MMCs namely (i) Al-60%SiC, (ii) Al-10%SiC-5% quartz and (iii) Al-30%SiC with tools as used in stage II. L_{27} orthogonal array was selected to conduct the experimentation with the level of process parameter identified in the previous stage. The response variables with aforesaid design were MRR, TWR, SR, micro-hardness, residual stress, and recast layer thickness. The analysis of recast layer formation and material deposition on the

workpiece were completed using X-Ray diffraction and electron scanning microscopy techniques.

1.8 ORGANIZATION OF THE THESIS

The thesis has been divided into six chapters. Brief description of the contents of each chapter is given below:

Chapter - 1 highlights the introduction to the Metal Matrix Composites there fabrication techniques, applications and features. This chapter also addresses the methods to overcome the uniform distribution of reinforced particle in matrix phase. Various aspects of electrical discharge machining have been detailed: including basic principle of machining, phenomena of material removal, surface integrity of ED machined surface. Residual stresses and its effect on the service life of the component have been classified. A brief classification and its measuring techniques have also been included in this chapter. The Taguchi's approach, multiple response optimizations objectives, scope and overall methodology of the experimental work have been outlined.

Chapter - 2 presents an account of available literature in the fabrication methods of MMCs and machining characteristics of EDM process such as MRR, TWR, SR and surface integrity. The impact of various input process parameters such as peak current, pulse-on time, pulse-off time, polarity of machining and duty factor on electrode wear and material transfer has been discussed. The literature also addresses the magnitude and measuring methods of induced residual stress during fabrication as well as after EDM. After an elaborate scrutiny of the published work, the gaps in this research area listed.

Chapter - 3 details the selection of input parameters and factors levels for the experimentation (pilot experimentation), statistical planning of experimentation and execution of experiments, followed by data collection and recording of results for MRR, TWR, SR, micro-hardness, residual stress. In Stage II, residual stress was identified as the most important response factor hence the relevance of low discharge current and low pulse duration on the phenomenon of machining has been established through literature review. The actual impact of these parameters and their ranges has been investigated through pilot experimentation conducted by varying one-parameter-at-a-time approach. After considering all the variables, L_{18} and L_{27} orthogonal arrays were selected for the experimentation in Stage II and Stage III respectively. The factors included in the array

were work piece, electrode, peak current, pulse-on time and pulse-off time and dielectric medium.

Chapter - 4 gives detailed account of experimentation stages on MMCs. The selection of input factors and their levels for experimentation, statistical planning of experiments and execution of experiments based on selected design, followed by data collection and recording of response parameters has been disscussed. The experimentation has been divided into three distinct Stages, namely Stage I, Stage II and Stage III. The experimentation in Stage I was done on the basis of full-factorial design by considering only two (current and pulse-on time) input variables with three levels, which was modeled by using regression statistical technique for global optimization. For Stage II and Stage III, the machining time, voltage, type of flushing, polarity and powder concentration were kept constant for all the experiments. The residual stress on the machined surface was analyzed using X-ray diffraction technique. The micro-hardness of the machined surface has been evaluated by the micro-hardness tester.

Chapter - 5 highlights the analysis of results obtained from the selected design of experiments, followed by discussions. A collective view of the results obtained by machining MMCs with different electrode materials in the selected powders suspended in the dielectric medium are presented. It presents the comparative analysis with the help of graphs. The results were optimized by using Lexicographic Goal Programming in Stage I. In Stage II the residual stress induced during machining has been modelled by using an effective technique known as Feed Forward Back Propagation Neural Network. The microstructure of machined surface has been obtained using scanning electron microscopy (SEM) has been dicussed.

Chapter - 6 lists down the conclusions of this research work. Recommendations for future work in this area are also listed.

CHAPTER – 2

LITERATURE REVIEW

Processability of metal matrix composites depends upon how appropriately their elements are chosen, their properties, distribution and interface between them. The ductile property of matrix embedded with ceramics reinforced particles serve to reduce the coefficient of thermal expansion, increase strength and modulus. High tool cost in traditional machining processes results in limiting the application of these materials in advance technologies hence electric discharge machining (EDM) process is widely accepted machining option for geometrically complex shaped components.

This Chapter presents the basic selection of elements and fabrication methods of MMCs and a review of the research work carried in the field of EDM to explore ways to improve the efficiency of the machining process. Later, research work related to measurement of residual stresses is reviewed along with scope of future work.

2.1 INTRODUCTION

A composite material is the multiphase, judicious artificial combination of different materials to attain the enhanced properties which the individual component cannot and is a result of combined action of two or more distinct materials. The specific properties of the composite can be wisely tailored by choosing their components (material), their distribution, orientation and crystallographic texture. The metal matrix composite (MMCs), also known as cermets, is one such class which, gained popularity for its lower coefficient of thermal expansion (CTE) with higher strength and modulus. The combination of these proprieties of MMCs makes them suitable for automobile industries such as brake system, piston, piston rod, shaft etc. They are also used in various applications such as electronic packaging and thermal management solutions such as microprocessor lids, flip chip lids, microwave housing, optoelectronic housing, armors etc with the potential to replace existing high cost alloy materials such as titanium-based alloy etc.

Several MMCs are developed by reinforcing various matrix materials. Among these aluminium matrix has been identified as a promising material due to its low density, lower melting temperature (660^0C), higher process ability and ductility (FCC crystal structure). Although, magnesium has a lower density as well as lower melting point as

compared to aluminium, but the presence of HCP crystal structure of magnesium restrict ductility as a number of slip system are fewer in non cubic structure as compared to FCC crystal structure of aluminium. In general, ductility of the matrix is an important factor in MMC because the reinforcement or filler element is brittle and the ductility of matrix compensates the brittleness and helps to restrict the propagation of cracks. In high temperature applications, titanium matrix was selected thus compromising its high density and brittleness. The common ceramic fillers were SiC, Si_3N_4, AlN, Al_2O_3, TiB_2, ZrO_2, and Y_2O_3. However, if the matrix material is similar then the selection of filler, interface bonding with matrix and its amount (%) and distribution pattern particularly poses challenges [27]. The basic characteristics of filler component of the composite are also considered in the selection criteria. As the strengthening of the composite is directly affected by the elastic modulus of filler and this factor is prominent in SiC and TiB_2 ceramics. The thermal conductivity of AlN is the highest but its reactivity with water results in formation of aluminium oxy-nitride, which results in, lowering the thermal conductivity. Thus, usage of significantly higher thermal conductivity of SiC as filler is also justified. After the brief introduction to the basic of MMCs, the emerging class of particulate reinforced MMCs has been reviewed and particularly Al-MMCs reinforced with SiC ceramic particulate has been the main interest of researchers.

2.2 FABRICATION OF COMPOSITE

The process of fabrication of MMCs depends upon the state of matrix material (solid, liquid, vapour phase). The most popular method as reported in literature is liquid state processing such as stir casting, pressurized liquid infiltration, plasma spray decomposition and in solid state processing powder metallurgy is preferred. In a liquid state process, uniform distribution of filler ceramic in the matrix was attained by the usage of the preform of filler in the shape of the finished product. The filler particles are held in position by using binders such as silica or aluminium meta-phosphate [28]. The infiltration, with pressure ranges from 50-90kgf of designed perform, was done by the low viscosity liquid metal as shown in Figure 1.1. The method is suitable for MMCs with a high fraction of filler particulate. Another method called plasma spray in which decomposition of molten matrix and heated filler particles is done by a co-spray process. This method involves higher operating cost. A common method for the low cost fabrication of MMCs is stir casting [29]. In this process, matrix material is superheated over its melting temperature. The particles are preheated at around 1000-1200^{0}C to make

the surface oxidized. The melted matrix is stirred at an average stirring speed of 300-400 rpm as the vortex is formed during stirring [30, 31]. The preheated particle is added at the vortex of matrix melt. The final temperature of pouring is controlled to be approx. 600^0C, or when a thin layer of aluminium appeared on the top of melt. Thereafter, the melt is poured into the mold by using down pouring gate system. The process becomes complicated due to the lower density of filler ceramic which tends to float on the surface of molten metal and particles are not uniformly distributed in the matrix or may causes aggregation [32]. Figure 2.1 represents the schematic operational sequence of stir casting process. The stability of dispersion of filler units may be achieved on lowering the filler-liquid matrix interface energy by using suitable dispersants or by providing the electric charge to fillers or by improving the wettability.

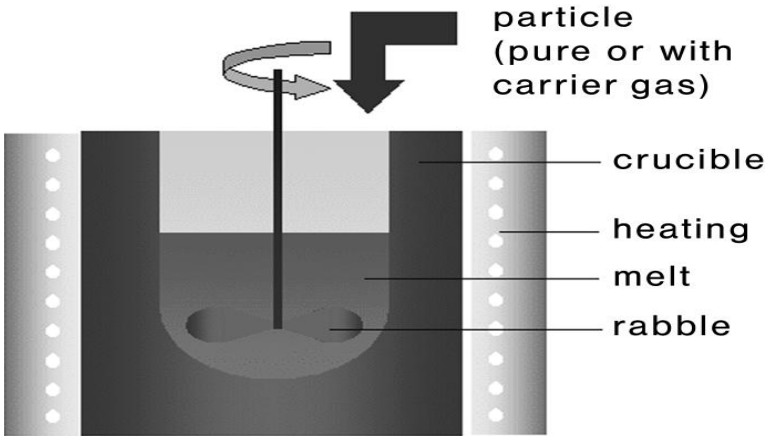

Figure 2.1 Schematic diagram of operational sequence during stir casting process [31]

During fabrication of MMCs, the reaction between the components of composite material degraded the resultant property of composites. Lai et al. [30] observed that at elevated temperature, some amount of silicon carbide (SiC) particles is consumed according to the reaction.

$4Al + SiC \text{ ----------} \rightarrow Al_4C_3 + 3Si$

They also concluded that the formation of brittle aluminium carbide weakens the interface of filler and matrix and the formed silicon dissolves in aluminium matrix causing non uniform distribution of mechanical properties. To alleviate this problem, the appropriate filler particles surface modification may be implemented such as a coating or oxidation.

In powder metallurgy (PM) which is a solid state processing method, an appropriate amount of matrix particles are mixed with the filler particle and the solid state diffusion is attained by sintering process. The PM process is a low temperature process hence the optimum combination of pressure and the temperature is required to reduce the porosity defect and retain the shape of the final product.

The above section provides a brief introduction of fundamentals of the fabrication process. The finished product of MMCs can be tailored in simple geometrical shapes by using various manufacturing processes. A proper method for machining is equally important for the versatile application of MMCs in various sectors. The advantageous properties of MMCs are limited by traditional machining process which causes high surface damages, severe tool wear and cracks impossible to machine in intrinsic shapes with high accuracy [34]. Amongst various non-traditional machining processes, reviewers particularly focused on electric discharge machining (EDM) process on MMCs due its ability to machine intrinsic shapes with close precision with good finish and satisfactory metal removal rate [13, 35]. The origin of EDM can be traced to 1770 reported by the English scientist Joseph Priestly when erosion effect of spark between the conductors was identified. In 1943, the pioneering work in EDM was carried out by Lazarenko and Lazarenko and observed that if the discharge takes place in the presence of dielectric the thermal energy can be focused to a small area. The relaxation circuit (RC Circuit), also known as Lazarenko circuit (Figure 2.2), was widely used in EDM system in 1950s and became a foundation for subsequent development EDM technology [36, 37]. The EDM process work on the principle of thermal energy generated due to the excitation of progressive rectangular electric pulses resulting in formation of plasma channel with temperature range of about 20000^0C between the conductive tool and the work piece [38].

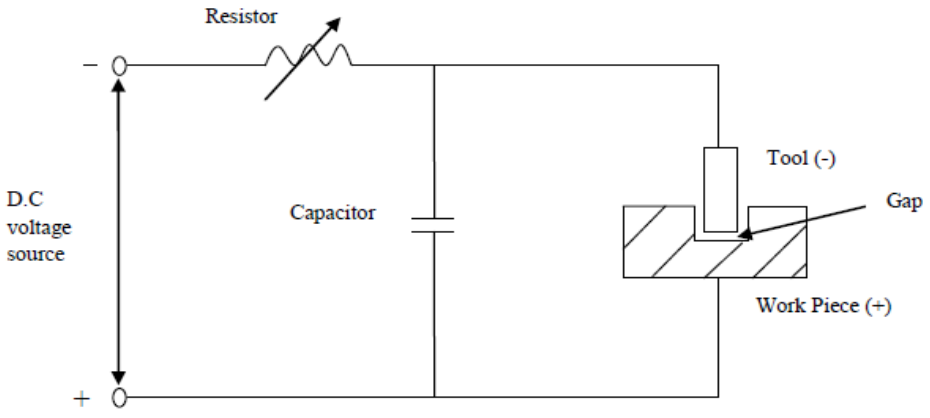

Figure 2.2 Schematic diagram of electric discharge machining using relaxation circuit

2.3 PERFORMANCE EVALUATION OF EDM ON MMCs

Pioneering research in this area has demonstrated the ability of electric discharge machining process [13]. The performance of EDM process is measured in term of material removal rate (MRR), tool wear rate (TWR), surface roughness (SR), which directly depends upon electrical parameters such as current, voltage, pulse-on/off time polarity etc., as well as non- electric parameters such as dielectric etc. Along with these responses, several authors have also reported on the surface integrity.

2.3.1 Material removal

Material removal mechanism

The rate of material removal is measured in terms of weight of material removed from the workpiece over a period of time. Several researchers have attempted to study the material removal mechanism and diffusion of elements between the electrodes i.e. tool and work piece. Mahdavinejad and Mahdavinejad [39] machined WC-Co composite EDM process. They reported that due to the difference in melting and evaporation points of basic elements in composite, cobalt matrix melts and evaporates before even melting of WC particles. The early removal of matrix phase of the composite material due to its lower melting point as compared to reinforced particle resulted in entrapment of particulates between the electrodes resulting in unstable machining (arcing). This agglomeration of particle in the matrix resulted in initiation of fatigue cracks [40-42]. The stock removal by EDM process of WC-Co composite were consistent with the results presented by Gadalla and Tasi [43] who also reported the formation of W_2C and WC_{1-x} on the machined surface. Seo et al. [34] investigated the machinability on 15-35 Vol% SiC/Al composite. It was reported that, under fine cutting conditions, the matrix material is not completely melted to detach the SiC particles. However, during rough machining (higher MRR), the melting of the matrix as well as decomposing of SiC particle in silicon was confirmed by EDX-ray analysis of surface. There was a complete absence of SiC particle in the heat affected zone (HAZ). However, Liu et al. [44] upon analysis of the debris in ED machining process observed that spalling was the major factors that contribute to metal removal mechanism in SiC/Al composite. Due to less thermal conductivity and brittleness, thermal spalling mechanism of metal removal is more prominent. This was also confirmed by the several researchers for various class of particulate reinforced composite [45-47].

Figure 2.3 represents schematic diagram for thermal spalling of SiC particles during EDM of composites. The machined surface of 65% SiC/A356.3 composite is shown in Figure 2.4 when machined using current (12 Amps), pulse-on time (45µs) and pulse-off time (45µs) and electrolytic copper as tool. The reinforced particle size was 50 microns (average).

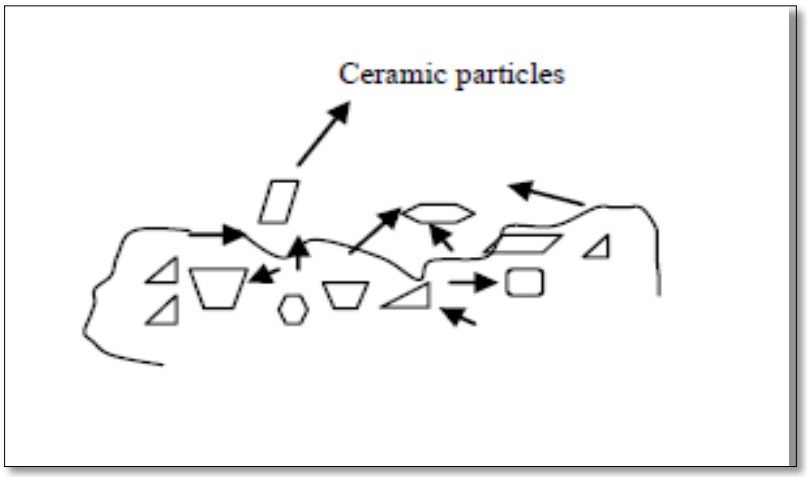

Figure 2.3 Schematic diagram shows the spalling mechanism due to conflict in coefficient of thermal expansion of composite materials

Ponappa et al. [48] studied the effect of EDM process parameters on drilled hole quality such as tapercity and surface finish. The work piece selected for the evaluation of EDM process parameters was Microwave-sintered magnesium nano composites (reinforced with 0.8 and 1.2 wt.% of nano alumina). They reported that pulse-on time and servo speed were the significant factor affecting hole accuracy and surface finish of the machined work piece.

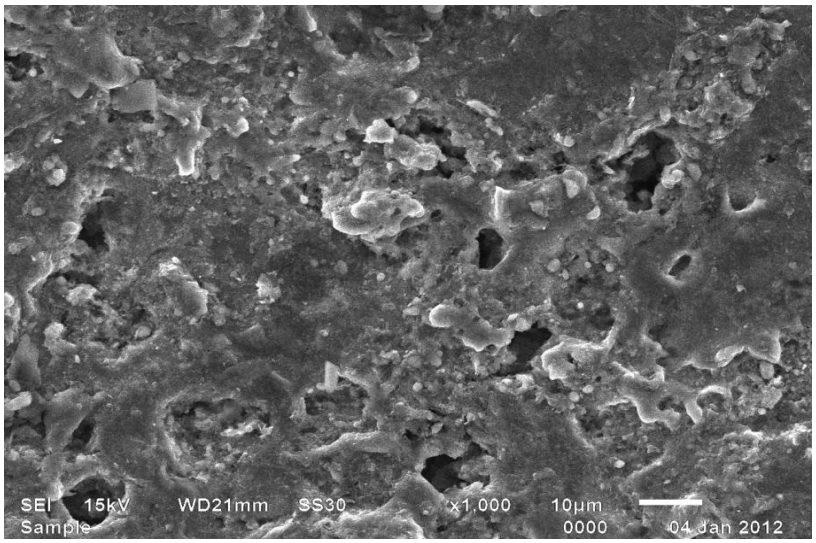

Figure 2.4 SEM micrograph of ED machined 65%SiC/A356.2 composite

Effect of EDM parameters on MRR

Singh et al. [35] conducted an experiment on machining of 10% SiC/Al and investigated the effect of current, pulse-on time and dielectric flushing pressure on MRR. It was found that current and pulse on time significantly affects the MRR. MRR increases at high spark energy but at the expense of tapercity, radial overcut and surface finish. It was further observed that the entrapment of SiC particle between the spark gap hinders the machining process which is in-line with the findings of Mahdavinejad and Mahdavinejad[39] and Hocheng et al. [49]. Hocheng et al. [49] also suggested larger current and shorter pulse-on time for effective EDM. The problem may be resolved with optimum setting of flushing pressure as higher flushing pressure hinders the ionized bridge between the electrodes which results in ignition delay and decrease in discharge energy. The study was further extended by Seo et al. [34], who conducted an experiment by increasing the reinforced SiC particle percentage content varying from 15-35 vol%. It was noted that increasing trend of MRR is a function of product of current and pulse-on time up to 100A and 500µs respectively (Figure 2.5), and then drops drastically due to loss of energy through conductive matrix material and is irrespective of SiC particles content. This was also observed by Tasi et al. [50], but the magnitude of MRR was greater for a higher percentage of SiC reinforced composite which directly effects the dimensional errors.

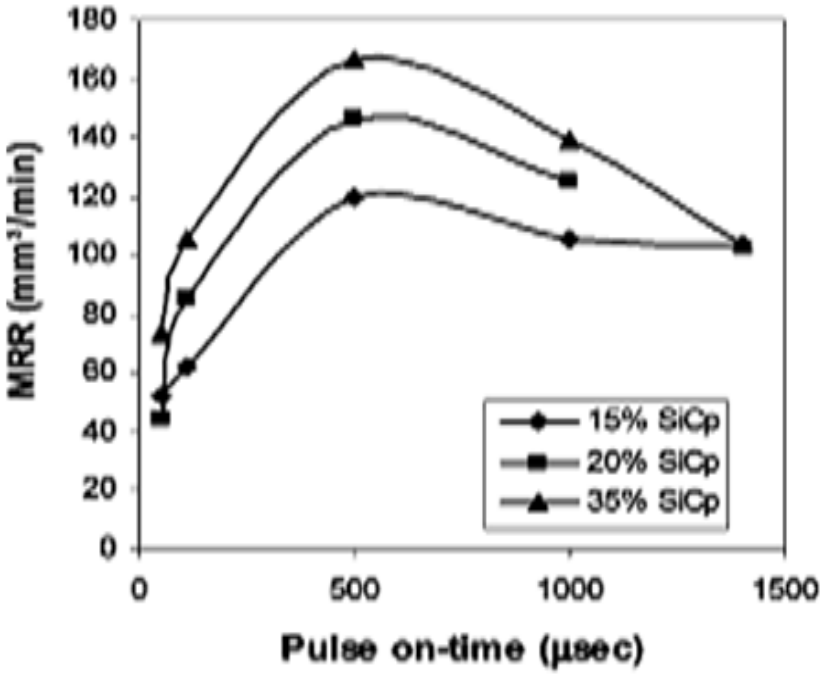

Figure 2.5 Variation of material removal rate and with current and pulse-on time [34]

Ahamed et al. [2] studied the effect of machining parameters on hybrid MMCs, namely Al-5%SiC-5% B_4C and Al-5%SiC-5% glass. The machining parameters were current, pulse-on time, pulse-off time and flushing pressure. The effect on responses were analyzed individually and reported an increase in MRR as the current, pulse-off time and flushing pressure increase but reduced with higher pulse-on time. In both types of hybrid composites, the magnitude of machining parameters also depended upon the wettability and density of reinforced particles.

Senthilkumar and Omprakash [51] tried EDM of Al-TiC_p with reinforced particle size of average 45μm and varying its percentage from 2.5% and 5%. The composite was prepared by using powder metallurgy. They concluded that MRR depends upon the ionized bridge intensity which increases as the current increases. The reinforced particles act as a shield to a composite and lower the intensity of bridged, but it can be eliminated by using proper flushing pressure to maintain the conductive path between the electrodes. Pulse-on time was directly proportion to the MRR up to a certain limit but greater pulse-on time formed larger craters thus hindering the conductive path between the electrodes which results in drop in MRR. Similar results were reported by Gopalakannan et al. [52] while ED-machining of Al7075-B_4C MMC.

Effect of EDM parameters on TWR

The tool wear rate was usually measured in terms of material removed per unit time. The mechanism is quiet similar to MRR, as a tool and workpiece act as electrodes to generate sparks in EDM process. The amount of material eroded from both the electrodes depends upon the contribution of electrons and ions generated during the process.

Singh et al. [35] concluded that while machining Al-10%SiC composite, TWR was directly proportional to pulse-on time and current. Ko-Ta-Chiang [53] argued that influence of current has a direct effect on TWR but pulse-on time has an inverse effect on TWR. The claim quoted was supported by other researchers [55, 55] who reported that TWR increases with increase in current magnitude as it plays the major role in magnifying the discharge energy between the electrodes. On the other hand, prolonged pulse energy declines the energy density by enlarging the discharge diameter [45].

The accuracy of machining is measured in terms of replica of tool produced in a workpiece. This can be achieved by reducing tool wear rate close to zero. Various methods were proposed by the researchers to diminish TWR, and one such method was rotary tube electrode. This method was adopted for machining of Al-SiC MMC and

shown reduction in TWR due to effective flushing conditions [55, 56]. Jeswani [17] proposed that addition of conductive power in dielectric significantly affects the EDM process due to the reduction of the insulating strength of dielectric by the formation of bridging effect between the electrodes. The method is classified as powder mixed EDM (PMEDM) and also termed as additive EDM. Number of researchers has investigated the effect of addition of different types of powder and varying their concentration in the dielectric [57].

The commonly used copper and graphite electrodes in EDM process have low wear resistance which results in high probability of inaccurate machining. The high tool wear constraint in the process was overcome by using the tool material having higher electric, thermal, wear resistance and easy fabricability. Mostly tool material fabricated was done by powder metallurgy, infiltration technique or liquid phase sintering [58-60]. Norasetthekul et al. [38] developed ZrB_2-Cu electrode by infiltration technique proved to be higher wear resistance as compared to Cu and graphite electrode. Khanra et al. [61] evaluated the performance ZrB_2-Cu composite electrode by varying the composition of both the elements. They observed that MRR increases rapidly when the %wt of Cu in the electrode increases from 20-40% and thereafter it was observed to be decreased. The rapid increasing trend of TWR was observed for 30-40%wt. of Cu thereafter slow increase in tool wear was observed. Hence they concluded that the tool performed best when the composition of elements in the electrode was ZrB_2-40%wt. Cu. This class of the tool was also used to enhance the machined surface due to metal transfer during the machining process, and the process is also known as electric discharge alloying (EDA). Tasi et al. [62] evaluated the performance of Cu/Cr-based composite tool electrodes. They concluded that tool wear was observed to be lesser and also the surface modification of the work piece due the transferred Cr element from the tool electrode results in good corrosion resistance property. Bai et al. [63, 64] presented the alloying technique by using green-compact Al-Mo composite electrode.

2.3.2 Modeling of EDM process

For commercializing the EDM process, the prediction of response parameters with respect to the input parameter must be correlated during machining. Karthikeyan et al. [65] attempted to develop a mathematical model for EDM of SiC particulate (25μm size) reinforced LM aluminium matrix composite and correlated the response factors such as MRR, TWR and SR to current, pulse-on time and the percentage of SiC reinforced particulate. They concluded that MRR decreases as the percentage of SiC and pulse-on

time increase whereas TWR and SR increases as the current and percentage SiC increases. The proposed model was validated with experimental results within the operating limits. Dhar et al. [66] used MATLAB software to develop quadratic (second order) mathematical model to relate response and process parameters of EDM while machining cast Al-4Cu-6Si alloy reinforced with 10% SiC particulate. They concluded that MRR, TWR, radial overcut increases significantly with current but gap voltage was found to contribute little in effecting the response parameters.

Gopalakannan et al. [52] presented a mathematical model for EDM process using response surface methodology for the machining of Al 7075-B_4C MMC. They proposed the quadratic model for the response variable such as MRR, TWR, SR.

Sidhu et al. [67] presented the Lexicographic Goal Programming (LGP) method for optimization of EDM process parameters while machining Al-10%Al_2O_3 MMC with copper as a tool electrode. The methodology adopted for the application of Lexicographic technique is discussed as in the next section.

Development of a mathematical model, to relate the machining parameter with response factor is very difficult due to its complexity and nonlinearity in the EDM process. The literature is rich with the use of various artificial neural network (ANN) models of suitable architecture to predict most accurate response factors by organizing effectively qualitative and quantitative factors. In manufacturing the most popular ANN model is multilayered perception (MLP) networks, for example, Lee et al. [68], Ozcelik et al. [69], Spedding and Wang [70], Nabil and Ridha [71] used feed forward back propagation to predict the surface roughness in various machining processes. Katz and Naude [72], Indurkhya and Rajurkar [73], Panda and Bhoi [74] applied various neural networks for the prediction of machining parameter in EDM. Mediliyegedara et al. [75] used a feed forward neural network to classify the wave form generated from electrolyte incorporated modified EDM.

But still research work related to developing a model of ED machined particulate reinforced MMCs by using ANN technique has not been seen in the literature. For making this process commercially viable for MMCs, the prediction of induced residual stresses at various settings of input parameter is very important so that these could be controlled to improve the service life of the components. Developing a reliable mathematical model relating the machining parameters with residual stresses is very difficult due to complexities involved and also the nonlinearity of the EDM process.

However, many researchers have reported use of various neural network models to predict some responses accurately by effectively organizing the qualitative and quantitative factors. The foundation for the growth of neural network architecture was started from 1943. The models were further modified with the construction of electronic discrete variable automatic computer [115]. Currently the most widely used Artificial Neural Network (ANN) is multilayer perceptions based on back propagation techniques. The technique was employed for controlling and modeling various selected parameters. For example, in many studies feed forward back propagation neural networks were adopted to predict the surface roughness in machining processes [68-71]. Similarly, back propagation neural network control was used to predict tool wear and the resultant failures in drilling and turning operation [116-118].Various neural networks techniques have been used for prediction of responses during EDM [72-74]. Feed forward neural network with back propagation learning algorithm has been used to estimate of height of the workpiece online and distinguish the machining condition in wire EDM [119].

A process control system consisting of a fuzzy gap-width controller adapted by neural network was introduced [120]. Experiments were conducted to develop a model of EDM using back propagation neural network with current, pulse-on time and pulse-off time as an input parameter for predicting the metal removal rate (MRR) and tool wear rate (TWR) [121]. A neural network was developed to study the steel transformation curve. [122]. Feed forward neural network was used to classify the wave form generated from electrolyte incorporated modified EDM [75]. Taguchi's L_{18} orthogonal array was used to conduct experiments on explosive electric discharge grinding. The results were analyzed using genetic algorithm developed using neural network for optimization of the results [123]. In another study, Taguchi's L_{27} orthogonal array was used to present feed forward neural network based on back propagation along with a regression model to predict the surface roughness in abrasive jet machining process [124]. The artificial neural networks (ANNs) were applied successfully during machining and can accurately predict the responses during EDM [125-129].

The literature review shows that ANN is a powerful tool to develop models particularly in manufacturing applications to predict, generalize and analyze non-linear multivariate data. Also, no study has been reported that applies ANNs to predict the induced residual stresses in particulate reinforced metal matrix composites during EDM.

2.4 EDM SURFACE INTEGRITY

Due to thermal nature of process, machining leaves many types of surface defects, which results in reduction of service life of the finished product. Therefore, it is essential to optimize the EDM parameters for better surface integrity. The surface integrity of Electric discharged machined (EDMed) surface deals with two factor i.e. surface topography and surface metallurgy (Change in layer due to heat or elements migrations). The surface quality of machined surface is underpinned by increasingly sophisticated equipments such as X-ray diffraction or microscopic techniques.

The examination of machined surface layer reveals that the change not only occurs on the surface of component but also effect the property of component at subsurface [76]. Machined surface consists of three distinctive layers recast layer, heat effected zone (HAZ) and converted layer. The recast layer on the work piece is created due to deposition of molten metal on the machined surface due to insufficient flushing. This recast layer also consist of a small amount of metal transferred from the tool electrodes or dielectric medium. The layer next to recast layer that changes the metallurgy and determine the life of the component is HAZ. Due to rapid high temperature melting and cooling process, subsurface defects such as cracks, spalling, porosity, residual stresses, metallurgical transformation are responsible for this zone [2]. The last layer is the conversion layer or annealed layer, which was characterized by change in grain structure.

Muller et al. [77] carried out machining on AA2618 20%SiCand A356-35%SiC with copper electrode in the presence of paraffin oil as a dielectric. It was observed that the crater size or surface roughness depends upon the energy used in discharge energy, which is a function of current and pulse-on time. The results were not in agreement with the finding of Hung et al. [78] as they reported that current is the only dominating factor that effects the surface roughness.

The deposition of molten metal and formation of gas bubbles during the process causes porosity and voids. The presence of reinforced particles decreases the removal efficiency and also the reinforced ceramic do not melt during the machining. Hence this is a more viscous operation which results in thicker recast layer as compared to un-reinforced material. It was also observed that the reinforced particles were flushed away or deposited below the recast layer with the melted portion of matrix at higher rating of discharge energy [35, 51, 79, 80].

2.5 RESIDUAL STRESSES

Among the various defect generated during electro discharge machining, residual stress which is generated due to uneven solidification of molten metal is the most significant defect that leads to failure especially under tensile loading or may cause corrosion [81, 82]. When the induced residual stresses exceeds the ultimate strength of material the failure was appeared in the form of cracks [83].

A frequent collapse of bridges and heavy structures in March 1938 in Belgium attracted attention of designer towards a factor called residual stresses, which is induced during processing. The collapse was mainly due to residual stresses generated due to the welding process, resulting in generation of cracks which get eventually extended into the base metal, causing failures [84]. The same type of thermal stresses was reported during EDM process.

Many electric and non-electric parameters such as pulse durations, peak current, voltage, polarity, material properties of electrodes (workpiece and tool) and dielectric affects the surface integrity.

Surface integrity plays a vital role in indicating the early failure of structure and researcher are mostly focusing in the area of non-destructive testing methods. The most popular non destructive testing methods are X-ray diffraction technique (Penetration in the matrix is < 50μm (Al), <5 μm (Ti) and resolution is 1mm in a plane and 20 μm vertically), Neutron diffraction (penetration 200mm (Al), 4mm (Ti) resolution 500 μm) Ultrasonic technique (Penetration>10cm and resolution 5mm), Eddy current technique, Active magnetic technique and Passive magnetic (Penetration 10mm and resolution 1mm) techniques.

Withers et al. [85] presented the overview of residual stress effect on fatigue life and surface integrity and covered the recent advancement in measuring methods (Figure 2.6). Till date, no significant attempt has been reported that evaluates the residual stresses in ED machined MMCs. In the literature, contribution of researchers for the evaluation of residual stresses induced in steels during EDM process was reported. These contributions may be used in ED machined MMCs to estimate the service life of composite materials.

Earlier Crookall [86] attempted to measure residual stresses in tool steel and inspected the formation of white layer due the deposition of elements of dielectric and tool electrode. They evaluated the residual stresses by using bending deflection method and concluded that the residual stresses are tensile in nature and maximum value below the machined

surface. The magnitude and depth of residual stresses varies with discharge energy. The finding was also confirmed by, Lloyd et al. [87], Barash et al. [88], Konig et al. [89].

Mamalis et al. [90] adopted X-ray diffraction technique to determine the residual stresses in ED machined steel. They found that peak residual stress was at the subsurface layer and independent of discharge energy. They pointed out that the depth of maximum surface is a function of discharge energy and approaches to the ultimate strength thus intensifying the surface crack network. Rebelo et al. [91] used the same technique to measure residual stress in steel and found the same pattern of responses. Ghanem et al. [92] studied the effect of EDM process on two hardened and non hardened steel. They measured residual stress by X-diffraction and reported that the profile of residual stress for harden steel depends on the quenching condition of the steel. The scanning electron micrograph shows an increase in crack density on the surface depending on the hardenability of material. They also proposed a finite element based model to predict the residual stress induced during machining.

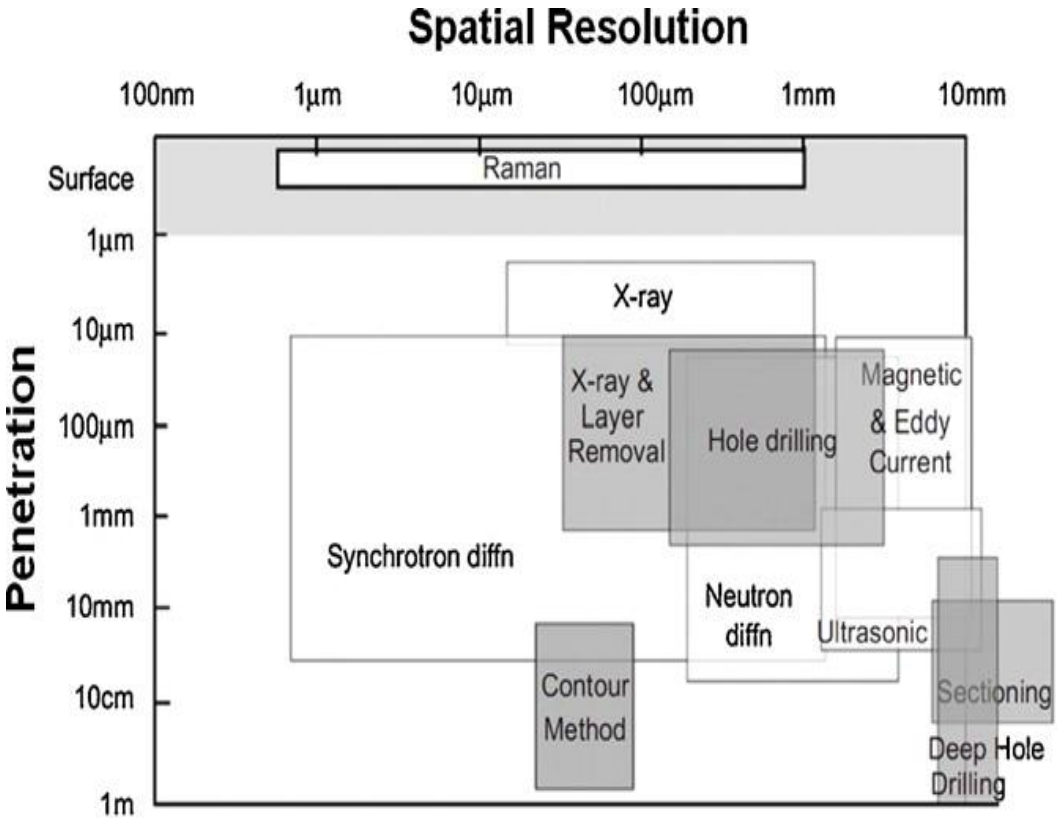

Figure 2.6 Methods and capabilities of various residual stress measuring techniques[85]

During EDM, it was found that peak tensile residual stress was present in the subsurface layer and approaches to the ultimate strength of the workpiece which causes cracks. This results in relaxation of residual stress and gives way to small compressive residual stress in the core of material [92, 93].

The nondestructive X-ray diffraction technique was chosen by Ekmekci [94] to study the effect of dielectric (kerosene and de-ionized water) and the electrodes (copper and graphite) on residual stress and retained austenite. They found that surface non-homogeneity contributes more for residual stress and micro-crack distribution as compared to phase transformation. Ll et al. [95] revealed that not only discharge current and pulse-on time affects the surface residual stress but pulse-off time also plays the significant role.

Ekmekci et al. [96] presented the residual stress profile as a function of depth of machined steel surface while machining in the presence of de-ionized water as a dielectric. The electrochemical machining process was used to remove thin layers form the workpiece, and the corresponding deformation was reported. The parametric study demonstrated the state of stress and was presented with a semi-empirical model. They found that the residual stress pattern remains unchanged with the process parameters and related this pattern with thermal properties of the workpiece and the dielectric medium. Various attempts were made to present the model to predict the residual stress induced in EDM process. Das et al. [97] simulated the EDM process for predicting residuals stress by using commercially available finite element solver DEFORM. Biswas et al. [98] chose ANSYS software to model EDM process to evaluate the residual stress. The recent advances to map the residual stress were highlighted by Wither et al. [99]. Recently, Jawahir et al. [100] compared various conventional and non-conventional material removal processes for the surface integrity. The majority of work to estimate residual stress reported till date is on ferrous/non-ferrous material. Now, with the potential application of composite materials in industries, researchers have started to focus on service life of machined and un-machined composite material. Broadly, composite materials are a result of judicious selection of two or more distinct materials leading to a synergetic improvement in properties when combined together. Due to the difference in the coefficient of thermal expansion between the constituent of MMCs it leads to thermal residual stress which affects the service life of the work piece.

Sun et al. [101] reported that the residual stress induced in SiC-Al MMC is hydrostatic in nature. They found that the residual stress in aluminium matrix was tensile in nature

whereas compressive in reinforced SiC particles. The magnitude of residual stresses may be reduced by under cooling the composite in nitrogen and again heating to a room temperature. Various models to estimate the residual strain (stresses) of SiC reinforced MMC's were proposed [102,103].

In case of composite materials, the crack propagation and nucleation, plastic deformation usually takes place near the interface of constituents, that is, near reinforced particles and the matrix material [104].

Cheng et al. [105] used diffractometer with 30μm resolving power to investigate the residual stresses in Al-MMC. They found that hoop and radial residual stress in the matrix and at the interface of constituent was tensile and compressive respectively. They also concluded that the maximum residual stress was observed at the interface and it decreases as distance from the interface increases. The maximum residual stress also depended upon the size, density and coefficient of thermal expansion of reinforced constituent [106, 107].

The introduction of MMCs in the manufacturing industry has been a viable option in producing low density, high coefficient of thermal expansion, and high stiffness components at economic cost.

The specific properties of composite depend upon their components properties (matrix and reinforced particles), their distribution, orientation, reactivity crystallographic texture, wettability and the process used in the fabrication. There are a number of matrix materials and reinforced particles listed to form composite, depending upon the area of their application. But due to high ductility and low melting point of aluminium, it is widely accepted matrix material for composites, hence most of published work belongs aluminium matrix material reinforced with SiC particulates.

After an elaborate scrutiny of the published work, the following gaps have been observed:

No research work on ED machining of 65vol%SiC/A356.2; 10vol% SiC-5vol% quartz/Al and 30vol%SiC/A359 has been done.

- Though MMCs has been used as a work material by some researchers, no study has been made to measure residual stresses induced after machining.
- Most of the available research work on powder-mixed dielectric reports the impact of machining on material removal rate, surface roughness and tool wear

rate. The emphases on surface modification and residual stresses, using copper, graphite and copper- graphite electrodes have not been addressed.

- No work has been reported on the use of copper and graphite powders in the dielectric medium to machine MMCs.
- The effect of discharge current and pulse-on time has been taken into consideration in various research works, but variation in pulse-off time has not been investigated. There is a need to study the effect of this important input process parameter to study the phenomena of residual stresses for MMCs.
- The artificial neural network modeling has not been used to estimate the induced residual stresses.
- Multiple goal decision criteria tools have not been applied for globally optimization of EDM process response parameters in MMCs.

CHAPTER - 3
DESIGN OF STUDY

Several factors that affect the machining performance in EDM process which is measured in terms of material removal rate (MRR), tool wear rate (TWR), surface roughness (SR), micro-hardness, residual stresses and surface integrity in this study.
These factors or input process parameters can be classified as follows:

1. Electrical parameters: Current, pulse-on time, pulse-off time, supply voltage, electrode gap, polarity.
2. Non-electrical parameters: Flushing pressure, jump time, electrode rotation, tool rotation, material type (work piece/ tool electrode).
3. Dielectric medium. The property of dielectric medium depends upon the insulating strength which may be altered by the suspended powder concentration, size and type.

The effect of each of these parameters on EDM process in general, and on the phenomenon of material removal and surface integrity in particular, has been discussed in detail in Chapter 2 on literature review. It is also known from previous research work that out of the above listed factors, parameters that directly affect the phenomenon of material removal (work piece and tool electrode) and surface integrity (residual stresses, surface roughness, micro-hardness, recast layer) in electrical discharge machining are:

1. Work piece material
2. Tool material
3. Pulse-on time
4. Pulse-off time
5. Current
6. Dielectric medium

These parameters have been investigated thoroughly in this research work. The levels of all these parameters could be easily changed from the control panel switches on the EDM machines that are currently being used by the tool and die making industry. The range of these process parameters for this experimental work was decided on the basis of the results of pilot experimentation conducted by ‘varying-one-parameter at a time’ approach i.e. accesses the influence of specific parameters on the machining characteristics of interest.

The work material used in the experimentation was particulate reinforced metal matrix composite. One set of experimentation was conducted on MMC reinforced with 10% Al_2O_3 composite (Particle size 50 microns) prepared by stir casting technique. In this method, steel mold of rectangular shape was used to prepare the specimen.

The parameters were selected in such a way so that a higher material removal rate is realized and were tested for both polarities (straight and reverse polarity). In second and third set of experimental study, various MMCs reinforced by SiC particulates of different particle size were selected for parametric comparison of machining characteristics such as residual stresses, micro-hardness, recast layer, MRR, TWR, SR.

3.1 PILOT EXPERIMENTATION

3.1.1 Selection of parameters for Stage I experimental plan.

During the experimentation study conducted in Stage I, the response variables selected were MRR, TWR and SR. Several literature based on these responses in EDM is available for various types of alloys/composites. From the literature, the most influencing factors effecting the above responses were current and pulse-on time, which usually defines the spark energy of the plasma generated between the electrodes. The maximum recommended value for the current and pulse-on time for this setup of experimentation was 16Amps and 50μs, beyond which the machining became unstable. The higher values of pulse-off time were chosen (as permissible in the manual for a particular setting of pulse-on time) with the aim of providing adequate cooling time to the recast material. Moreover, low pulse-off time results in unstable machining and may cause arcing. Machining below 8Amps and 10μs showed very less change in machining characteristics. The 3-levels for both input parameters for effective machining were selected and are given as below:

Current (Amp): 8, 12, 16.

Pulse-on time (μs): 10, 30 50

Since only two factors were studied, a full factorial design was chosen with nine trials conditions for two factors varied at three levels each. The experimental plan is shown in the first section of Chapter 4.

3.1.2 Selection of parameters for Stage II and Stage III.

The work material selected for the pilot experimentation was high density particulate reinforced MMC. As dense reinforced MMCs causes arcing due to entrapment of particle between the electrodes [48]; thus a 65vol%SiC/A356.2 was used as the work material for pilot experimentation to identify the process parameters settings. The effect of variation in peak current, pulse-on time and pulse-off time was studied on three response characteristics. The work material was supplied by Ceramic Process System (CPS), 111 South Worcester Street, Norton, MA, USA. The values of the input process parameters taken from the operation manual of EDM machine [121] for pilot experimentation are as under:

Peak Current	:	4, 6, 8, 12 and 16 Amp
Pulse-on time	:	5, 10, 30, 50 and 75 µs
Pulse-off time	:	15, 30, 45, 60 and 75 µs

The response variable for this investigation was selected as MRR, TWR, SR, residual stresses and micro-hardness. The functional characteristics (residual stresses or surface integrity) of the machined component are more important than the efficient machining objective (MRR, TWR). Hence responses such as residual stresses and the surface integrity (micro-hardness and SR) were the most important factors which determine the quality of the machined component for service. Having established the relevance of low discharge current and low pulse duration on the phenomenon of surface integrity through literature review, the actual impact of these parameters and their ranges was investigated through pilot experimentation. The impact of variation in pulse-off time as an independent parameter (it has been used as part of duty cycle along with pulse-on time) was missing in the available literature and this was further explored. Though the two response characteristics selected for the experimentation were residual stresses and micro-hardness (component functional characteristics); a third characteristic, namely electrode wear (efficient machining objective), was also studied as part of the pilot experimentation.

Effect on residual stresses

The graphs showing the effects of variation of current, pulse-on time and pulse-off time on residual stresses for three electrode materials are given in Figure 3.1 to 3.3.

The variation is as follows:

Factors	***Machining condition***	***Machining condition***	***Machining condition***
Current (Amp)	Variable factor	4	4
Pulse-on time (μs)	30	Variable factor	30
Pulse-off time (μs)	45	45	Variable factor

It was found during machining that the current and pulse-on time setting of 16 Amp and 75μs respectively resulted in unstable machining conditions causing arcing. It could be due to the entrapment of SiC particle between the gap of electrodes and inadequate flushing mechanism of the spark gap. Hence, these values of current and pulse-on time were eliminated and experimentation was carried out with the remaining four values. It was also observed during experimentation that stable and continuous machining took place at higher values of pulse- off time. The dielectric medium used in these experiments was EDM oil (Dielectric strength: 40 KV min, Appearance: Bright and clear) supplied by the OSCARMAX, EDM Company.

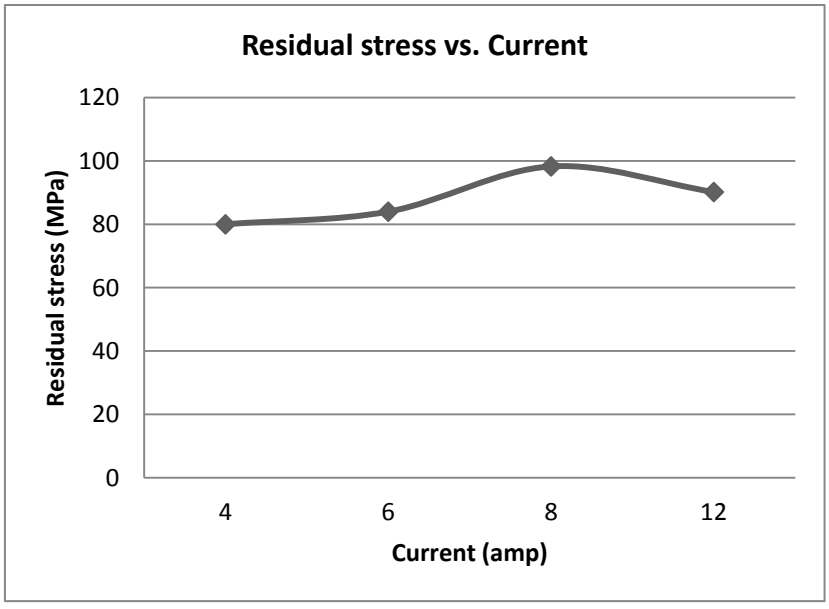

Figure 3.1 Residual stresses vs. Current using copper electrode

The current was varied of four levels (Range 4 to12Amp) as with current less than 4Amp the machining efficiency was unusually low (low MRR) which is not desirable. The experiment was conducted with pulse-on and pulse-off time treated as constant factors. The results are shown in Figure 3.1

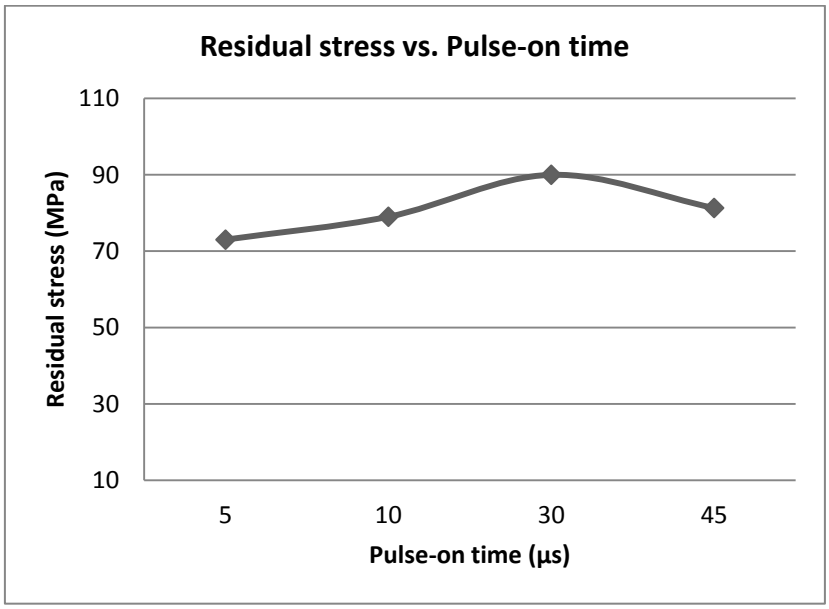

Figure 3.2 Residual stresses vs. Pulse-on time using copper electrode

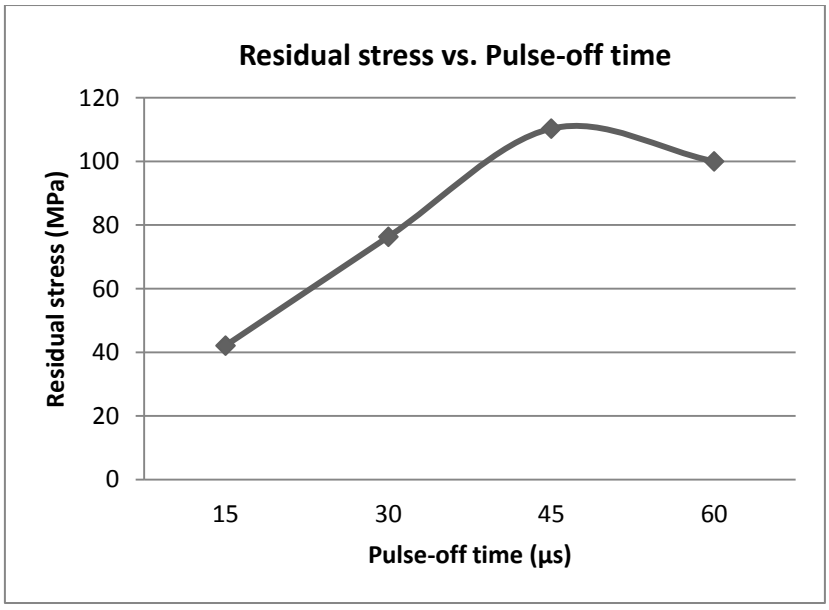

Figure 3.3 Residual stresses vs. Pulse-off time using copper electrode

For the second set of pilot experimentation the current and pulse-off time was kept constant while the pulse-on time levels was varied from 5µs to 45µs. The entire experimentation was conducted in the similar manner as in the previous set. The output variables (residual stresses) were plotted as shown in Figure 3.2. Similarly, the residual stresses were recorded with the variation in the pulse-off (range 15µs to 60µs) as shown in Figure 3.3. It can be seen from the plots that maximum variation in residual stresses takes place with an increase in the magnitude of pulse-off time up to 45µs. It was

observed that the residual stresses decreases beyond this setting. This was due the formation of cracks on the machined surface which results in stress relaxation. Moreover, a change in residual stress was minimum at low values of pulse-on time and a steady increase was observed as process setting on EDM was raised. This is due to increased spark energy between the electrodes. But a marginal decrease in residual stresses at higher values of current and pulse-on time was seen.

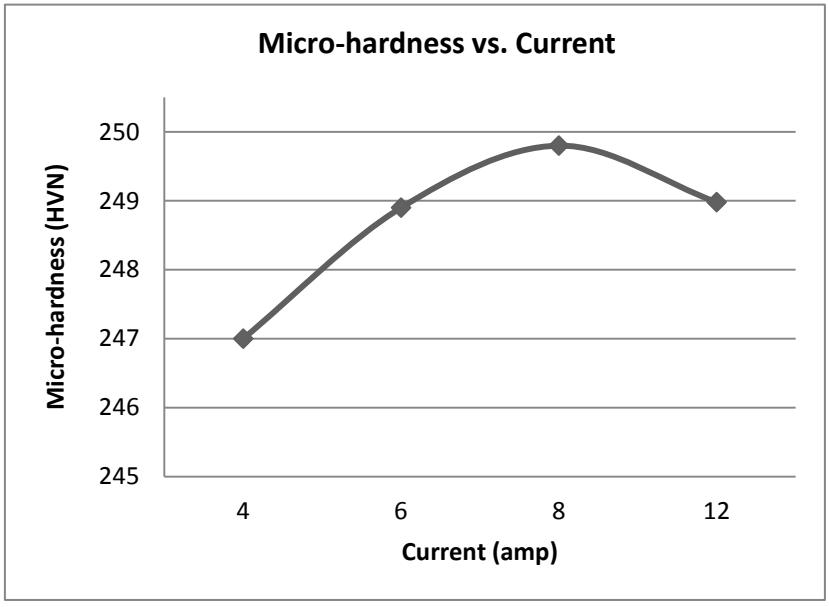

Figure 3.4 Micro-hardness vs. Current using copper electrode

The best value of micro-hardness was achieved at the peak current of 8Amp which is due to the transfer of electrode material or formation of compound on the work piece surface (Figure 3.4).

It was reported in the literature, during EDM, improvement in micro-hardness is achieved by the combined effect of material transfer and hardening due to the heating and quenching cycle. While hardening is more at higher values of peak current, it can be inferred that the maximum impact of material transfer takes place at 4Amp peak current.

The XRD analysis revealed that along with copper compound with aluminium the formation of silicon oxide is prominent in contributing to the increased micro-hardness. The micro-hardness reported when pulse-on time was set at 5µs was lowest as compared to range from 10µs to 45µs. The maximum micro-hardness was achieved between 10 to 30µs pulse-on time (Figure 3.5).

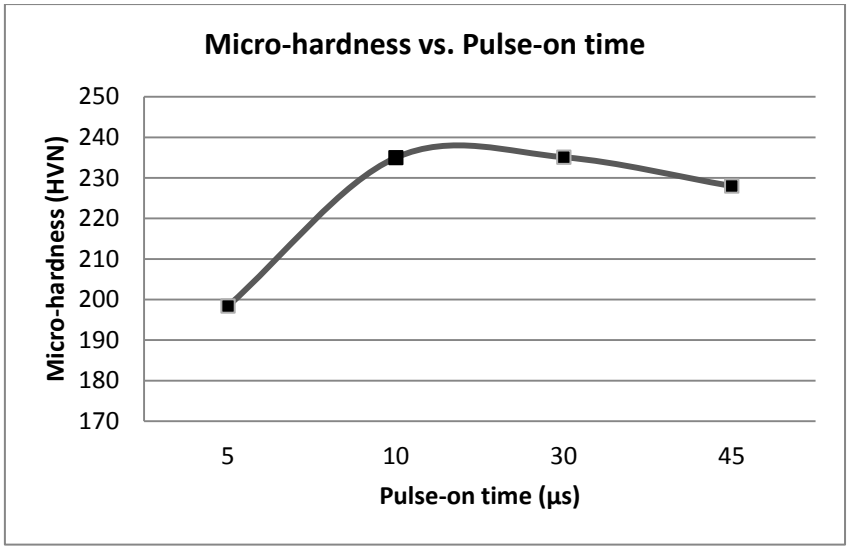

Figure 3.5 Micro-hardness vs. Pulse-on time using copper electrode

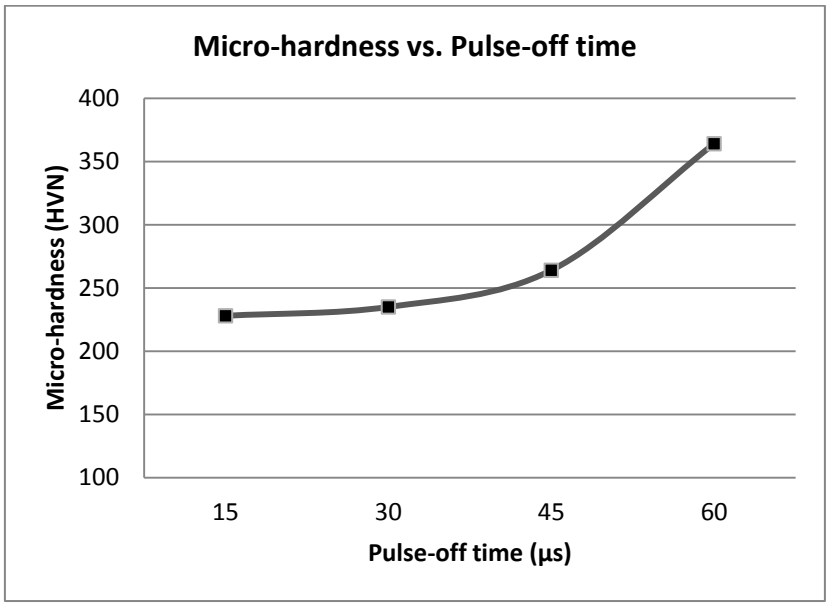

Figure 3.6 Micro-hardness vs. Pulse-off time using copper electrode

It was observed from the plots that there is a steady increase in micro-hardness with an increase in pulse-off time (Figure 3.6). It is expected because more pulse-off time results in increase in solidification process time of molten material and phase transformation under rapid cooling condition.

The highest micro-hardness (Figure 3.6) was reported at the highest pulse-off time situation i.e. 60µs, but on microscopic examination, the formation of cracks on the

machined surface was observed (defective part). Hence it was eliminated from the experimental plan.

It has been reported in many research papers that low values of current and pulse-on time causes a low intensity of spark which results in a smoother surface and lesser TWR. Surface roughness showed a marked improvement with an increase in pulse-off time, which may be due to adequate flushing and sufficient deionization of the dielectric at high pulse-off time.

Selection of Input Process Parameters for Stage II of experimentation

Based on the observations made during pilot experimentation conducted by varying-one parameter at a time, it was concluded that there is a large scope of exploring the machining characteristics of particulate reinforced aluminium matrix composite by using the different process parameters concluded from pilot experiment. As an outcome of the pilot study, four machine parameters namely (1) Current (2) Pulse-on time (3) Pulse-off time and (4) Type of dielectric were identified for detailed study using Taguchi's experimental design methodology. Also, three different types of Metal Matrix Composite (MMC) materials and three combinations of electrode materials were used during the experimental study. Maximum level for current was set at 12Amp as beyond this level arcing was caused on the workpiece. Similarly, the lower most level was used at which adequate material removal took place during machining and was thus set at 4Amp. A third level representing the middle setting as 8Amp was used to provide a clearer picture on the effect of current to emerge. Similarly, the pulse-on time and pulse-off time were selected and on the basis of control panel settings available on the machine. Also, three combinations of dielectric namely (1) Commercial grade EDM oil which represents conventional EDM; (2) EDM oil mixed with copper powder; and (3) EDM oil mixed with graphite powder were used. The last two levels represented powder mixed electric discharge machining (PMEDM) process used to measure their effect on the residual stresses in MMC materials. The following issues have been taken up during the research work in Stage II:

1. Material removal rate (MRR) of MMCs (65vol%SiC/A356.2 and 10vol%SiC-5vol% quartz/Al) was explored during Electric discharge machining process with the following tool material: Electrolytic copper, Fine grained graphite and Copper-graphite composite.

2. Surface roughness (SR) of a foresaid work materials has been explored with variant tool material.
3. The effect of dielectric medium has been investigated. Dielectric medium selected were: EDM oil (supplied by the company); Suspended copper particles mixed EDM oil; Suspended graphite powder mixed EDM oil.
4. Relationship between different machining characteristics (Current, pulse-on time, pulse-off time and dielectric medium) and the machining characteristics (MRR, SR, residual stresses) was established.
5. The residual stresses induced on the machined surface were investigated and further it was modeled to predict the magnitude of residual stress under different machining conditions.

Considering the objective, the levels of chosen factors were decided, keeping in view the machine tool capability and experimental limitation. To conduct the experiments it is usually unnecessary to run all possible combinations of factor levels. A fractional factorial experiments in which only a subset of runs were made for concluding the results. Based on the pilot experimentation, Table 3.1 details the different process parameter (Control variables) and their levels used during the experimentation.

Taguchi's methodology was used to plan experimental trials. Before finalizing, a particular orthogonal array for the purpose of designing the experiments a number of parameters and their level of interest must be established [108, 112]. In the present study, six different process parameters were used, as already listed. The workpiece materials had two levels whereas all other parameters had three levels each.

Table3.1 Factors of interest and their levels

Factors	**levels**	**Levels**		
		Level – 1	**Level – 2**	**Level– 3**
Work piece	2	65vol%SiC/A356.2	10vol%SiC-5vol% quartz/Al	-----
Electrode Type	3	Copper	Graphite	Copper-Graphite composite
Current	3	4 amp	8 amp	12 amp
Pulse-on	3	10μs	30 μs	45 μs
Pulse-off	3	15 μs	30 μs	45 μs
Dielectric	3	EDM oil	EDM oil mixed with Copper Powder	EDM oil mixed with Graphite powder

Since the factors chosen for the study were a combination of two and three levels, a mixed experimental design (L_{18}) developed by Taguchi was used for this study. L_{18} denote 18 different trial conditions which were conducted randomly to eliminate any undesirable bias in the study. The L_{18} is designed in a way that it accommodates the two-level factor in column 1 and the remaining three levels factors are assigned to other columns. As can be seen from this design matrix [108], the first column represents the types of work piece materials used in the study. Thus, the first nine trials represents 65vol% SiC/A356.2 MMC hereafter represented as Sample I and the remaining nine trials (Trial 10 to 18) represent results for 10vol% SiC-5 vol% quartz in aluminium, hereafter referred to as Sample II. The second column was used for electrodes (Cu, Gr, Cu-Gr); third column was assigned for pulse-on time; column 5, 6 and 7 was assigned for dielectric medium, current, pulse-on time respectively. Each run was conducted at random. The final control log for experimentation is represented in Table 4.7 (S*ection 4.3.3)*. Hence eighteen rows of L_{18} orthogonal array represents the eighteen experiments to be conducted during the experimentation (Appendix A, Table A.1). Thus, experiments number 1 has to be conducted at level 1 for each of the six process parameters. The remaining experiments are conducted according to the allocation of process parameters levels. The detail of these response variables are given in Table 3.2

Table 3.2 Response variables

Response	Response 1	Response 2	Response 3
Response Name	MRR	SR	Residual stresses
Response Unit	mg/min	µm	MPa

Selection of Input Process Parameters for Stage III

In experimental Stage III, the machining characteristics of particulate reinforced MMCs were explored by adding a composite in the experimental plan. The composite 30vol% SiC/ A359 was procured from MC-21, Inc., USA.

The following issues were taken up during the research work in Stage III;

1. Material removal rate (MRR) of three variants of MMCs namely 65vol%SiC/A356.2, 10vol%SiC-5vol% quartz/Al and 30vol% SiC/A359 was explored in this stage with following tool materials: electrolytic copper, fine grained graphite, copper-graphite composite.

2. Tool wear rate (TWR) and surface roughness (SR) of aforesaid combination of process parameters was explored.
3. The residual stresses induced on the machined surface of selected MMCs were investigated under different machining conditions.
4. Surface integrity was determined by observing the surface morphology, recast layer thickness and micro-hardness for the given MMCs.

The factors varied during the experimentation were the work piece material, electrode material, current, pulse-on time, pulse-off time and the dielectric medium. Each of these factors was varied at three levels as shown in Table 3.3.

Considering the linear graph of L_{27} orthogonal array, work piece was assigned to column 1 of the array; Electrodes: column 2; Current: column 12 ; Pulse-on time: column 13; Pulse-off time: column 5 and finally the dielectric medium was allocated to column 10 of the array. Left out columns were unassigned for further exploration of process parameters. Table 3.3 details the different control variables and their levels.

Table 3.3 Factors of interest and their levels

Factors	**Levels**	**Levels**		
		Level – 1	**Level – 2**	**Level– 3**
Work piece	3	65vol%SiC/A356.2	10vol%SiC-5vol% quartz/Al	**30vol%SiC/A359**
Electrode Type	3	Copper	Graphite	Copper-Graphite composite
Current	3	4 amp	8 amp	12 amp
Pulse-on	3	10µs	30 µs	45 µs
Pulse-off	3	15 µs	30 µs	45 µs
Dielectric	3	EDM oil	EDM oil mixed with Copper Powder	EDM oil mixed with Graphite powder

The final control log for the experimentation is shown in Table 4.24 (*Section-4.4*). The six response parameters studied are given as under:

(1) Response Name : Material removal rate,
Response Type : Higher-the better
Units : mg/min

(2) Response Name : Tool wear rate, Surface roughness
Response Type : Lower-the better
Units : mg/min (TWR), R_a value in microns (SR)

(3)	Response Name	:	Residual stresses
	Response Type	:	Lower-the better
	Units	:	MPa (Mega-Pascal)
(4)	Response Name	:	Micro-hardness
	Response Type	:	Higher-the better
	Units	:	HVN (Vickers Hardness Number)
(5)	Response Name	:	Recast layer thickness
	Response Type	:	Lower-the better
	Units	:	μm (micro meter)

Signal-to-Noise Ratio for Response Characteristics:

The multiple data values for each response were further transformed into a signal-to-noise (S/N) ratio. The change in quality characteristic of a product under investigation in response to a factor introduced in the experimental design is the 'signal' of the desired effect. The effect of external factors (uncontrollable factors) on the outcome of quality characteristic is termed as 'noise'. Thus, signal-to-noise ratio measures the sensitivity of the quality characteristic being investigated in a controlled manner, to those external influencing factors, (noise factors) not under control. The aim of any experiment is always to determine the highest possible S/N ratio for the result irrespective of the quality characteristics. A high value of S/N implies that signal is much higher than the random effects of noise factors. Depending upon the objective of the performance characteristic, there are various types of S/N ratios. In a particular design of experimentation problem, there can be three different type of performance characteristic employed in practice. The selection of an appropriate S/N ratio is very important for optimization of performance characteristic. These are described as:

Higher the better type problem: In this type of problem, the quality characteristic is continuous and non negative and it is made as large as possible or maximizing the objective function. It is expressed as follows:

$$(S/N)_{HB} = -10 \log (MSD_{HB})$$

$$\text{where } MSD_{HB} = \frac{1}{R} \sum_{j=1}^{R} (1/y_j^2) \qquad (3.1)$$

MSD_{HB} = Mean Square Deviation for Higher-the-better response

Lower the better type problem: The quality characteristic is always continuous and non negative. Its most desirable value is zero. As there are no adjustment factors in such type of problem, the thrust is to minimizing the quality loss thus expressed as follows:

$$(S/N)_{LB} = -10 \log (MSD_{LB})$$

$$\text{where } MSD_{LB} = \frac{1}{R} \sum_{j=1}^{R} (y_j^2) \qquad (3.2)$$

MSD_{LB} = Mean Square Deviation for Lower-the-better response

Nominal the best type problem: In nominal-the-best type of problems, the quality characteristic is continuous and non-negative, but its target value is non zero and assumes some finite value. For these types of problems, if the mean becomes zero the variance also tends to become zero. A scaling factor can be used as an adjustment factor to shift the mean closer to the target for such type of problems. The function can be expressed as:

$$(S/N)_{NB} = -10 \log (MSD_{NB})$$

$$\text{where } MSD_{NB} = \frac{1}{R} \sum_{j=1}^{R} (y_j - y_o)^2 \qquad (3.3)$$

MSD_{NB} = Mean Square Deviation for Nominal-the-best response

y_j = Observed value of the response characteristic

y_o = Nominal or target value of the results, R = Number of repetitions

For smaller-the-better type, target value is zero. For larger-the-better type, inverse of each large value becomes a small value and again the target value is zero. For nominal-the-best type of characteristic, the standard definition of MSD has been used. Therefore, for all the three expressions, the smallest magnitude of MSD is being sought. The constant 10 has been purposely used to magnify S/N ratio for each analysis and negative sign is used to set S/N ratio of larger-the-better type relative to the square deviation of smaller-the-better type [108].

CHAPTER - 4
EXPERIMENTATION

The experimental layout as shown in Figure 4.1 was planned to conduct experiments in three Stages (Stage I, Stage II, and Stage III). The experiments are conduct on the basis of availability of resources on the particular stage of the plan.

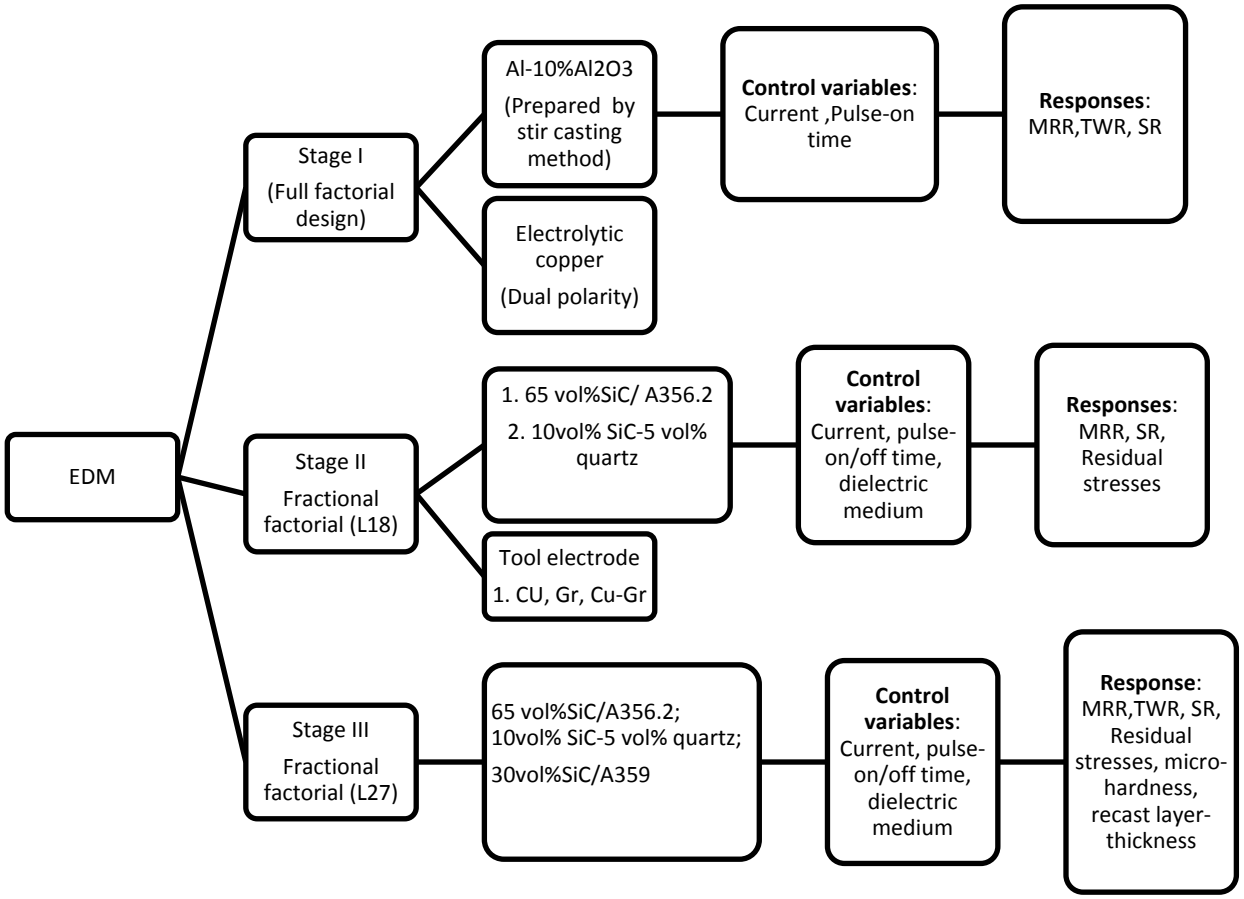

Figure 4.1 Summary of experimental program

The Stage I of experimentation was started with the selection of an appropriate method to prepare the Metal Matrix Composite (MMC). The preparation of MMC was finalized keeping in view the cost-effectiveness and availability hence, stir casting method was used [32]. The matrix material used was aluminium reinforced with Al_2O_3 ceramic particle. The correlated chemical composition of as-received composite material was tested on an Optical Emission Spectrometer (model DV-6, make Baird, USA) and is presented in Table 4.1

Table 4.1Composition of aluminium metal matrix Composite

Si	Fe	Cu	Mn	Mg	Al
0.8	0.318	5.8	0.03	0.62	Balance

4.1 PREPARATION OF THE COMPOSITE MATERIAL

To ensure effective reinforcement, small particle sizes of about 50microns was used and distributed evenly throughout the matrix. In this process, the matrix material was superheated over its melting temperature. The particles were also preheated at around 1000-1200^{0}C to produce an oxidized surface and remove the moisture content from the surface. The melted matrix material was stirred using an automated stirrer at a speed of 300-400 rotations/minute thus forming a vortex during stirring. The preheated particles were added at the vortex of mushy state matrix material [29]. The final temperature of pouring was controlled at 720^{0}C, or the point when a thin layer of aluminium appeared on top of the melt. Thereafter, the melt was poured into a sand mold. For the development of composite material, the low pressure infiltration process proposed by Park et al. was used [28]. A picture of the polished sample after examination under an electron microscope (Make Nikon Epiphot-200) is shown in Figure 4.2

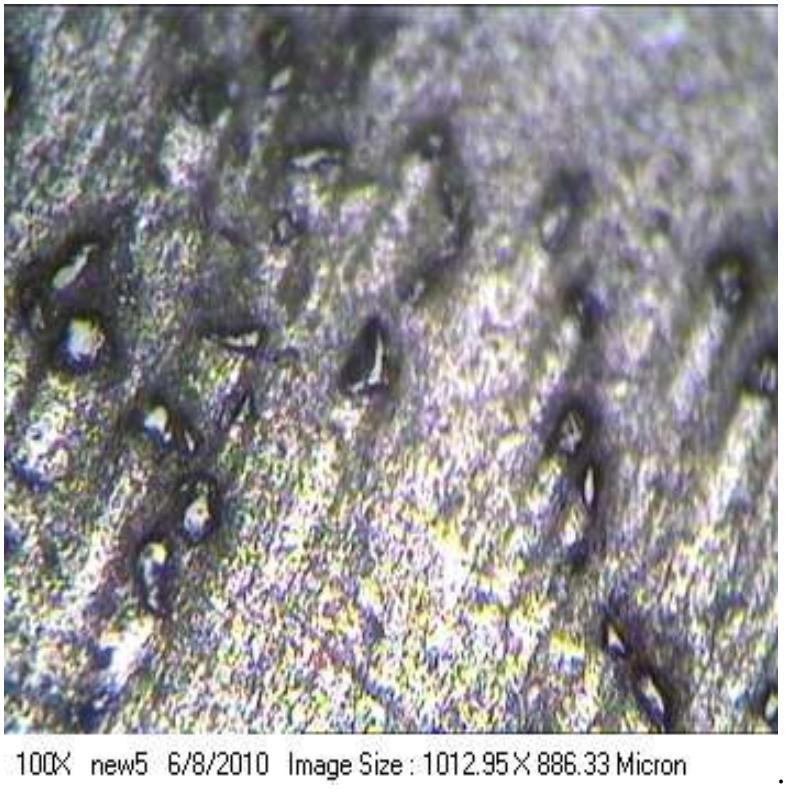

Figure 4.2 Microstructure of as-received MMC (100X)

4.2 DESCRIPTION OF EXPERIMENTAL SET-UP FOR Stage I

The experiments were carried out on an Electric Discharge Machine (Make Electronica – 6040) equipped with a pulse generator. Electrolytic copper electrode machined to cylindrical shape of diameter 10mm was used for machining and was fed downwards with servo control mechanism. The fixed parameters for the present experimentation were input voltage (40V); pulse-off time (12μs); dielectric medium (commercial grade kerosene). The process parameters as listed in Chapter 3 were current and pulse-on time. Table 4.2 shows the input (control) parameters (Current (Amp), X_1 and Pulse-on time (μs), X_2) and the response parameters (MRR, TWR, SR) for both the polarity (conventional and reversed). The ranges of parameter settings values were taken as per EDM bibliography and pilot experimentation for stable machining of composite materials.

4.2.1 Conduct of Experimental Trials

A set of nine experiments as per full factorial experimental designs (Table 4.2) were conducted for each combination of Current (X_1) and Pulse-on time (X_2). Positive and negative polarity of the tool electrode (copper) and kerosene dielectric with constant side flushing was used for all the experiments. Time for each machining cut was fixed at 20 minutes.

Table 4.2 Input process parameters layout

Exp. No.	Process parameters	
	Current (X_1)	Pulse-on time (X_2)
1	8	10
2	8	30
3	8	50
4	12	10
5	12	30
6	12	50
7	16	10
8	16	30
9	16	50

A total 9 trials with values of peak current and pulse on-time for each experiment were set on the control panel of the machine according to the control log given in Table 4.2. The effect on the three response parameters MRR, TWR and SR was studied and is presented

in this section. The study was completed by considering the effect of process parameters on recast cast layer thickness of the MMC, machined under conventional polarity conditions. The results were optimized using Lexicographic Goal Programming (LGP) technique applied on nonlinear models of response function.

The observed values of MRR, TWR and SR after machining with copper tool electrode in dual polarity are shown in Table 4.3.

Table 4.3 Observation table for responses parameter

EXP. No.	TWR (mg/min)		MRR (mm^3/min)		SR (µm)	
	Positive Polarity	*Negative Polarity*	*Positive Polarity*	*Negative Polarity*	*Positive Polarity*	*Negative Polarity*
1	10.52	12.58	17.00	18.27	5.72	5.35
2	4.26	5.55	10.21	9.98	6.38	3.99
3	2.45	3.02	5.70	5.98	6.69	6.33
4	25.4	20.25	25.2	22.23	7.39	6.36
5	8.72	6.56	10.7	10.18	7.83	7.12
6	5.11	3.72	9.72	7.23	8.22	7.42
7	30.94	24.92	31.02	26.02	8.97	8.12
8	12.99	8.97	17.28	14.23	9.43	7.92
9	7.86	5.13	14.22	18.27	9.66	8.44

4.2.2 Regression analysis

Regression analysis is the mathematical measure of the average relationship between two or more variables in terms of the original units of the data. In regression analysis, there are two types of variables. The variables, the value of which can be predicted (such as MRR, TWR, SR), is called predicted or dependent variables and the variables which is used for the prediction (such as current or pulse-on time) is called independent or predictor variables. To illustrate, suppose the empirical model developed is represented by

$$y = \beta_0 + \beta_1 x_1 + \beta_2 x_2 \quad (4.1)$$

The equation 4.1 is a multiple linear regression model with two independent variables. The independent variables often called the predictor variable or regressors. The term linear is used because the equation 4.1 is a linear function of the unknown parameters β_0, β_1 and β_2. The model describes a plane in the two-dimensional x_1, x_2 space. The parameters β_0 defines the intercept of the plane.

The model developed may be of first-order or second-order in two variables. For example

$$y = \beta_0 + \beta_1 x_1 + \beta_2 x_2 + \beta_{12} x_1 x_2 \quad (4.2)$$

In equation 4. 2 the term(x_1x_2) is represented as interaction between x_1 and x_2. The term $x_1x_2 = x_3$ and $\beta_{12} = \beta_3$, then the equation 4.2 can be written as

$$y = \beta_0 + \beta_1 x_1 + \beta_2 x_2 + \beta_3 x_3 \quad (4.3)$$

The equation 4.3 is a standard multiple linear regression model with three regressors.

Regression model fitting was completed by using statistical software MINITAB 15 package. In multiple regression problems, certain tests of hypotheses about the model parameters are helpful in measuring the usefulness of the model. The test procedure involves an analysis of variance partitioning of total sum of square SS_T into the sum of square due to model SS_R (regression) and the sum of square due to residual SS_E (error in prediction) i.e. (Equation 4.4)

$$SS_T = SS_R + SS_E \quad (4.4)$$

The reported output from the software, the coefficient of multiple determination R^2 for the model measured in terms of reduction in the variability of y (output) is obtained by using regressor variables x_1, x_2 in the model. The term R^2 is calculated as (equation 4.5)

$$R^2 = \frac{SS_R}{SS_T} = 1 - \frac{SS_E}{SS_T} \quad (4.5)$$

Determination of Regression model for response parameters

The regression model includes the experimental data, mathematical methods and statistical analysis. A general regression analysis was performed to predict the responses using MINITAB15 software. From the results obtained, the final regression models for machining with tool electrode in positive polarity condition are given by equation (4.6) for MRR, equation (4.7) for TWR and equation (4.8) for SR. A second order polynomial regression equation representing the MRR, TWR and SR (both polarity) can be expressed as a function of EDM machining parameters such as current(X_1) and pulse-on time (X_2).

From the results (Table 4.3) and the removal of some insignificant terms the final regression model for the response are presented as follows:

$$MRR = 12.5625 + 1.74937X_1 - 0.818917X_2 + 0.011033{X_2}^2 \quad (4.6)$$

R^2=97.50%

$$TWR = -1.27208 + 2.84719X_1 - 0.624292X_2 - 0.0469062X_1 * X_2 + 0.0126417{X_2}^2 \quad (4.7)$$

R^2=97.35%

$$SR = 2.07125 + 0.4125X_1 + 0.047X_2 - 0.000875X_1 * X_2 - 0.00002625{X_2}^2 \quad (4.8)$$

R^2=99.95%

The regression model obtained for negative polarity was obtained similarly and are given by equations (4.9), (4.10) and (4.11) for MRR, TWR and SR respectively.

$$MRR = 42.8517 - 2.78104X_1 - 1.19275X_2 + 0.140313{X_1}^2 + 0.0141875X_1 * X_2 + 0.012175{X_2}^2 \quad (4.9)$$

R^2= 94.95%

$$TWR = 8.35042 + 1.70365X_1 - 0.6852X_2 - 0{,}0319687X_1 * X_2 + 0.0114{X_2}^2$$

R^2= 98.92% (4.10)

$$SR = 2.09083 + 0.428958X_1 - 0.054X_2 - 0.00206X_1 * X_2 + 0.00165{X_2}^2 \quad (4.11)$$

R^2= 89.51%

The R^2 value indicates the variance in response parameter with machining parameters and explains the validation of presented data.

4.3 DESCRIPTION OF EXPERIMENTAL SET-UP FOR Stage II

4.3.1 Material used for experimentation

During Stage II, the two types of particle reinforced MMCs were used. Sample I with 65vol%SiC/A356.2 Metal Matrix Composite was procured from Ceramics Process System, MA, USA, in the form of a rectangular strip (Appendix B). Sample II was a hybrid Metal Matrix Composite with 10vol% SiC-5 vol% quartz in aluminium metal (matrix) and was prepared by using stir casting method as explained in Stage I. The composition of this material as measured with optical emission spectroscopy (Make: Arun Technology Poly-Spek-M Spectrometer) read as 96.129% Al, 0.498% Cu, 0.018%

Mg, 2.063% Si, 0.424% Fe, 0.075% Mn, 0.384% Zn, 0.354% Pb, 0.035% Sn, 0.009% Ti, 0.011% Cr. The detailed properties of the materials selected are listed in Table 4.4.

Table 4.4 Properties of MMCs

	Sample I	**Sample II**
Work Piece	65vol%SiC/A356.2	10vol%-SiC-5vol% quartz/Al
Average Reinforced Particle size (Microns)	40-60	50(SiC), 14 (Quartz)
Density (g/cm^3)	3.01	2.84
Thermal Conductivity (W/mk)	200	215
Coefficient of Thermal expansion ($ppm/^0C$)	8.00	25.6
Modulus of Elasticity (GPa)	179	78
Poisson's Ratio	0.25	0.33

The three electrodes used in the study were electrolytic copper, fined grained graphite (Particle size 5.0μm) and copper- graphite composite (50% Cu, Grade 673, resistivity 2.03 μΩ-m, density 2.95 g/cm^3) procured from SGL Corporation, USA.

4.3.2 Equipment and measurement method

The parts were machined on an OSCARMAX (S645 ZNC, Taiwan) die sinking EDM machine (Appendix C), and conventional polarity for the selected electrodes was used to conduct the experiment. The electrodes were machined to a cylindrical shape of diameter 18 mm. The trials were conducted in EDM oil as dielectric and with suspended copper/graphite particles in EDM oil. To ensure uniform mixing of powder, a stirring pedal set at 1400rpm was used during machining as shown in Figure 4.3. The other process parameters such as voltage (~135V), flushing pressure ($0.6kg/cm^2$), were kept constant.

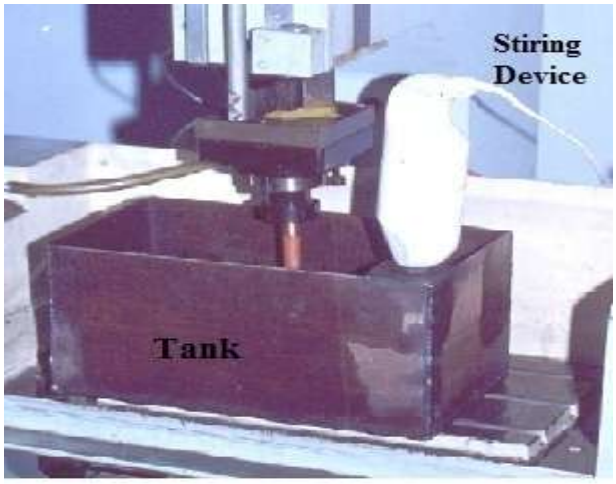

Figure 4.3 Experimental set-up for machining with powder-mixed dielectric

The residual stresses generated during machining were measured by X-ray diffraction method on PANalytical's X'PertPro MPD (Netherlands) diffractometer. This diffractometer is a horizontal fixed, laboratory based system. The maximum 2θ angle accessible to the instrument was limited to 145^0.

Table 4.5 shows the brief experimental condition for X-ray stress analysis.

Table 4.5 Residual stress measuring conditions

Parameters	Conditions
Characteristic X-Ray	Cu-Kα1+2
Measure method	Ω-Diffractometer method
Diffraction plane, (hkl)	(422)
Tube Voltage, KV	45
Tube current, mA	40
Diffraction angle (2θ)	40^0-140^0

4.3.3 Conduct of experimental trials

The experimental study was conducted using the Taguchi's design of experiments technique. A pilot study coupled with information available from literature was used to identify the machine and process parameters to be varied during the study.

Based on this study, current, pulse-on time, pulse-off time and dielectric fluid were identified for detailed study of their effect on MRR, SR and residual stresses generated during machining. To draw valid conclusions from the experiments, each of these factors were varied at three levels to understand their impact on response parameters. Thus, a total of six factors namely Material type (Sample I & Sample II), Current (I), Pulse-on time (t_{on}), Pulse-off time (t_{off}) and electrode materials (Copper, graphite and Copper-Graphite composite). Three combinations of dielectric namely (1) Commercial grade EDM oil, which represents conventional EDM; (2) EDM oil mixed with copper powder; and (3) EDM oil mixed with graphite powder dielectric medium were chosen for study.

The last two levels represent powder mixed electric discharge machining (PMEDM) process which is used to measure their effect on the response parameters in MMC materials was analyzed.

The list of factors studied with their respective levels is shown in Table 4.6.

Table 4.6 Representation of factor levels for Stage II

Factors (Symbol)	**Levels**		
	Level – 1	**Level – 2**	**Level – 3**
Work piece (w)	65vol%SiC/A356.2 (Sample I)	10vol%SiC-5vol% quartz/Al (Sample II)	-----
Electrode(e)	Cu	Gr	Cu-Gr
Current (I) Amp	4	8	12
Pulse-on (t_{on})µs	10	30	45
Pulse-off (t_{off}) µs	15	30	45
Dielectric(d)	EDM oil (D)	EDM oil + Cu Powder (D+Cu)	EDM oil+ Gr powder (D+Gr)

Since the factors chosen for the study were a combination of two and three levels, a mixed experimental design (L_{18}) developed by Taguchi was used for this study. The trial conditions after the assignment of factors to an L_{18} array are listed in Table 4.7.

Table 4.7 Experimental layout (L_{18})

Exp. No.	W/Pc (w)	Electrode (e)	Pulse-off (t_{off}) µs	Pulse-on (t_{on}) µs	Dielectric (d)	Current (I) Amp
1	Sample I	Cu	15	10	D	4
2	Sample I	Cu	30	30	D+Cu	8
3	Sample I	Cu	45	45	D+Gr	12
4	Sample I	Gr	15	45	D+Cu	8
5	Sample I	Gr	30	10	D+Gr	12
6	Sample I	Gr	45	30	D	4
7	Sample I	Cu-Gr	15	30	D	12
8	Sample I	Cu-Gr	30	45	D+Cu	4
9	Sample I	Cu-Gr	45	10	D+Gr	8
10	Sample II	Cu	15	30	D+Gr	8
11	Sample II	Cu	30	45	D	12
12	Sample II	Cu	45	10	D+Cu	4
13	Sample II	Gr	15	45	D+Gr	4
14	Sample II	Gr	30	10	D	8
15	Sample II	Gr	45	30	D+Cu	12
16	Sample II	Cu-Gr	15	10	D+Cu	12
17	Sample II	Cu-Gr	30	30	D+Gr	4
18	Sample II	Cu-Gr	45	45	D	8

L_{18} denotes 18 different trial conditions which were conducted randomly to eliminate any undesirable bias in the study. The L_{18} is designed in such a way that it accommodates the two-level factor in column 1 and the remaining three levels factors are assigned in other columns.

As can be seen from this design matrix, the first column represents the type of work piece materials used in the study. Thus, the first nine trials represent 65vol% SiC/A356.2 MMC hereafter represented as Sample I and the remaining nine trials (Trial 10 to 18) represent results for 10vol% SiC-5vol% quartz in aluminium, hereafter referred to as Sample II. The assignment of other factors to remaining columns is listed in as Table 4.7.

Residual stress

The efficiency of the machining process depends upon various process parameters such as spark energy, flushing pressure, dielectric medium and the electrode. During EDM of MMCs, a localized high temperature electric discharge occurs in the presence of dielectric which may result in change in mechanical and physical properties and also develop residual stresses within the material. The residual stresses affect the fatigue life of the workpiece and often cause distortion or cracking and in some cases also premature failure of the part in service [2, 31, 91, 114]. The parts were machined as per the trial conditions listed in Table 4.7. The machining takes place as a result of application of consecutive spark discharges, which bring overlapping craters that are randomly distributed over the entire surface. The discharge is assumed to be axisymmetric which results in equal magnitude of biaxial stress field generated on the surface of machined work piece [90]. Thus, a unidirectional stress evaluation was done with the help of X-ray diffraction classical procedure.

X-ray diffraction method was used for measuring residual stresses in machined surface layer employ the characteristics radiation emitted from an X-ray. The change in *d*-spacing due to strain in the sample is very small, so the highest possible 2θ angle peak was selected. To calculate the residual stress, a number of independent X-ray runs with different ψ angles were performed. The residual stress was then obtained from the slope of *d* versus $\sin^2\psi$ plot. This method is called $\sin^2\psi$ technique [84, 85,109].

The advantage of this method is that repeated measurements are possible on the specimen. Figure 4.4 shows the schematic of concepts used in residual stress analysis.

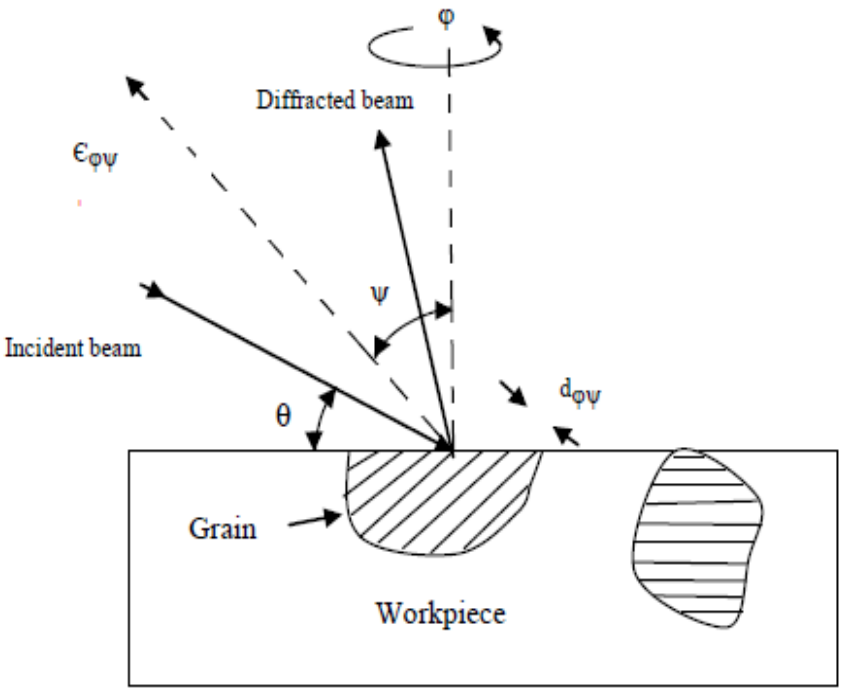

Figure 4.4 Concept of X-ray diffraction stress analysis

The general equation for measuring the residual stresses is represented by equation 1.3 given below (From Chapter 1). The lattice strain $Є_{φψ}$ is defined as a ratio of the change in lattice spacing of atomic layer due to the machining process to the un-machined lattice spacing tilted by ψ angle and rotated by φ angle of the sample.

$$Є_{φψ}=\frac{1}{2} S_2 \sin^2ψ(σ_φ – σ_{33})+ \frac{1}{2}S_2τ_φ\sin(2ψ) + Є_{φ0}{}^0$$

Where

$$Єφψ = \frac{d_{φψ}-d_0}{d_0}$$

$$Є_{φ0}{}^0 = \frac{1}{2}S_2σ_{33} + S_1 (σ_{11} + σ_{22} + σ_{33})$$

$$σ_φ = σ_{11}\cos^2φ + σ_{12}\sin(2φ) + σ_{22} \sin^2φ$$

$$τ_φ = σ_{13}\cosφ + σ_{23}\sinφ$$

S_1 = -ν/E, $1/2S_2$ = (1+ν)/E, S_1 and $1/2S_2$ are the X-ray elastic constants (XEC's) [82, 106, 107 121].

The calculated values of X-ray elastic constant utilized in the present study for both the sample are represented in Table 4.8.

Table 4.8 X-ray elastic constants

	Sample I	Sample II
Elastic constants $T^{-1}Pa(1/2S_2)$	6.98	16.84

From general equation for stress (equation 1.3), in order to measure the unidirectional normal residual stress, the parameters a^+ was calculated by using the lattice strain for positive and negative value of ψ (psi) for the particular rotational angle φ of the sample and is given by equation 4.12

$$a^+ = \frac{1}{2}(\epsilon_{\varphi\psi+} + \epsilon_{\varphi\psi-}) = \frac{1}{2} S_2 \, sin^2\psi(\sigma_\varphi - \sigma_{33}) + \epsilon_{\varphi 0^0} \quad (4.12)$$

where σ_{33}=0, φ=0^0

The residual stresses induced during machining were measured using X-ray machine (Make :PANalytical's X'PertPro MPD (The Netherlands)). The evaluation of residual stress was completed using XRD classic technique using only one plane (hkl) to calculate the magnitude of residual stresses. The machined surface was cleaned to remove the re-solidified globules of molten metal to reduce measurement errors. In this experiment, the highest peak (2θ ≥125^0) also known as Bragg's peak diffracted from the matrix phase of composite was selected for precise measurements. The small change in lattice spacing gives considerable change in peak angle and it is represented by the equation 4.13.

$$\frac{\Delta d}{\Delta \theta} = (-)\Delta\theta cot\theta \quad (4.13)$$

A number of independent XRD measurements of the isolated diffracted peak from the matrix phase of composite material were made at a different angle of ψ (psi) tilts. The obtained $d_{\varphi\psi}$ spacing at different angles ψ tilt (positive and negative) was used to calculate the lattice strain. The calculated a^+ was plotted against $\sin^2\psi$ and the slope of the linear fit curve was compared with equation 4.12. The residual stress with accepted uncertainty value due to the goodness of curve fitting was obtained. Sikarskie [113] presented various factor contributing to the uncertainty in measurement of stress by X-ray diffraction method. The inhomogeneous stress state generated during certain trials causes preferred orientation which leads to lower peak intensities and less accurate peak location resulting in higher uncertainty. This effect of texture in measurement can be overcome by choosing appropriate tilts or translation of the sample to bring more grains in diffraction condition. The measured residual stresses values with uncertainty are shown in Table 4.9. The absolute residual stresses (σ_φ) values with uncertainty were measured after each trial by above methodology and are given in the Table 4.9.

Table 4.9 Observation table for residual stress measured by X-ray diffraction technique

Exp. No.	Residual stress (MPa) (σ_φ)	Uncertainty (±MPa)
1	63.3	5.7
2	74.6	3.9
3	82.8	4.0
4	36.3	13.5
5	63.6	6.0
6	110.3	11.4
7	61.4	2.6
8	78.5	5.9
9	129	10.3
10	70.4	12.1
11	104	11
12	78.1	9.7
13	41.8	13.2
14	149.3	19.3
15	132.9	20.1
16	77.7	10.4
17	89.2	9.6
18	231.5	15.8

Sample calibration and data analysis for Trial 6

Residual stress was measured in matrix phase (Al-Phase) of the machined sample. The measurement was performed by selecting the isolated peak diffracted at the highest value of 2θ from (422) plane when using Cu-K-α radiations (λ=1.5406 A^0). Table 4.10 for Trial 6 (Sample I) represents the change in lattice spacing measured from 19 ψ tilts (Figure 4.6). The calculated lattice strain for positive and negative ψ tilt is represented in the last column of the Table 4.10. Residual stress was analyzed by comparing the linear fit regression equation obtained from the plot of a^+ versus $\sin^2\psi$ (Figure 4.5) with equation 4.12 as follows:

$$0.000767 = \frac{1}{2} S_2 (\sigma_\varphi)$$

where $1/2S_2$ =6.98 T^{-1}Pa. Hence the normal residual stress for Trial 6 is 110 MPa with uncertainty of ±11.4 MPa.

Table 4.10 Peak table and lattice strain for Trial 6

ψ	Sin^2 ψ	2θ	$d_{\varphi\psi}$	$\epsilon_{\psi\varphi}$
0.00	0	133.1585	0.839462	0
12.92	0.049993	133.1723	0.839418	-0.000324034
18.44	0.100053	133.1904	0.839360	-0.000393157
22.79	0.150044	133.1858	0.839375	-0.000375279
26.57	0.200069	133.1826	0.839385	-0.000363361
30.00	0.25	133.1504	0.839487	-0.000241814
33.21	0.299985	133.1631	0.839447	-0.000289476
36.27	0.34998	133.1537	0.839477	-0.000253729
39.23	0.399974	133.1733	0.839415	-0.000327609
42.13	0.449993	133.1725	0.839417	-0.000325226
12.92	0.049993	133.1235	0.839573	-0.000139357
18.44	0.100053	133.1334	0.839541	-0.000177478
22.79	0.150044	133.1097	0.839616	-8.81355E-05
26.57	0.200069	133.0696	0.839744	6.43053E-05
30.00	0.25	133.0547	0.839791	0.000120268
33.21	0.299985	133.0741	0.839730	4.76344E-05
36.27	0.34998	133.0172	0.839911	0.000263123
39.23	0.399974	132.9901	0.839997	0.000365477
42.13	0.449993	132.9874	0.840006	0.000376188

Figure 4.6 shows the shift of diffraction peak with change in the value of ψ. The corresponding value of $\sin^2\psi$ and d-spacing is listed in Table 4.10 for the analysis of change in d-spacing or strain induced.

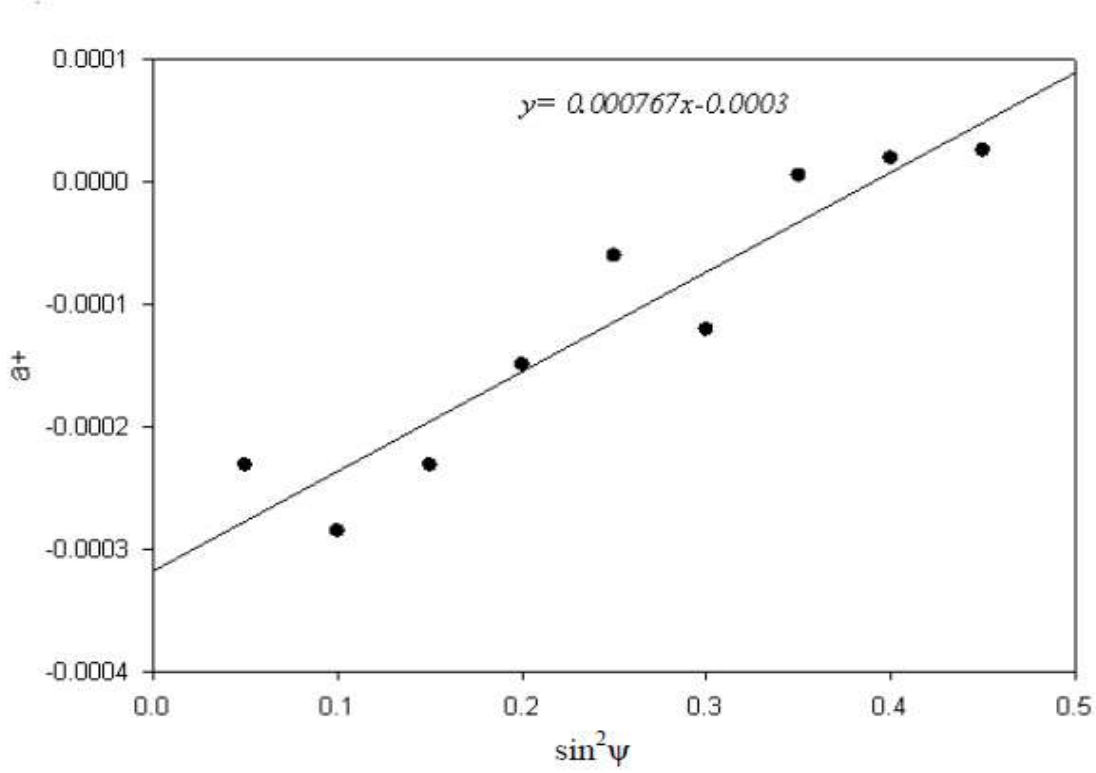

Figure 4.5 Represents a^+ vs. $\sin^2\psi$ plot with regression equation of Trial 6

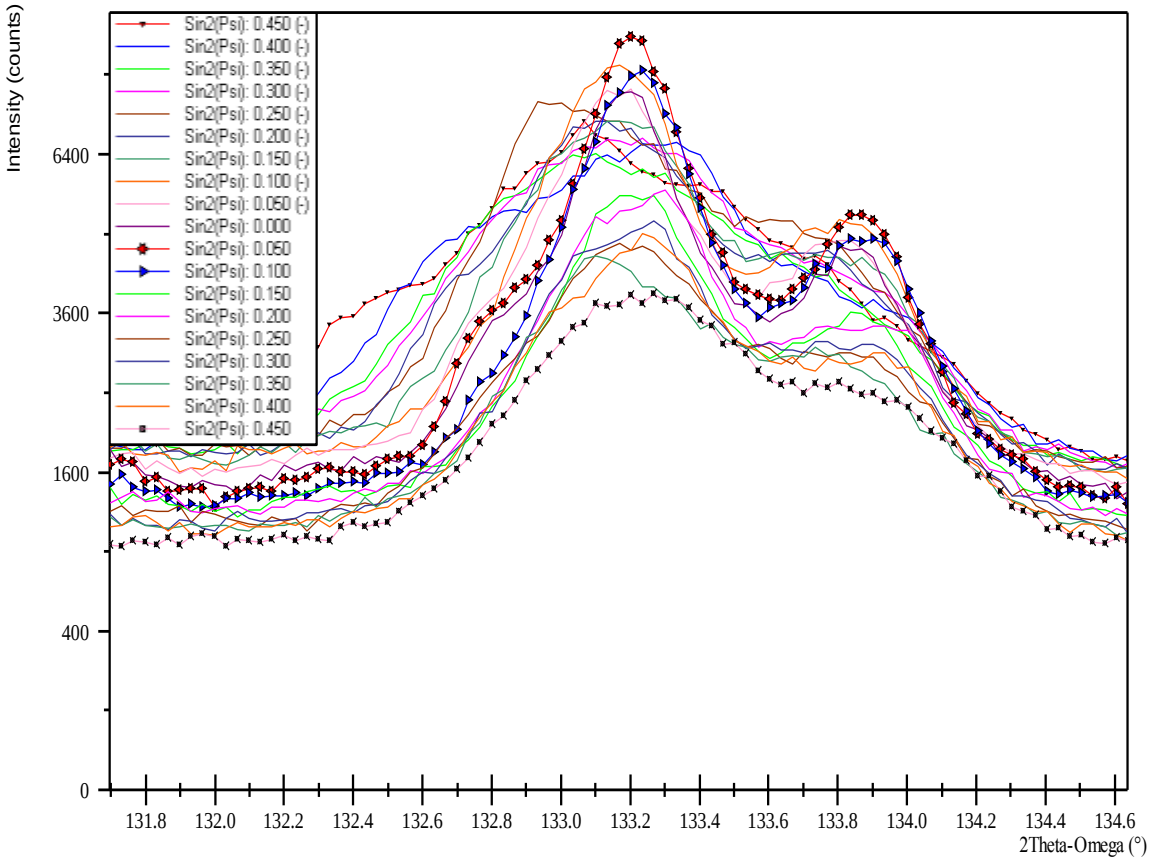

Figure 4.6 Representation of shift in selected peak at different ψ angles of Trial 6.

Metal Removal Rate (MRR) and Surface Roughness (SR)

The MRR and SR were also evaluated in the present stage (Stage II) experimentation for each trial run. The machining rate from both the tool and the work piece was measured by subtracting the weight at the beginning and completion of machining using a digital weighing machine (Chyo (MJ-300), readability 0.001g). The machining rate is given by equation 4.14.

$$Machining\ rate = \frac{(w_i - w_f)1000}{T}\ mg/min \qquad (4.14)$$

where w_i = weight before machining (mg) and w_f = weight after machining (mg) (measured after cleaning the retained dielectric) and T= time for machining (minutes).

The SR was measured using Mitutoyo SJ-400 surface roughness tester in terms of arithmetic average of absolute value R_a (µm). Each sample was measured diametrically from three locations on the machined surface and was averaged for further analysis. The observed value of response parameters (MRR and SR) for each trial listed in Table 4.11.

Table 4.11 Observation table for MRR, (SR) and modified value of residual stress

Exp. No.	MRR (mg/min)	SR (µm)	σ_n (MPa) calculated from Eq.4.15
1	2.64	2.94	66.7
2	14.275	2.05	55.4
3	23.17	5.67	47.2
4	23.38	2.09	93.7
5	18.97	4.12	66.4
6	3.04	3.00	19.7
7	22.240	5.01	68.6
8	9.860	2.06	51.5
9	9.460	5.06	1
10	20.90	6.69	162.1
11	60.67	10.46	128.5
12	10.860	4.69	154.4
13	57.99	6.46	190.7
14	18.86	8.44	83.2
15	29.96	4.44	99.6
16	65.5	6.76	154.8
17	10.07	6.12	143.3
18	45.72	7.95	1

The value of residual stress in the modified form, according to equation 4.15 is also listed in the last column of the Table 4.11.

4.3.4 Analytical Hierarchical Process

The optimization of the three responses individually would have thrown up vastly different parametric combinations of the machining parameters. For example, if MRR is optimized individually it would have resulted in identification of some parameters of the process that maximize MRR (as MRR is a higher the better function). These parameters may not have resulted in lower SR as roughness was not considered during optimization. The vice versa would have been true if SR was optimized individually. Same thing applies for residual stresses. In order to get a more useful and global optimization result, it is important that all the responses are optimized together. The Analytical Hierarchy Process (AHP) offers one such technique for multiple optimization. AHP is simply structured and is widely used to deal in multiple goal decision makings technique and is classified as decision making tool under certainty i.e. the data is known deterministically and designed for the situation in which ideas, feeling and emotion are quantified into numerical scale [131]. The main steps used in implementation of AHP are:

- Define the objective, the evaluation criteria and develop the hierarchical structure with an objective at the top level, the criteria, and sub-criteria at the intermediate level and the lowest level which consist of available alternative.
- Form pair wise comparison matrix for each level with respect to a higher level and determine the relative importance of different alternative with respect to its immediately above sub criteria. The comparison is made on 9-point "fundamental scale of Saaty" represented in Table 4.12

Table 4.12: Saaty's fundamental scale [132]

Scale value	Explanation
1	Equally preferred
3	Slightly more preferred
5	Strongly more preferred
7	Very strongly more preferred
9	Extremely preferred
2,4,6,8	Used to reflect compromise between scale value

- Compute relative weight for the pairwise comparison matrices using eigenvector methods.
- Judge the scope of inconsistency by using the largest Eigenvector (λ_{max}). The judgment of accepted degree of consistency can be checked by means of consistency ratio (CR) of consistency index (CI) with the appropriate value of the random index (RI) from Table 4.13.

Table 4.13: Random consistency index

k	**1**	**2**	**3**	**4**	**5**	**6**	**7**	**8**	**9**	**10**	**11**	**12**	**13**
RI	0.00	0.00	0.58	0.90	1.12	1.24	1.32	1.41	1.45	1.49	1.51	1.48	1.48

- Repeat the above steps for all levels in the hierarchy and the overall relative value is evaluated by linear addition function.

Implementation of AHP for global optimization of responses in EDM process

In the present study, Analytical Hierarchy Process (AHP) was applied to choose the best combination of input parameter. The criteria used were to minimize the residual stress and surface roughness and maximize the metal removal rate. In this experimental design layout, 9 Trials are conducted for each type of MMCs and the orthogonality was maintained by selecting L_{18} experimental design. In the present design given in Table 4.7, Trials 1 to 9 is the available alternative for MMC Sample I and Trial 10-18 for MMC Sample II. The steps designed for the determination of global optimization {MCDM problem (Finite alternative)} are summarized in Figure 4.7.

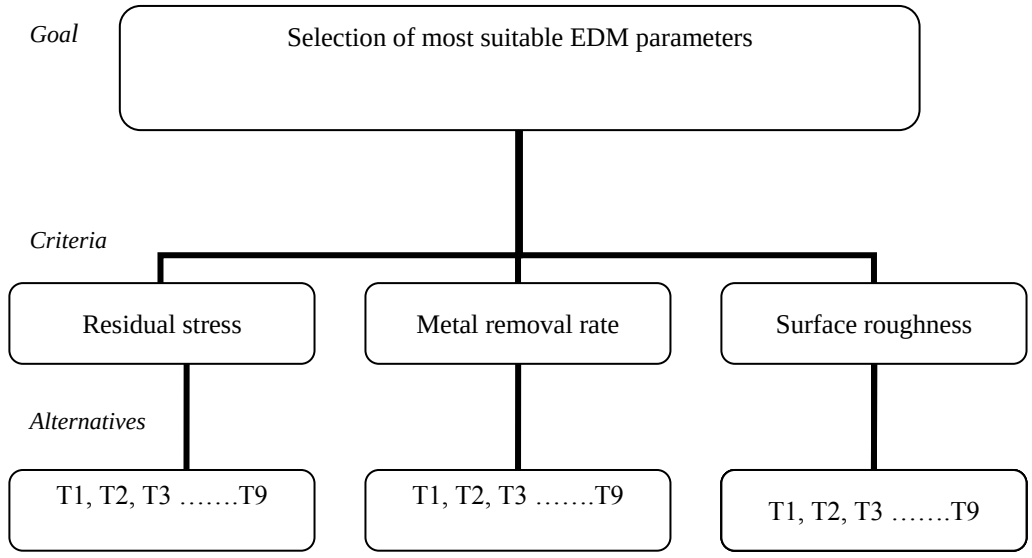

Figure 4.7 Hierarchy layout of analytic hierarchy process used

The MMCs selected in the present study are generally used for very high end applications in aerospace and mining, and the residual stresses developed during the EDM process effect the service life of the product. Residual stress was assigned the largest weight followed by material removal rate and surface roughness. To attain the desired objective, the residual stress results were slightly modified as follows:

$$\sigma_n = (\sigma_{max} - \sigma_\varphi) + 1 \tag{4.15}$$

where σ_{max} is the maximum value of residual stress in the corresponding set of trial of each work piece, σ_φ is residual stress measured with X-ray diffraction method, σ_n a modified residual stress value (Refer 4.11) was calculated from equation 4.15.

Using the criteria of assigning weights to residual stress, MRR and SR a (3x1) weight column matrix as shown in Table 4.14 was established for pair wise comparison.

Table 4.14: Pairwise comparison of criteria

	Residual stress	**MRR**	**SR**	**Priority vector**
Residual stress	1	2	5	0.581552
MRR	½	1	3	0.308996
SR	1/5	1/3	1	0.109452
	λ_{max} = 3.00369	CI= 0.0018473, RI= 0.58, CR=0.003		

Subsequently a pair wise comparison of experimental trials (alternatives) was developed for, Residual stress(σ_n), MRR and SR for each work piece and is shown in Tables (4.15, 4.17-4.21). It was also ensured during pair wise comparison of alternatives that, if the value attained during comparison is more than the maximum limit of Saaty's fundamental scale, the highest value of the scale (9) was selected to avoid inconsistency.

Table 4.15: Pairwise comparison of residual stress with respect to their alternatives for Sample I

	T1	**T2**	**T3**	**T4**	**T5**	**T6**	**T7**	**T8**	**T9**	**Priority vector**
T1	1	1	1	1	1	3	1	1	9	0.130829
T2	1	1	1	½	1	3	1	1	9	0.12105
T3	1	1	1	½	1	2	1	1	9	0.115577
T4	1	2	2	1	1	5	1	2	9	0.180525
T5	1	1	1	1	1	3	1	1	9	0.130829
T6	1/3	1/3	1/2	1/5	1/3	1	1/4	1/3	9	0.050517
T7	1	1	2	1	1	4	1	1	9	0.136302
T8	1	1	1	½	1	3	1	1	9	0.12105
T9	1/9	1/9	1/9	1/9	1/9	1/9	1/9	1/9	1	0.0133204
	λ_{max} = 9.23034				CI= 0.0287927, RI= 1.45, CR=0.0198					

Table 4.16 Synthesized matrix of residual stress for Sample I

	T1	T2	T3	T4	T5	T6	T7	T8	T9
T1	0.13434	0.10405	0.10405	0.17208	0.13433	0.12442	0.13585	0.11843	0.12329
T2	0.13434	0.10405	0.10405	0.08604	0.13433	0.12442	0.13585	0.11843	0.12329
T3	0.13434	0.10405	0.10405	0.08604	0.13433	0.08295	0.13585	0.11843	0.12329
T4	0.13434	0.20809	0.20809	0.17208	0.13433	0.20737	0.13585	0.23685	0.12329
T5	0.13434	0.10405	0.10405	0.17208	0.13433	0.12442	0.13585	0.11843	0.12329
T6	0.04478	0.05202	0.05202	0.03442	0.04478	0.04147	0.03396	0.03948	0.12329
T7	0.13434	0.20809	0.20809	0.17208	0.13433	0.16590	0.13585	0.11843	0.12329
T8	0.13434	0.10405	0.10405	0.08604	0.13433	0.12442	0.13585	0.11843	0.12329
T9	0.01493	0.01156	0.01156	0.01912	0.01493	0.00461	0.01509	0.01316	0.01370

Table 4.17 Pairwise comparison of MRR with respect to their alternatives for Sample I

	T1	T2	T3	T4	T5	T6	T7	T8	T9	Priority vector
T1	1	1/5	1/9	1/9	1/7	1	1/8	1/4	1/4	0.02080
T2	5	1	1/2	1/2	1	5	1/2	1	1	0.09982
T3	9	2	1	1	1	9	1	3	3	0.19547
T4	9	2	1	1	1	8	1	2	2	0.17520
T5	7	1	1	1	1	6	1	2	2	0.15448
T6	1	1/5	1/9	1/8	1/6	1	1/7	1/3	1/3	0.02328
T7	8	2	1	1	1	7	1	2	2	0.17034
T8	4	1	1/3	1/2	1/2	3	1/2	1	1	0.08303
T9	4	1	1/3	1/2	1/2	3	1/2	1	1	0.08303
	$\lambda_{max} = 9.02762$				CI= 0.00640, RI= 1.45, CR=0.0023					

Table 4.18 Pairwise comparison of SR with respect to their alternatives for Sample I

	T1	T2	T3	T4	T5	T6	T7	T8	T9	Priority vector
T1	1	1	1/2	1	1	1	1/2	1	1/2	0.0834519
T2	1	1	1/3	1	1/2	1	1/2	1	1/2	0.0728733
T3	2	3	1	3	1	2	1	3	1	0.176214
T4	1	1	1/3	1	1/2	1	1/2	1	1/2	0.0728733
T5	1	2	1	2	1	1	1	2	1	0.133865
T6	1	1	1/2	1	1	1	1/2	1	1/2	0.0834519
T7	2	2	1	2	1	1	1	2	1	0.152199
T8	1	1	1/3	1	1/2	1/2	1	1	1/2	0.0728733
T9	2	2	1	2	1	1	1/2	2	1	0.152199
	λ_{max} = 9.10338				CI= 0.0129221, RI= 1.45, CR=0.008911					

Table 4.19 Pairwise comparison of residual stress with alternatives for Sample II

	T10	T11	T12	T13	T14	T15	T16	T17	T18	Priority vector
T10	1	1	1	1	2	2	1	1	9	0.138612
T11	1	1	1	1/2	2	1	1	1	9	0.119842
T12	1	1	1	1	2	2	1	1	9	0.138612
T13	1	2	1	1	2	2	1	1	9	0.165782
T14	1/2	1/2	1/2	1/2	1	1	1/2	1/2	9	0.0758749
T15	1/2	1	1/2	1/2	1	1	1/2	1/2	9	0.089421
T16	1	1	1	1	2	2	1	1	9	0.129583
T17	1	1	1	1	2	2	1	1	9	0.128872
T18	1/9	1/9	1/9	1/9	1/9	1/9	1/9	1/9	1	0.0134007
	λ_{max} = 9.1803				CI=0.0225376, RI= 1.45, CR= 0.0155					

Table 4.20 Pairwise comparison of MRR with alternatives for Sample II

	T10	T11	T12	T13	T14	T15	T16	T17	T18	Priority vector
T10	1	1/3	2	1/3	1	1	1/3	2	1/2	0.068095
T11	3	1	6	1	3	2	1	6	1	0.185247
T12	1/2	1/2	1	1/5	1/2	1/3	1/6	1	1/4	0.0330161
T13	3	3	3	1	3	2	1	6	1	0.181600
T14	1	1	1	1	1	1/2	1/3	2	1/2	0.0629946
T15	1	1	1	1	1	1	1/2	3	1/2	0.0923417
T16	3	3	3	3	3	3	1	6	1	0.1852470
T17	1/2	1/2	1/2	1/2	1/2	1/2	1/2	1	1/5	0.0314636
T18	2	2	2	2	2	2	2	2	1	0.159995
	λ_{max} = 9.05235				CI= 0.00654334, RI= 1.45, CR= 0.00451					

Table 4.21 Pairwise comparison of SR with their alternatives for Sample II

	T10	T11	T12	T13	T14	T15	T16	T17	T18	Priority vector
T10	1	1/2	1	1	1	2	1	1	1	0.107181
T11	2	1	2	2	1	2	2	2	1	0.171361
T12	1	1/2	1	1	1/2	1	1	1	1/2	0.0858196
T13	1	1/2	1	1	1	1	1	1	1	0.0990902
T14	1	1	2	1	1	2	1	1	1	0.126548
T15	1/2	1/2	1	1	1/2	1	1/2	1	1/2	0.0741207
T16	1	1/2	1	1	1	2	1	1	1	0.107181
T17	1	1/2	1	1	1	1	1	1	1	0.0990902
T18	1	1	2	1	1	2	2	1	1	0.12661
	λ_{max} = 9.16155				CI= 0.0201939, RI= 1.45, CR= 0.0139					

The assignment of pair wise comparison (9x9 matrix) of alternatives was completed by comparing and rounding-off the response ratio obtained in experimental trials. For example, if Trial 1 gives a value of 16.5 and the Trial 2 gives 4.5, then the response ratio is the ratio of the values of two trials (Trial 1 / Trial 2) and is 3.66 (rounding off as 4). The same procedure was adopted for all the response parameters to assign the weights. This was followed by calculation of percentage increase in variable magnitude to assign the weight in pairwise comparison matrix [132]. To illustrate this calculation, the pair wise matrix for residual stress (Sample I) as shown in Table 4.16 was considered.

Step 1: The matrix was normalized by dividing each element of matrix by its column total. For example, for T (1, 1) element, a value 0.13434 was obtained by dividing T (1,1) element i.e. 1 by the column total 7.444 (1+1+1+1+1+1/3+1+1+1/9). The same procedure was adopted for each element of matrix and is given in Table 4.16.

Step 2: The estimation of priority vector was done by taking the row average i.e. (0.13434+0.10405+0.10405+0.17208+0.13433+0.12442+0.13585+0.11843+0.12329) divided by 9. The priority vector, consistency index (CI) and maximum Eigen value (λ_{max}) for above matrix is indicated in the last column of Table 4.16.

Similarly the synthesized pair wise comparison matrix, priority vectors and validation of constructed matrix were evaluated for each response parameter.

The overall weight was calculated by multiplying the alternative available priority vectors for each sample with the criteria weight and is given in Table 4.22. The overall priority for each EDM parameter setting was calculated as demonstrated below:

Table 4.22: Overall weight matrix of sample I for priority

Trials	Residual stress (0.581552)	MRR (0.308996)	SR (0.109452)	Overall priority vector	Ideal weight vector
T1	0.130829	0.02080	0.0834519	0.091645	0.548453
T2	0.12105	0.09982	0.0728733	0.109219	0.653623
T3	0.115577	0.19547	0.176214	0.146899	0.879124
T4	**0.180525**	**0.17520**	**0.0728733**	**0.167097**	**1.000000***
T5	0.130829	0.15448	0.133865	0.138471	0.828682
T6	0.050517	0.02328	0.0834519	0.045707	0.273534
T7	0.136302	0.17034	0.152199	0.148560	0.889066**
T8	0.12105	0.08303	0.0728733	0.103185	0.617514
T9	0.0133204	0.08303	0.152199	0.049217	0.294540

***Ist rank, ** IInd rank**

Table 4.23: Overall weight matrix of sample II for priority

Trials	Residual stress (0.581552)	MRR (0.308996)	SR (0.109452)	Overall priority vector	Ideal weight vector
T10	0.138612	0.068095	0.107181	0.113791	0.73091
T11	0.119842	0.185247	0.171361	0.146440	0.940701
T12	0.138612	0.0330161	0.0858196	0.100555	0.645949
T13	**0.165782**	**0.181600**	**0.0990902**	**0.155672**	**1.000000***
T14	0.0758749	0.0629946	0.126548	0.077638	0.498728
T15	0.089421	0.0923417	0.0741207	0.088929	0.571260
T16	0.129583	0.1852470	0.107181	0.149991	0.963508**
T17	0.128872	0.0314636	0.0990902	0.095874	0.615871
T18	0.0134007	0.159995	0.12661	0.071110	0.456796

***Ist rank, ** IInd rank**

Overall weight of T1 (Sample I)**: Overall Weight = 0.132856(0.130829) + 0.02362(0.02080) + 0.0549692(0.0834519) = **0.091645.

Similarly, the overall weight was calculated for each trial conducted with two work pieces. The remaining calculations were completed by combining the assigned criteria weight with the alternative priority weight to get the overall priority results (Table 4.22, 4.23) as per the hierarchical steps given in Figure 4.7. The ideal weight vector was obtained by dividing the priority vector with the largest priority weight element in the matrix.

The advantage of using idealized weight vector is that the ranking of trials does not change due to the influence of newly introduced non-optimal identical alternative [133].From the calculated overall priority; the trials were ranked for each type of MMCs.

4.4 DESCRIPTION OF EXPERIMENTAL SET-UP FOR Stage III

The experimental set-up was similar to section 4.3 (Stage II). In this stage, Sample III 30vol%SiC/A359 provided by MC-21, Inc.,USA was included in the experimental design. Hence the MMCs selected for the study was; 65 vol%SiC/ A356.2; 10vol% SiC-5 vol% quartz in aluminium metal matrix; 30vol%SiC/A359. The detailed properties of the Sample III are listed in Table 4.24.

Table 4.24 Properties of work piece (Sample III)

Work Piece	SiC Particle size (Average)	Density	Thermal Conductivity	Coefficient of Thermal expansion	Modulus of Elasticity	Poisson's ratio
30 vol% SiC/ A359	14 microns	2.8 g/cm^3	170 W/mk)	14.5 ppm/^oC	110 GPa	0.29

Experimental design was completed using the Taguchi's fractional factorial experiments in which, certain treatment conditions are chosen to maintain the orthogonality among the various factors. The list of factors interest and their levels is shown in 4.25.

Table 4.25 Representation of factor levels for Stage III

Factors (Symbol)	**Levels**		
	Level – 1	**Level – 2**	**Level – 3**
Work piece (w)	65vol%SiC/A356.2 (Sample I)	10vol%SiC-5vol% quartz/Al (Sample II)	30vol%SiC/A 359 (Sample III)
Electrode(e)	Cu	Gr	Cu-Gr
Current (I) Amp	4	8	12
Pulse-on (t_{on})µs	10	30	50
Pulse-off (t_{off}) µs	15	30	45
Dielectric(d)	EDM oil (D)	EDM oil + Cu Powder (D+Cu)	EDM oil + Gr powder (D+Gr)

In this experimental situation, there are three levels for each factor and a possible matrix is a 27 trials orthogonal array (OA) labeled as L_{27} matrix. The 27 trials provide 26 degrees of freedom (dof) for the entire experiment allocated to 13 columns of three levels with each column having two degrees of freedom (dof). There are six factors which are varied during the experiment. Each factor is varied at three levels with two dof associated with each factor. The total degrees of freedom for the orthogonal experiment are calculated to be 12. In this study, both L_{18} and L_{27} could be potentially used for designing the experimental trial conditions. However, since L_{18} is a mixture of two and three level factors, L_{27} was preferred for the present study. The additional degrees of freedom

provided by the array are used to examine the uncontrolled error or other random factors. The assignment of factors was carried out using MINITAB15. In this experimental stage, the allocation of control variables (factors) in orthogonal array was; workpiece (Sample I, II, III): column 1, Electrode (Cu, Gr, Cu-Gr): column 2, Current (4, 8, 12): column 12, Pulse-on time: column 13, Pulse-off time (15, 30, 45): column 5, Dielectric medium: column 10. The experiment was conducted as per experimental design layout for the Stage III is shown in Table 4.26.

Table 4.26 Experimental design layout

Exp. No.	Work piece (w)	Electrode (e)	Current (Amp) (I)	Pulse-on (µs)(t_{on})	Pulse-off (µs) (t_{off})	Dielectric medium (d)
1	Sample I	Cu	4	10	15	D
2	Sample I	Cu	8	30	30	D+Cu
3	Sample I	Cu	12	45	45	D+Gr
4	Sample I	Gr	12	45	15	D+Cu
5	Sample I	Gr	4	10	30	D+Gr
6	Sample I	Gr	8	30	45	D
7	Sample I	Cu-Gr	8	30	15	D+Gr
8	Sample I	Cu-Gr	12	45	30	D
9	Sample I	Cu-Gr	4	10	45	D+Cu
10	Sample II	Cu	8	45	15	D+Gr
11	Sample II	Cu	12	10	30	D
12	Sample II	Cu	4	30	45	D+Cu
13	Sample II	Gr	4	30	15	D
14	Sample II	Gr	8	45	30	D+Cu
15	Sample II	Gr	12	10	45	D+Gr
16	Sample II	Cu-Gr	12	10	15	D+Cu
17	Sample II	Cu-Gr	4	30	30	D+Gr
18	Sample II	Cu-Gr	8	45	45	D
19	Sample III	Cu	12	30	15	D+Cu
20	Sample III	Cu	4	45	30	D+Gr
21	Sample III	Cu	8	10	45	D
22	Sample III	Gr	8	10	15	D+Gr
23	Sample III	Gr	12	30	30	D
24	Sample III	Gr	4	45	45	D+Cu
25	Sample III	Cu-Gr	4	45	15	D
26	Sample III	Cu-Gr	8	10	30	D+Cu
27	Sample III	Cu-Gr	12	30	45	D+Gr

Six responses parameters were studied in Stage III of experimentation namely MRR, TWR, SR, micro-hardness, recast layer thickness and residual stresses. The experimentation for the study undertaken consisted of 27 trial runs, with each trial having three replications for the responses MRR, TWR, SR, and micro-hardness. For the analysis of recast layer thickness and residual stresses, an average value was considered.

The EDM process trials were conducted in random order such that the results obtained may not be biased due to the effect of noise factors. The machining condition (constant parameters) was similar as in Stage II. MRR, TWR and SR were measured using similar methods explained in Stage II. Micro-hardness was measured using digital micro-hardness tester (Model: MVH-2) coupled with computer. The load applied for indentation was 9 N and dwelling time was set to 14sec. The machining characteristics (response parameters) such as MRR, TWR, SR, micro-hardness and the calculated S/N ratio are presented in Table 4.27 and 4.28. The responses such as residual stress and recast layer thickness and their calculated S/N ratio are presented in Table 4.29.

In Table 4.27 and 4.28 the replication of experimentation is represented by R1, R2 and R3 for each machining response parameters.

The machined surface was analyzed using a by X-ray diffraction method on PANalytical's X'PertPro MPD (Netherlands) (Appendix E). The typical XRD spectra of EDM machined work piece was carried out using Cu- Kα radiations (λ= 1.5406 A^0) to examine the changes on the machined surface using a scan rate of 1^0/ min and range up to 140^0 with the generator setting of 40mA and 45 kV. Micrograph analysis of the work piece was completed using SEM (Make: JSM-6610LV Joel, Japan) at suitable magnification.

The study of recast layer was completed by cutting work piece along cross-section using water cooled precise cutting machine. The Wire-cut EDM was avoided for the cross-sectional wise cut of the work piece, as the heat generated during the process may alter the specimen microstructure. The cross-section of the work piece was polished using various grid size (400 to 3500 grits) emery papers (Make: 3M). The recorded mean values of recast layer thickness and the residual stresses is tabulated in Table 4.29

Table 4.27: Observation table for the MRR, TWR and their calculated S/N ratio

Exp. No.	Output Responses							
	MRR (mg/min)			S/N ratio (dB)	TWR (mg/min)			S/N ratio (dB)
	R1	R2	R3		R1	R2	R3	
1	3.11	2.17	2.14	7.49	0.89	0.72	0.72	2.14
2	12.73	15.82	13.27	22.77	5.9	5.67	5.5	-15.10
3	25.99	20.35	22.06	27.02	10.74	9.87	9.99	-20.17
4	29.14	27	27.33	28.87	3.4	4.35	3.6	-11.60
5	3.14	3.6	3.2	10.35	1.1	0.25	0.57	2.737
6	8.14	8.025	8.12	18.16	0.42	0.38	0.4	7.951
7	17	9.93	14.22	22.08	93.87	78.42	88.3	-38.8
8	30.3	23.86	25.36	28.33	114.4	35.8	77.8	-38.33
9	3.57	2.7	3.2	9.81	12.22	5.43	7.6	-18.96
10	57.99	58.1	58	35.2	2.54	2.12	2.34	-7.38
11	67.34	44.5	54.32	34.5	6.5	7	6	-16.27
12	16.26	15.34	15.4	23.81	0.9	0.74	0.7	2.105
13	11.4	30.45	14.32	23.42	0.65	0.2	0.48	6.376
14	63.9	81.7	77.1	37.26	2.6	0.28	1.6	-4.95
15	21.23	21.45	21.3	26.57	2.1	1.36	1.5	-4.52
16	56.67	74.33	63.89	36.09	145.2	130.2	130	-42.63
17	10.08	11	10.3	20.37	20.33	23.92	22.9	-27.01
18	45.44	70	59.98	34.91	99.6	63.54	79.7	-38.30
19	55.74	57.9	55.86	35.03	33.2	34.17	33.4	-30.52
20	11.97	12.38	11.98	21.65	0.48	0.5	0.4	6.70
21	11.27	8.2	10.1	19.64	6.06	8.67	7.68	-17.5
22	7.057	7.82	7.22	17.31	0.3	0.2	0.2	12.46
23	19.06	15.68	17.97	24.80	0.285	1.43	0.59	0.836
24	7.5	5.59	5.99	15.86	0.09	0.025	0.05	24.34
25	11.2	10.7	10.1	20.53	52.41	13.8	30.7	-31.11
26	5.81	6.2	6.27	15.68	46.7	50.73	47	-33.65
27	13.65	12.57	13.02	22.31	87.64	92.67	88.4	-39.04
	Mean (S/N) = 23.71				**Mean (S/N)= - 13.72**			

Table 4.28: Observation table for the SR and Micro-hardness and their calculated S/N ratio

Exp. No.	Output responses							
	SR (µm)			S/N ratio (dB)	Micro-hardness(HVN)			S/N ratio (dB)
	R1	R2	R3		R1	R2	R3	
1	1.97	1.87	1.97	-5.743	257.5	264	261.3	48.3292
2	3.12	3.19	3.15	-9.975	429.8	302.4	323	50.0415
3	3.58	3.77	3.58	-11.23	241.2	305.2	276.8	48.4838
4	5.22	5.18	5.25	-14.3	501.5	623.7	570.7	55.3201
5	3.17	3.23	3.23	-10.13	520.5	399.6	523.8	54.3190
6	4.52	4.03	4.57	-12.82	327.5	563.3	345.6	52.0501
7	3.11	3.06	3.15	-9.84	334.7	341	330.8	50.5118
8	3.08	3.25	3.01	-9.869	480.5	429	445.2	53.0656
9	3.78	3.8	3.62	-11.44	625.8	653.8	634.7	56.0935
10	7.4	7.35	5.51	-16.66	117.2	91.32	100.4	40.0002
11	9.42	11.1	6.24	-19.23	110.7	71.9	83.3	37.8595
12	5.09	5.64	8.86	-16.57	97.55	94.62	96.3	39.6576
13	5.76	6.17	5.96	-15.51	209.3	185.4	198.1	46.3288
14	7.1	8.56	11.82	-19.43	90.6	95.8	114.6	41.5888
15	5.28	5.6	5.21	-14.59	114.5	114.3	116.35	41.2169
16	7.71	9.75	9	-18.94	53.64	60	62	37.8034
17	18.5	16.6	17.54	-24.90	70.1	67.76	61.43	38.3713
18	8.92	9	8.53	-18.90	134.8	123.5	133.6	42.3008
19	5.79	5.63	5.31	-14.93	210.7	180.5	198.7	45.8199
20	3.92	3.82	3.8	-11.70	189	254.8	230.6	46.5372
21	3.6	3.56	3.56	-11.06	365.3	533.9	423.9	52.1300
22	3.43	3.41	3.25	-10.53	219.1	258.8	240.2	47.9247
23	5	5.89	5.09	-14.55	474.7	477.9	422.5	53.1821
24	4.48	4.25	4.58	-12.94	203	216	218.8	46.5372
25	4.74	4.58	4.33	-13.16	240.5	210.7	222.5	46.9887
26	3.59	3.24	3.66	-10.88	281.4	334.5	319.1	50.0340
27	4.18	4.13	4.16	-12.37	323.7	316.9	300.7	49.9196
	Mean (S/N) = -13.79				**Mean (S/N) = 47.13**			

Table 4.29 Observation table for the residual stresses and recast layer thickness

Exp. No.	Residual stresses (MPa)	Recast layer thickness (µm)
1	50.3	33.727
2	69.6	28.791
3	78.8	89.093
4	(-)31.3	61.978
5	60.5	37.005
6	98.3	125.043
7	69.4	100.368
8	89.5	31.917
9	134.0	28.193
10	59.4	71.726
11	89.2	36.082
12	(-)70.1	10.412
13	(-)41.8	6.103
14	139.3	35.872
15	122.9	23.000
16	(-)89.7	17.942
17	95.2	8.374
18	(-)208.5	39.874
19	30.5	33.166
20	35.9	19.178
21	28.6	6.002
22	21.2	12.409
23	59.3	31.268
24	37.5	26.480
25	60.5	7.674
26	44.9	4.730
27	51.5	6.338

The residual stress measuring condition was as indicated in Stage II {X-ray= Cu-Kα1; (hkl) = (422)}. The X-ray elastic constant for the sample III was calculated as $11.73T^{-1}Pa$ i.e. ($1/2S_2$= 11.73 $T^{-1}Pa$).

Sample calibration of residual stress in Sample III (Trial 23)

The method of measuring residual stress was similar to previously mentioned method, but the representation of the graph was between d-spacing vs. $\sin^2\psi$. This representation of the graph may help to identify the presence of shear stress on the machined surface. In the present study, only absolute normal residual stress was considered.

The diffractometer was then positioned to record the shift of selected peak at positive and negative ψ angles and it measures the value of d-spacing correspondingly as shown in Figure 4.8. The values obtained at various ψ angles are represented in Table 4.30

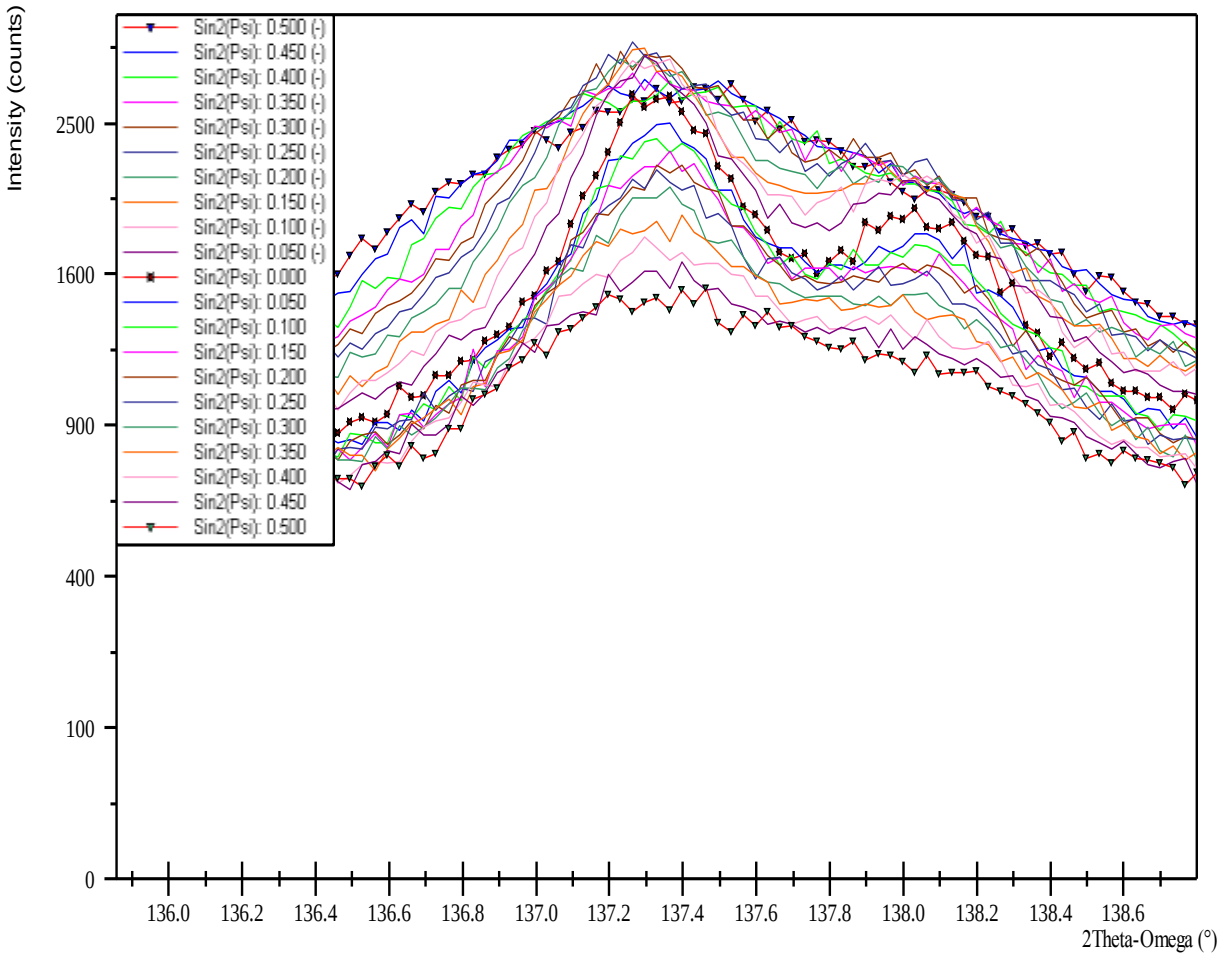

Figure 4.8. Representation of shifts in selected peak at different ψ angles.

Table 4.30 Represents the results of Trial 23 (Sample III) diffracted from (422)

	ψ	Sin ψ	Sin^2 ψ	2θ	d
Positive ψ	0.00	0	0	137.3189	0.827004
	12.92	0.22359036	0.049993	137.3323	0.826967
	18.44	0.3163114	0.100053	137.3192	0.827004
	22.79	0.38735469	0.150044	137.3115	0.827025
	26.57	0.44729085	0.200069	137.3231	0.826993
	30.00	0.5	0.25	137.2946	0.827073
	33.21	0.54770926	0.299985	137.2934	0.827076
	36.27	0.59159111	0.34998	137.2872	0.827094
	39.23	0.63243498	0.399974	137.2616	0.827166
	42.13	0.67081502	0.449993	137.2764	0.827124
	45.00	0.70710678	0.5	137.2924	0.827079
Negative ψ	12.92	0.22359036	0.049993	137.3048	0.827044
	18.44	0.3163114	0.100053	137.295	0.827072
	22.79	0.38735469	0.150044	137.2772	0.827122
	26.57	0.44729085	0.200069	137.2603	0.827170
	30.00	0.5	0.25	137.2458	0.827211
	33.21	0.54770926	0.299985	137.241	0.827224
	36.27	0.59159111	0.34998	137.2161	0.827295
	39.23	0.63243498	0.399974	137.2051	0.827326
	42.13	0.67081502	0.449993	137.1854	0.827382
	45.00	0.70710678	0.5	137.1722	0.827419

The d-spacing and $\sin^2\psi$ for negative and positive ψ tilts are plotted in Figure 4.9.

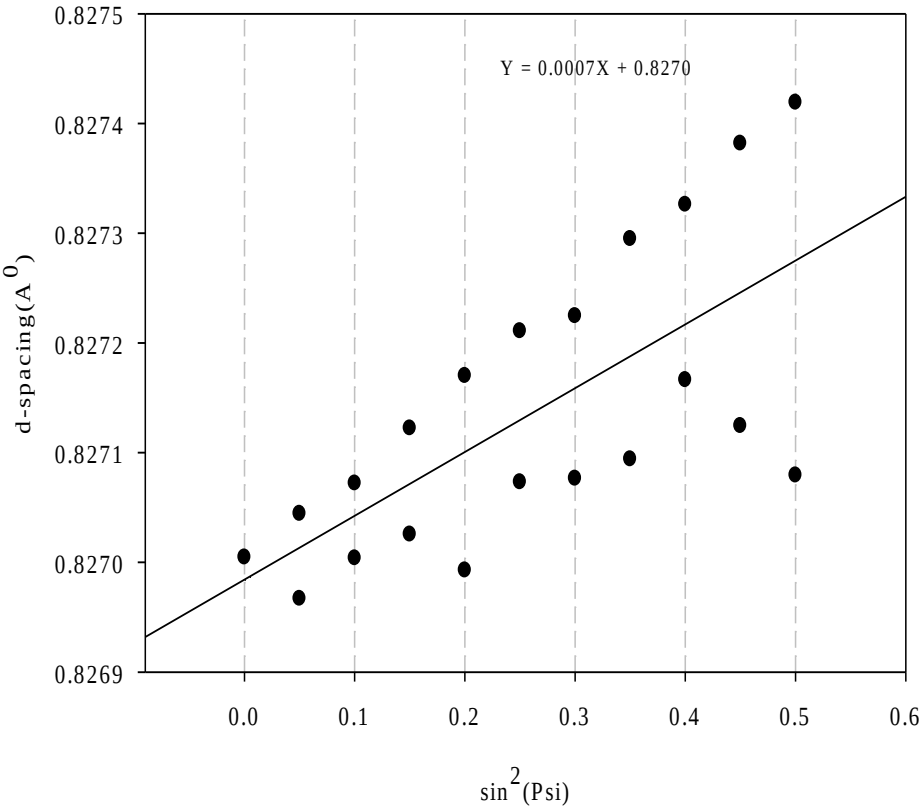

Figure 4.9 The d-spacing vs. $\sin^2\psi$ plot with regression equation of Trial 23

A linear fit was obtained with both values using regression method and is given by equation 4.16.

$$Y = 0.0007X + 0.8270 \tag{4.16}$$

The above equation was compared with residual stress equation 4.12 and σ_φ was calculated to be 59.3 MPa by utilizing the value of elastic constants for the Sample III i.e. 11.73 ($T^{-1}Pa$). The splitting of a graph indicates the presence of shear stress. The shear stress component of equation (1.3) may be utilized for future studies of induced shear stresses.

CHAPTER - 5

ANALYSIS AND DISCUSSION OF THE RESULTS

After conducting the experiments with different process (control) parameters (variables), the values of output responses were recorded as per selected design of experiments methodology (For Stage I: full factorial; Stage II: L_{18} (Fractional factorial) and Stage III: L_{27} (Fractional factorial)). The results were analyzed and are described in this Chapter.

5.1 RESULTS AND DISCUSSION FOR STAGE I

The variation in MRR and TWR for positive polarity is shown in Figure 5.1 and 5.2 respectively (from the Table 4.3).

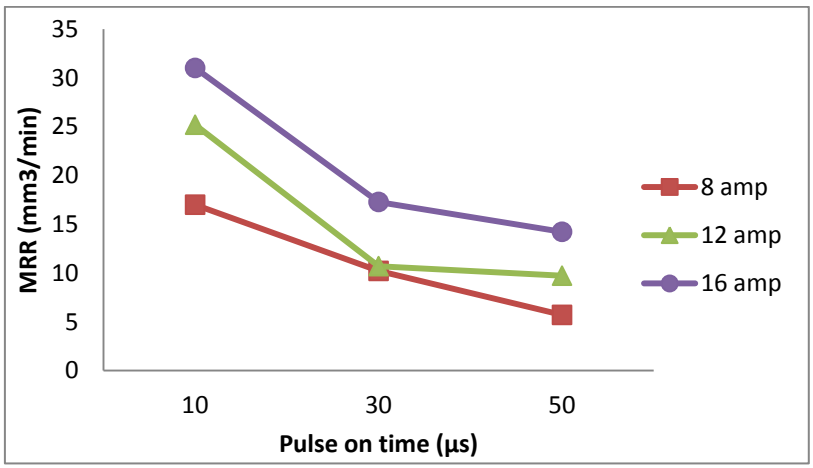

Figure 5.1 Variation of MRR at conventional polarity

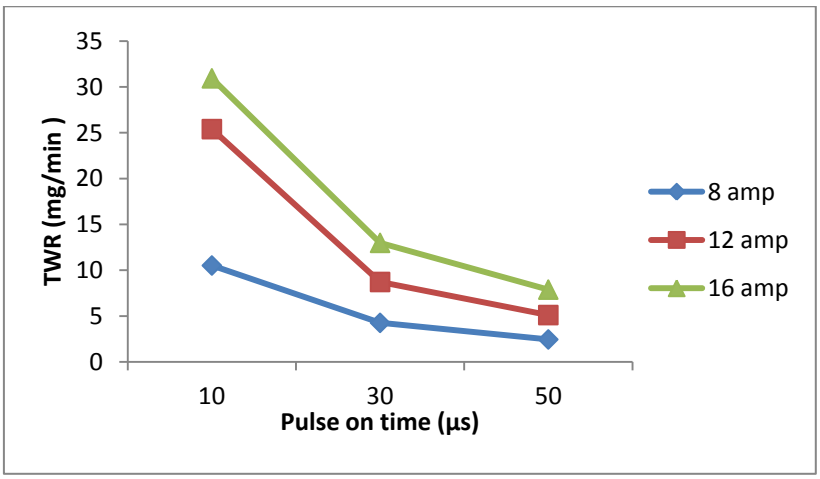

Figure 5.2 Variation of TWR at conventional polarity

The results show that MRR increases with an increase in current as current intensity plays a significant role in intensifying the spark energy. On the other hand, MRR decreases

with increased pulse-on time due to reduction in spark frequency which results in deposition of carbon due to breakdown of dielectric (dielectric used was kerosene). A similar trend was observed in the Trials completed using negative polarity as shown in Figure 5.3 (a).

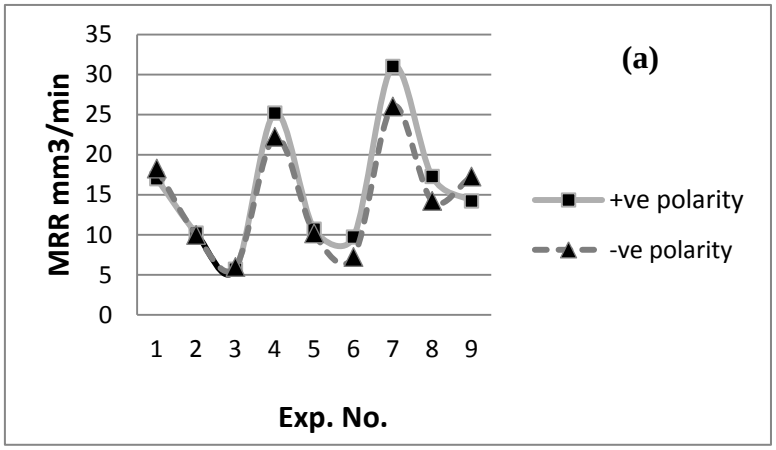

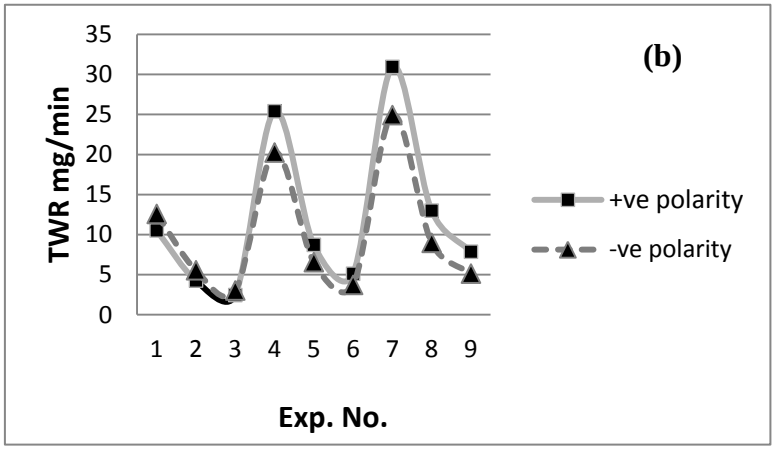

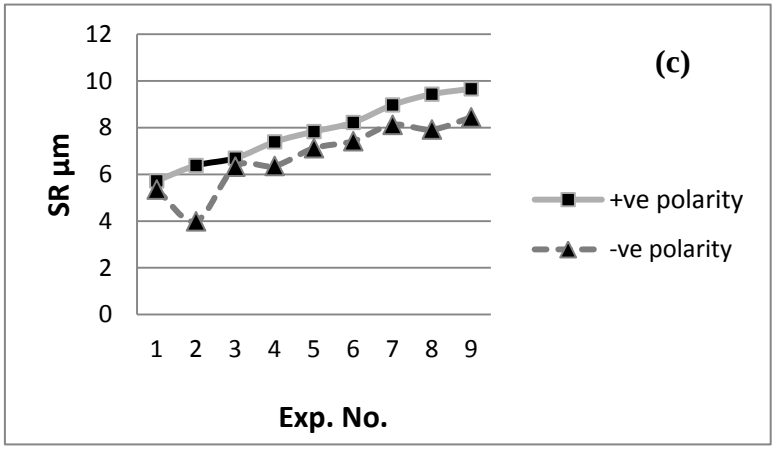

Figure 5.3 Comparison of results for (a) MRR, (b) TWR and (c) SR at normal (+ve) and reverse polarity(-ve)

From the Figure 5.3 (a) maximum metal removal rate (MRR) was observed when the current is set at its highest level, and correspondingly pulse-on time is set at its lowest level. However, this also leads to higher TWR at these settings (Figure 5.3 (b)). It can be concluded that the effect of machining parameters on output responses for composite materials is similar to that of other materials used during EDM. A review of Figure 5.3 (c) shows that surface roughness (SR) deteriorated with the increase in the pulse-on time and current due to increase in pulse energy per spark. This leads to the formation of larger craters resulting in poor surface finish. Reverse polarity with low spark energy leads to a superior surface finish. The setting of machining parameters was decided according to the application of processed components. If higher surface finish was required the machining process parameter should be set at its lowest speak energy, on the other hand the lowest spark energy reduces the MRR and vice versa. For global optimization, the results comprehensively cover all the output responses for optimization.

To overcome these limitations, Lexicographic Goal Programming (LGP), a multiple criteria decision making tool was used. The focus of LGP process is on selecting the best preferred alternatives from a finite set of alternatives under given constraints.

5.1.1 Lexicographic Goal Programming

In multi-objective model, realistic size, especially one with more than two objectives, the range of efficient solution can be enormous (Pareto optimal solution). To obtain useful results, the multi-objective model must be reduced to sequence of a single objective. One such method used to drives the response in the sequential order is Lexicographic Goal Programming which is also known as preemptive optimization [134].

The LGP method begins by prioritizing the goals in order of their relative importance and then optimize by considering the goal hierarchy one at a time in such a way that higher priority is never dishonored by the lowest priority goal. Thus, if $f_1$and f_k denotes the most and the least important function respectively i.e. (f_1>f_2…….f_k), then f_1 is considered to be first objective function, subjected to constraints considered in experimentation. The solution obtained for above formulated model is added as one of the constraint in the second level formulation of a problem to protect the goal hierarchy. The procedure is adopted until the lowest priority objective is considered i.e k^{th} objective and the final solution obtained is the desired solution for multiple objective optimization problem

Preemptive or Lexicographic optimization performs multi-objective optimization by considering objectives one at a time. The most important factor is optimized first; then

second most important is optimized subject to a requirement achieved in first optimal process; and so on. In this method, the objectives are ranked in order of its importance by the designer.

The optimal solution X* is found by minimizing the objective function starting from most important and proceeding according to the order of importance of the objectives. Let $f_1(X)$ and $f_k(X)$ denote the most and the least important objective function. The priority of objective can also be denoted as $f_1(X)>f_2(X)\ldots..>f_k(X)$. The first problem is formulated by considering the first priority i.e. f1(X) and it is represented as

$$Minimize/Maximize f_1(X)$$

Subject to $$g_j(X) \leq 0, j = 1,2, \ldots\ldots, m$$

And its solution X_1^* and $f^*_1=f_1(X_1^*)$. In second problem, the formulation includes the optimal value achieved in first stage of optimization and formulated as below:

$$Minimize/Maximize f_2(X)$$

Subject to $$g_j(X) \leq 0, j = 1,2, \ldots\ldots, m$$

$$f_1(X_1^*) = f_1^*$$

The solution of this problem is obtained as X_2^* and $f_2^* = f_2(X_2^*)$. This procedure is repeated until all the $f_k(X)$ objective has been considered. The k^{th} problem is given by

$$Minimize/Minimize\ f_k(X)$$

Subject to $$g_j(X) \leq 0,\ \ j = 1,2, \ldots., m$$

$$f_l(X) = f_1^*, \qquad l = 1,2, \ldots\ldots, (k-1)$$

The final solution obtained at the end (i.e. X^*_k) is taken as the desired solution of the original multi-objective optimization problem.

Implementation of LGP on response parameters

The developed non-linear models (Equation 4.6 - 4.11) from Chapter- 4 were used to optimize the results by using LGP technique.

Estimation of optimized results for positive polarity

The goal was identified and ranked in the order of priority. For experiments conducted with positive polarity, TWR was given the least priority (Rough machining). The objective was then written using the following sequence of priority.

$$MRR_{max} > SR_{min} > TWR_{min}.$$

The objective of maximizing MRR was implemented using equations (4.6, 4.7 and 4.8) obtained for positive polarity and these were solved as per the priority sequence using the Simplex method, with constraints subjected to:

$$8 \leq X_1 \leq 16 \text{ and } 10 \leq X_2 \leq 50.$$

A sample calculation is given below to explain the steps used during optimization. The optimization of non-linear equation was completed by using LINGO 9.0 software.

Step 1: For maximizing MRR (Priority 1), the objective function is written using equation (1):

$$Max\ (MRR) = 12.5625 + 1.74937X_1 - 0.818917X_2 + 0.011033{X_2}^2;$$

Subjected to $8 \leq X_1 \leq 16$ and $10 \leq X_2 \leq 50$

The optimum solution showed that maximum MRR obtained was 32mm^3/min with current set at (X_1 =16Amp) and pulse on-time set at (X_2=10µs). The results obtained are in confirmation with the experimental results within the acceptable range for error.

Step 2: The next priority was to minimize the SR without degrading the first priority. The optimal result obtained was 32mm^3/min. In second step, the value obtained in first step should not be degraded, hence equation (4.6) can be re-written using the optimal MRR solution as

$$12.5625 + 1.74937X_1 - 0.818917X_2 + 0.011033{X_2}^2 \geq 32$$

After considering the constraints, the most optimal solution that minimizes SR is X1 = 15.744Amp, (~16Amp) and X_2 = 10µs. This would results in an SR of 8.87µm.

Step 3: During the third step, the least priority (minimize TWR) was considered. The MRR should not be less than 32mm^3/min and SR should be not more than 8.87 µm. The Goal Programming formulation can be written as

$$Min\ (TWR) = -1.27208 + 2.84719X_1 - 0.624292X_2 - 0.0469062X_1 * X_2 + 0.0126417{X_2}^2$$

The above equation is subject to

$$12.5625 + 1.74937X_1 - 0.818917X_2 + 0.011033{X_2}^2 \geq 32 \quad \text{and}$$

$$2.07125 + 0.4125X_1 + 0.047X_2 - 0.000875X_1 * X_2 - 0.00002625{X_2}^2 \leq 8.87;$$

with constraints as $8 \leq X_1 \leq 16$ and $10 \leq X_2 \leq 50$

The optimum solution obtained after 53 iterations were X_1= 15.74Amp (~16Amp) and X_2= 11.75 µs (~10µs). TWR, thus obtained in this case was 29.28 mg/min. Table 5.1 shows the sensitivity analysis of the above model to identify the range in which the optimized results remains unchanged. Since MRR was given the highest priority in this case, the optimal solution represents the useful settings for rough machining.

Table 5.1: Sensitivity analysis

Objective Coefficient range		
Variable	Allowable increase	Allowable decrease
X_1	-19.03094	Infinity
X_2	0.3312822	-1.211636
Right hand side Ranges		
Constraints	Current RHS value	Allowable increase	Allowable decrease
MRR (1st priority)	32	0	0
TWR(2nd priority)	8.87	0	0

A similar calculation was done for finish machining by changing the order of priority represented as:

$$SR_{min} > MRR_{max} > TWR_{min}$$

Using the same procedure as described above, the optimum results obtained for TWR after 59 iterations was 12.77mg/min with X_1 at 8Amp and pulse on-time at 10µs. On

comparing both the priority sequences, there was approximately 50% and 67% reduction in setting of X_1 and X_2 respectively.

Estimation of optimized results for negative polarity

The primary reason for machining the workpiece using negative polarity to achieve a lower SR. Thus, objective function in this case is $SR_{min}>MRR_{max}>TWR_{min}$

The above objectives were input as priority tool in equations (4.9- 4.11). The optimal results obtained after 30 iterations suggest that X_1 be set at 8Amp and X_2 be set at 10µs. Using the same logic, if the objective is $SR_{min}>TWR_{min}>MRR_{max}$, then the optimum results obtained after 50 iterations suggested that X_1 to be set at 8Amp and X_2 be set at 30µs. For negative polarity, the process parameters show no change in X_1 but an increase by 67% in X_2.

The results show that if higher MRR is the desirable output, positive polarity should be used. The optimal solution in such a case would be to set the current at 16Amp and pulse-on time at 10µs. However, for finishing operations (SR_{min}), the current should be set at 8Amp and pulse on-time at 10µs. The results showed that MRR achieved with negative polarity is lesser as compared to positive polarity, and the reverse was true for SR.

The optimal results for parts machined using negative polarity and having priority setting for responses as SR>MRR>TWR reveals that current be set at 8Amp and pulse-on time at 10µs. If the priority is changed to SR>TWR>MRR, the current setting should remain at 8Amp and the pulse-on time should be increased to 30µs. The results show that if MRR is placed as 2^{nd} priority instead of TWR, the surface roughness obtained will be of higher magnitude.

5.1.2 Thickness of the Recast Layer

The work piece machined using the positive polarity was evaluated for the thickness of recast layer as this machining condition gives a clear view of the recast layer formation due to high spark energy. The machined composite was cut vertically to examine the recast layer thickness from the cross section of specimen.

The recast layer was measured using an optical microscope assisted with inbuilt MIAS 4.0 (Metallurgical Image Analysis system) software and is given in Table 5.2. The thickness of recast layer increases with increase in spark energy and results in a more wave-like morphology, voids due the flow of molten material.

Table 5.2: Mean thickness of recast layer (µm)

Parameter setting		Current		
		8 Amp	12 Amp	16 Amp
Pulse-on time	10 µs	40.3	41	44.3
	30 µs	42.7	43.2	48
	50 µs	48.1	49.4	52.3

It was also observed that the few reinforced particle dislodged with molten metal result in non-uniform distribution in matrix, hence may reduce the service life of the machined work piece (Figure 5.4).

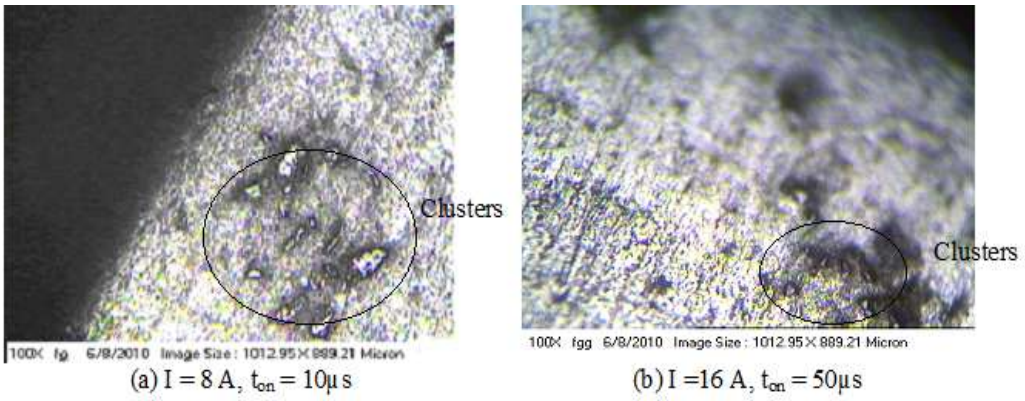

Figure 5.4 Optical micrographs of the recast layers

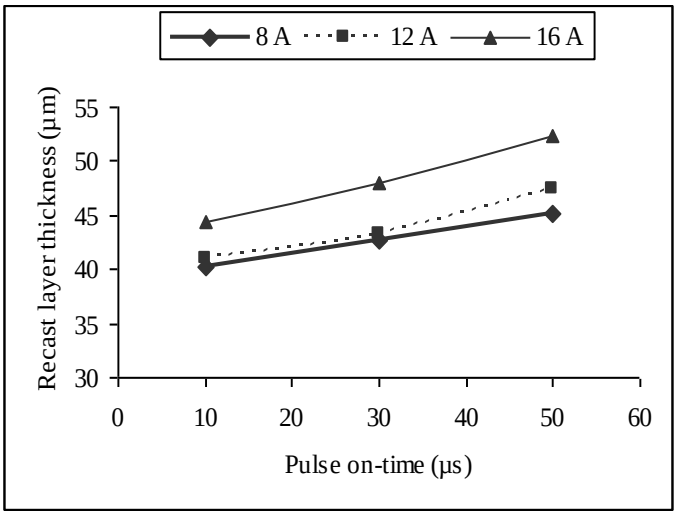

Figure 5.5 Variation of Recast layer thickness with Pulse-on time

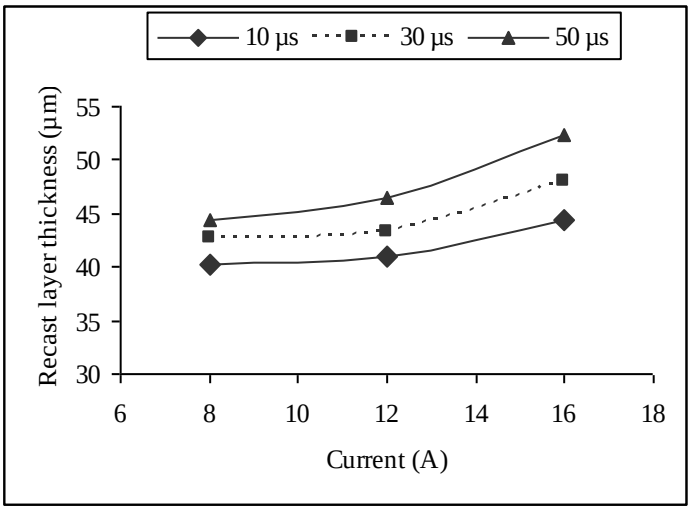

Figure 5.6 Variation of Recast layer thickness with Current

From the plot of the recast layer thickness, (Figure 5.5, 5.6) it can be inferred that there is continuous change in thickness with change in parameter settings. The slope of the response values in the two plots indicates that change in pulse-on time has greater influence on recast layer thickness than current.

The analysis of variance (ANOVA), which is proven statistical technique to measure the impact of the factors on a response, was used to identify significant input parameters affecting the recast layer thickness. The results of ANOVA are given in Table 5.3. The results shows that pulse- on time followed by current significantly affect the thickness of the recast layer thickness.

Table 5.3: Analysis of variance for means of recast layer thickness

Factors	DOF	Sum of Squares	Variance	F-value	p- value
Current (X_1)	2	47.056	23.528	17.29	0.011*
Pulse-on time (X_2)	2	162.282	81.141	59.61	0.001**
Residual Error	4	5.444	1.361		
Total	8	214.782			

**** Most significant, * Significant**

5.2 RESULTS AND DISCUSSION OF STAGE II

The responses in this experimental stage were Residual stresses, MRR and SR. The analysis of results is discussed as follows:

5.2.1 Residual stresses

Analysis of variance (ANOVA) for residual stresses

The analysis of variance (ANOVA) for residual stresses induced into the machined surface was completed and the results are given in Table 5.4.

Table 5.4 Analysis of means for the residual stresses

Factors	Degree of freedom	Sum of Squares	Variance	F-value	P-value	Contribution (%)
W/Pc	1	4204.4	4204.4	9.13	0.023*	10.436
Electrodes	2	3284.0	1641.98	3.57	0.095*	6.586
Pulse off	2	14262.5	7131.27	15.49	0.004*	37.188
Pulse on	2	110.5	55.26	0.12	0.889	(Pooled)
Dielectric	2	6526.1	3263.04	7.09	0.026*	15.623
Current	2	4725.5	2362.75	5.13	0.050*	10.604
Error	6	2762.6	460.44			
Total	17	35875.7				

*** Significant factors**

The factors with a larger value of F-test indicate there significant effect in inducing the residual stresses. Similarly, the p-value indicates the significance level for each factor. The contribution percentage of each input factor was measured by analyzing the F-value and the p-value. From the results, it is clear that pulse-off time is the most significant factor followed by dielectric medium, current, work piece and electrode material. On the other hand, the effect of pulse-on time is negligible. The main effect of various input parameters are presented in Figure 5.7.

For compressive, qualitative and quantitative analysis of EDM process, ANN was used to establish the relationship between input and output parameters and also to understand and predict the process performance.

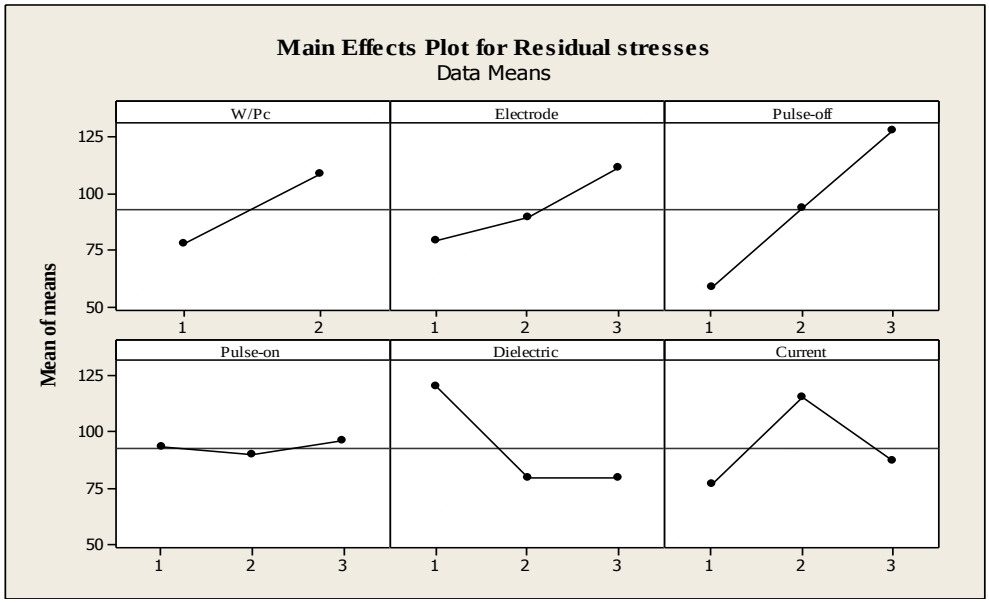

Figure 5.7 Main effect plots for residual stresses

Neural- network based modeling of residual stresses

In the present study, two types of particulate reinforced aluminium MMCs were machined using EDM and a superior and reliable process model was developed using ANN to predict the residual stresses. A features borrowed from the physiology of the brain is the basis for the development of modeling technique known as artificial neural network systems or simply neural networks. A neural network is defined by a collection of parallel processors connected together in the form of a directed graph, organized in such a way that the network structure lends itself to the problem being considered. A network consists of processing element or unit in the network as a neuron, with connections between units indicated by the arc. The flow of information is indicated by the arrowhead on the connections. Figure 5.8 shows the general processing element or neuron model.

Once the net input is calculated, it produces final output passing on to a non-linear filter called activation function. There are several types of activation function used in neural network, but activation function mostly utilized in multilayer network are continuous in nature that varies gradually between the asymptotic values 0 and 1 or -1 and +1 and is given by equation as:

Sigmoid function

$$f(x) = \frac{1}{1+e^{-x}} \qquad \text{Range (0, 1)}$$

Hyperbolic function

$$f(x) = \frac{e^x - e^{-x}}{e^x + e^{-x}} \quad \text{Range (-1, 1)}$$

The identity function (f(x) = x) is available for the output layer neuron.

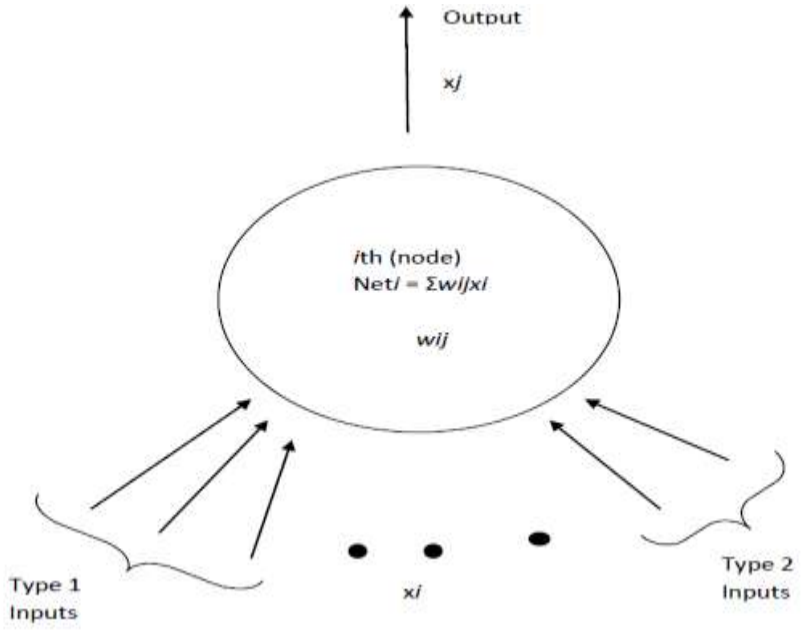

Figure 5.8 Schematic illustration of single neuron in a network. The input connections are modeled as an arrow from other nodes. Each input connection has associated with it a quantity w*ij*, called weight.

The neural network is broadly classified into three basic types namely (i) Supervised, (ii) Unsupervised and (iii) Reinforced as shown in Figure 5.9.

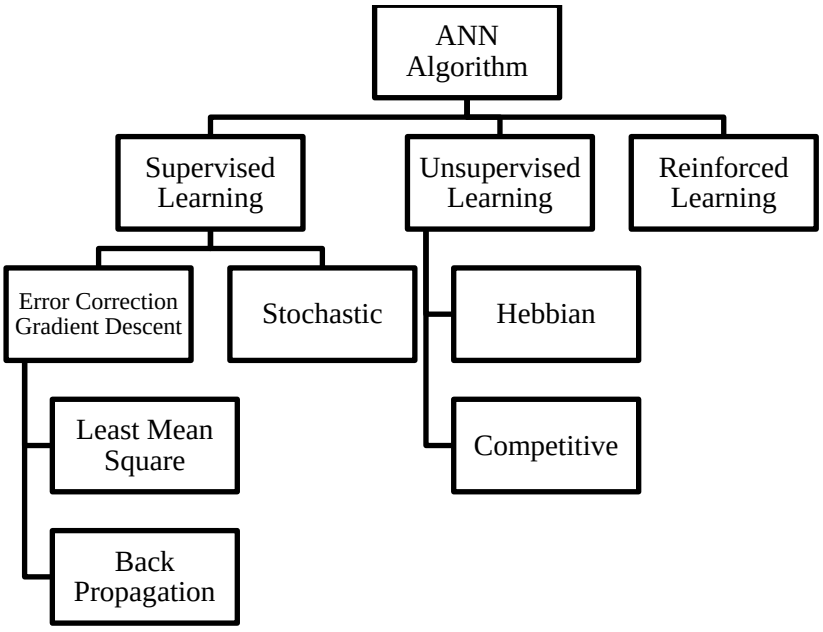

Figure 5.9 Classification of learning algorithm

The back propagation (BP) method has been proven to be the most useful in manufacturing related applications as reported in the literature. The network learns from the predefined set of input-output example pairs by using a two phase propagate-adapt cycle. After the input pattern is applied as a stimulus to the first layer of network units, it is propagated through each hidden layers until an output is generated. This output is then compared to desired output, and an error signal is computed for output nodes.

The difference between the output generated by network model (T_{or}) and the actual output (O_{or}) is given as below:

$$E_r = \frac{1}{2}\sum_{r=1}^{n}(T_{or} - O_{or})^2$$

Based on error signal, a connection weight is updated using BP algorithm. The neural network algorithm used for the modeling was supervised learning, as the results obtained from the experimentation were compared.

The estimation of model in neural network comprise of two stages (i) Training and (ii) Testing of the network with the experimental machining data. The network consists of one input, two hidden and one output layer and was assumed to be 6-n_1-n_2-1, where six are the input factors with seventeen neurons in the input layer, n_1, n_2 neurons in the hidden layer and one neuron in the output layer. The number of neurons in the hidden layer is determined by trial and error as there is no general methodology available to estimate.

The criterion is to select a minimum number of nodes which would not affect the performance of network by minimizing the storage memory for synaptic weight. When the number of hidden nodes is equal to the number of training patterns, the learning could be fastest, but on the other hand, it loses the generalization capabilities. The error criterion adopted in the present model is a sum of square error.

The procedure followed is outlined as under (Appendix D, Figure D.1)

- Divide the data set randomly in the training set and the testing set groups in appropriate percentage.
- Apply different network architecture to train the network.
- Evaluate the network architecture by comparing the normalized importance of each parameter obtained from the network with the ANOVA output results and percentage relative error.

- Test the network for its generalized ability by using group of data classified for testing.

The experimental data given in Table 4.9 consists of 18 groups with the levels of input parameters/factors and residual stresses as output response. Out of these, 12 group of data (given by Trial # 1,2,3,5,7,8,11,12,13,15,16,18) were randomly selected (about 67%) of all data groups were associated with training of network and the remaining 6 groups of data (represented by Trial # 4,6,9,10,14,17) or 33% of data were used to test the network. For training of network, a commercial window based ANN software, IBM-SPSS was used. The number of the network was constructed, and the best network was selected based on minimum absolute relative error. This was interestingly achieved with 1^{st} and 2^{nd} hidden layer having 9 and 7 nodes respectively. The learning rate and the momentum values were selected as 0.001 and 0.7 respectively. The summarized neural network architect for the prediction of residual stresses is shown in Figure 5.10.

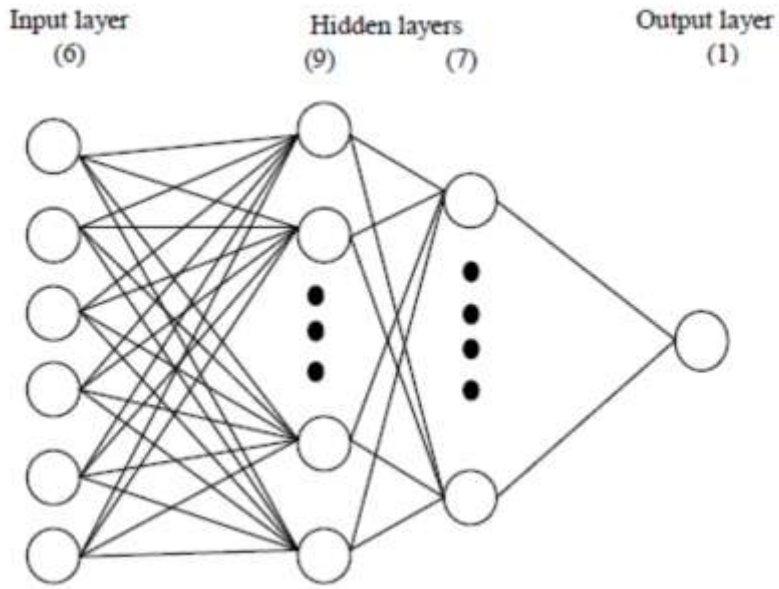

Figure 5.10 Neural network architect for residual stresses calculation

The weights were updated and the activation function in hidden layers and output was selected as hyperbolic tangent and identity function respectively. It was observed that the outcome of network directly depends upon the weight distribution done randomly. Thus, the network was trained repeatedly to update the weight until the hierarchy of normalized importance of each input parameter in the network showed consistency with the results obtained during ANOVA analysis (Table 5.4). The results of neural network model are shown in Table 5.5.

Table 5.5 Comparison of ANN with experimental results

Experiment No.	Experimental response	ANN response	% Relative error
Training data			
1	63.3	61	3.633491
2	74.6	75.4	1.07239
3	82.8	82.6	0.241546
5	63.6	64.5	1.41509
7	61.4	61.7	0.4886
8	78.5	78.1	0.509554
11	104	104.2	0.19231
12	78.1	80.1	2.56082
13	41.8	43.2	3.34928
15	132.9	132	0.677201
16	77.7	76.2	1.930502
18	231.5	233.1	0.69114
Testing data			
4	36.3	56.6	55.3747
6	110.3	91.9	16.68178
9	129.0	142.1	10.155
10	70.4	74.9	6.39205
14	149.3	142.4	4.621567
17	89.2	78.6	11.88341

The normalized importance bar chart (Figure 5.11) shows the importance of the factors for allocation of weights in neural network architecture sorted in the descending order. It appears from the chart that, variables related to pulse-off time is the most significant factor that affects the residual stresses while ED-machining followed by type of dielectric medium used. The other factors have relatively smaller significance with pulse-on time having the least significance. The summary of selected network and the normalized importance of each factor are shown in Appendix D.

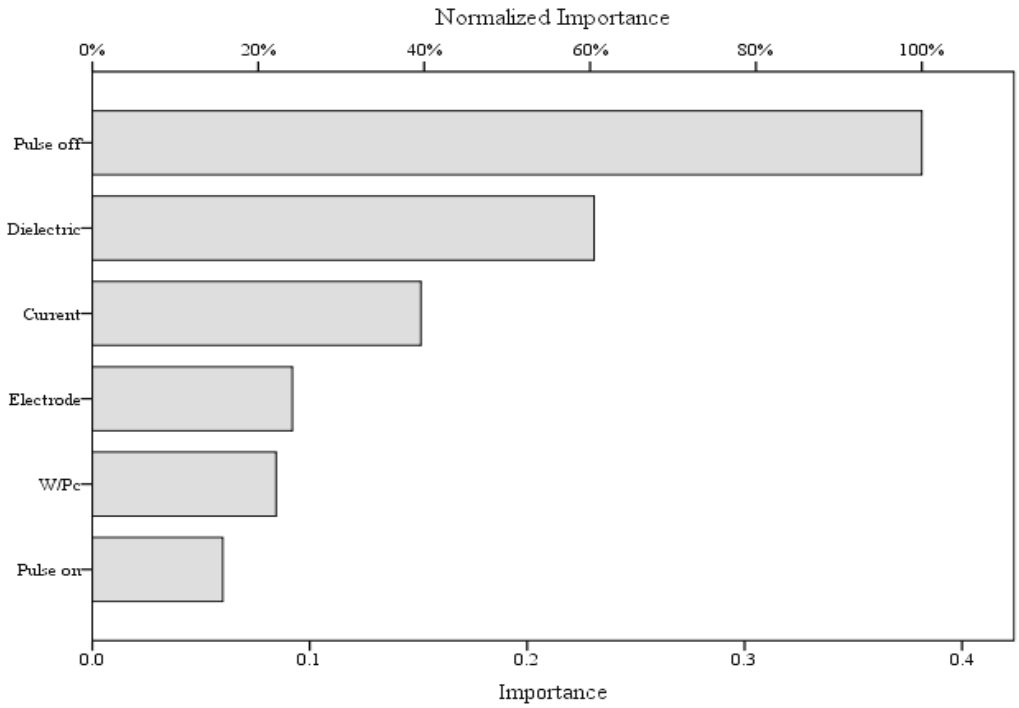

Figure 5.11 Normalized importance of each input factor on the residual stresses

The performance of ANN was measured with absolute % relative error between the output of network with the experimental value and was calculated by equation 5.1.

$$|\%\ Relative\ error| = \frac{Experimental\ value - predicted\ value}{Experimental\ value} X100 \qquad (5.1)$$

Figure 5.12 shows that the predicted data of network is remarkably close to the experimental data results in verifying the network generalization capabilities.

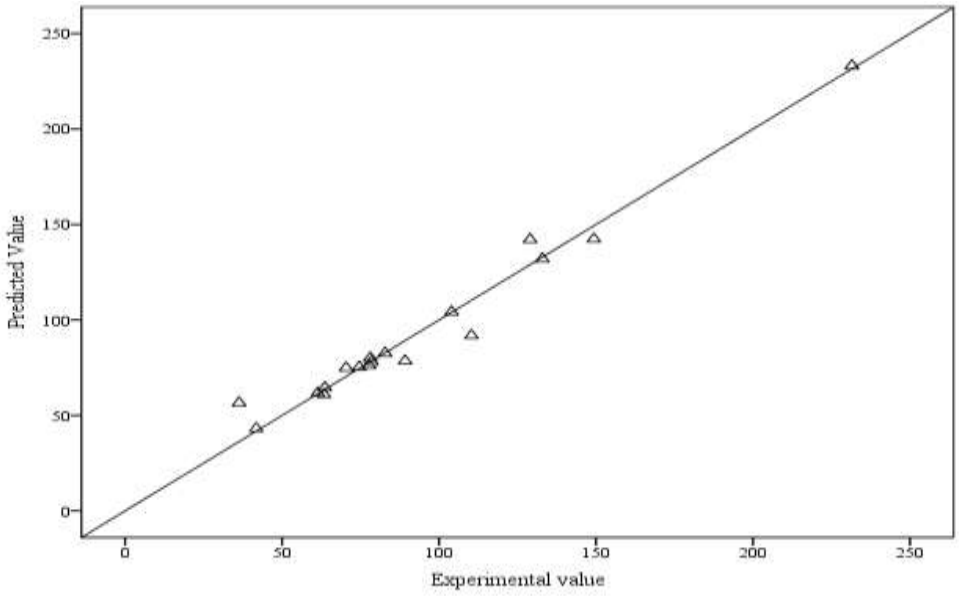

Figure 5.12 Comparison of ANN results and the experimental outputs

Other statistical tools such as paired-sample t-test and correlation were also completed to measure the amount of association between the experimental value and predicted value obtained from the network. The results are summarized in Table 5.6 and 5.7.

Table 5.6 Correlation between the experimental value and ANN model value

Variables	N	Mean	Std. deviation	Std. error mean	Correlation	Significance
Experimental value	18	93.039	45.9384	10.8278	0.984	0.000
ANN model value	18	93.266	44.9631	10.5979		

Table 5.7 Paired sample t- test (Experimental value and ANN model value)

Pair (N=18)	**Paired Differences**					t-test	Significance
	Mean	Std. Deviation	Std. Error Mean	95% Confidence Interval of the Difference			
				Lower	Upper		
Experimental and ANN values	-0.227	8.1328	1.9169	-4.2717	3.8170	-0.119	0.91

Table 5.6 shows that experimental value and the predicted value are positively correlated, r (N=18) = 98.4%. Also, from Table 5.7, it can be concluded that the mean residual stresses value increased from the experimental value to the predicted value by -0.227, t (17) = -0.119, p=0.907 > 0.05. The experimental value and the results obtained from ANN model are not significantly different at 95% confidence range.

Microstructure Analysis

For understanding the topography of EDM machined surfaces in relation to the residual stresses induced during machining, an SEM study was completed on select samples for both materials used in this study. Figures 5.13 and 5.14 shows the comparative residual stresses induced in Sample I and Sample II respectively. Figure 5.13 (a) shows the traces of pull-out of particulate and micro-shrinkage which was less deep. The pattern of machined surface shows the residual stresses of lesser magnitude.

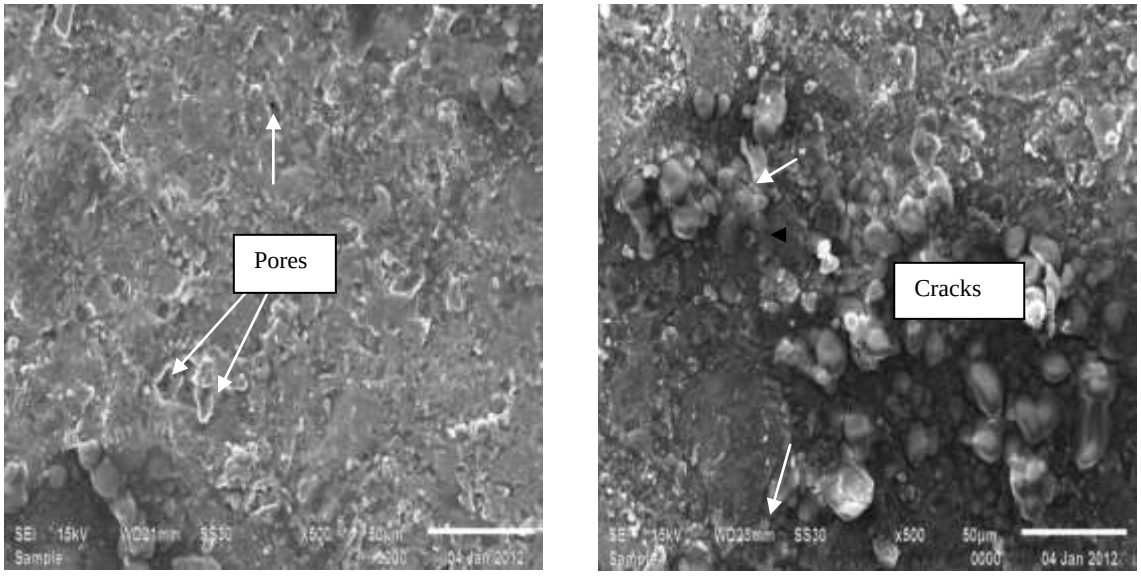

Figure 5.13 EDM machined specimen of Sample I

(a) Residual stresses = 36.3 MPa obtained for Trial 4 (I= 8 Amp; t_{on}= 45 µs; t_{off}= 15 µs, e= Gr, d= EDM oil + Cu Powder).

(b) (b) Residual stresses =129 MPa obtained for Trial 9 (I= 8 Amp; t_{on}= 10 µs; t_{off}= 45 µs, e= Cu-Gr, d= EDM oil + Gr powder).

Similarly, the maximum residual stresses for Sample I was obtained in Trial 9 shown in Figure 5.13 (b) (I= 8 Amp; t_{on}= 10 µs; t_{off}= 45 µs, e= Cu-Gr, d= EDM oil + Gr powder).

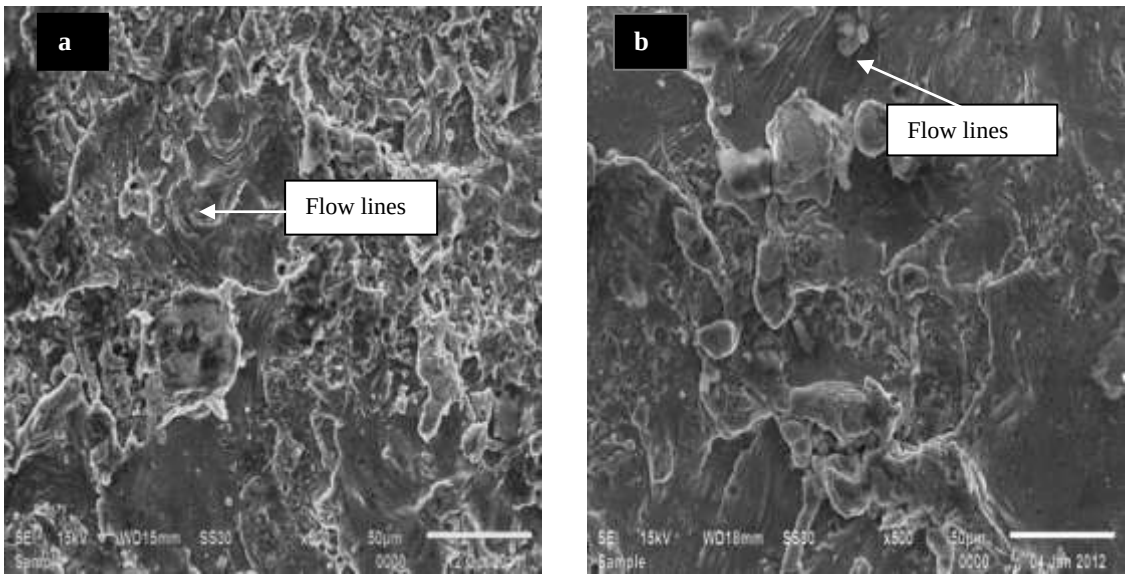

Figure 5.14 EDM machined specimen of Sample II

(a) Residual stresses = 41.8 MPa obtained for Trial 13 (I= 4 Amp; t_{on}= 45 µs; t_{off}= 15 µs, e=Gr, d= EDM oil + Gr powder).

(b) Residual stresses =231.5 MPa obtained for Trial 18 (I= 8 Amp; t_{on}= 45 µs; t_{off}= 45 µs, e= Cu-Gr, d= EDM oil)

In Figure 5.14, the expelled material is re-solidified on the work piece in the form of globules leading to the formation of micro cracks due to high energy level resulting in larger residual stresses. Figure 5.14 (a, b) shows the minimum and maximum residual stresses for Sample II (10vol%SiC-5vol% quartz/Al matrix composite). The minimum residual stresses was obtained for Trial 13 (I= 4 Amp; t_{on}= 45 µs; t_{off}= 15 µs, e=Gr, d= EDM oil + Gr powder) and maximum residual stresses was obtained for Trial 18 (I= 8 Amp; t_{on}= 45 µs; t_{off}= 45 µs, e= Cu-Gr, d= EDM oil). Both micrographs show the flow line of molten metal. However, these flow lines are more predominant in Figure 5.14 (b) due to severe melting leading to high residual stresses.

The SEM pictures of the machined surface represent the comparison of surface having highest and lowest residual stresses. This SEM analysis of the sample also reflects the surface properties of the machined surface such as surface roughness, porosity, crack etc. The machined surface in both the composites has a porous structure which shows that the metal removal process was a result of melting, evaporation and spalling [135].

Further, the surface topography reveals that the residual stresses may be caused due to metal flow, globules pockmarks, voids and crack. For Sample I, the flow lines of molten matrix are not as severe as observed in Sample II due to a low coefficient of thermal expansion and the density of reinforced particulate, but there is a formation of pores and voids in the micrograph.

The Sample I (65vol%SiC/A356.2) does not show large flow lines phenomena on the machined surface as seen in Sample II (10vol%SiC-5vol% quartz/Al composite). This could be due to low heat expansion coefficient and high density of reinforced particles in Sample I and thus do not experience high thermal gradient and volume change during EDM. The typical XRD spectra of un-machined and EDM machined work piece was carried out for both materials using Cu-Kα1 radiations (λ= 1.5406 A^0) to examine the changes on the machined surface using a scan rate of 1^0/ min and range up to 140^0 with the generator setting of 40mA and 45 kV. The resulting scans are shown in Figure 5.15 and 5.16. The lower most plots in both figures are for the un-machined surface and the other two plots are for trials which exhibited lowest and the highest residual stresses. The XRD of machined surface in Figure 5.15 and 5.16 indicates the formation of new phases. The peak intensity reduces as the residual stresses magnitude increases due to dislocation of planes of atoms.

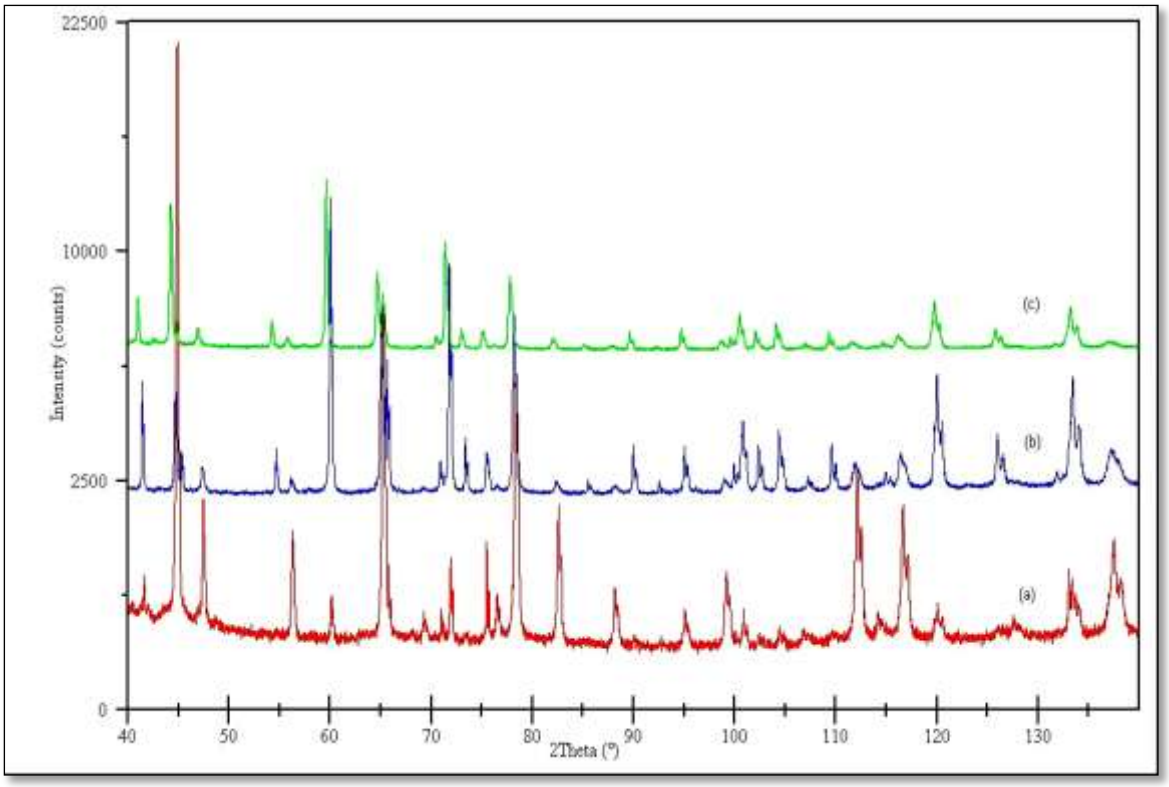

Figure 5.15 XRD spectra of Sample I (a) before EDM (b, c) ED machined surface with residual stresses 36.3MPa, 129MPa respectively.

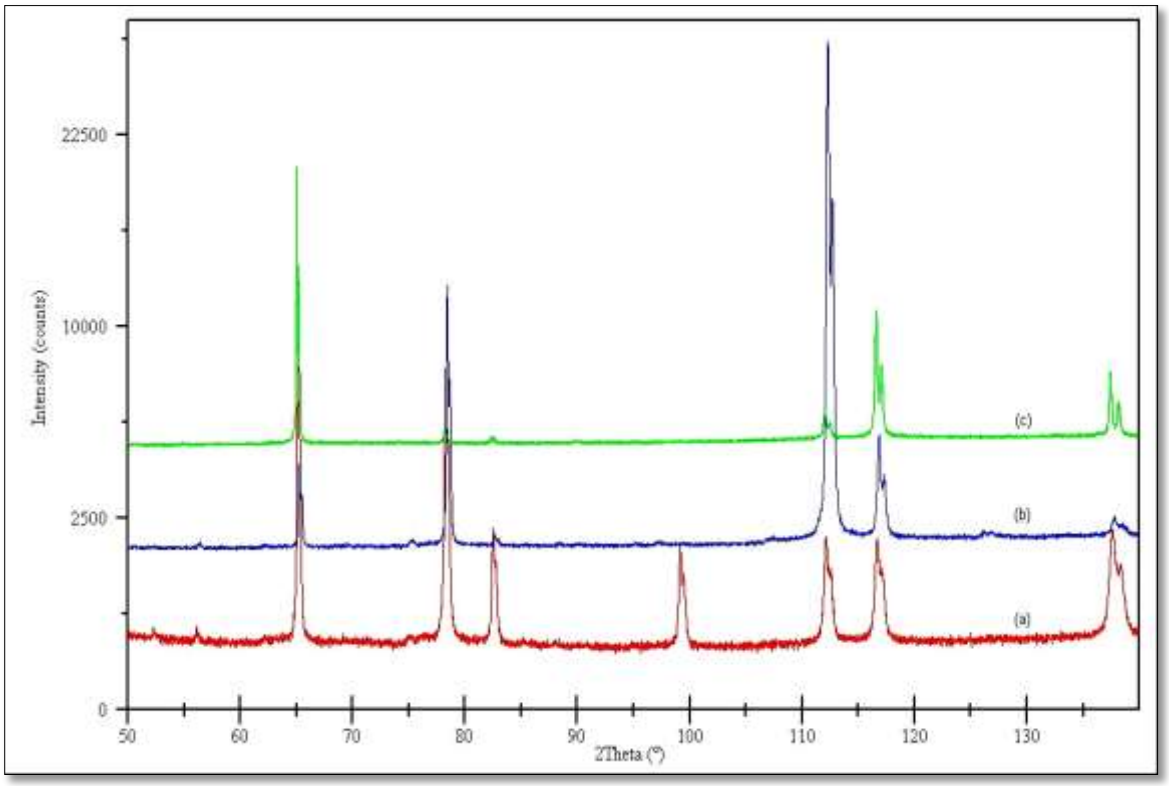

Figure 5.16 XRD spectra of Sample II (a) before EDM (b, c) ED machined surface with residual stresses 41.8MPa, 231.5MPa respectively.

5.2.2 Metal Removal Rate (MRR) and Surface Roughness (SR)

Analysis of variance of MRR and SR

The results for MRR and SR were analyzed using Analysis of Variance (ANOVA). Summary of ANOVA for MRR and SR is provided in Table 5.8, 5.9 respectively. Comparing the data F-values with the F-critical at a confidence level of 95%, the significant factors were identified. The higher the F value more is the effect of the parameter on the response.

Table 5.8 Analysis of variance for MRR

Factors	Degree of freedom	Sum of Squares	Variance	F-value	P-value
Work piece	1	1977.26	1977.26	10.50	0.018*
Electrodes	2	62.50	31.25	0.17	0.851
Pulse-off	2	435.50	217.75	1.16	0.376
Pulse-on	2	1448.53	724.26	3.85	0.084*
Dielectric	2	10.67	5.33	0.03	0.972
Current	2	1494.86	747.43	3.97	0.080*
Error	6	1129.73	188.29		
Total	17	6559.04			

*** Significant factor**

Table 5.9 Analysis of variance for SR

Factors	Degree of freedom	Sum of Squares	Variance	F-value	P-value
Work piece	1	50.0333	50.0333	80.99	0.000*
Electrodes	2	1.9590	0.9795	1.59	0.280
Pulse off	2	0.9768	0.4884	0.79	0.496
Pulse on	2	4.6520	2.3260	3.77	0.087*
Dielectric	2	22.5037	11.2519	18.21	0.003*
Current	2	10.6571	5.3286	8.63	0.017*
Error	6	3.7064	0.6177		
Total	17	94.4886			

*** Significant factor**

ANOVA for MRR shows that current and pulse-on time contributed significantly to change in MRR. Also, the change in work piece material resulted in a significant effect on MRR. In relative comparison, dielectric, pulse off time and electrode material had no significant effect. It was observed that with the increase in pulse-on time and current the MRR increases significantly due to the fact that increased current and pulse-on time increases the amount of spark energy and due to increased heat input the temperature rises resulting in higher melting or evaporation rate of the work piece. Surface roughness of the machined surface was significantly influenced by factors like powder concentration, current and pulse-on time. Also, the two materials showed significantly different SR. The roughness increased with the increase in current and pulse-on time whereas addition of powder in dielectric improved the finish. Increase in current or pulse-on time increases the spark energy which leads to the formation of bigger and deeper craters leading to rough machined surface. Addition of powder consistently improved the finish of the machined surface as the addition of metallic powder; the spark becomes more uniform with increased frequency and widening of the spark gap. Widening of the spark gap reduces the breakdown voltage in relative comparison to conventional EDM. This reduces the magnitude of impact force resulting in small and shallow craters lowering the surface roughness [136]. The main effect plots of these responses are given in Figure 5.17 and Figure 5.18. The figure shows the variation in the responses plotted on y-axis with change in parameter settings.

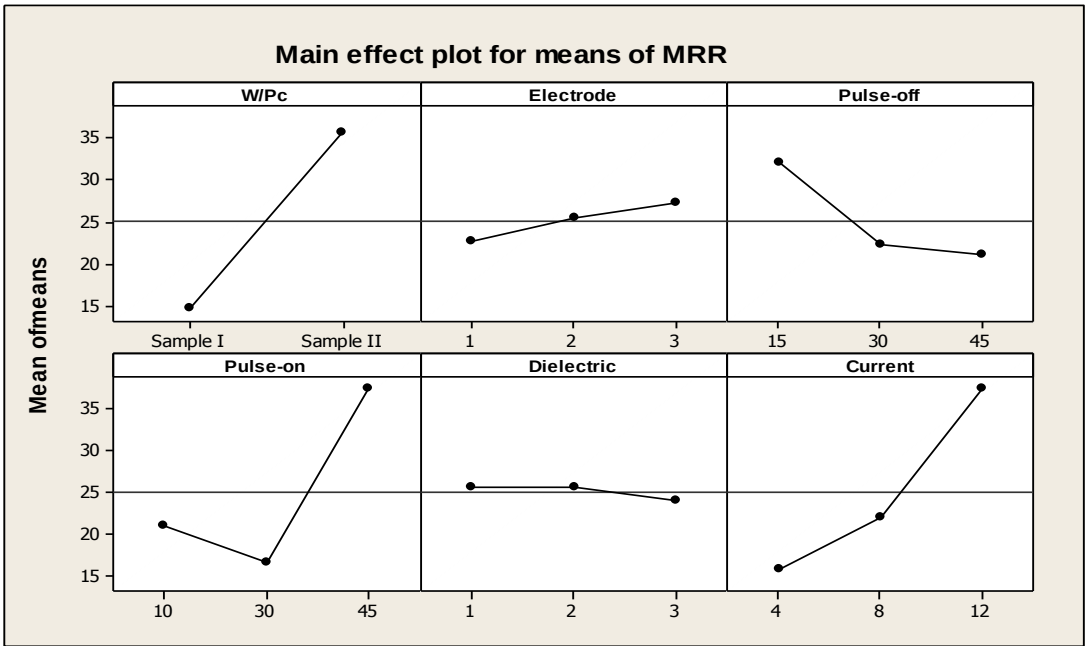

Figure 5.17 Main effect plots for MRR

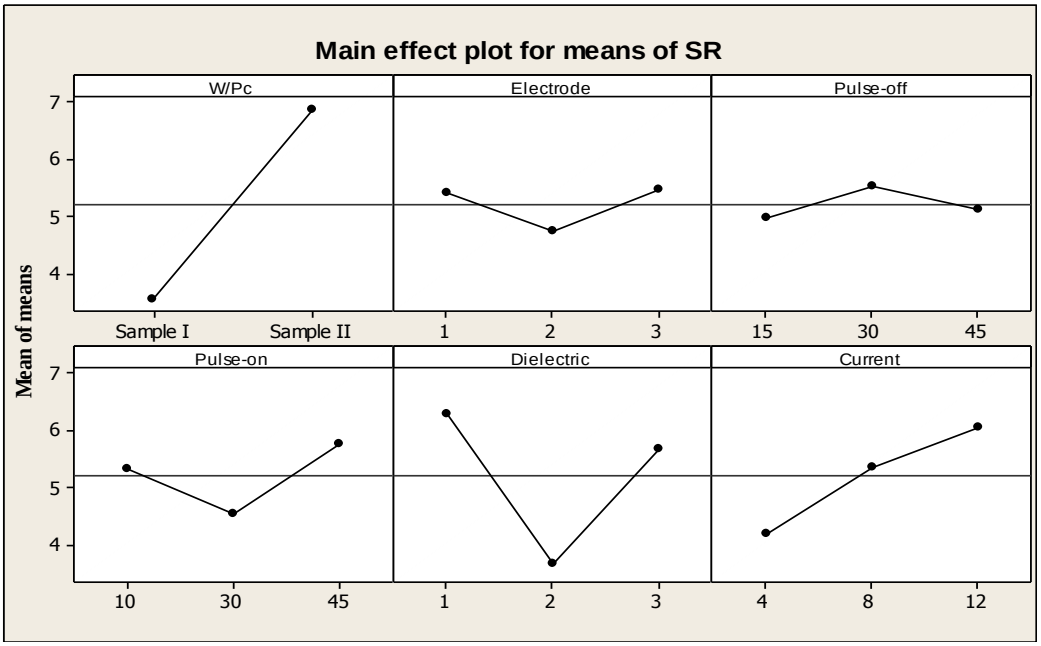

Figure 5.18 Main effect plots for SR

5.2.3 Results of Analytical hierarchy processes (AHP)

The results corresponding to the evaluation of global optimality (*Section 4.3.4*) of responses such as Residual stresses, MRR and SR by using AHP, a multiple criteria decision making technique reveal that the maximum overall weight or composite performance score for Sample I was obtained for T4 as given in Table 4.22 (*Section 4.3.4*) which corresponds to Trial number 4 in the original L_{18} array (See Table 4.7, Section 4.3.3) which was performed with graphite electrode, dielectric mixed with Cu powder, pulse-off and pulse-on time of 15 µs, and 45 µs respectively and current of 8 Amps. Similarly, the maximum overall weight or composite performance score for sample II as obtained in Table 4.23 (*Section 4.3.4)* corresponds to Trial 13 of the original L_{18} array. This Trial was completed with graphite electrode, dielectric mixed with graphite powder, pulse-off and pulse-on time of 15 µs and 45 µs respectively with a current setting of 4 Amp. So the solution that globally optimizes residual stresses, MRR and SR for the two types of MMCs used in the experiment are given by the following.

Parameter	***Sample I (65vol%SiC/A356.2)***	***Sample II (10vol%SiC-5vol% quartz/Al)***
Electrode	Graphite	Graphite
Dielectric mixed with	Copper powder	Graphite Powder
Pulse-off time	15 µs	15 µs
Pulse-on time	45 µs	45 µs
Current	8 Amp	4 Amp

5.3 RESULTS AND DISCUSSION OF STAGE III

The responses in this experimental stage were MRR, TWR, SR, micro-hardness, residual stresses, and recast layer thickness. The analysis of results is discussed as follows:

5.3.1 Analysis of variance of S/N ratio for MRR, TWR, SR and Micro-hardness

The S/N ratio was obtained for MRR, TWR, SR and micro-hardness (responses) measured after each experiment with repetitions. The responses were analyzed using statistical analysis of variance (ANOVA) of S/N ratio using Taguchi's methodology. From the objective, larger-the-better type of S/N ratio was applied for transforming the raw data for MRR and micro-hardness, as larger values of MRR and micro-hardness are desired. Whereas, smaller-the- better characteristic of S/N ratio was applied to TWR and SR process parameters. The ANOVA based on raw data affects the average response rather than reducing variation. But ANOVA based on S/N ratio takes in account both these aspects.

The Analysis of Variance (ANOVA) for responses is presented in Table 5.10. Table 5.10 also shows the significant parameters based on F-test. The purpose of ANOVA was to establish the contributing factors to estimate MRR, TWR and SR**.**

Table 5.10 Analysis of variance for S/N ratio of responses

Factors	dof	Sum of Squares(SS)			Variance (V)			F-Value		
		MRR	TWR	SR	MRR	TWR	SR	MRR	TWR	SR
Work piece	2	596.93	42.27	291.2	298.466	21.23	145.51	40.2**	0.37	23.5**
Electrode	2	35.46	6603.91	9.809	17.729	3301.9	4.904	2.38	57.13**	0.78
Current	2	690.01	1621.97	6.166	345.006	810.98	3.083	46.4**	14.03**	0.49
Pulse-on	2	290.26	17.10	22.75	145.129	8.55	11.375	19.5**	0.15	1.81
Pulse-off	2	44.24	76.09	7.485	22.119	38.04	3.742	2.97*	0.66	0.60
Dielectric	2	28.04	14.29	4.871	14.022	7.14	2.435	1.88	0.12	0.39
Error	14	104.16	809.22	87.98	7.440	57.80	6.285			
Total	26	1789.1	9185.04							

**** Most significant at (99%) *Significant at (90%)**

The ANOVA for MRR shows that work piece material, peak current and pulse duration (on and off time) affected MRR. During pulse-off duration, the entrapped reinforced particles or debris between the two electrodes are flushed out with the pressure of

dielectric fluid. ANOVA results for TWR showed tool material and current as the significant factors. Cu-Gr electrode showed higher tool wear as compared to Cu and Gr electrode due the easy disintegration of less compactly packed particles. Similarly, for SR, no process parameter showed any effect on SR except the work piece material. 65vol%SiC/A356.2 (Sample I) showed the lowest roughness as compared to the other two materials (Sample II, III) used in the study. The concentration of reinforced particles plays a major role in dispersing the spark energy channel resulting in shallow and hence lowers SR. The main effect plot represents the variation of MRR, TWR and SR with input parameters as shown in Figure 5.19-5.21 respectively.

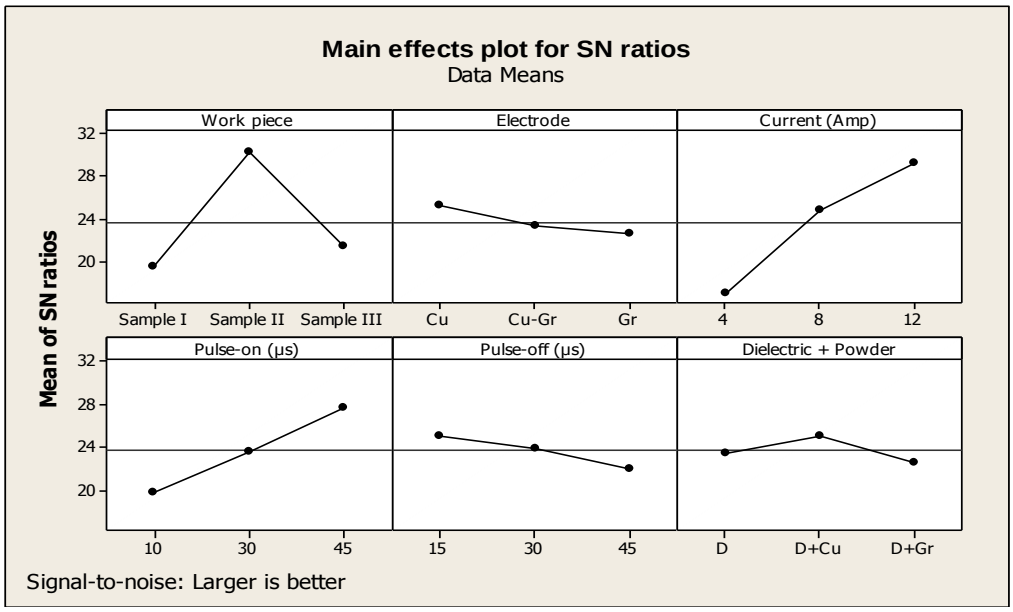

Figure 5.19 Main effects plot of MRR for S/N ratio

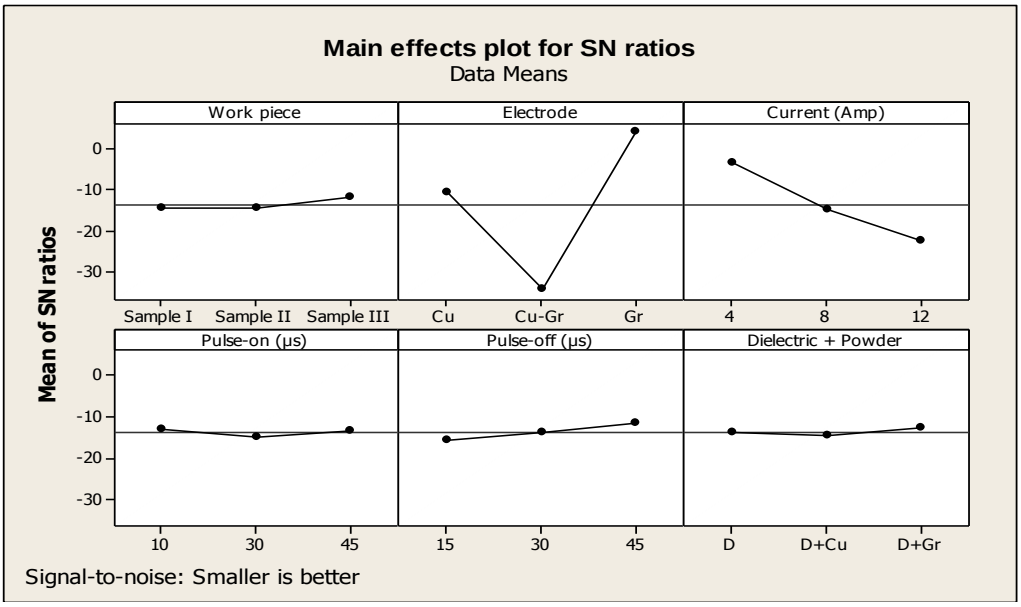

Figure 5.20 Main effects plot of TWR for S/N ratio

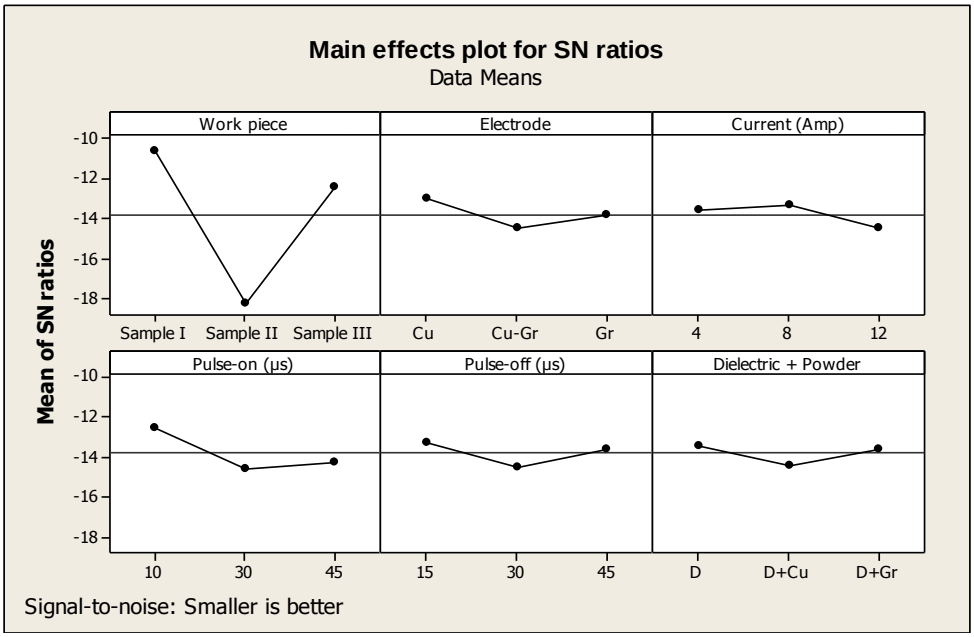

Figure 5.21 Main effects plot of SR for S/N ratio

Table 5.11 represented the ANOVA results for S/N ratio of micro-hardness. The main effect plot of S/N ratio represents the variation micro-hardness with input parameters, as shown in Figure 5.22. The plot shows that the density of reinforced particle is directly proportional to the micro-hardness of the matrix material after machining. This is due to the decomposition of SiC particles into Si and C thus particle forming silicon dioxide (SiO_2) due the oxidation of reinforced particles. The work piece machined with graphite results in higher micro-hardness as compared to copper. The mean value micro-hardness of each material machined with graphite electrode was, Sample I: 486.24, Sample II: 137.66, Sample III: 303.45. By observing the unprocessed matrix material the micro-hardness is generally lower than 117HVN.

Table 5.11 Analysis of means for the Micro-hardness

Factors	Degree of freedom	Sum of Squares	Variance	F-value	P-value
Work piece	2	627.568	313.784	39.34	0.000**
Electrode	2	48.855	24.427	3.06	0.079*
Current	2	1.009	0.504	0.06	0.939
Pulse-on	2	1.834	0.917	0.11	0.892
Pulse-off	2	4.993	2.497	0.31	0.736
Dielectric	2	12.675	6.337	0.79	0.471
Error	14	111.655	7.975		
Total	26				

**** Most significant *Significant**

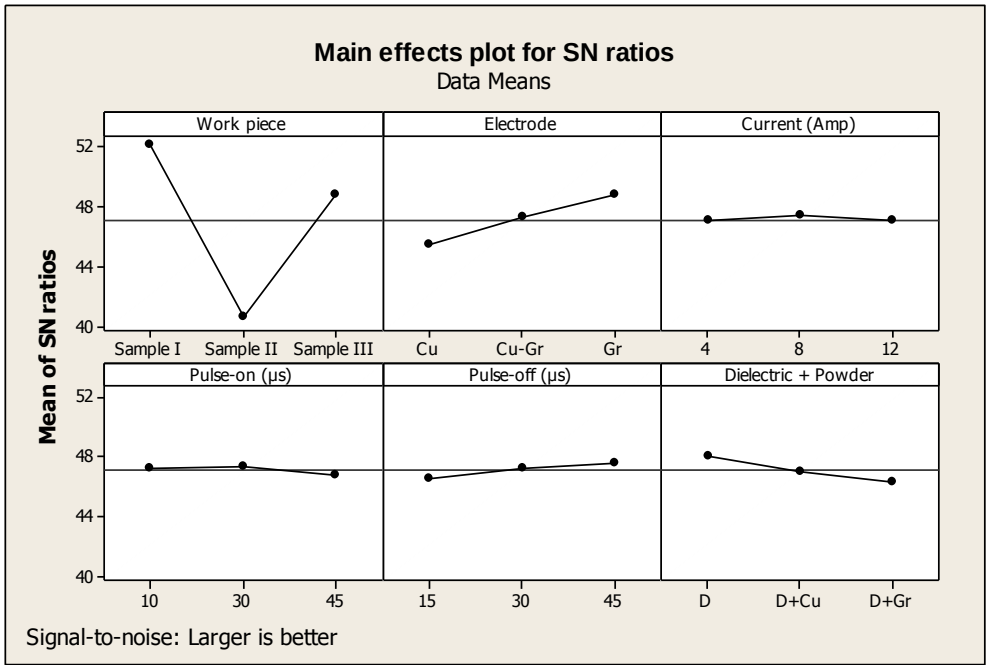

Figure 5.22 Main effects plot for S/N ratios of micro-hardness

5.3.2 XRD analysis

The machined MMCs surface was tested by XRD analysis to study the deposition of electrode material and the suspended particles from the dielectric. The deposition of these particles helps the machined surface to improve its surface properties and micro-hardness.

The XRD pattern of Sample I (65 vol% SiC/ A356.2 MMC) machined during Trial 1 (e =Cu, I=4Amp, t_{on}= 10µs, t_{off}=15 µs, d= No additives) is shown in Fig 5.23 (a). The pattern shows the deposition of copper oxide (Cu_8O=32%) and silicon oxide (SiO_2= 39%) on the surface of machined MMC. The copper act as corrosion resistive agent whereas SiO_2 impart micro-hardness to the machined surface. The copper oxide formed on the surface is due the transfer of material from the electrode, but the formation of SiO_2 is due the oxidation of silicon carbide reinforced particle at high operation temperature on the surface. Whereas (Fig. 5.23 (b)) when the work piece machined at the condition selected in Trial 3 (e=Cu, I=12Amp, t_{on}=45 µs, t_{off}=45 µs, d= D+Gr) results in formation of copper oxide (Cu_8O=3%), and silicon oxide (SiO_2=17%) and a large amount of carbon deposited on the surface of machined work piece was observed. On comparing the results, it was observed that when EDM electric parameters are at its lower level results in high deposition rate as compared to the parameters at a higher level.

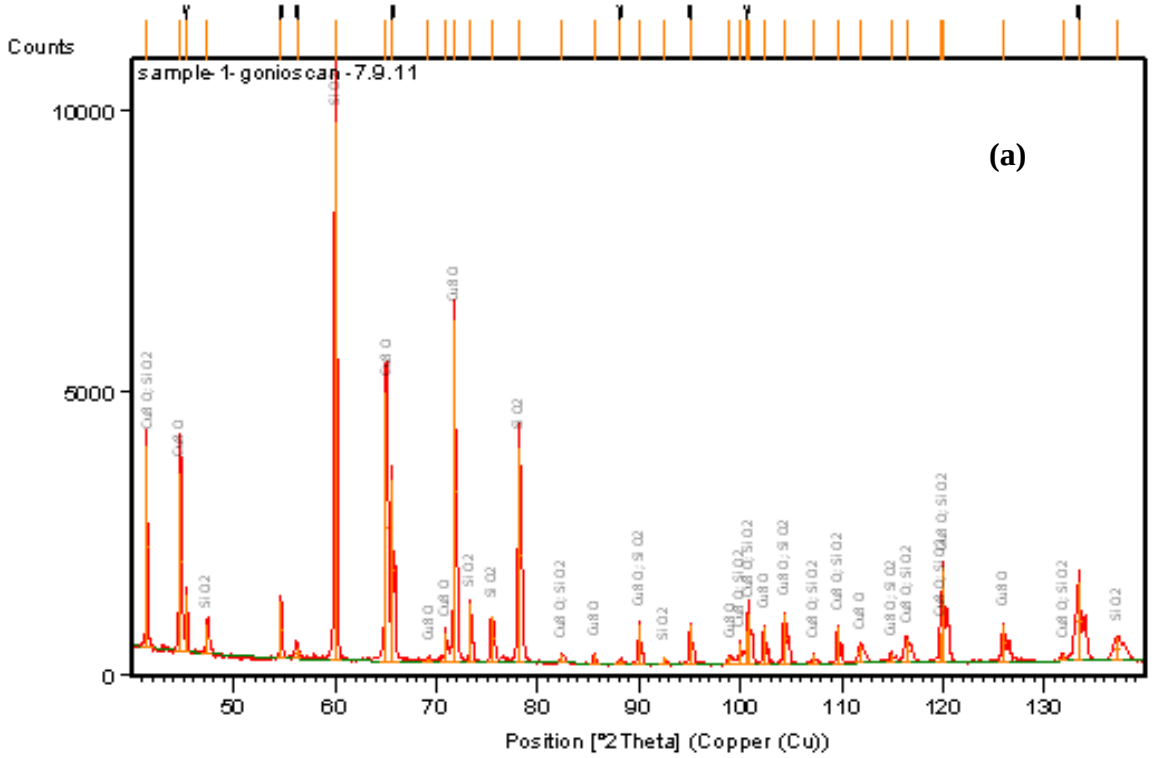
Counts
sample-1-gonioscan-7.9.11
10000
5000
0
50
60
70
80
90
100
110
120
130
Position [°2Theta] (Copper (Cu))
(a)

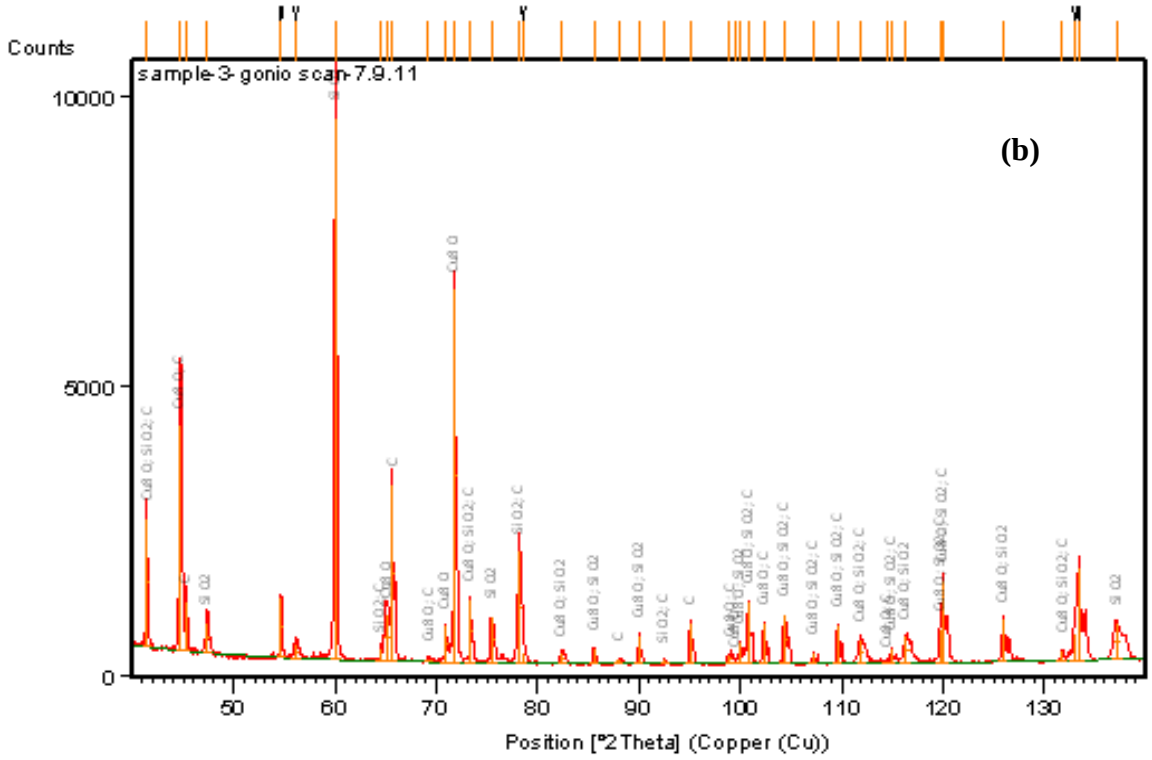
Counts
sample-3-gonio scan-7.9.11
10000
5000
0
50
60
70
80
90
100
110
120
130
Position [°2Theta] (Copper (Cu))
(b)

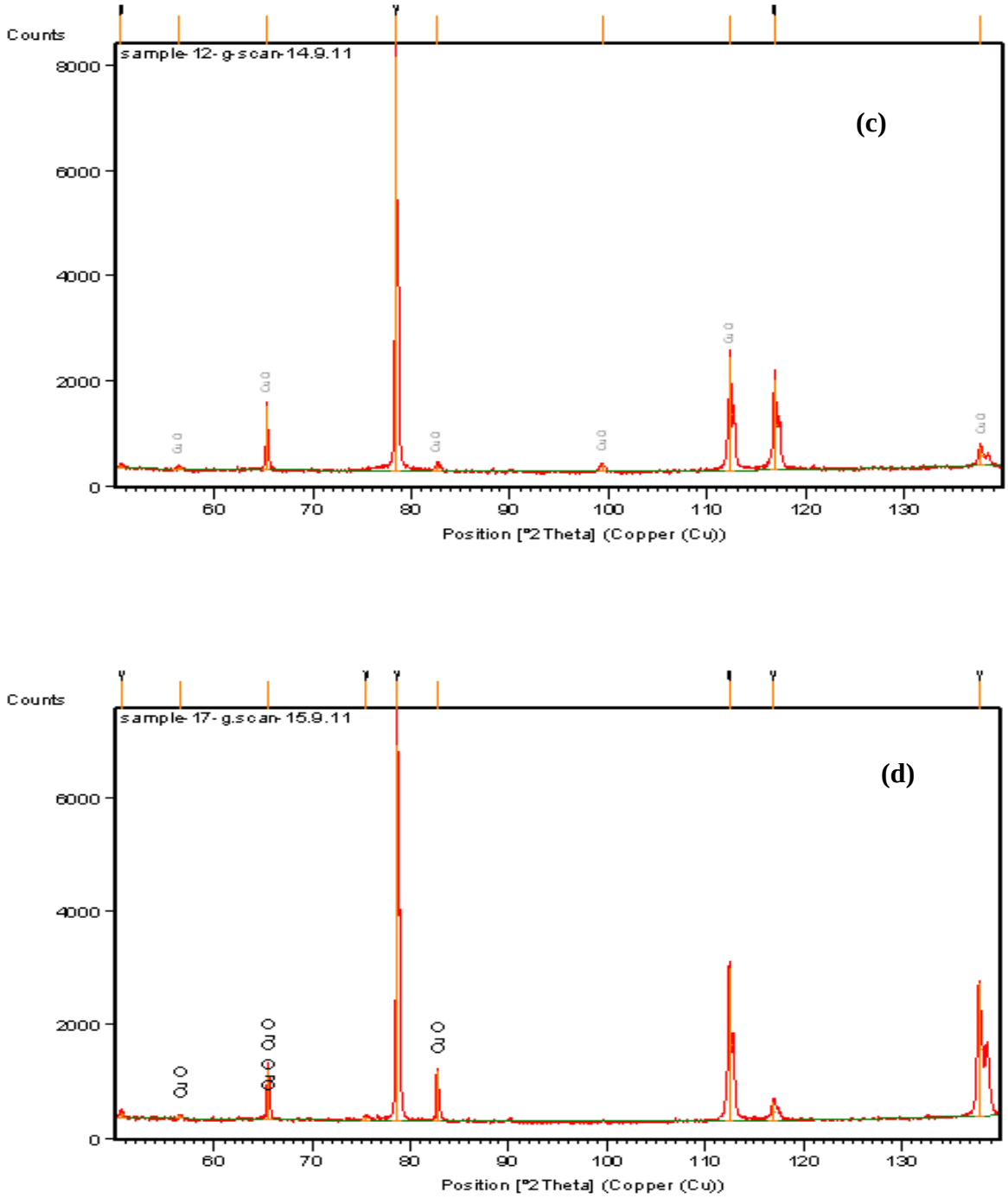

Figure 5.23 XRD spectra (2θ vs. intensity counts) of machined surface

(a) Material I, Cu electrode, I=4amp, ton=10µs, toff=15µs, d= No additives.

(b) Material I, Cu electrode, I=12amp, ton=45µs, toff=45µs, d= D+Gr.

(c) Material II, Cu electrode, I=4amp, ton=30µs, toff= 45µs, d=D+Cu.

(d) Material II, Cu-Gr electrode, I=4amp, ton=30µs, toff= 45µs, d= D+Gr.

It was also observed that the matrix material of the composite reacts with copper to form aluminium-copper (Al_4Cu_9 / $AlCu_3$) compounds due rapid cooling rate which enhanced the strength and hardness of the matrix phase (Figure 5.24).

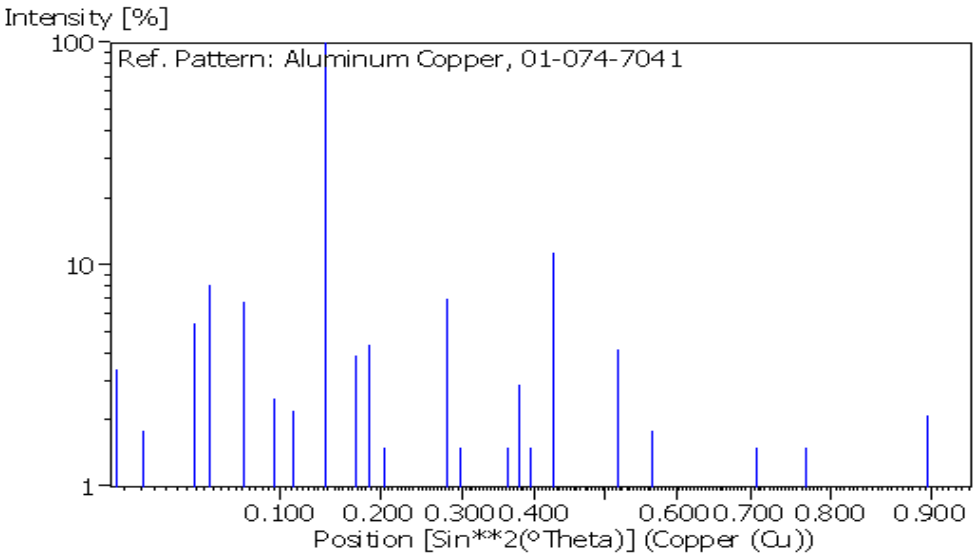

Figure 5.24 XRD pattern showing the formation of Al-Cu compound (Trial 9)

The XRD pattern for Sample II machined at the settings selected in Trial 12 (e=Cu, I=4Amp, t_{on}=30 µs, t_{off}=45 µs, d=Cu+D) is shown in Figure 5.23 (c). The major element deposited on the surface is copper oxide (CuO) which is transferred from the electrode as well as from the suspended copper particles. The traces of copper-oxide were also observed on the surface when the work piece was machined with copper-graphite electrode (Trial 17, Figure 5.23 (d)) in the presence of suspended graphite powder dielectric but the formation of CuO on the surface is lesser (34%) as compared to Trial12 conditions.

The XRD pattern for Sample III is shown in Figure 5.25. The pattern shown in Figure 5.25 (a) is for the Trial19 (e=Cu, I=12Amp, t_{on}=30 µs, t_{off}=15 µs, d=D+Cu). The spectrum shows the formation of copper oxide (Cu_8O), silicon oxide (SiO_2) and copper silicon ($Cu_{15}Si_4$). The compound Cu_8O (34%) and SiO_2 (49%) was formed due the oxidation of transferred elements and the reinforced SiC particles but the trace off reaction of Cu particles with SiC was also observed for this specimen. The XRD spectra (Figure 5.25 (b)) of Trial 24 (e=Gr, I=4Amp, t_{on}=45 µs, t_{off}=45 µs, d= D+Cu) reveal that deposition of copper on the machined surface as a major element, but the traces of graphite was negligible.

Similarly, the spectra (Figure 5.25(c)) of Trial 27(e=Cu-Gr, I=12Amp, t_{on}=30 µs, t_{off}=45 µs, d=D+Gr) the major deposited material on the machined surface was copper oxide (CuO=84%). The small traces of silicon dioxide (SiO_2=13%) and silicon copper (Si_9Cu=3%) were also identified.

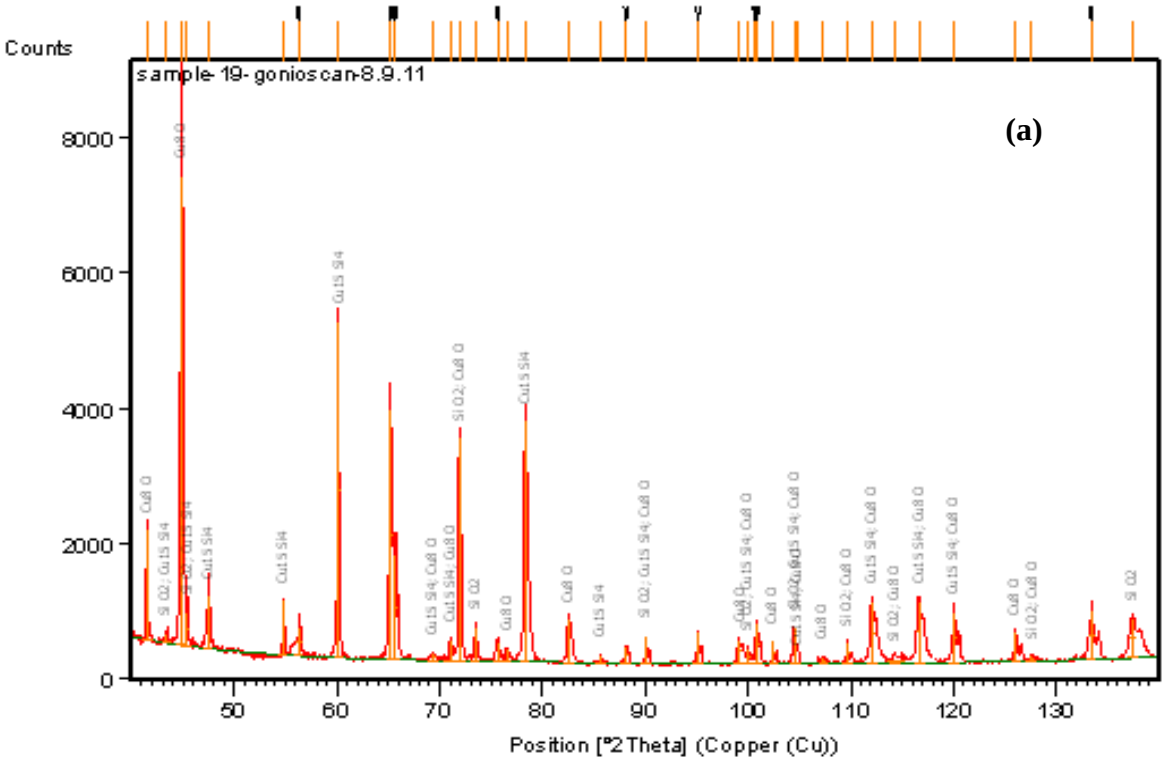
Counts
sample-19-gonioscan-8.9.11
(a)
8000
6000
4000
2000
0
50
60
70
80
90
100
110
120
130
Position [°2Theta] (Copper (Cu))

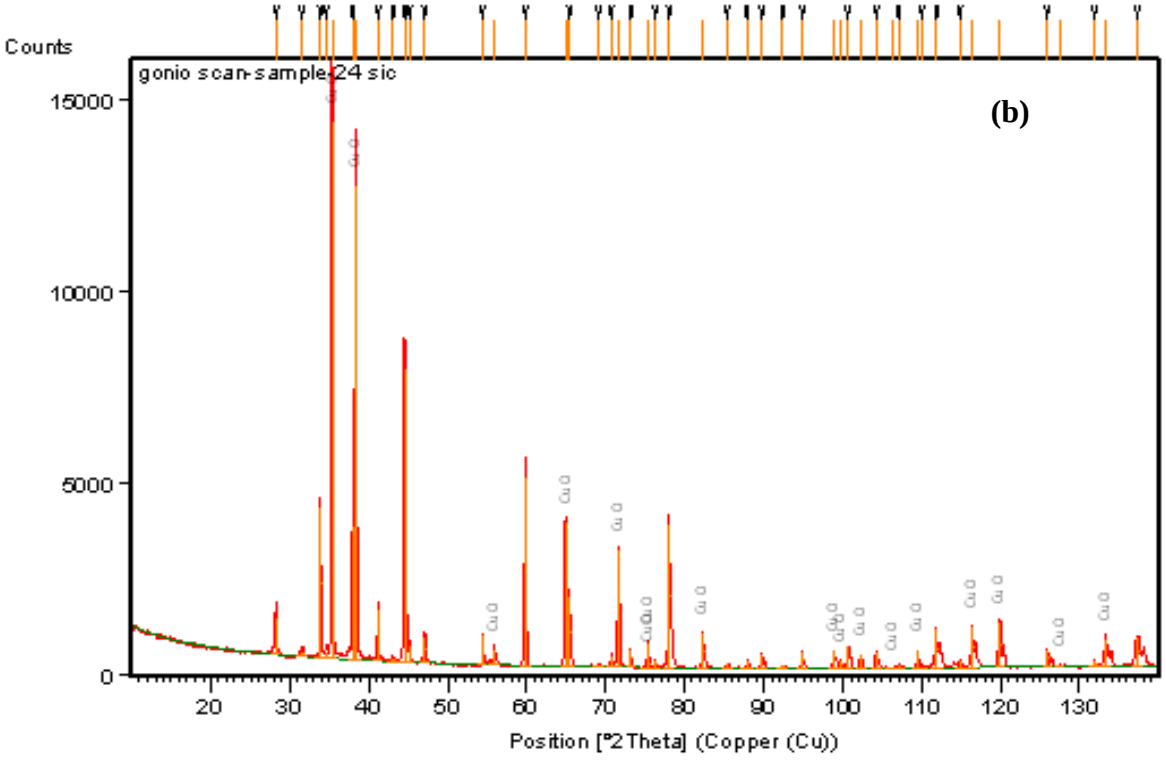
Counts
gonio scan-sample-24 sic
(b)
15000
10000
5000
0
20
30
40
50
60
70
80
90
100
110
120
130
Position [°2Theta] (Copper (Cu))

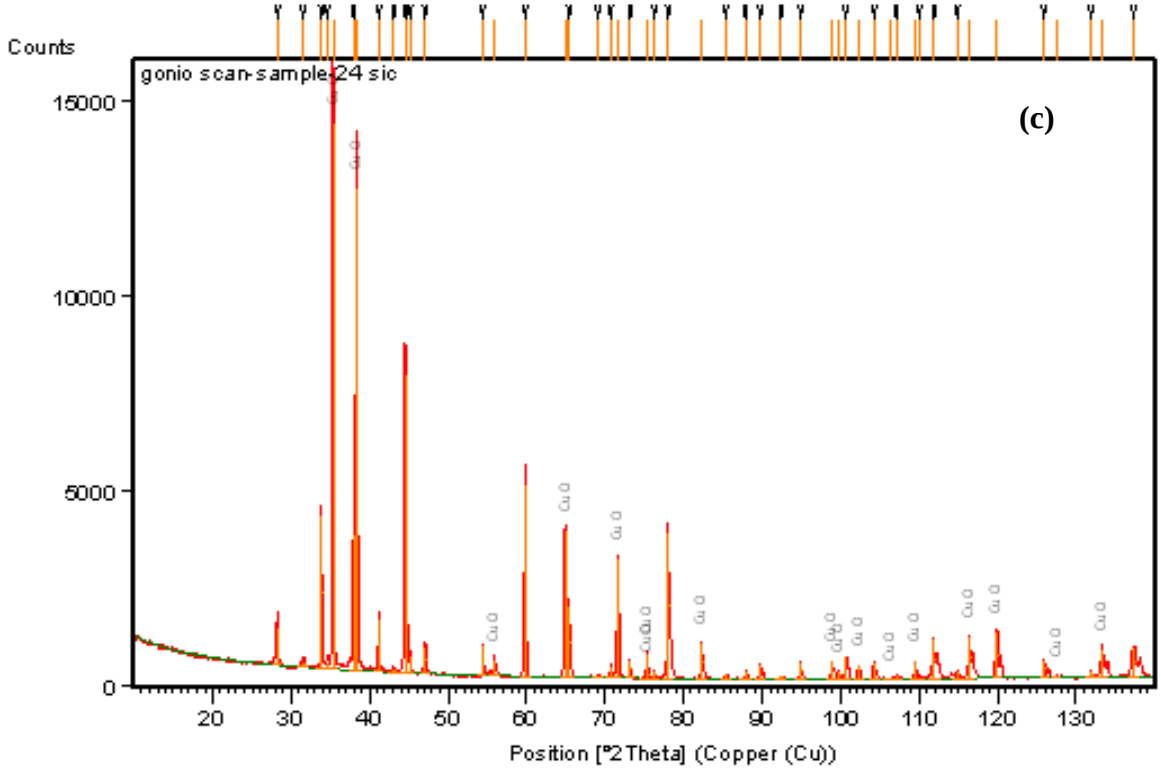

Figure 5.25 XRD pattern of Sample III

(a) Cu electrode, I=12amp,ton=30µs, toff=15µs, d=D+Cu

(b) Gr electrode, I=4amp, ton= 45µs, toff=45µs, d=D+Cu.

(c) Cu-Gr electrode, I=12amp,ton= 30 µs, toff=45 µs, d=D+Gr

5.3.3 Microstructure analysis

Figure 5.26, 5.27, 5.28 shows the micrograph of as-received machined surface of Sample I. The Figure 5.26 micrograph corresponds to the setting parameters at Trial 3 while Figure 5.27 is for Trial 4. In both the Trials the spark energy i.e. current (I=12Amp) and pulse-on time (t_{on}=45µs) remain same while the suspended additive particles in dielectric are graphite powder is for Trial 3 and copper powder is for Trial 4.

It was observed that the surface of MMCs consist of voids, but the higher density and the deeper voids/pitting were observed in case of graphite additive powder. This is due to high conductivity of copper suspended particles which results in enlarged spark and reduced the insulating strength of dielectric to form plasma channel between the electrodes hence efficient transfer of energy. The Figure 5.27 was compared with the micrograph obtained at the lowest sparks energy condition (Trial 1, Figure 5.28) i.e. I= 4Amp, t_{on}=10µs and without additive in dielectric. The topography of both the Trial (Trial 4 and Trial 1) reveal the almost similar topography with fewer number of voids/pitting,

but in Trial1 the metal removal rate from the MMC is considerably sacrificed as compared to Trial 4.

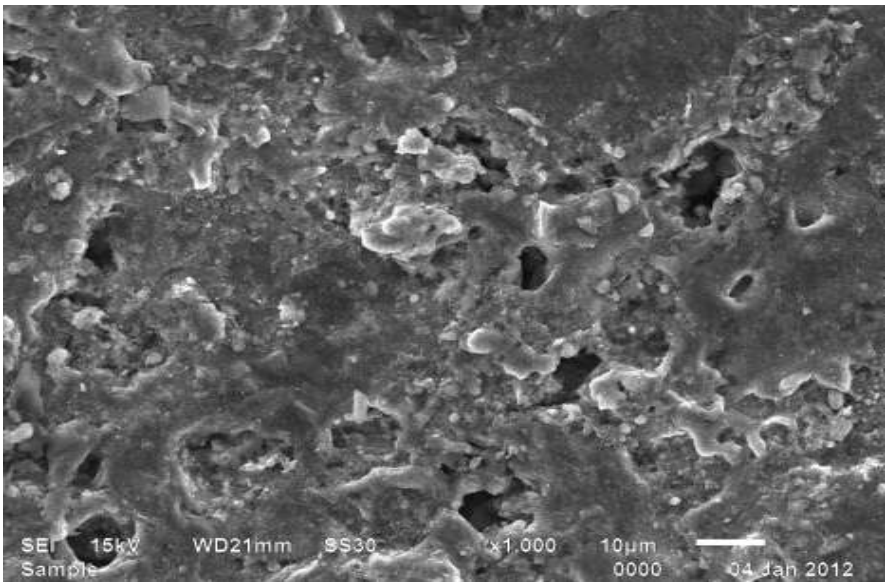

Figure 5.26 SEM micrograph of Sample I for Trial 3 (Cu electrode, I=12Amp,ton=45µs, toff=45µs, d=D+Gr)

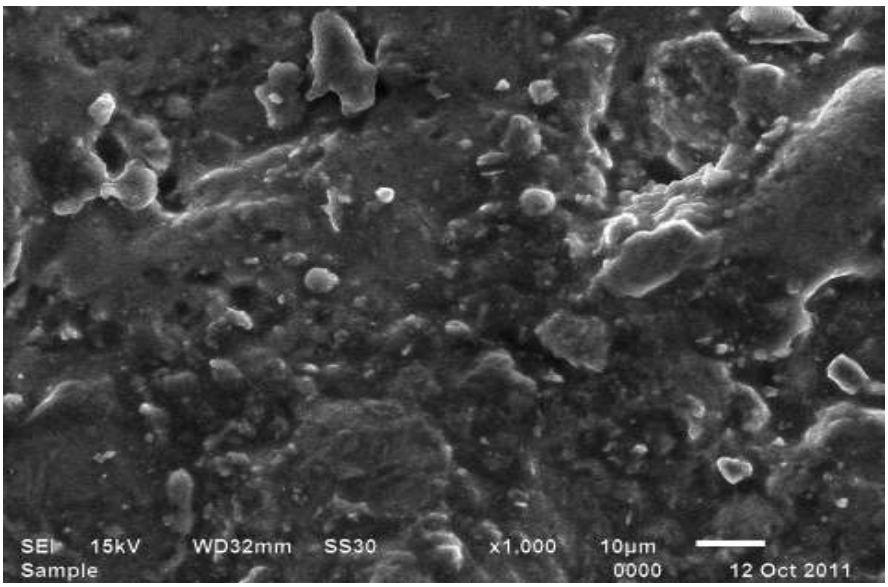

Figure 5.27 SEM micrograph of Sample I for Trial 4 (Gr electrode, I=12Amp, ton=45µs, toff=15µs, d=D+Cu)

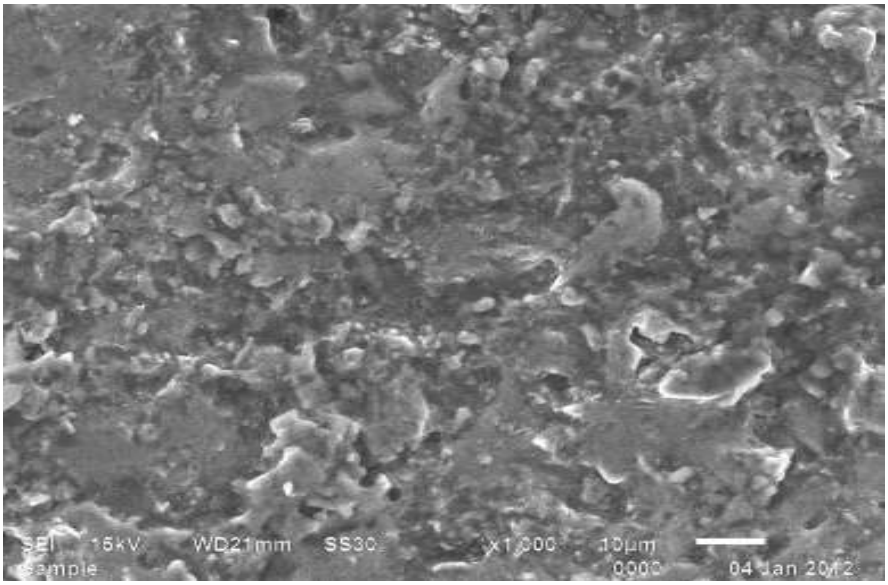

Figure 5.28 SEM micrograph of Sample I for Trial 1(Cu electrode, I=4Amp, ton=10µs, toff=15µs, d=D (without powder))

Figure 5.29 corresponding to Trial 12 for the Sample II. Figure 5.29 shows traces of material transfer (CuO) but at the same time has a rough surface with void formation due to oxidation reaction. The topography of this material is due to the fewer number of reinforced SiC particles in aluminium matrix which may act as a shield to the matrix material against spark energy.

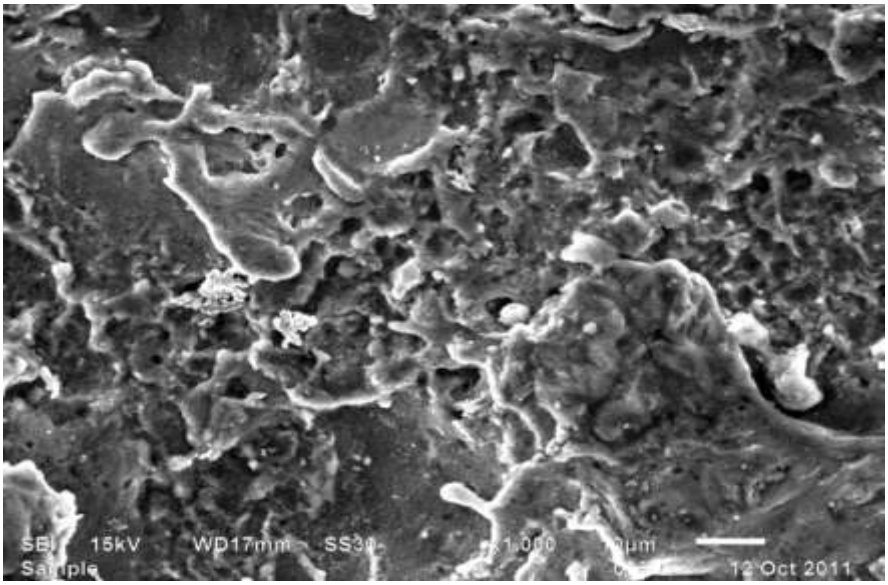

Figure 5.29 SEM micrograph of machined surface of Sample II

Figure 5.30 (a, b) represents the micrograph for Sample III. The material was machined at same spark energy level (I=12Amp, t_{on}=30µs). In Figure 5.30 (a) the work piece was machined using copper electrode in the presence of suspended copper additive in the dielectric medium (Trial 19) while Figure 5.30 (b), represents the part machined with Cu-

Gr electrode in the presence of suspended graphite additive in a dielectric medium (Trial 27). The surface shows a voids in Trial 27 which in line with micrograph studied for Sample I.

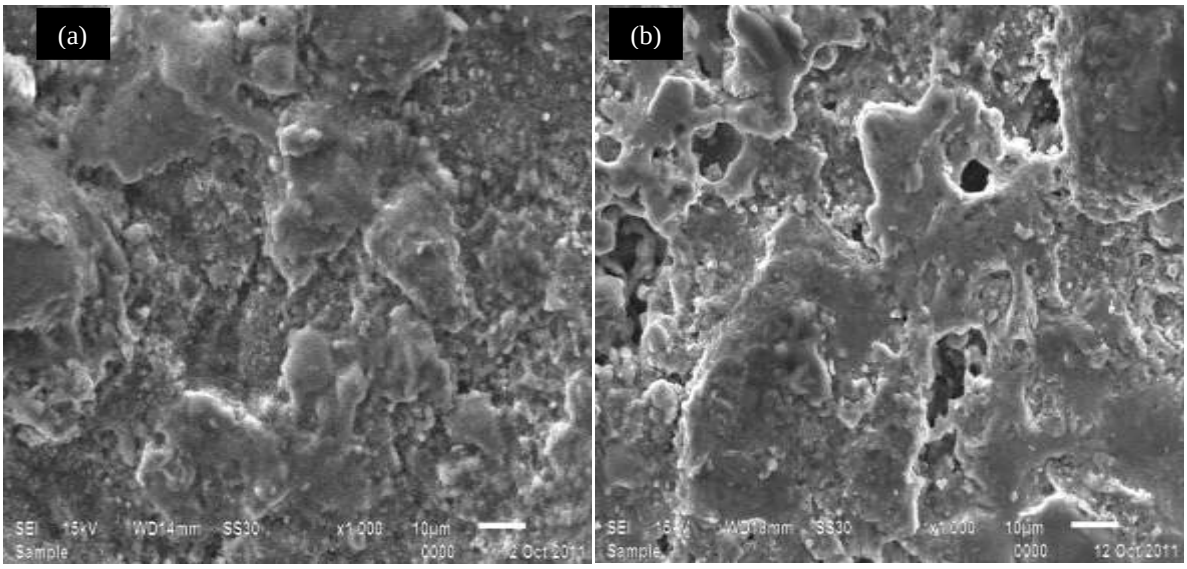

Figure 5.25 Typical PMEDM surface of Sample III a) Cu electrode, I=12amp, Ton=30µs, Toff=15µs, d=D+Cu b) Cu-Gr electrode, I=12Amp, Ton=30µs, Toff=45µs, d= D+Gr.

The formation of voids was further magnified to 1500X where the micro-shrinkage pattern was observed from the expelled out reinforced particles (Figure 5.31).

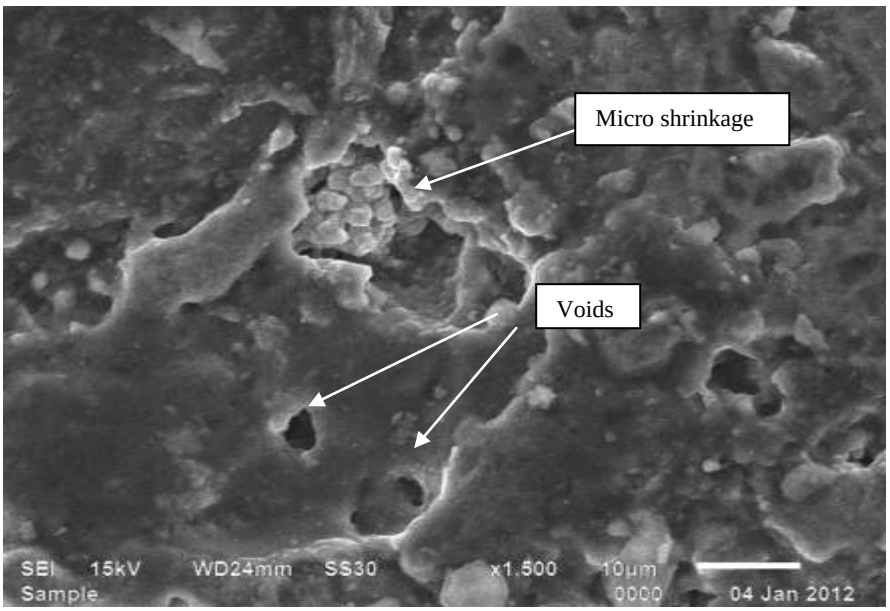

Figure 5.31 Scanning electron micrograph of EDMed surface of sample III machined

5.3.4 Analysis of variance of means for recast layer thickness and residual stresses

The percentage contribution of various process parameters on the recast layer thickness and residual stresses is estimated in this section. The ANOVA (general linear model) for the raw data was performed to identify the significant parameters and to quantify their effect on the performance characteristics. The ANOVA for recast layer is presented in Table 5.11 and the main effect plot is shown in Figure 5.32.

Table 5.11 Analysis of means for recast layer thickness

Factors	Degree of freedom	Sum of Squares	Variance	F-value	P-value
Work piece	2	9032.1	4516	9	0.003**
Electrode	2	768.4	384.2	0.77	0.483
Current	2	3473.6	1736.8	3.46	0.060*
Pulse-on	2	2148.1	1074	2.14	0.154
Pulse-off	2	1011.0	505.5	1.01	0.390
Dielectric	2	806.7	403.3	0.80	0.467
Error	14	7023.1	501.6		
Total	26	24162.9			

**** Most significant *Significant**

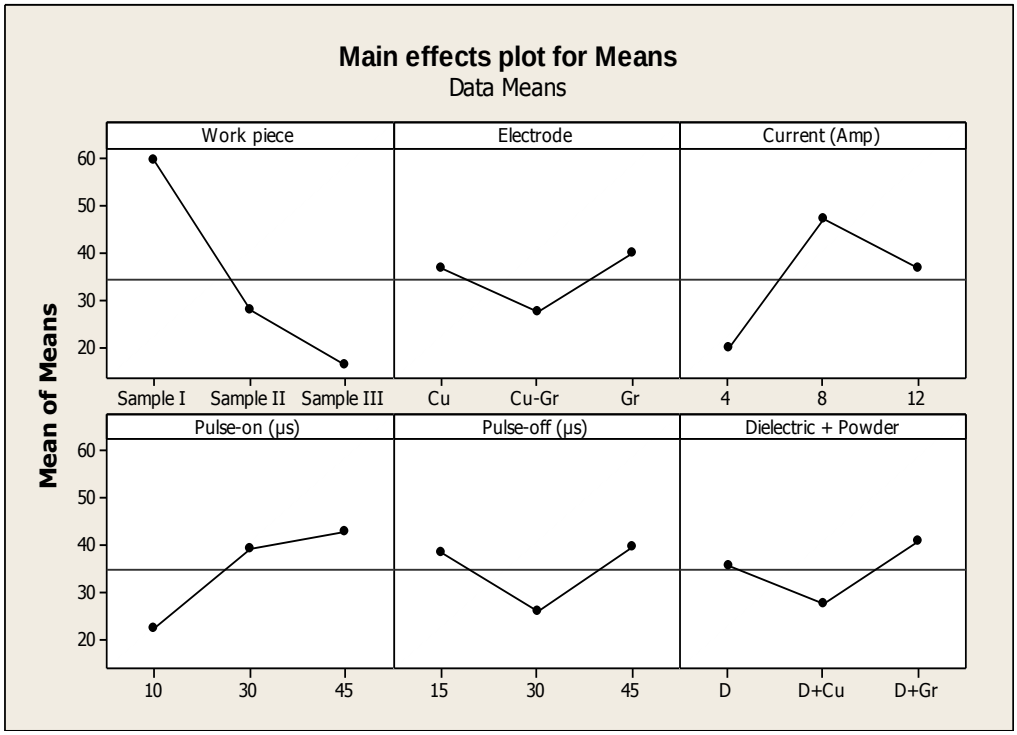

Figure 5.32 Main effects plot for recast layer thickness

From the main effect plot, it was observed that the sample reinforced densely (Sample I), resulting in thicker recast layer as compared to Sample II and III. This was due the heat absorption capacity of dense and bigger size reinforced particles of Sample I (Sample I: SiC= 65%, avg. size = 55μm; Sample II: SiC+SiO_2=15%,avg. size=50 μm; Sample III: SiC= 30%, avg. size= 14 μm). The heat absorbed by these particles leads to deeper heat affected zone i.e. thicker recast layer.

Microstructure analysis of Recast layer

The study of recast layer was completed by cutting work piece along cross-section using water cooled precise cutting machine. The cross-section of the work piece was polished using various grid size (400 to 3500 grits) emery papers (Make: 3M). Figure 5.33 depicts the microstructure of sample I after machining with EDM under the experimentation conditions corresponding to the Trial 1 (Cu electrode, I=4Amp, t_{on}=10μs, t_{off}=15μs, d=D (without additives)). It was observed that the deep irregular crater was formed due to uneven distribution of spark energy between the electrodes. As the spark energy was set at lowest intensity, the distribution of craters on the machined surface was not dense. It could be attributed to extremely low energy input during experimentation hence, low magnitude of SR. The average micro-hardness measured during this Trial was 260 HVN.

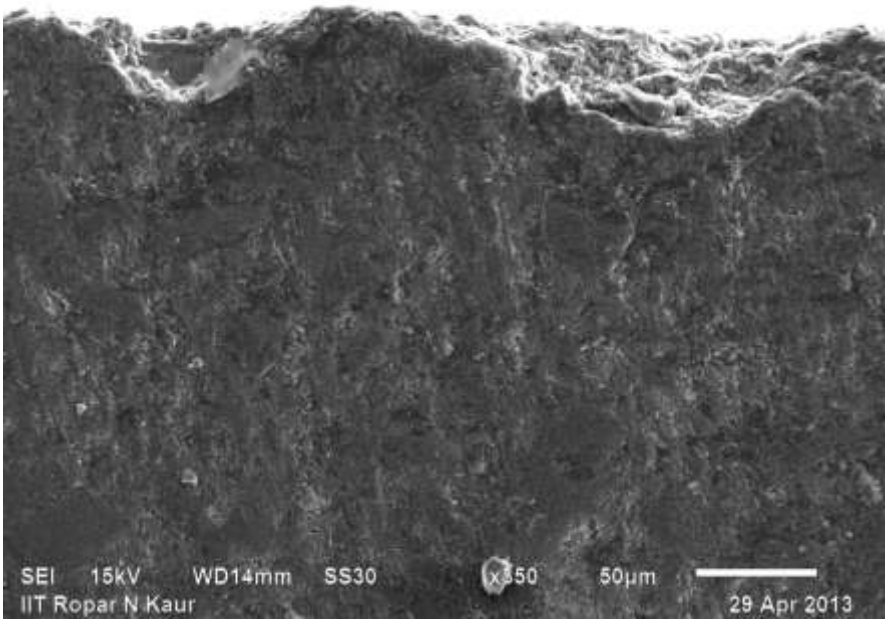

Figure 5.33 SEM micrograph of recast layer in EDM for Sample I (Trial 1)

Figure 5.34 (a, b) depicts the microstructure of Sample I machined under the condition corresponding to Trial 2 (Cu electrode, I=8Amp, t_{on}=30μs, t_{off}=30μs, d=D+Cu). It was observed that the depth of craters and recast layer depth was almost similar to Trial 1.The

moderate machining parameters during this trial results in continuous formation of recast layer. The formation of pits/voids and the white layers on the surface were observed in this trial (Figure 5.34 (b)). These white layers on the surface were associated with the probable locations of crack propagation. The presence of copper compound and silicon dioxide (SiO_2) was traced during the XRD examination. These compounds enhanced the conductivity and surface micro-hardness of the machined surface. The presence of additive in EDM oil results in reduction of recast layer thickness but there is considerable increase in MRR. The residual stresses induced in the sample were marginally increased.

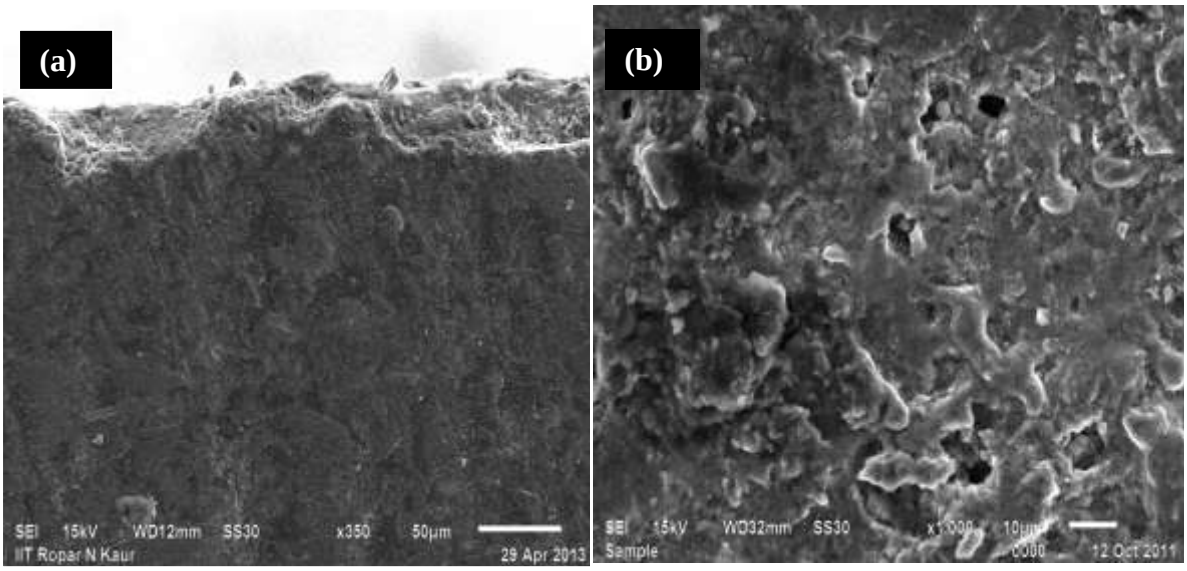

Figure 5.34 SEM micrograph of Sample I for Trial 2 (a) Cross-sectional view representing recast layer and (b) Surface morphology.

Figure 5.35 depicts the microstructure of Sample I under experimental conditions corresponding to Trial 3. The recast layer formation was almost uniform through out the section. The machining parameters used were at its highest level (I=12 Amps, t_{on}= 45, t_{off} = 45) in the presence of graphite powder-mixed dielectric medium. The formation of crack formation was observed in the domain of recast layer and it propagated towards the base portion of MMC. The direction of cracks shown in Figure 5.35 is along the horizontal and along cross-sectional direction of the material. Hence it was concluded that the material removal mechanism was mainly due to spalling and melting of matrix phase of MMCs. The topography of machined surface is shown in Figure 5.36. The void formation in Trial 3 was wider and deeper as compared to the morphology studied for Trial 2. The deposition of melted portion of the sample was also observed which increases surface roughness and residual stresses. But on the other hand, the micro-hardness was reduced and it was measured as 274 HVN

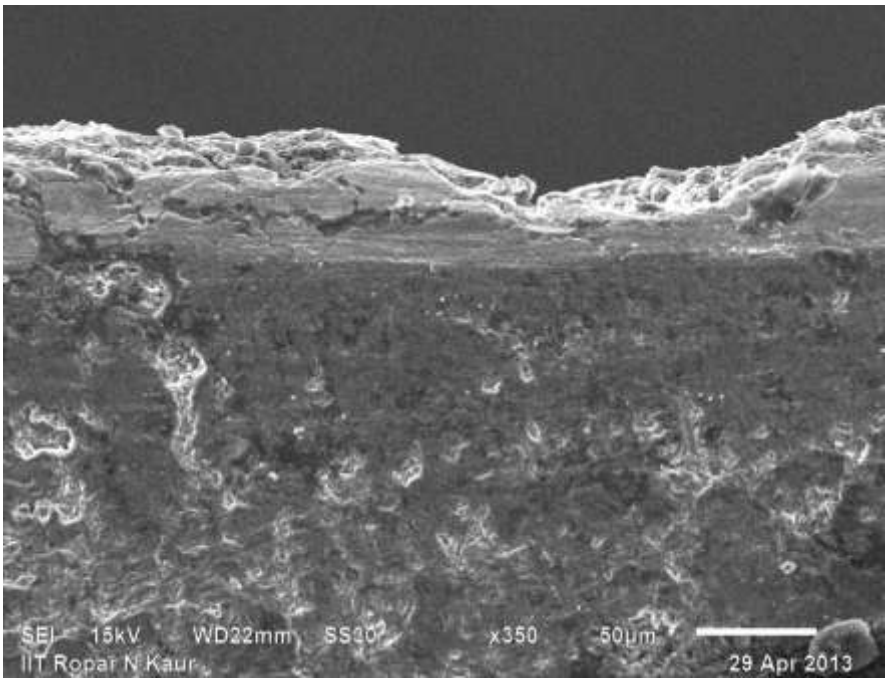

Figure 5.35 SEM photograph for Sample I (Trial3) representing the cracks

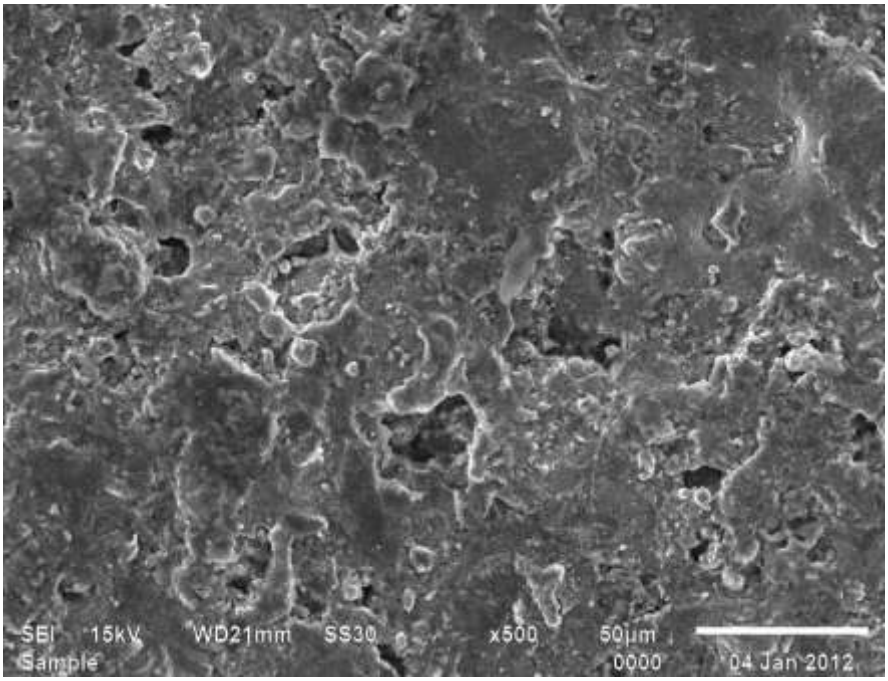

Figure 5.36 Topography of Sample I (Trial 3) showing the formation of white layers and voids.

Figures 5.37, 5.38, 5.39 correspond to Trial 4, 5, 6 respectively. The samples were machined using graphite as a tool electrode under the given conditions (Ref. Table 4.24). Trial 4 and Trial 5 were conducted in additives (Copper and Graphite powder) mixed in EDM oil while Trial 6 was conducted in EDM oil (without additives).

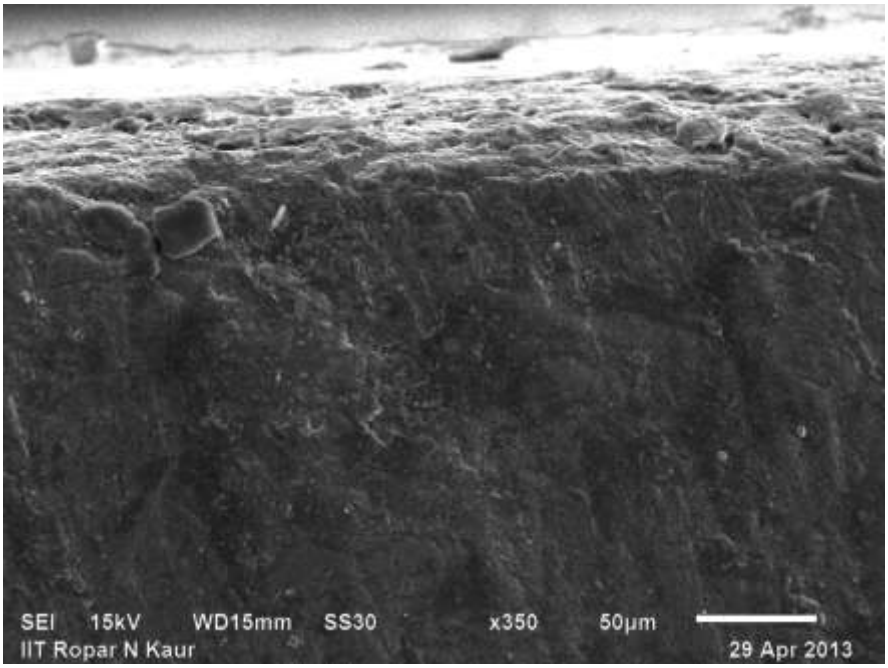

Figure 5.37 SEM micrograph of Sample I for Trial 4

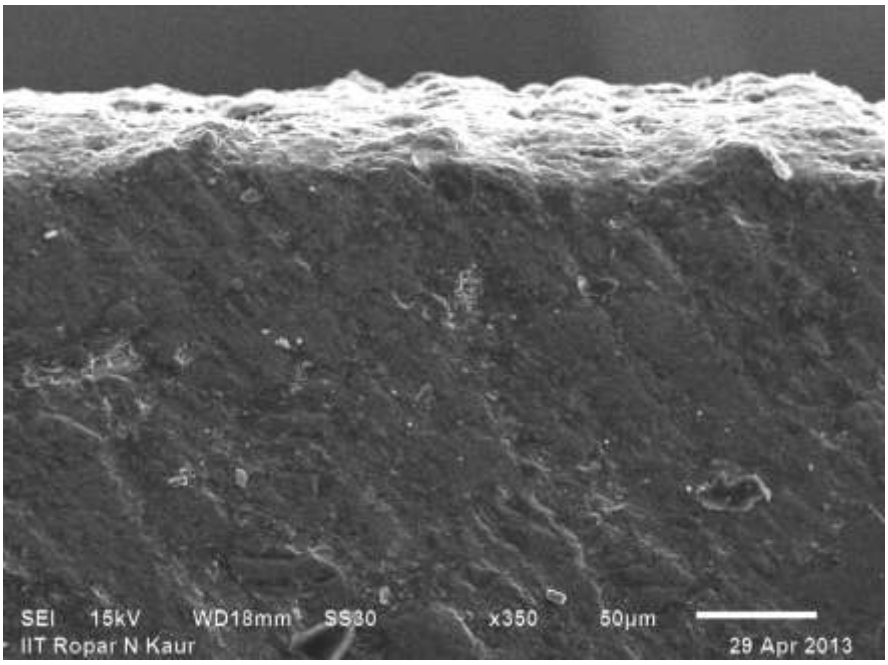

Figure 5.38 SEM micrograph of Sample I for Trial 5

The formation of crater was observed in Trial 6 which was similar to Trial 1 (without-additive). In Trial 6 the depth of crater was shallow due the less conductive property of graphite tool electrode as compared to copper electrode. The machined surface is shown in Figure 5.39. The morphology of machined of Sample I conducted according to condition laid in Trial 8 was also analyzed. It was observed that uneven trend craters appeared while machining without additive mixed in EDM oil. The SEM obtained for Trial 8 is shown in Figure 5.40.

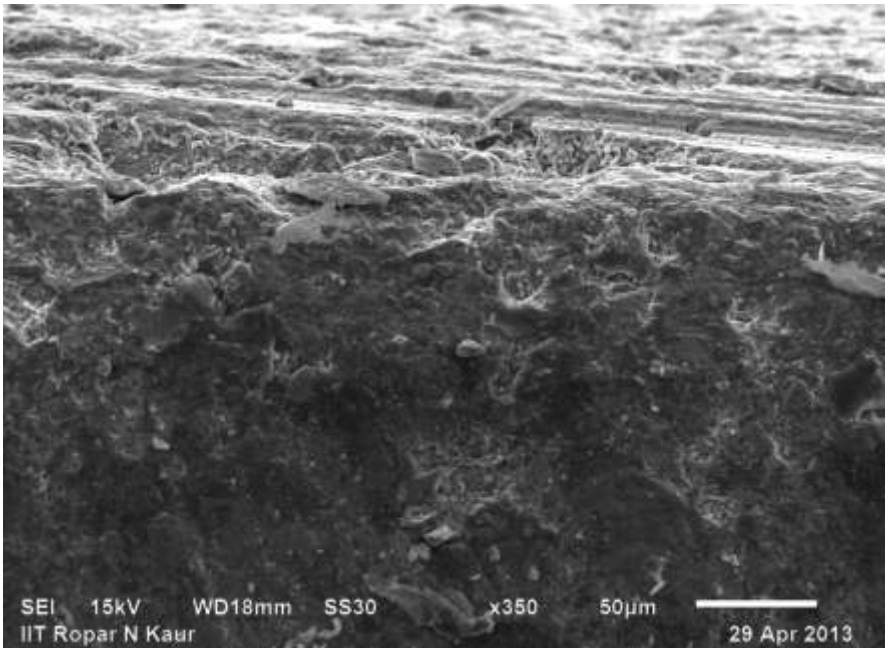

Figure 5.39 SEM micrograph of Sample I for Trial 6

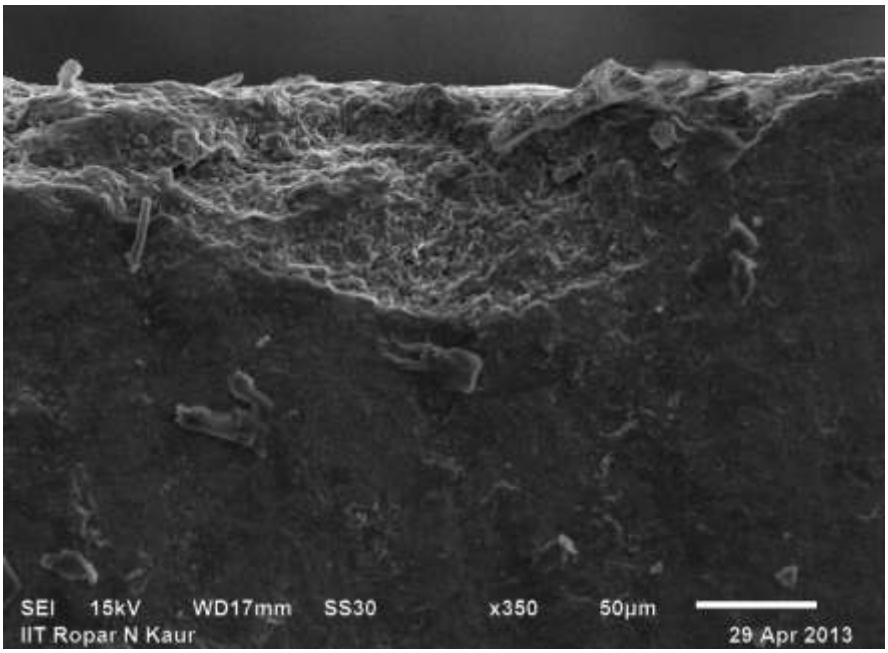

Figure 5.40 SEM micrograph of Sample I for Trial 8

Figure 5.41 and 5.42 depicts the microstructure of Sample I corresponding to Trial 9 at X350 and X1000 magnification. The formation of recast layer was uniform throughout the cross-section. The thin recast layer with mild pits was observed as shown in Figure 5.41. The depositions on recast layer were due to the disintegration of loosely bounded Cu-Gr composite electrode. The re-solidified melts and cracks after EDM were observed on the topography of machined surface (Figure 5.43)

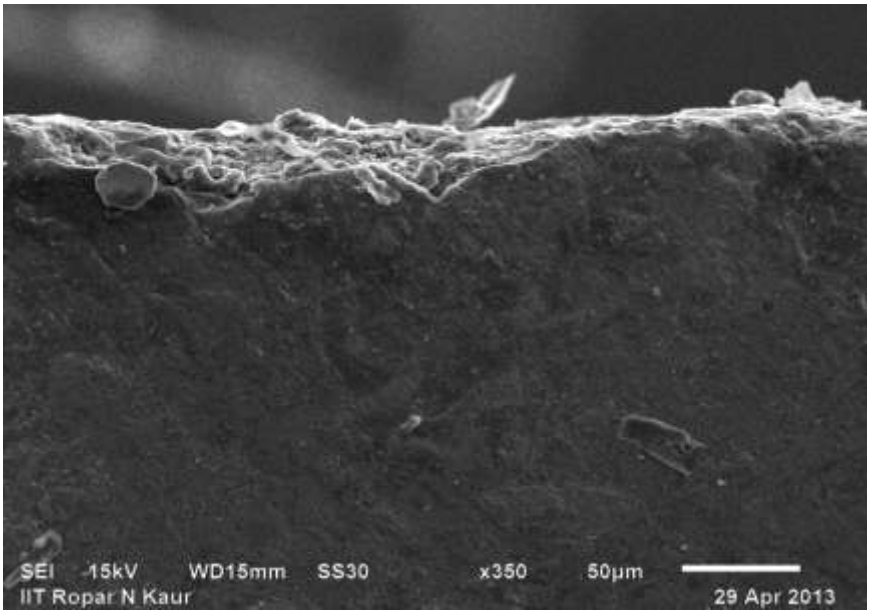

Figure 5.41 SEM photograph of Sample I for Trial 9 (X350)

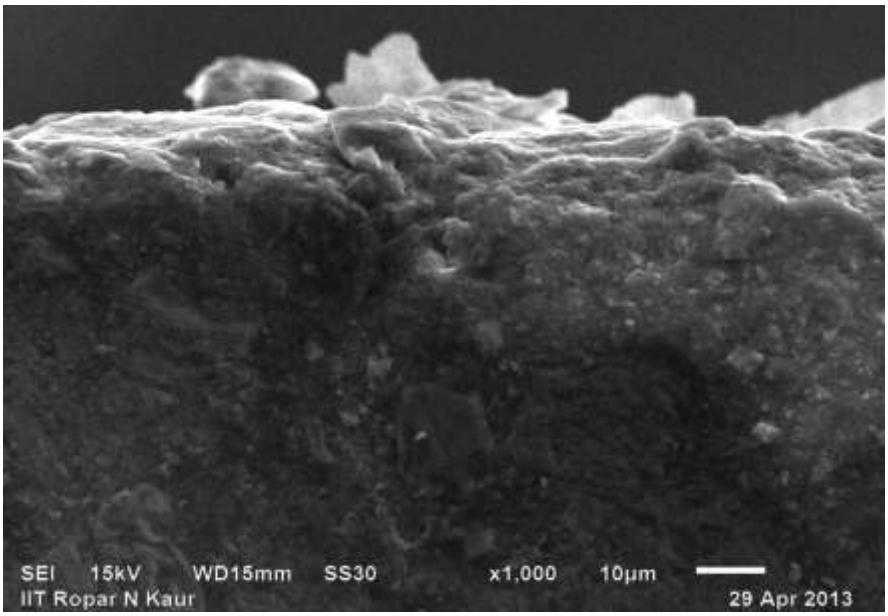

Figure 5.42 SEM photograph of Sample I for Trial 9 (X1000)

The cracks appeared on the surface were due to imperfect joining of droplets of melts including a lot of stresses gradient exceeding the ultimate strength of MMC. The matrix material melts and recast on the machined surface causing cracks and voids. The rounded edge of the grains in contact indicates that the material was molten during the EDM process. These depositions also results in higher magnitude of residual stresses and was measured to be 134.0 MPa. From the Figure 5.43 the cracks were observed on the surface of machined MMC. The recast layer thickness was observed to be minimum during this

trial. To enhance the service life of the component obtained during Trial 9, the thin recast layer should be removed by using suitable finishing process.

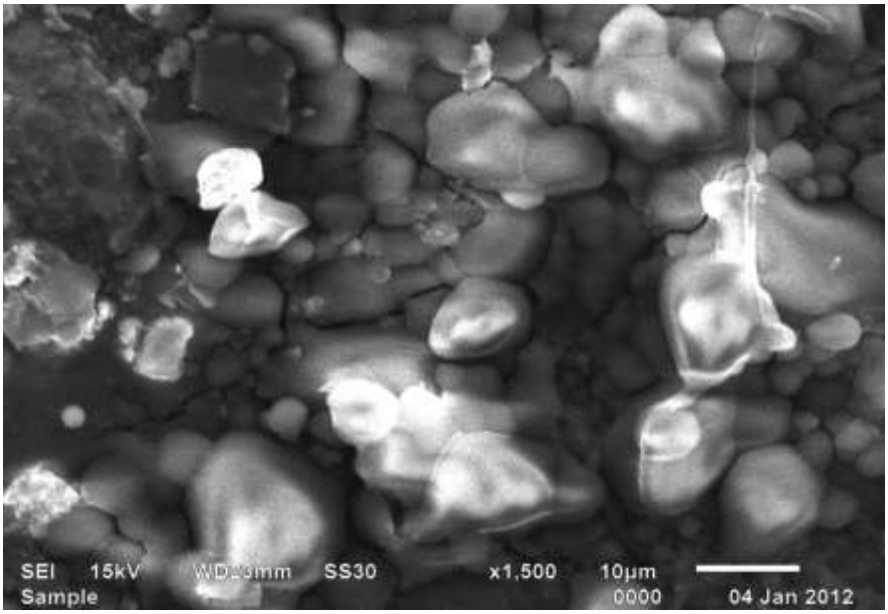

Figure 5.43 SEM photograph of Sample I for Trial 9 representing depositions and cracks

Figure 5.44 and 5.45 shows the cross-sectional view of Sample II machined as the parameters corresponding to Trial 11 and Trial 12. The formation of recast layer was smoother as compared to SEM obtained for sample I. This was due to easy metal removal rate during machining. The metal removal rate in these sample was maximum as compared to sample I and sample III.

The presence of dense reinforced particles hinders the formation of plasma between the electrodes hence craters was observed in cross-section of the specimen. In Sample II the metal removal mechanism is mainly due to melting or thermal fractures. As the particulate reinforcement was minimum in these samples the thermal fractures was observed on the topography machined sample.

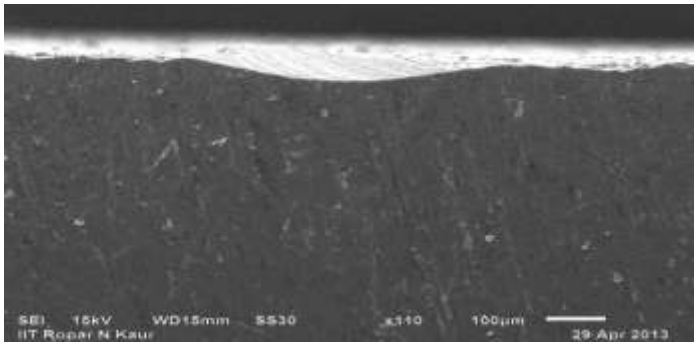

Figure 5.44 SEM photograph for Sample II (Trial 11)

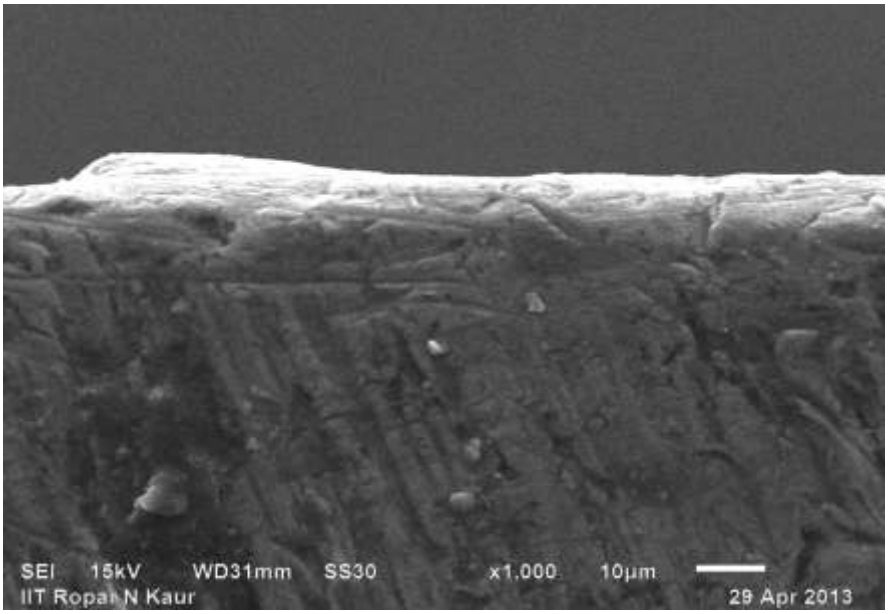

Figure 5.45 SEM photograph for sample II (Trial 12)

The topography of MMC machined corresponding to Trial 12 is shown at in Figure 5.46, 5.47.

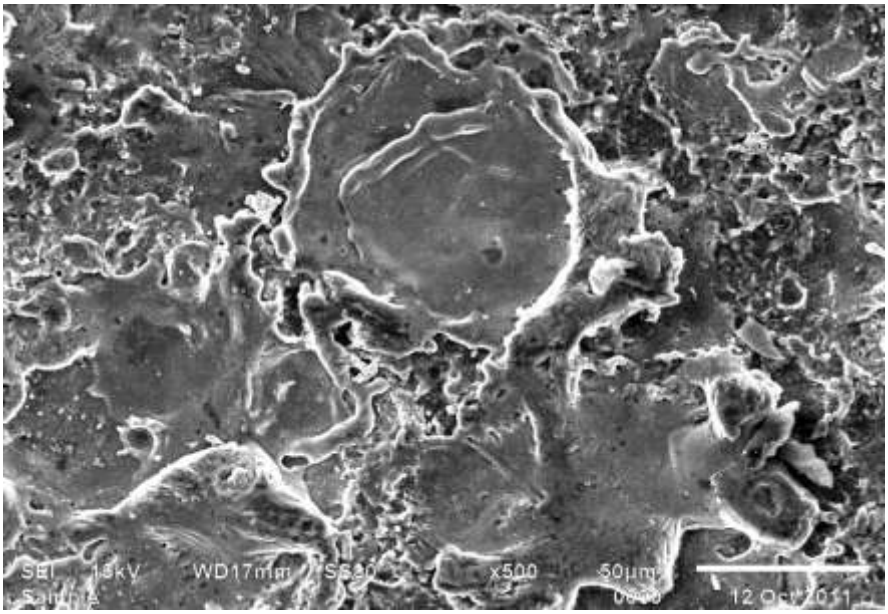

Figure 5.46 Topography of Sample II for Trial 12

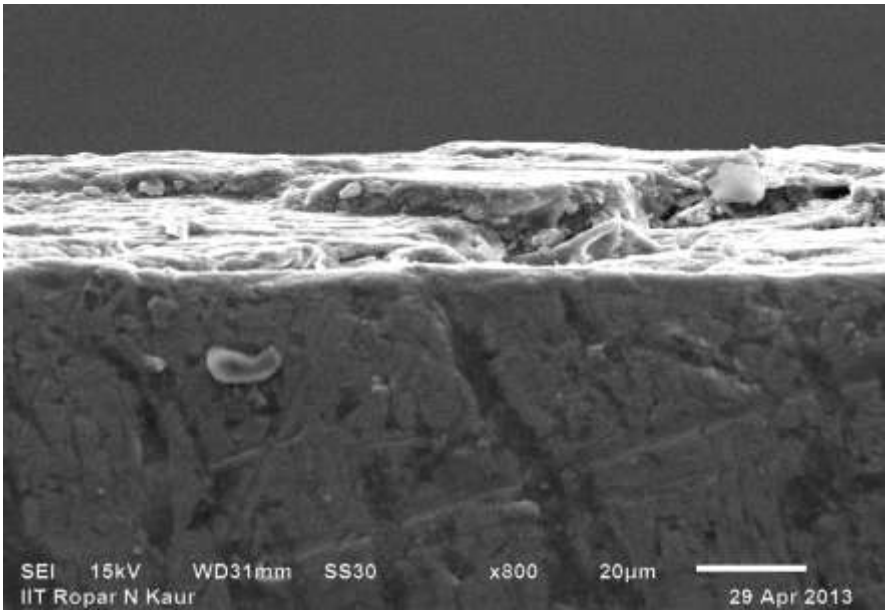

Figure 5.47 SEM of Sample II showing the machined surface for Trial 12

The Figure 5.48-5.56 shows the microstructure of Sample III machined under different condition corresponding to Trial 19-27 as shown in the experimental design (L_{27})matrix. It was observed that, the formation of recast cast layer was uniform and the heat affected zone was also confirmed on the surface of the specimen, hence had least residual stresses and high surface finish. The heat effected zone was maximum in dense particle reinforced MMC. The reinforced particles absorbed the heat generated during EDM process and contributing in thickening the recast layer or heat effected zone.

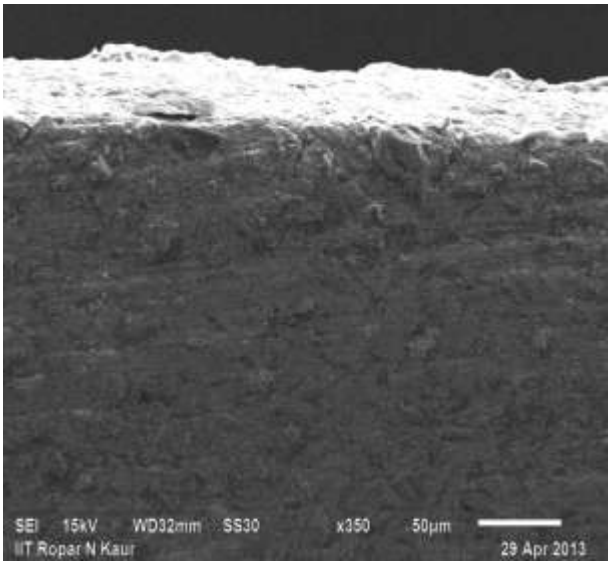

Figure 5.48 SEM of Trial 19 (Sample III)

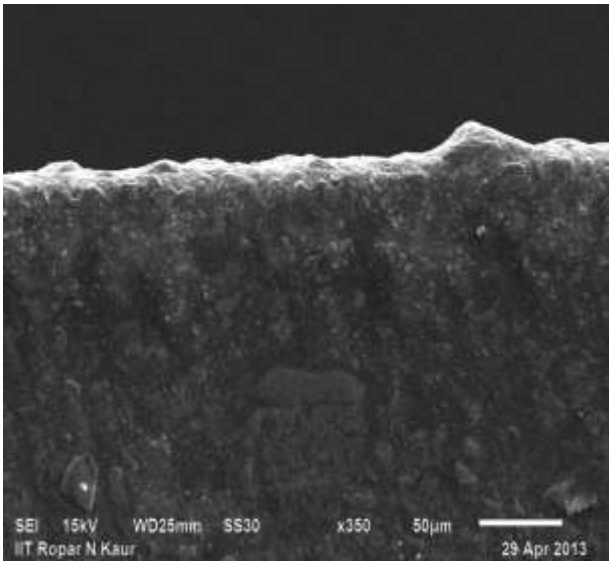

Figure 5.49 SEM of Trial 20 (Sample III)

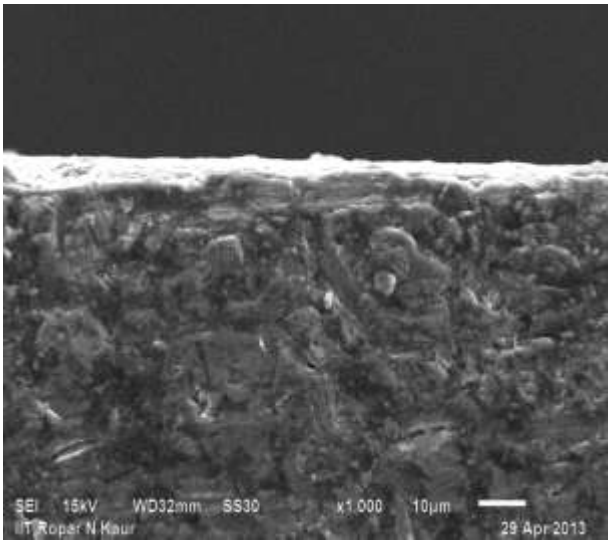

Figure 5.50 SEM of Trial 21 (Sample III)

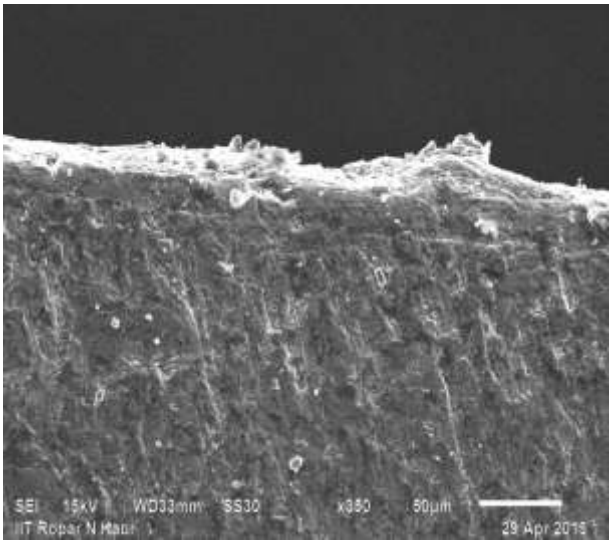

Figure 5.51 SEM of Trial 22 (Sample III)

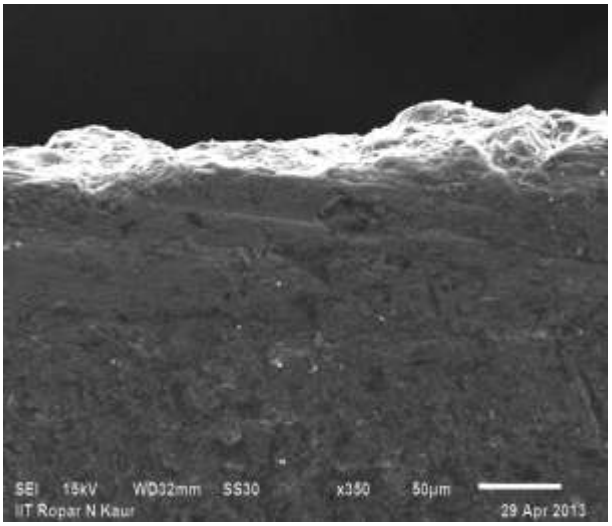

Figure 5.52 SEM of Trial 23 (Sample III)

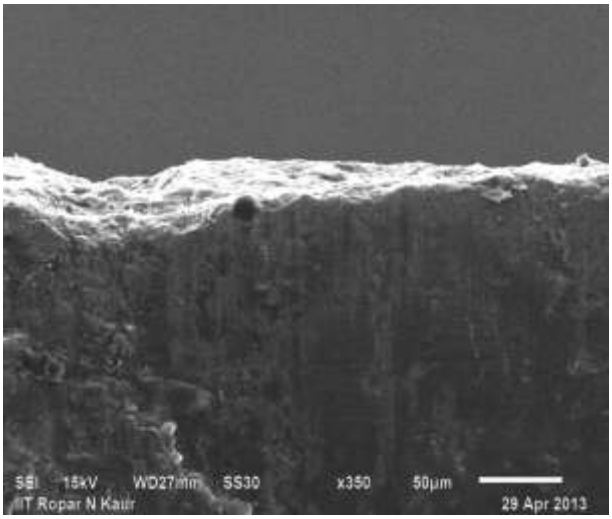

Figure 5.53 SEM of Trial 24 (Sample III)

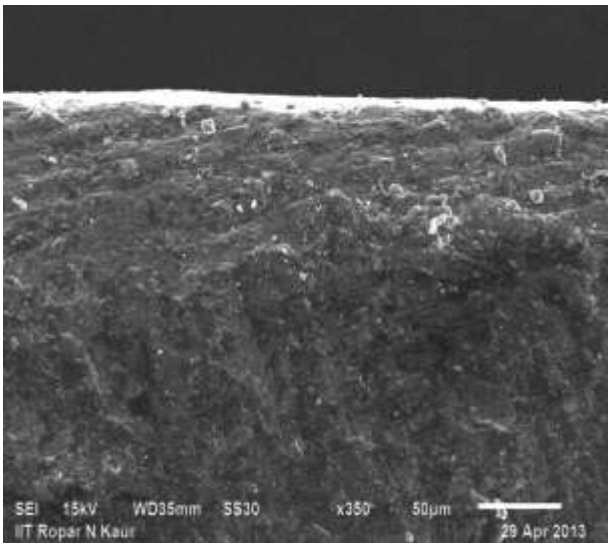

Figure 5.54 SEM of Trial 25 (Sample III)

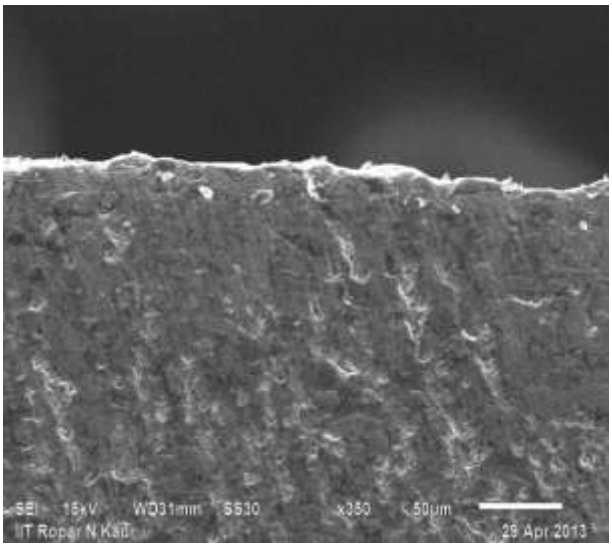

Figure 5.55 SEM of Trial 26(Sample III)

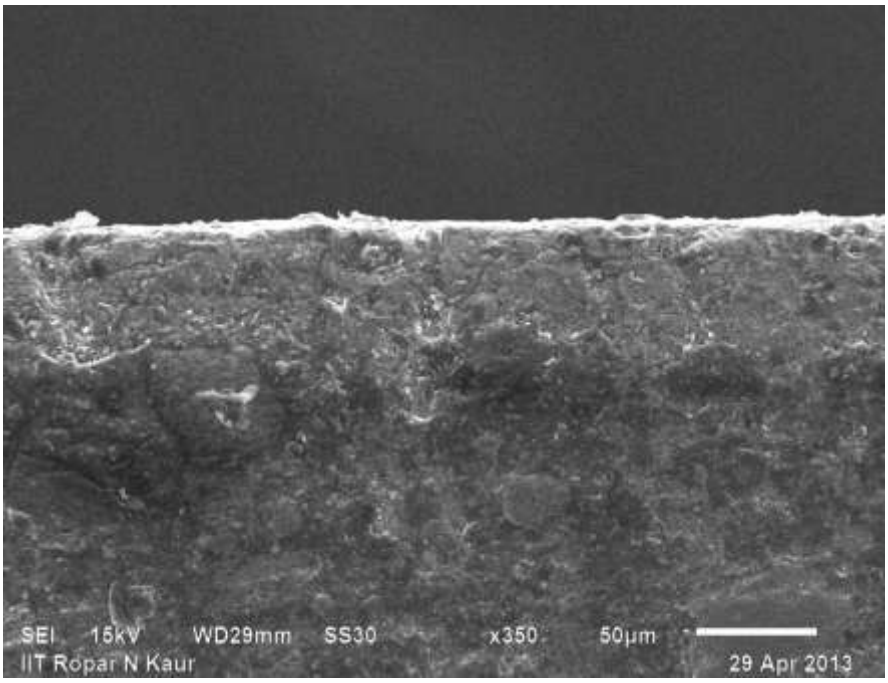

Figure 5.56 SEM micrograph of Trial 27 (Sample III)

It was observed from the microstructures corresponding to Trial 19 and Trial 23, that the recast layer was maximum for these trials, followed by Trial 24. On comparing Trial 19 and Trial 23 process parameters, it was observed that current and pulse-on time was same but the electrolytic copper tool electrode in the copper -powder mixed dielectric medium was used in Trial 19. The higher energy transfer between the electrodes results in maximum recast layer thickness. In Trial 24 the current was at its lowest level as compared to current setting in Trial 19. From Trial 19 and Trial 24, it was concluded that current is more significant factor contributing the recast layer thickness as compared to pulse-on time.

Residual stresses

The results for Residual stresses (Table 4.28, *Section 4.4*) were analyzed using Analysis of Variance (ANOVA) for identifying the significant factors affecting the residual stresses. The ANOVA data for the residual stresses is given in Table 5.12. The last and the 2nd last column of ANOVA table show the p-value and the F-value respectively for each factor. Those factors were significant which have a p-value less than 0.05 (for confidence level 95%) while the principle of the F- test is that the larger the F-value for a particular parameter, the greater is its effect on response values. Comparing the p-value and F- values from ANOVA table, the type of work piece material (type of MMC), type

of electrode material and pulse-off time was found to be the significant factors affecting residual stresses.

Table 5.12 ANOVA table of Residual stresses

Factors	Sum of squares	DOF	Variance	F-ratio	P-value
Work piece	16723.2	2	8361.6	11.18	0.001**
Electrode	6405.0	2	3202.5	4.28	0.035*
Current	1338.1	2	669.1	0.89	0.431
Pulse-on	1379.6	2	689.8	0.92	0.420
Pulse-off	7980.8	2	3990.4	5.34	0.019*
Dielectric	960	2	480.2	0.64	0.541
Error	10471.1	14	747.9		
Total	45258.4	26			

**** Most significant *Significant**

The main effect plot for residual stresses is shown in Figure 5.57. Main effect plots show the variation of residual stresses for each factor varied during experimentation. The x-axis represents the three levels at which each factor is varied and y-axis shows the resultant change in the residual stresses. The mean of response is indicated by a horizontal line.

The residual stresses were highest in Sample II and least in Sample III. Similarly, the residual stresses were highest with Cu-Gr electrode and least with Cu electrode. This may be due to higher coefficient of thermal expansion of work piece Sample II (See Table 4.4 for properties) of materials. Also, the higher percentage of reinforced particles in Sample I and Sample III helps in compensating the machining heating and cooling shocks (shielding effect). On the other hand, material with dense and bigger reinforced particles restrict the flow of molten matrix metal and cause larger mismatch between the thermal properties of matrix and reinforced particles [99, 104]. Hence it causes higher residual stresses in Sample II as compared to Sample III, which has lesser number of reinforced particles. The existence of conflicting compressive and tensile stresses between the soft matrix and hard particulates on the plane parallel and perpendicular to the surface during

intense temperature increase causes spalling and hot spots. This increases the severity of stresses differential which results in crack generation [39, 137].

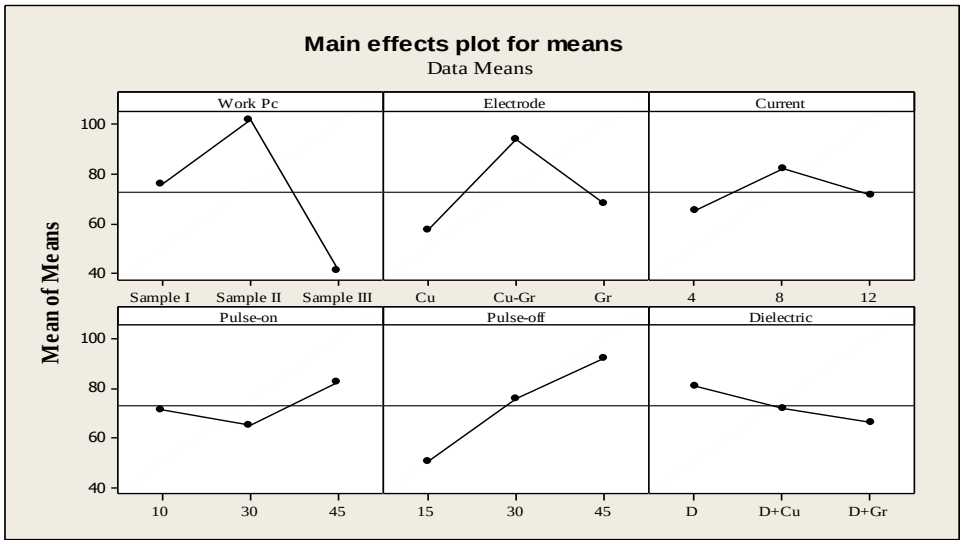

Figure 5.57 Main effect of control parameter on residual stresses

The presence of powder in dielectric reduces the thermal shocks by lowering the insulating strength of dielectric and these result in a stable EDM process. The highest level of pulse off time gives maximum residual stresses. The results have been further explained by plotting two factors at a time. Higher pulse off-time enhances the re-solidification time in the presence of dielectric medium and thus results in a bigger surface grains causing higher residual stresses.

In order to understand the effect of machining parameters on the residual stresses, the effect of factors taken two at a time are shown in Figures 5.58 to 5.59. The effect of current and pulse-off time on residual stresses is shown in Figure 5.58.

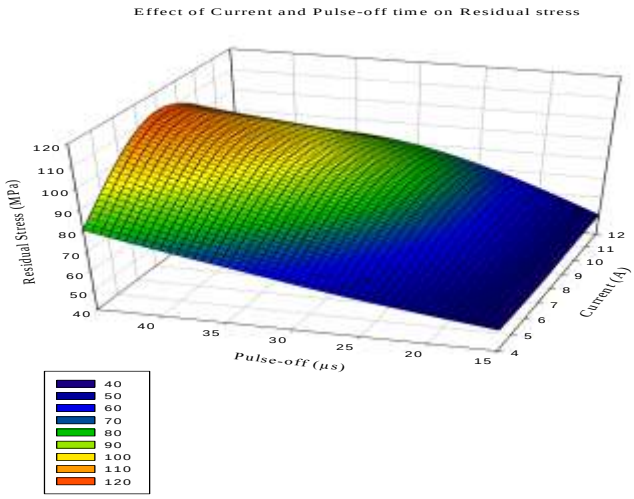

Figure 5.58 Effect of current and pulse-off time on residual stresses

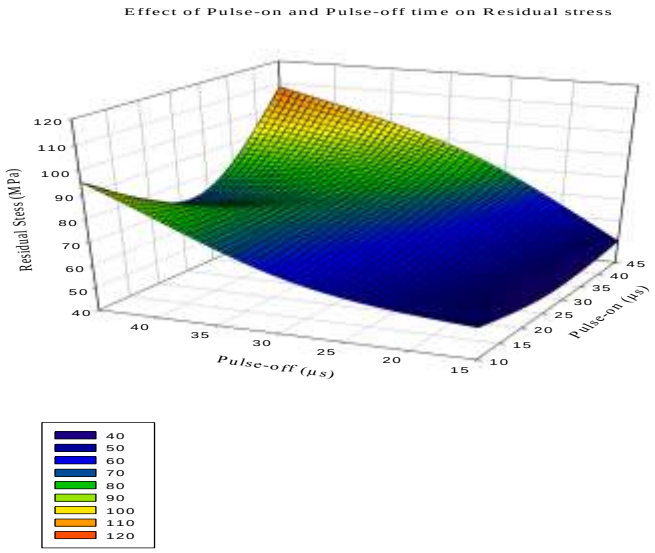

Figure 5.59 Effect of Pulse-on time and Pulse-off time on residual stresses

It reveals that at higher pulse-off time level, the increase in pulse-on time results in a decrease in residual stresses initially but it subsequently increases. The effect of tool electrode on different work piece materials is shown in Figure 5.60.

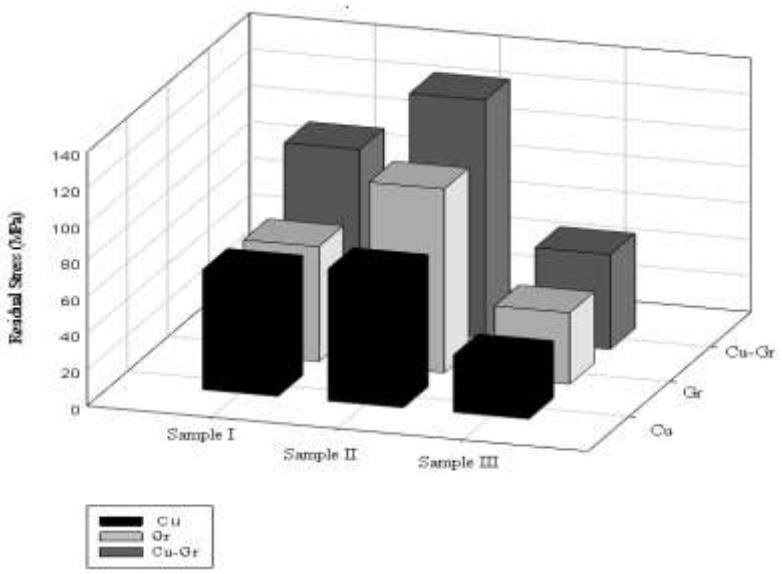

Figure 5.60 Effect of electrodes on residual stresses

The plots show that copper electrode, due to its higher conductivity, results in smooth plasma channel between the electrodes (anode and cathode) thereby causing lesser residual stresses. In case of composite electrode (Cu-Gr), discharge energy disintegrates weakly bonded particles from the electrode. These particles deposit on the work piece surface and this phenomenon results in higher residual stresses.

CHAPTER - 6

CONCLUSIONS AND SCOPE FOR FUTURE WORK

6.1 CONCLUSIONS

Experimental investigations were conducted on variant MMCs using electrical discharge machining process. Based on the experiments conducted, the following conclusions have been drawn:

1. During electric discharge machining of Al-10%Al_2O_3 MMC, the motivation factors at Stage I of experimentation were to enhance the productivity leading to higher MRR and better SR. The results show that all the responses (MRR, TWR, and SR) have a direct relationship with current but an inverse relationship with pulse-on time. This is because the increased pulse-on time decreases the frequency of spark occurrence.
2. The parts machined using conventional (+ve) polarity results in higher MRR as compared to those with negative polarity. Whereas, highest surface finish was obtained for reverse polarity (-ve polarity) when current was set at 8 Amps and pulse-on time at 30μs.
3. The regression statistical tool was used to develop the non-linear mathematical model to predict the machining response parameters. These models were further optimized using lexicographic goal programming (LGP).
4. The LGP proved to be a powerful tool in determining the setting of response parameters under given constraints. The optimal solution obtained using the LGP matched with experimental results and thus it can be used as a powerful tool for optimization of multiple responses. With straight polarity, high current (16 Amp) and low pulse on-time (10μs) should be used for maximizing MRR and for good surface finish, the current (8Amp) and pulse-on time (10μs) should be set at low levels. Experiments conducted with negative polarity showed similar results for finish machining. However, if TWR is a priority as compared to MRR, then current should be set at a lower level (8Amp) and pulse-on time (30μs) should be increased to an intermediate level.
5. The recast layer thickness is significantly affected by current and pulse-on time, and pulse-on time is found to be more significant. The formation of clusters or uneven distribution of reinforced particles deteriorates the properties of the machined surface. Hence due to least presence of reinforced particles in recast

layer, it is desirable to remove it. The responses in the present stage of study are consistent with the conclusions drawn by other investigators.

The study was extended by selecting two variants of MMCs; namely 65vol%SiC/A356.2 and 10vol%SiC-5vol% quartz/Al. The machining process parameters such as electrode material (Copper, Graphite and Copper-Graphite composite), peak current, pulse-on/off time and dielectric medium were varied during the study. Due to high carbon emission/deposition at high current and high pulse-on time conditions, the kerosene was replaced by EDM oil. Some experiments were also conducted in dielectric mixed with suspended powders. The following conclusions have been drawn from Stage II of experiments:

1. The residual stresses induced in the MMCs after machining were analyzed by X-ray diffraction method. Pulse-off time was identified as the most significant factor resulting in residual stresses in both the MMCs.
2. The analysis of results shows that MMCs with low coefficient of thermal expansion and a high density of reinforced particle have lower residual stresses.
3. The electrode material with high conductivity resulted in smooth formation of plasma channel between the electrodes; hence the induced residual stresses were minimum.
4. The increase in pulse-off time causes a steep rise in residual stresses due to extended solidification period while pulse-on time has no effect.
5. The addition of powder in the dielectric lowers the residual stresses. However, the conductivity of powder particles has no effect on residual stresses.
6. ANN model was developed to predict the residual stresses in such materials. The capability of ANN to predict residual stresses during EDM was achieved with feed forward back propagation neural architecture with two hidden layers with 9 and 7 neuron in each layer. The learning rate and momentum were selected as 0.001 and 0.7 respectively. The model accurately predicts the residual stresses and can be used as a reliable tool for study of residual stresses in case of complex problems that involve qualitative and quantitative factors.
7. The XRD patterns indicate the formation of new phases on the machined surface. The peak intensity after machining is reduced due to dislocation of atomic layer resulting in residual strains.

8. Current and pulse-on time significantly affected MRR while the addition of powder, current and pulse-on time affected SR. While pulse-off time had no significant effect on MRR and SR, it had the largest effect on residual stresses followed by powder mixed dielectric, current and the type of electrode used.
9. Analytic Hierarchy Process (AHP), a multiple criteria decision making tool for finite alternative was used for optimizing three output response parameters; namely residual stresses, material removal rate and surface roughness. The identification of process parameters and other requirements involves complex decision making due to conflicting parameter setting for different output responses. In the present stage, AHP was used to obtain more reliable global composite performance score for various machining conditions in a powder-mixed electric discharge machining of MMCs.
10. The optimal conditions for both types of materials were identified. The overall process settings for both the samples reveal that machining of MMCs with graphite electrode, higher pulse-on time and lowest pulse-off time in the presence of suspended particles dielectric gives minimum residual stresses with desired MRR.
11. Due to the presence of dense ceramic reinforced particles in Sample I as compared to Sample II, the desired results were obtained at intermediate level of current and higher conductivity suspended particles in a dielectric medium.
12. The optimal settings suggested that graphite electrode should be used with pulse-on and pulse-off time of 45µs and 15µs respectively. Addition of powder in the dielectric improved the MRR as the electrical conductivity of powder reduces the dielectric insulating strength. Also, copper powder suspended in the dielectric resulted in an optimal solution for 10vol%SiC-5vol% quartz/Al MMC and graphite powder gives better results for 65vol%SiC/A356.2 MMC. It may be concluded that to overcome problems of poor finish at high current setting in EDM, the dielectric should be mixed with powder.
13. Higher density of reinforced particles in the matrix results in lesser MRR, SR and residual stresses as ceramic particles act as a shield of matrix material against sparks energy. MRR variation with current was in line with results obtained while machining Al-10%Al_2O_3 composite. It decreased when the pulse-on time was stepped up from 10 to 30 µs. Further, it increased drastically as prolonged

pulse-on time causes intense melting and evaporation of matrix material and easy removal of reinforced particle by spalling mechanism.

14. Copper powder mixed EDM results in smoother machined surface as compared to graphite powder in the dielectric due to its higher conductive properties.

In Stage III, the EDM performance on three variants of MMCs (65vol%SiC/A356.2, Al-10vol%SiC-5vol% and 30vol%SiC/A359) was compared. The machining conditions of this stage were similar to Stage II. The following conclusions have been drawn:

1. Current and pulse-on time increases the spark energy which affects MRR. The density of reinforced particles shields the matrix material from spark energy; hence high MRR and high SR were observed with lowest reinforced particle matrix.
2. The pulse-off duration at its lowest level is sufficient to remove entrapped debris by the flushing pressure of dielectric which helps in improving MRR.
3. TWR was highest with Cu-Gr electrode due to disintegration of the weakly bonded particles in the composite electrode. High current also affects TWR adversely.
4. The effect of material properties and machining parameters on the residual stresses of a machined surface was investigated by measuring the shift in selected peak at highest angle by diffractometer method. It was observed that the residual stresses were tensile as well as compressive in nature due to conflicts in thermal properties of matrix and reinforced particles. The splitting of graph (d vs. $\sin^2\psi$) in the observation indicates a stress-gradient that represents the presence of shear stresses.
5. The surface residual stresses were observed to be mainly dependent upon concentration/ particle size and the conductivity of the work piece. The residual stresses increase with an increase in pulse-off time due to higher re-solidification time of the recast layer (as observed in Stage II of the experimental plan). Also, the residual stresses increase with increase in current from 4Amp to 8Amp but decrease with any further increase in current.
6. The depositions on the work piece due to the presence of copper powder in dielectric result in higher residual stresses as compared to conditions where graphite powder is mixed. Due to weak bonding in composite electrode (Cu-Gr),

significant quantities of disintegrated particles were deposited to form thick recast layer on the work piece.

7. The study also reports the phenomenon of surface modification while machining with EDM process. The density of reinforced ceramic forming oxides (SiO_2) at elevated temperature (above 1700^0C) is the most significant factor imposing micro-hardness on the machined surface.
8. The XRD spectra reveal the formation of copper oxide as the major transferred element from electrode/dielectric medium which is responsible for the modification of machined surface. This is due to its higher conductivity as well as reactivity potential of copper as compared to graphite, which is less reactive to form compounds or surface modifier. This results in improved conductivity and corrosive resistance of the surface.
9. The traces of carbon particles were observed under optical microscopical examination in the free form on the surfaces and the craters of the machined MMCs.
10. The deposition of carbon was observed when the machining parameters setting were at the highest level. Finally, the cross-sectional view of recast layer analysis reflected the profile of sparks generated during EDM. Hence, PMEDM may be designated as the most suitable machining option for MMCs to enhance surface properties.
11. In the SEM analysis, the thickness of recast layer is found to be maximum for dense reinforced particles MMCs due to its higher heat absorption tendency. Hence, high density matrix material also shows high extent cross-sectional residual stresses distribution. It also depends upon the size of reinforced particles. The recast layer thickness increases as the current increases from 4Amps to 8Amps but it shows a decreasing trend as the magnitude of current further increases. The PMEDM with copper as an additive shows a minimum recast layer thickness due to improved electrical conductivity and consistent discharges.

6.2 SUGGESTIONS FOR FUTURE STUDY

1. As is evident from the literature (see Figure 6.1), most of the published research work of EDM on MMCs has been carried out in the field of aluminium matrix composites, but very less work has been reported for the composite with other matrix phase such cobalt, steel etc. The EDM of matrix phase reinforced with

two or more different type of particulates/fibers, classified as a hybrid composite, are still an open area of research.

2. The abrasive nature of reinforcements hinders the applicability of MMCs which is overcome by highly acceptable EDM process and the controlled process parameters, to achieve the desired dimensional accuracy and surface finish. But still the area related to change in a matrix material property with EDM process parameters has not been tried yet.

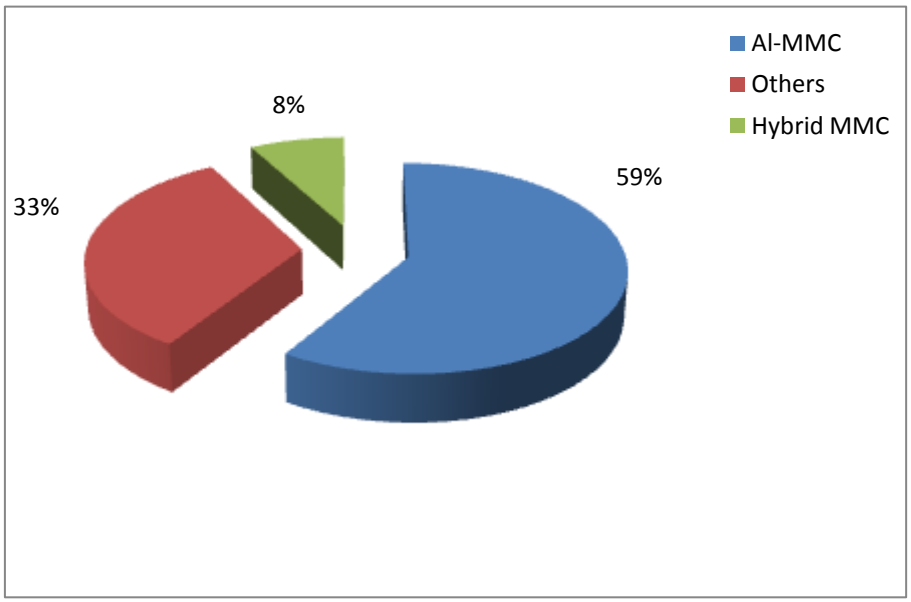

Figure 6.1 Research studies conducted in EDM on different MMCs

3. EDM process involves multi-input parameters, which makes this process a complex operation thus construction of a universally accepted mathematical model for prediction is responses is very difficult. The implementation of ANN modeling technique can overcome this complexity and the prediction of responses are more close to the experimental value which was successful applied in various manufacturing processes. But still this technique of modeling of EDM of MMCs is yet to be explored.
4. Due to heating and cooling shocks in EDM process, the investigation of residual stresses is subject of considerable emphasis to ensure the service life of a component. Out of various non destructive testing, X-ray diffraction method is mostly adopted by the researcher to measure residual stresses. The measure of residual stress in composite after machining is still open for the future work. The magnitude of residual stresses through-out the heat affected zone can be

measured by removing the machined thin layer by using the electro-polishing method.

5. The full tensor residual stresses on the machined surface can be explored to understand the nature of EDM process.
6. In this work, the process parameters have been optimized using Taguchi orthogonal array design. However, the study does not account the interaction between the process parameters.

REFERENCES

[1]. http://en.wikipedia.org/wiki/Mongol_bow (2013).

[2]. A.R. Ahamd, P. Asokan and S. Aravindan, Electric discharge machining of hybrid Al-SiC-B_4C and Al-SiC-Glass MMC's, *International Journal of Advanced Manufacturing Technology* 44 (2009) 520-528.

[3]. P. K. Rohatgi, Cast metal-matrix composite, In: Casting ASM Handbook, 9th edition, *ASM International* 15 (1992) 840-854.

[4]. P.C Pandey and H.S. Shan, Modern machining process, 7th edition, *Tata McGraw hill*, New Delhi (1993) 2.

[5]. A. Banerjee, M.K. Surappa and P.K. Rohatgi, Cast aluminum alloys containing dispersions of zircon particles, *Metallurgical and Material Transactions* B 4 (1983) 273-283.

[6]. P. K. Rohatgi, B.C.Pai and S.C. Panda, Preparation of cast aluminum-silicon particulate composites, *Journal of Materials Science* 14(1979) 2277-2283.

[7]. M.K. Surappa and P.K. Rohatgi, Preparation and properties of cast aluminum-ceramic particle composites, *Journal of Materials Science* 16(1981) 983-993.

[8]. F.A. Badia and P.K. Rohatgi, Dispersion of graphite particles in aluminum castings through injection of melt, *Transaction AFS* 77 (1969) 402-406.

[9]. B.C. Pai and P.K. Rohatgi, Production of cast aluminum graphite particles composites using a pellet method, *Journal of Materials Science* 13 (1978) 329-335.

[10]. G. Boothroyd and A.K. Winston, Non-conventional machining process, In: Fundamental of machining and machine tools, *Marcel Dekker Inc.*, New York (1989), 491-497.

[11]. J.A. McGeough, Electro-discharge machining, In: Advanced methods of machining, *Chapman & Hall*, London (1988) 130-136.

[12]. K. Ojha, R. K. Garg and K. K. Singh, MRR improvement in sinking electrical discharge machining: A review, *Journal of Minerals & Materials Characterization & Engineering* 9 (2010) 709-739.

[13]. R.K. Garg, K.K. Singh, A. Sachdeva, V. S. Sharma, K. Ojha and Sharanjit Singh, Review of research work in sinking EDM and WEDM on metal matrix composite materials, *International Journal of Advanced Manufacturing Technology* 50 (2010) 611-624.

[14]. T. Hidekazuh, S. Takumi and M. Kiyonori, Surface hardening of titanium using EDM process, *Titanium Japan* 48 (2000) 143-145.

[15]. F. Y. Tzeng and C.Y. Lee, Effects of powder characteristics on electro-discharge machining efficiency, *International Journal of Advanced Manufacturing Technology* 17 (2001) 586-592.

[16]. K. Furutani, A. Saneto, H. Takezawa, N. Mohri and H. Miyake, Accretion of titanium carbide by electric discharge machining with powder suspended in working fluid, *Precision Engineering* l25 (2001) 138-144.

[17]. M.L. Jeswani, Effect of the addition of graphite powder to kerosene used as the dielectric fluid in electric discharge machining, *Wear* 70 (1981) 133-139.

[18]. Y.S. Wong, L.C. Lim, I. Rahuman and W.H. Tee, Near mirror-finish phenomenon in EDM using powder-mixed dielectric, *Journal of Materials Processing Technology* 79 (1998) 30-40.

[19]. Mukund R. Patel, Maria A. Barrufet, Philip T. Eubank and Daryl D. DiBitonto, Theoretical models of electric discharge machining process- The anode erosion model, *Journal Of Applied Physics* 66 (1989) 4104-4111.

[20]. Daryl D. DiBitonto, Philip T. Eubank, Mukund R. Patel, and Maria A. Barrufet, Theoretical models of the electrical discharge machining process. I. A simple cathode erosion model, *Journal of Applied Physics* 66 (1989) 4095-4103.

[21]. Y. H. Guu, H. Hocheng, C. Y. Chou and C.S. Deng, Effect of electric discharge machining on surface characteristics and machining damage of AISI D2 tool steel, *Material Science and Engineering* A 358 (2003) 37-43.

[22]. B. R. Lazarenko and N. I. Lazarenko, Technological characteristics of electro-spark machining of current conducting materials In: Electro-spark machining of metals *Consultant Bureau* 2 (1964) 1.

[23]. Sanjeev Kumar, To investigate the phenomenon of surface modification in die steels using EDM process, *Ph.D. Thesis,* Thapar University, India (2008).

[24]. P.J Withers, M. Turski, L. Edwards, P.J. Bouchard and D.J. Buttle, Recent advances in residual stress measurement, *International Journal of Pressure Vessels and Piping* 85 (2008) 118-127.

[25]. T. B. Barker, Engineering quality by design: Interpreting the Taguchi approach, *Marcel-Dekker Inc.*, New York (1990) 78-82.

[26]. R. Hick and V.K. Turner, Fundamental concepts in the design of experiments, 5th edition, *Oxford University Press* (1999) 134-139.

[27]. Deborah D.L. Chung, Composite materials science and applications, 2nd edition, *Springer-Verlag* London limited (2010).

[28]. Wong Park, Chelhong Park, Hyungjin Kim and Sunchul Huh, Microstructure and wear characteristics on Al alloy matrix composite reinforced with Ni perform, *Journal of Mechanical Science and Technology* 26 (2012) 1741-1746.

[29]. Byeong-Choon Goo and Myung-Ho Kim, Characteristics of A356/SiCp and A390/SiCp composites, *Journal of Mechanical Science and Technology* 26 (2012) 2097- 2100.

[30]. S. Basavarajappa and G. Chandramohan, Wear studies on metal matrix composites: A Taguchi approach, *Journal of Materials Science and Technology* 21 (2005) 845-850.

[31]. Karl Ulrich Kainer, Metal matrix composites. Custom made materials for automotive and aerospace engineering, *Wiley-VCH KGaA*, Weinheim, (2006) 8-11.

[32]. M.K. Surappa, Aluminum matrix composites: Challenges and opportunities, *Sadhana*, 28 (2003) 319-334.

[33]. S.W. Lai and D.D.L. Chung, Consumption of SiC whiskers by the Al-SiC reaction in aluminum-matrix SiC whisker composites, *Journal of Materials Chemistry* 6 (1996) 469-477.

[34]. Y.W. Seo, D. Kim and M. Ramulu, Electric discharge machining of functionally graded 15-35Vol% SiC/Al composite, *Materials and Manufacturing Processes* 21 (2006) 479-487.

[35]. P. Narinder Singh, K. Raghukandan, M. Rathinasabapathi and B.C. Pai, Electric discharge machining of Al-10%SiC as-cast metal matrix composite, *Journal of Materials Processing Technology* 155-156 (2004) 1653-1657.

[36]. Sanjeev Kumar, Rupinder Singh, T.P. Singh and B.L. Sethi, Surface modification by electric discharge machining: A review, *Journal of Materials Processing Technology* 209 (2009) 3675-3687.

[37]. K.H. Ho and S.T. Newman, State of the art electric discharge machining (EDM), *International Journal of Machine Tools & Manufacture* 43 (2003) 1287-1300.

[38]. S. Norasetthekul, P.T. Eubank, W.L. Bradley, B. Bozkurt and S. Stucker, Use of zirconium diboride-copper as an electrode in plasma applications, *Journal of Materials Science* 34 (1999) 1048-1270.

[39]. R.A. Mahdavinejad and A. Mahddavinejad, ED machining of WC-Co, *Journal of Materials Processing Technology* 162 (2005) 637-643.

[40]. Javier Llorca, Fatigue of particle and whisker reinforced metal matrix composite, *Progress in Materials Science* 4 (2002) 283-353.

[41]. M. Karayaka and S. Huseyin, Thermo-mechanical fatigue of particulate-reinforced aluminum 2xxx-T4, *Metallurgical and Materials Transaction* A 22 (1991) 697-707.

[42]. M. Ramulu, G. Paul and J. Patel, EDM surface effect on the fatigue strength of a 15 vol% SiC/Al metal matrix composite material, *Composite Structures* 54 (2001) 79-86.

[43]. A.M Gadalla and W. Tasi, Electric discharge machining of tungsten carbide-cobalt composite, *Journal of the American Ceramic Society* 72 (1989) 1396-1401.

[44]. J.W. Liu, T.M. Yue and Z.N. Guo, An analysis of the discharge mechanism in electrochemical discharge machining of particulate reinforced metal matrix composites, *International Journal of Machine Tools & Manufacture* 50 (2010) 86-96.

[45]. Yan-Cherng Lin, A-Cheng Wang, Der-An Wang and Chin Cherng Chen, Machining performance and optimizing machining parameters of Al_2O_3-TiC ceramics using EDM based on the Taguchi method, *Materials and Manufacturing Processes* 24 (2009) 667-674.

[46]. A.M. Gadalla, B. Bozkurt and N.M. Faulk, Modeling of thermal spalling during electric discharge machining of titanium diboride, *Journal of the American Ceramic Society* 74 (1991) 801-806.

[47]. J.H. Zhang, T.C. Lei and W.S. Lau, Study on the electrode-discharge machining of a hot presses aluminum oxide based ceramic, *Journal of Materials Processing Technology* 63 (1997) 908-912.

[48]. K. Ponappa, S. Aravindan, P. V. Rao, J. Ramkumar, and M. Gupta, The effect of process parameters on machining of magnesium nano alumina composites through EDM, *International Journal of Advanced Manufacturing Technology* 46 (2010) 1035-1042.

[49]. H. Hocheng, W.T. lei and H.S. Hsu, Preliminary study of material removal in electric discharge machining of SiC/Al, *Journal of Materials Processing Technology* 63 (1997) 813-818.

[50]. D.C. Tasi, T.S. Lui and L.H. Chen, Effect of silicon particles on the EDM characteristic of Al-Si alloys, *Material Transactions* 43 (2002) 199-205.

[51]. Velusamy Senthilkumar and Bidwai Uday Omprakash, Effect of titanium carbide particles addition in the aluminum composite on EDM process parameters, *Journal of Manufacturing Processes* 13 (2011) 60-66.

[52]. S. Gopalakannan, T. Senthilvelan and S. Ranganathan, Modeling and optimization of EDM process parameters on machining of Al 7075-B_4C MMC using RSM, *Procedia Engineering* 38 (2012) 685-690.

[53]. Ko-Ta Chiang, Modeling and analysis of the effects of machining parameters on the performance characteristics in the EDM process of Al_2O_3+TiC mixed ceramic, *International Journal of Advance Manufacturing Technology* 37 (2009) 523-533.

[54]. Che-Chung Wang and Yao Chien Lin, Feasibility study of electric discharge machining for W/Cu composite, *International Journal of Refractory Metal & Hard Materials* 27 (2009) 872-882.

[55]. B. Mohan, A. Rajadurai and K.G. Satyanarayana, Effect of SiC and rotation of electrode on electric discharge machining of Al-SiC composite, *Journal of Materials Processing Technology* 124 (2002) 297-304.

[56]. B. Mohan, A. Rajadurai and K.G. Satyanarayana, Electric discharge machining of Al-SiC metal matrix composite using rotary tube electrode, *Journal of Materials Processing Technology* 153 (2004) 978-985.

[57]. H.K. Kansal, Sehijpal Singh and Pradeep Kumar, Technology and research developments in powder mixed electric discharge machining (PMEDM), *Journal of Materials Processing Technology* 184 (2007) 32-41.

[58]. S. Singh, S. Maheshwari and P.C. Pandey, Some investigations into the electrode discharge machining of hardened tool steel using different electrode materials, *Journal of Materials Processing And Technology* 149 (2004) 272-277.

[59]. J. Marafona and C. Wykes, A new method of optimizing material removal rate using EDM with copper-tungsten electrodes, *International Journal of Machine Tools & Manufacture* 40 (2000) 153-164.

[60]. M.P. Samuel and P.K. Philip, Powder metallurgical tool electrodes for electric discharge machining, *International Journal of Machine Tools & Manufacture* 37 (1997) 1625-1633.

[61]. A.K. Khanra, B.R. Sarkar, B. Bhattacharya, L.C. Pathak and M.M. Godkhindi, Performance of ZrB_2-Cu composite as an EDM electrode, *Journal of Materials Processing Technology* 183 (2007) 122-126.

[62]. H.C. Tasi, B.H. Yan and F.Y. Huang, EDM performance of Cr/Cu-based composite electrodes, *International Journal of Machine Tools & Manufacture* 43 (2003) 245-252.

[63]. Ching-Yuan Bai and Chun-Hao Koo, Effect of kerosene or distilled water as dielectric on electric discharge alloying of superalloy Haynes 230 with Al-Mo composite electrode, *Surface & Coating Technology* 200 (2006) 4127-4135.

[64]. Ching-Yuan Bai, Effect of electric discharge surface modification of super alloy Haynes 230 with aluminum and molybdenum on oxidation behavior, *Corrosion Science* 49 (2007) 3889-3904.

[65]. R. Karthikeyan, P.R. Lakshmi Narayanan and R.S. Naagarazan, Mathematical modeling for electric discharge machining of aluminum-silicon carbide particulate composites, *Journal of Materials Processing Technology* 87 (1999) 59-63.

[66]. Sushant Dhar, Rajesh Purohit, Nishant Saini, Akhil Sharmaand and G. Hemanth Kumar, Mathematical modeling of electric discharge machining of cast Ai-4Cu-6Si alloy-10% SiC_p composites, *Journal of Materials Processing Technology* 194 (2007) 24-29.

[67]. Sarabjeet Singh Sidhu, Ajay Batish and Sanjeev Kumar, EDM of metal matrix composite for parameter design using lexicographic goal programming, *Materials and Manufacturing Processes* 28 (2013) 495-500.

[68]. B. Y. Lee, H.S. Liu and Y.S. Tarng, Modeling and optimization of drilling process, *Journal of Materials Processing Technology* 74 (1998) 149-157.

[69]. B. Ozcelik, H. Oktem and H. Kurtaran, Optimization surface roughness in end milling Inconel 718 by coupling neural network model and genetic algorithm, *International Journal of Advance Manufacturing Technology* 27 (2005) 234-241.

[70]. T.A. Speeding and Z.Q. Wang, Study on modeling of wire EDM process, *Journal of Materials Processing Technology* 69 (1997) 18-28.

[71]. B.F. Nabil and A. Ridha, Ground surface roughness prediction based upon experimental design and neural network models, *International Journal of Advance Manufacturing Technology* 31 (2006) 24-36.

[72]. Z. Katz and J. Naude, A neural network/expert system approach for design improvement of products manufactured by EDM, ASME transactions*: Journal of Manufacturing Science and Engineering* 121 (1999) 733-738.

[73]. G. Indurkhya and K.P. Rajurkar, Artificial neural network approach in modeling of EDM process, *Intelligent Engineering System Through Artificial Neural Networks* USA 2 (1992) 845-850.

[74]. D.K. Panda and R.K. Bhoi, Artificial neural network prediction of material removal rate in electro discharge machining, *Materials and Manufacturing Processes* 20 (2005) 645-672

[75]. T.K.K.R. Mediliyegedara, A.K.M. De Silva, D.K. Harrison, J.A. McGeough and D. Hepburn, Designing steps and simulation results of a pulse classification system for the electrochemical discharge machining process-An artificial neural network approach, *Advances in Intelligent and Soft Computing* 34 (2006) 343-352.

[76]. J.P. Kruth, L. Stevens, L. Froyen and B. Lauwers, Study on the white layer of a surface machined by die sinking electro-discharge machining. *Annals of the CIRP* 44 (1995) 169-172.

[77]. F. Muller and J. Monaghan, Non-conventional machining of particle reinforced metal matrix composite, *International Journal of Machine Tool & Manufacture* 40 (2000) 1351-1366.

[78]. N.P. Hung, L.J. Yang and K.W. Leong, Electro discharge machining of cast metal matrix composite, *Journal of Materials Processing and Technology* 44 (1994) 229-236.

[79]. A. De Silva and J. Ranke, Electric discharge machining of metal matrix composite, In: *Proceeding of International Symposium for Electro Machining*, Switzerland (1995) 75-84.

[80]. T. Le Roux M.L.H. Wise and D.K. Aspinwall, The effect of electrical discharge machining on the surface integrity of an aluminum-silicon carbide metal matrix composite, *Journal of Processing Advanced Material* 3 (1993) 233-241.

[81]. M. Ramulu, M.G. Jenkins and J.A. Daigneault, Spark-erosion process effects on the properties and performance of TiB_2 particulate-reinforced/SiC matrix ceramic composite, *Ceramic Engineering and Science Proceedings* 8 (1997) 227-238.

[82]. P.F. Thomson, Surface damage in electro-discharge machining, *Journal of Material Science & Technology* 5 (1989) 1153-1157.

[83]. L.C. Lee, L.C. Lim, Y.S. Wong and H.H. Lu, Towards a better understanding of the surface features of electro-discharge machined tool steel, *Journal of Materials Processing Technology* 24 (1990) 513-523.

[84]. Willam R. Osgood, Residual stresses in metals and metal construction, *Reinhold Publishing Corporation*, New York, (1954).

[85]. P.J. Withers and H.K.D.H. Bhadeshia, Residual stress Part1- Measurement techniques, *Material Science and Technology* 17 (2001) 355-365.

[86]. J.R. Crookall and B.C. Khor, Residual stresses and surface effects in electro-discharge machining, In: *Proceedings of 13th International Machine Tool Design and Research Conference*, Birmingham (1972) 331-338.

[87]. H.K. Lloyd and R.H. Warren, Metallurgy of spark-machined surfaces, *Journal of Iron Steel Institute* 203 (1965) 238-247.

[88]. M. Barash and M.G. Sri-Ram, Some properties of spark machined heat treated steel, In: *Proceedings of Third International Machine Tool Design and Research Conference*, Birmingham (1962) 85-91.

[89]. W. Konig R. Wertheim, Y. Zvirin and M. Toren, Material removal and energy distribution in electric discharge machining, *CIRP Annal* 24 (1975) 95-100.

[90]. A.G. Mamalis, N.M. Vosniakos, N.M. Vacevanidis and X. Junzhe, Residual stress distribution and structural phenomena of high-strength steel surface due to EDM and ball-drop forming, *CIRP Annal* 37 (1988) 531-535.

[91]. J.C. Rebelo, A.M. Diaz, D. Kremer and J.L. Lebrun, Influence of pulse energy on the surface integrity of martensite steels, *Journal of Materials Processing Technology* 84 (1998) 90-96.

[92]. F. Ghanem C. Braham and H. Sidhom, Influence of steel type on electric discharge machined surface integrity, *Journal of Materials Processing Technology* 142 (2003) 163-173.

[93]. J.P. Kruth and P. Bleys, Measuring residual stress caused by wire EDM of tool steel, *International Journal of Electrical Machines* 5 (2000) 23-28.

[94]. Bulent Ekmekci, Residual stress and white layer in electric discharge machining (EDM), *Applied Surface Science* 253 (2007) 9234-9240.

[95]. X.S. Ll, A.H. Cai and J.J. Zeng, Effect of EDM conditions on surface residual stress of Cr12MoV steel, *Material Science Forum* 697 (2012) 171-175.

[96]. Bulent Ekmekci, Oktay Elkoca, A. Erman Tekkaya and Abdulkadir Erden, Residual stress state and hardness depth in electric discharge machining: De-ionized water as dielectric, *Machine Science and Technology* 9 (2005) 39-61.

[97]. Shuvra Das, Mathias Klotz and F. Klocke, EDM simulation: Finite element-based calculation of deformation, microstructure and residual stress, *Journal of Materials Processing Technology* 142 (2003) 434-451.

[98]. Chandan Kumar Biswas and Mohan Kumar Pradhan, FEM of residual stress of EDMed surface, *Advance Materials Research* 383 (2012) 872-876.

[99]. P.J Withers, M. Turski, L. Edwards, P.J. Bouchard and D.J. Buttle, Recent advances in residual stress measurement, *International Journal of Pressure Vessels and Piping* 85 (2008) 118-127.

[100]. I.S. Jawahir, E. Brinksmeier, R.M Saoubi, D.K. Aspinwall, J.C. Outeiro, D. Meyer, D. Umbrello and A.D. Jayal, Surface integrity in material removal process: Recent advances, *CIRP Annals- Manufacturing Technology*, 60 (2011) 603-626.

[101]. Z.M. Sun, J.B. Li, Z.G. Wang and W.J. Li, Residual stresses in silicon carbide particulate reinforced aluminum composite, *Acta Metallurgica Et Materialia* 40 (1992) 2961-2966.

[102]. H.M. Ledbetter and M.W. Austin, Internal strain (Stress) in an SiC-Al particle-reinforced composite: An X-ray diffraction study, *Material Science and Engineering* 89 (1987) 53-61.

[103]. A. Roatta and R.E. Bolmaro, An Eshelby inclusion- based model for the study of stresses and plastic strain localization in metal matrix composite : General formulation and its application to round particles, *Material Science and Engineering: A* 229 (1997) 182-191.

[104]. Tomohiko Adachi, Tohru Sekino, Tadachika Nakayama, Takafumi Kusunose and Koichi Niihara, Measurement of microscopic stress distribution of multilayered composite by X-ray stress analysis, *Materials Letters* 57 (2003) 3057-3062.

[105]. Liu Cheng, Zhang Fan and Zhang Guoding, Micro-X-ray diffraction study of thermal residual stresses in some model aluminum matrix composite, *Journal of Materials Science* 39 (2004) 2923-2925.

[106]. P.B. Prangnell, S.J. Barnes, S.M. Roberts and P.J. Withers, The effect of particle distribution on the damage formation in particulate reinforced metal matrix composites deformed in compression, *Material Science and Engineering: A* 220 (1996) 41-56.

[107]. J.J. Lewandowski, C. Liu and W.H. Hunt, Effect of matrix microstructure and particle distribution on fracture of an aluminum metal matrix composite, *Material Science and Engineering: A* 107 (1989) 241-255.

[108]. P.J. Ross, Taguchi techniques for quality engineering, *McGraw Hill*, New York, (1996).

[109]. B.D. Cullity, Elements of X-ray diffraction 2nd edition, *Addison-Wesley*, New York (1978)

[110]. U. Welzel, J. Ligot, P. Lamparter, A.C. Vermeulen and E.J. Mittemeijer, Stress analysis of polycrystalline thin films and surface regions by X-ray diffraction, *Journal Of Applied Crystallography* 38 (2005) 1-29.

[111]. D.C. Montgomery, Design & Analysis of Experiments, 5th edition, *John Wiley & Sons*, New Delhi (2005).

[112]. T. Bagchi, Taguchi methods explained: Practical steps to robust design, *Prentice Hall of India* (1993).

[113]. D.L. Sikarskie, On a series form of correction to stress measured using X-Ray diffraction, *AIME Transactions* 239 (1967) 577-580.

[114]. Jyh-Wei Lee, Microstructure evaluation and phase transformation of recast layer in electrical discharge machined dual phase Fe-Mn-Al alloy, *Journal of Materials Science*, 38 (2003) 1679-1687.

[115]. S. Rajasekaran and G.A. Vijayalakshmi Pai, Neural networks, fuzzy logic and genetic algorithms, *Eastern Economy Edition* (2003) 22-23.

[116]. S. Rangwala and D. Dornfeld, Sensor integration using neural networks for intelligent tool condition monitoring, *Journal of Engineering For Industry ASME*, 112 (1990) 219-228.

[117]. I. N. Tansel, C. Mekdeci, O. Rodriguez and B. Uragun, Monitoring drill conditions with wavelet based encoding and neural networks, *International Journal of Machine Tools Manufacturing* 33 (1993) 559-575.

[118]. Y.S. Trang, Y.W. Hseih and S.T. Hwang, Sensing tool breakage in face milling with a neural network, *International Journal of Machine Tools Manufacturing* 34 (1994) 341-350.

[119]. Y.S. Liao, M.T. Yan and C.C. Chang, A neural network approach for the on-line estimation of workpiece height in WEDM, *Journal of Materials Processing Technology* 121 (2002) 252-258.

[120]. A. Behrens and J. Ginzel, Neuro-Fuzzy process control system for sinking EDM, *Journal of Manufacturing Process* 5 (2003) 33-39.

[121]. Debabrata Mandal, Surjya K. Pai and Partha Saha, Modeling of electric discharge machining process using back propagation neural network and multi-objective optimization using non-dominating sorting genetic algorithm-II, *Journal of Materials Processing Technology* 186 (2007) 154-162.

[122]. P.H. Prevost, A. Isambert, D. Depeyre, C. Donadille, and R. Perisse, Some practical insights into neural network implementation in metallurgical industry, Computers & chemical engineering 18 (1994) 1157-1170.

[123]. Fengguo Caoand and Qinjian Zhang, Neural network modeling and parameters optimization of increased explosive electric discharge grinding process for large area polycrystalline diamond, *Journal of Materials Processing Technology* 149 (2004) 106-111.

[124]. Ulas Caydas and Ahmet Hascalik, A study on surface roughness in abrasive water-jet machining process using artificial neural networks and regression analysis method, *Journal of Materials Processing Technology* 202 (2008) 574-582.

[125]. N. Tosun and L. Ozler, A study of tool life in hot machining using artificial networks and regression analysis methods, *Journal of Materials Processing Technology* 124 (2002) 99-104.

[126]. J.T Lin, D. Bhattacharyya and V. Kecman, Multi regression and neural network analysis in composite machining, *Composite Science Technology* 63 (2003) 539-548.

[127]. Azlan Mohd Zain, Habibollah Haron, Sultan Noman Qasem and Safian Sharif, Regression and ANN models for estimating minimum value of machining performance, *Applied Mathematical Modeling* 36 (2012) 1477-1492.

[128]. N. Muthukrishnan and J. Paulo Davim, Optimization of machining parameter of Al/SiC-MMC with ANOVA and ANN analysis, *Journal of Materials Processing Technology* 209 (2009) 225-232.

[129]. P.G. Benardos and C.G. Vosniakos, Prediction of surface roughness in CNC face milling using neural networks and Taguchi's designs of experiments, *Robotics and Computer Integrated Manufacturing* 18 (2002) 343-354.

[130]. Lei Che, Masahide Gotoh, Shigeki Takago and Yukio Hirose, X-ray elastic constant determination and residual stress estimation of spherical carbide in JIS SK3, *International Offshore and Polar Engineering Conference*, USA (2006) 51-56 ISBN 1-880653-66-4.

[131]. Hamdy A. Taha, Operation research an introduction, In: Decision analysis and games, 7th edition, *Pearson Education* (2002) 503-511.

[132]. S. Das and A.B. Chattopadhyay, Application of the analytic hierarchy process for estimating the state of tool wear, *International Journal of Machine Tools and Manufacturing* 43 (2003) 1-6.

[133]. R. Venkata Rao, Material selection for a given engineering application, In: Decision making in the manufacturing environment, 1st edition, *Springer* (2007) 59-60.

[134]. Singiresu S. Rao, Further topics in optimization: In Engineering optimization-3rd edition, *New Age International (P) Limited* (2003) 785-786.

[135]. B. Lauwer, J.P. Kruth, W. Liu, B. Sahacht and P. Bleys, Investigation of material removal mechanism in EDM of composite ceramic materials, *Journal of Materials Processing Technology* 149 (2004) 347-352.

[136]. A. Bhattacharya, Ajay Batish and K. Singh**,** FE simulation and experimental validation of powder mixed EDM process for estimating the temperature distribution and volume removed in single crater, *International Journal of Modeling, Simulation, and Scientific Computing*, (2012) DOI: 10.1142/S1793962312500067.

[137]. C.S. Trueman and J. Hoddleston, Material removal by spalling during EDM of ceramics, *Journal of the European Society* 20 (2000) 1629-1635.

[138]. Sarabjeet Singh Sidhu, Ajay Batish and Sanjeev Kumar, Neural-Network-Based modeling to predict residual stresses during electric discharge machining of Al/SiC-MMCs, *Proceedings of the Institution of Mechanical Engineers Part:B* (2013) doi: 10.1177/0954405413492505.

APPENDIX – A

STANDARD ORTHOGONAL ARRAY

Table A.1 L18 orthogonal array

Trial No.	Col. 1	Col. 2	Col.3	Col.4	Col.5	Col. 6	Col. 7	Col. 8
1	1	1	1	1	1	1	1	1
2	1	1	2	2	2	2	2	2
3	1	1	3	3	3	3	3	3
4	1	2	1	1	2	2	3	3
5	1	2	2	2	3	3	1	1
6	1	2	3	3	1	1	2	2
7	1	3	1	2	1	3	2	3
8	1	3	2	3	2	1	3	1
9	1	3	3	1	3	2	1	2
10	2	1	1	3	3	2	2	1
11	2	1	2	1	1	3	3	2
12	2	1	3	2	2	1	1	3
13	2	2	1	2	3	1	3	2
14	2	2	2	3	1	2	1	3
15	2	2	3	1	2	3	2	1
16	2	3	1	3	2	3	1	2
17	2	3	2	1	3	1	2	3
18	2	3	3	2	1	2	3	1

Table A.2 L27 orthogonal array

Trial No.	Col. 1	Col. 2	Col. 3	Col. 4	Col. 5	Col. 6	Col. 7	Col. 8	Col. 9	Col. 10	Col. 11	Col. 12	Col. 13
1	1	1	1	1	1	1	1	1	1	1	1	1	1
2	1	1	1	1	2	2	2	2	2	2	2	2	2
3	1	1	1	1	3	3	3	3	3	3	3	3	3
4	1	2	2	2	1	1	1	2	2	2	3	3	3
5	1	2	2	2	2	2	2	3	3	3	1	1	1
6	1	2	2	2	3	3	3	1	1	1	2	2	2
7	1	3	3	3	1	1	1	3	3	3	2	2	2
8	1	3	3	3	2	2	2	1	1	1	3	3	3
9	1	3	3	3	3	3	3	2	2	2	1	1	1
10	2	1	2	3	1	2	3	1	2	3	1	2	3
11	2	1	2	3	2	3	1	2	3	1	2	3	1
12	2	1	2	3	3	1	2	3	1	2	3	1	2
13	2	2	3	1	1	2	3	2	3	1	3	1	2
14	2	2	3	1	2	3	1	3	1	2	1	2	3
15	2	2	3	1	3	1	2	1	2	3	2	3	1
16	2	3	1	2	1	2	3	3	1	2	2	3	1
17	2	3	1	2	2	3	1	1	2	3	3	1	2
18	2	3	1	2	3	1	2	2	3	1	1	2	3
19	3	1	3	2	1	3	2	1	3	2	1	3	2
20	3	1	3	2	2	1	3	2	1	3	2	1	3
21	3	1	3	2	3	2	1	3	2	1	3	2	1
22	3	2	1	3	1	3	2	2	1	3	3	2	1
23	3	2	1	3	2	1	3	3	2	1	1	3	2
24	3	2	1	3	3	2	1	1	3	2	2	1	3
25	3	3	2	1	1	3	2	3	2	1	2	1	3
26	3	3	2	1	2	1	3	1	3	2	3	2	1
27	3	3	2	1	3	2	1	2	1	3	1	3	2

APPENDIX – B

METAL MATRIX COMPOSITE ARRANGED FROM THE OUTSOURCES

The work piece 65vol%SiC/A356.2 (Sample I) was supplied by Ceramic Process System (CPS), 111 South Worcester Street, Norton, MA, USA.

The material was supplied in the form of rectangular strip of dimension 150mm x 120mm x 5mm. A multipurpose heat sinking component manufactured by the company is shown in Figure B.1.

Figure B.1 Pictorial view of 65%SiC/A356.2 components

The microstructure of these components is shown in Figure B.2. The Figure B.2 indicates the composite material provided was a mixture of three types of SiC particles.

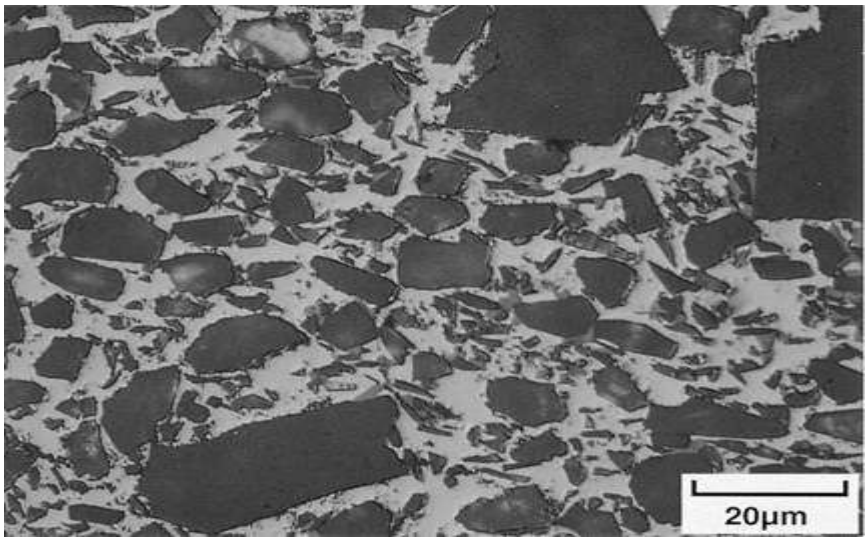

Figure B.2 Microstructure of un-machined 65%SiC/Al

The workpiece 30vol%SiC/A359 (Sample III) supplied by (Metallic Composites for 21st Century) MC-21, Inc. 5100, Convair Dr. Carson City, NV 89706.

The material supplied was also in the form of rectangular strip (Figure B.3). The material being supplied contains 30volume percent Silicon Carbide in A359 aluminum i.e. 30%SiC/A359. The SiC particles average ~ 14 microns in diameter.

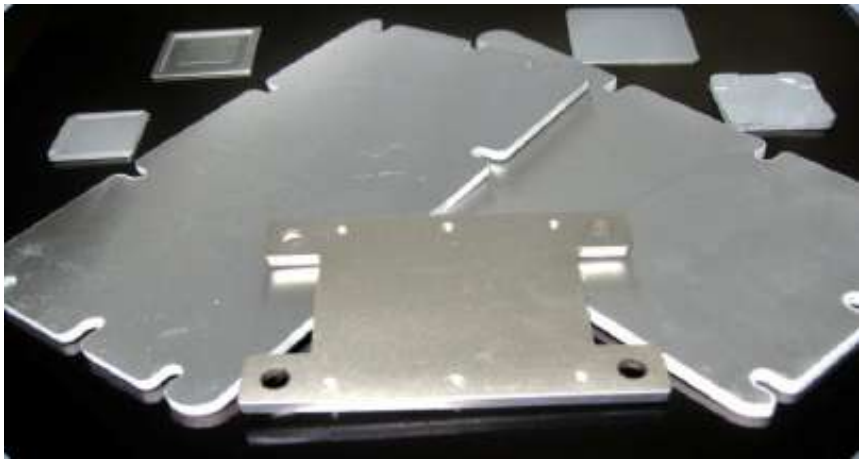

Figure B.3 Pictorial view of 30%SiC/A359 components

The application of this material was in the field of automobile and various manufacturing industries. The pictorial view of some automobile parts manufactured with this material is shown in Figure B.4.

Figure B.4 Some automobile parts manufactured with 30% SiC/A359 composite material

The microstructure of 30%SiC/A359 metal matrix composite is shown in Figure B.5.

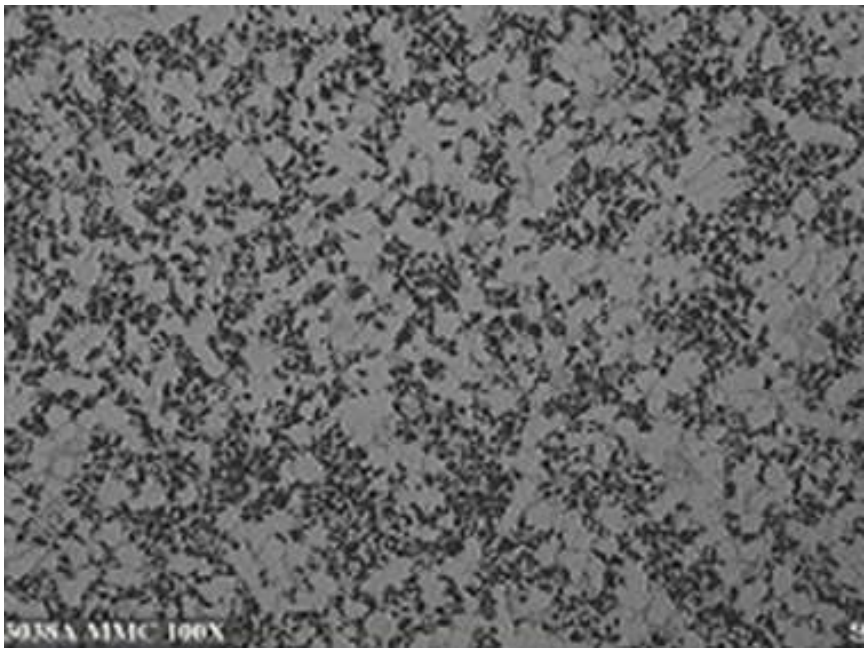

Figure B.5 Microstructure of 30%SiC/A359 metal matrix composite

The tool electrode used in the experimentation was electrolytic copper, fine grained graphite and copper graphite composite. The optical microscopic view of copper-graphite composite tool electrode is shown in Figure B.6.

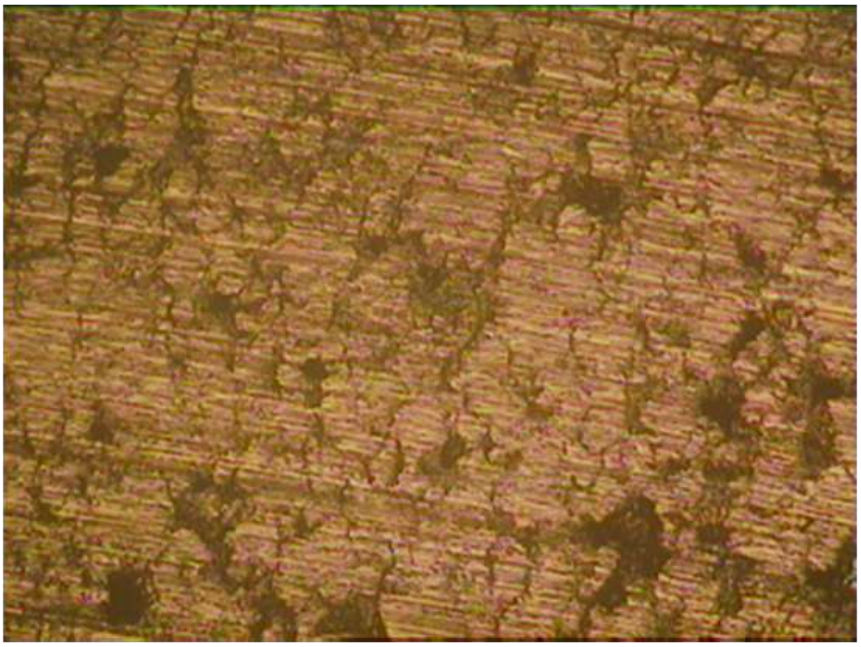

Figure B.6 Microstructure of copper-graphite composite tool electrode

APPENDIX – C

EDM MACHINE AND ITS TECHNICAL SPECIFICATIONS

The electric discharge machining used for experimentation was OSCARMAX- ZNC-S645 available at Central Institute of Hand Tools, Jalandhar. The Figures (C.1- C.2) shows the pictorial view of machined and its components used in the experimentation. The alignment of tool and workpiece was done with the help of in-build dial gauge.

Figure C.1 EDM machine used for the experimentation

(a) **(b)**

Figure C.2 Component of EDM (a) Position of tool electrode and workpiece (b) Control panel for EDM process parameters

The pictorial view of tool electrode and machined MMC with holders. The dielectric flushing nozzles are also shown in Figure C.3.

Figure C.3 Tool and workpiece set-up in EDM process

Technical data of the OSCAEMAX ZNC S-645 is as under:

1. **Power Supply Unit**

Supply Volts	:	415 V, 3 Ø, 50 Hz
Power input (Max.)	:	4.5 KVA
Open Gap Output Voltage	:	135 ± 5 % V
Machine Current (Max.)	:	60 A

2. **Machine Tool**

Electrode weight (Max.)	:	250 Kg.
Work piece weight (Max.)	:	2000 Kg.
Servo travel	:	400 mm
Reading accuracy of the dial gauge	:	0.01 mm

Work Tank

Length	:	1500 mm
Width	:	940 mm
Height	:	520 mm

Work Table

Mounting Surface

Length	:	1000 mm
Width	:	600 mm

Table Travel

Longitudinal Travel (X-axis)	:	600 mm
Transverse Travel (Y-axis)	:	450 mm

3. Dielectric Unit

Capacity	:	1200 Liters
Weight without Dielectric Fluid	:	350 Kg.
Filter Elements type	:	Paper
Filter Number	:	Two
Filter Rating	:	Below 20 microns
Outside Dimension (L x W x H)	:	2200 x 1300 x 580

The standard accessories are: X, Y axis double nuts balls screw, 14 inches CRT, Servo transverse on X, Y axis.

APPENDIX – D

THE BACK PROPAGATION NETWORK

Back propagation neural network

It is a systematic method for training multi-layer artificial neural networks. It has a mathematical foundation that is strong if not highly practical. It is a multi-layer forward network using extend gradient-decent based delta –learning rule, commonly known as back propagation (of error). Back propagation provides a computationally efficiency method for changing the weights in a feed forward network, with differentiable activation functions units, to learn a training set of input-output examples. It was first proposed by Paul Werbos in 1974, and further developed by D.E. Rumelhart, G.E. Hinton and R.O. Williams in 1986.

The training algorithm of back propagation involves four stages

1. Initialization of weights
2. Feed forward
3. Back propagation of errors
4. Updating of weights and biases.

Selection of initial weight

During first stage, the input and output values of the experimentation are normalized for the effect working of neural network. To get the best results the initial weight assignments (and Biases) are set to random numbers between -0.5 and 0.5 or between -1 and 1. The initialization of weight can be done randomly and there is no specific approach.

Selection of learning rate

A high learning rate leads to rapid learning but the weight oscillates, while a lower learning rate leads to slower learning.

Learning in back propagation

There are two types of learning:

(a) Sequential learning or pre pattern method
(b) Batch learning or pre-epoch method

In sequential learning a given input is propagated forward, the error is determined and back propagated, and the weights are updated.

In batch learning, the weights are updated only after the entire set of training network has been presented to the network. Thus, the weight update is only performed after every epoch.

How long we train network

The motivation for applying back propagation net is to achieve a balance between memorization and generalization; it is not necessarily advantageous to continue training until the error reaches a minimum value. The two disjoint sets of data used during training are

(a) Set of training patterns
(b) Set of training-testing pattern

The weights adjustments are based on the training pattern.

Momentum factor

In back propagation, the weight change is in a direction that is a combination of current gradient and the previous gradient. This approach is beneficial when some training data are very different from a majority of the data. A small learning rate is used to avoid major distribution of the direction of the learning when very unusual pair of training is presented. If the momentum is added to the weight update formula the convergence is faster.

Merits and demerits of back propagation

The merits and demerits of the back propagation network are a listed below:

Merits:

1. The mathematical formula presents present in this method can be applied to any network and does not require and special mention of the features of the function to be learn
2. The computing time is reduced if the weights chosen are small at the beginning.
3. The batch update of the weights exists, which provides a smoothing effect o the weight correction terms

Demerits:

1. The number of learning steps may be high, and also the learning phase has intensive calculations.
2. The selection of the number of hidden nodes in the network is a problem. If the number of hidden neurons is small, then the function to be learned may not be possibly represented, as the capacity of the network is small. If the number of hidden layer neurons is increased, the number of independent variables of the error function also increase, and the computing time also increase rapidly.
3. The network may get trapped in local minima even though there is much deeper minimum nearby.

In the present study, the experimental trials are divided in training and testing pattern by using Bernoulli's random variable method (training =70%: testing =30%). During training session, the updating of weight (training) stops when the error was minimum and the distribution of weight is according to the significance levels (from ANOVA table) of the input factors (process parameters). The methodology of training is represented diametrically (Figure D.1) as follows:

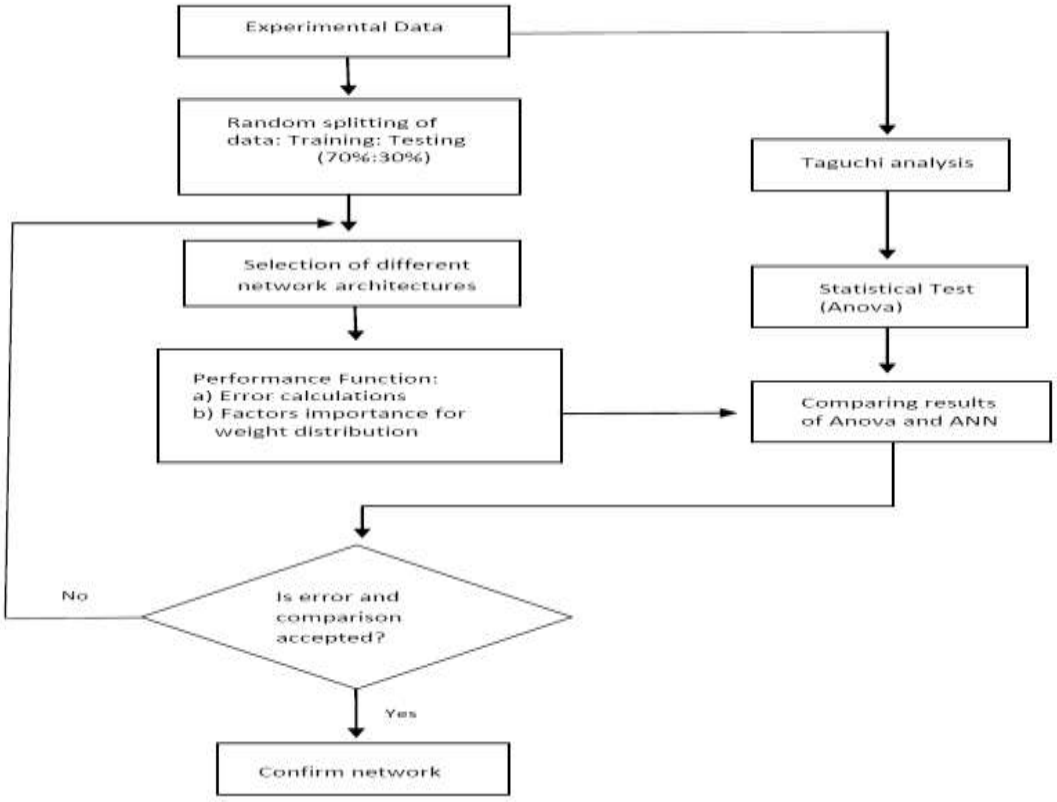

Figure D.1. Flow diagram represents the training methodology of the network

Table D.1 Summary of selected network to predict residual stress

Input Layer	**Factors**	1	Work piece
		2	Electrode
		3	Pulse-off
		4	Pulse-on
		5	Dielectric
		6	Current
	Number of Units		17
Hidden Layer(s)	Number of Hidden Layers		2
	Number of Units in Hidden Layer (n1)		9
	Number of Units in Hidden Layer (n2)		7
	Activation Function		Hyperbolic tangent
Output Layer	Dependent Variables	1	Residual stress
	Number of Units		1
	Rescaling Method for Scale Dependents		Standardized
	Activation Function		Identity
	Error Function		Sum of Squares

Table D.2 Independent importance of each factor for allocation of weight

Factors	**Importance**	**Normalized Importance**
Work piece	0.085	22.2%
Electrode	0.092	24.1%
Pulse-off(μs)	0.382	100.0%
Pulse-on(μs)	0.060	15.7%
Dielectric	0.231	60.5%
Current(amp)	0.151	39.6%

APPENDIX – E

X-RAY DIFFRACTOMETER (X'PERT PRO)

Figure E.1 XRD machine used for the residual stress measurments

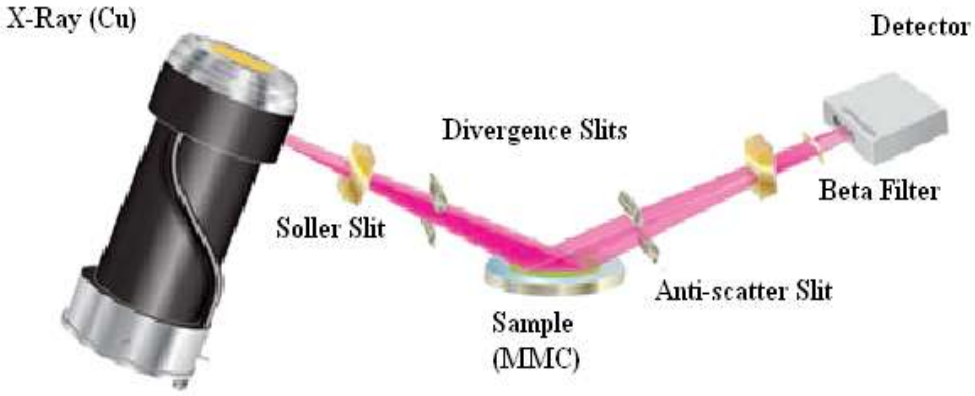

Figure E.2 Line diagram represntaion of XRD componenets

Key specification

Goniometer : Minimum step size : 0.0010

Radiation Safety: <1µS/Hr at 10cm

Power: Maximum generator output power: 3KW